# INVESTIGATION OF AN ADAPTATION-INDUCED TACTILE SPATIAL ILLUSION

# INVESTIGATION OF AN ADAPTATION-INDUCED TACTILE SPATIAL ILLUSION: PSYCHOPHYSICS AND BAYESIAN MODELING

By LUXI LI, Hon. B.Sc.

A Thesis Submitted to the School of Graduate

Studies in Partial Fulfillment of the Requirements

for the Degree Doctor of Philosophy


July 2017

McMaster University
DOCTOR OF PHILOSOPHY (2017)
Hamilton, Ontario
(Psychology)

TITLE: Investigation of an adaptation-induced tactile spatial illusion: psychophysics and Bayesian modeling

AUTHOR: Luxi Li, Hon. B.Sc. (McMaster University)

SUPERVISOR: Dr. Daniel Goldreich

NUMBER OF PAGES: xiv, 128

## Lay Abstract

Sensory adaptation can shape how we perceive the world. In this thesis, we showed that the perception of space in touch is pliable and subject to the influence of adaptation. Psychophysical testing in human participants showed that vibratory adaptation induced an illusion that expanded the perceived distance between stimuli on the skin. This illusion provides clues into how information about space in touch is normally processed and interpreted by the brain. In addition, we developed a computational model that used a powerful statistical framework – Bayesian inference – to investigate touch on a theoretical basis. To the best of our knowledge, the present thesis provides the first combined psychophysical and computational study on the effects of adaptation on tactile spatial perception. Our findings suggest that touch shares some common information processing principles with vision and hearing, and adaptation plays a functionally similar role in mediating this process across the senses.

## Abstract

Sensory adaptation is an important aspect of perception. A seemingly non-beneficial consequence of adaptation is that it produces perceptual illusions. For instance, following focal adaptation, the perceived separation between stimuli straddling the adapted attribute or region is often exaggerated. This type of illusion, known as perceptual repulsion, is both a consequence of and a clue to the brain's coding strategies and how they are influenced by recent sensory events. Adaptation-induced perceptual repulsion has been well documented in vision (e.g. the tilt aftereffect) and to a lesser extent in audition, but rarely studied in touch. The present thesis investigated the effects of adaptation on tactile spatial perception using a combination of human psychophysics and computational modeling. In a two-interval forced choice task, participants compared the perceived separation between two point-stimuli applied on the forearms successively. The point of subjective equality was extracted as a measure of perceived two-point distance. We showed that tactile spatial perception is subject to an adaptation-induced repulsion illusion: vibrotactile adaptation focally reduced tactile sensitivity and significantly increased the perceived distance between points straddling the adapted skin site (Chapter 2). This repulsion illusion, however, was not observed when the intervening skin was desensitized with topical anesthesia instead of vibrotactile adaptation, suggesting that peripheral desensitization alone is insufficient to induce the illusion (Chapter 3). With Bayesian perceptual modeling, we showed that the illusion was consistent with the hypothesis that the brain decodes tactile spatial input without awareness of the adaptation state in the nervous system (Chapter 4). Together, the empirical and theoretical work furthers the understanding of dynamic tactile spatial coding as the somatosensory system adapts to the sensory environment. Its main findings are consistent with the adaptation-induced repulsion illusions reported in vision and audition, suggesting that perception in different sensory modalities shares common processing features and computational principles.

# Preface

This thesis is composed of five chapters. Chapter 1 overviews the background literature in tactile perception, sensory adaptation, and perceptual illusions, and introduces the reader to Bayesian ideal observer analysis. Chapters 2 and 3 are empirical studies using psychophysical experimentation in human participants. Chapter 2 is published in the open-access journal *Frontiers in Human Neuroscience* [1], and is permitted for inclusion in the thesis under the terms of the Creative Commons Attribution License[2]. Chapter 4 is a computational modeling study exploring the empirical results described in Chapters 2 and 3. Chapter 5 discusses the findings and implications of these studies.

The research detailed in this thesis was supported by a Natural Sciences and Engineering Research Council of Canada (NSERC) Discovery Grant awarded to Dr. Daniel Goldreich. It was also supported through an annual graduate stipend from 2011 to 2016 by McMaster University.

[1] Li, L., Chan, A., Iqbal, S. M., & Goldreich, D. (2007). An adaptation-induced repulsion illusion in tactile spatial perception. *Front. Hum. Neurosci. 11: 331*. doi: http://10.3389/fnhum.2017.00331

[2] https://creativecommons.org/licenses/by/4.0/

# Declaration of Academic Achievement

## Chapter 2

I was involved in all aspects of this empirical research: experimental design, programming, data collection, statistical analysis, and writing. My graduate supervisor Dr. Goldreich made major contributions to the experimental design and programming. An undergraduate thesis student, Shah Mehran Iqbal, assisted in the data collection and statistical analysis for the pilot phase of the research (not included in this thesis). Another undergraduate thesis student, Arielle Chan, assisted in the data collection for the pilot phase and for Experiments 2 and 3. Several undergraduate laboratory study students also assisted in the data collection: Soumya Saini, Kyle Gauder, Vy Ngo, Faiza Shafaqat, Hiral Patel, Kaitlyn Gonsalves, and Cecelia Dai.

## Chapter 3

I was involved in all aspects of this empirical research: experimental design, programming, data collection, statistical analysis, and writing. Dr. Daniel Goldreich contributed to the experimental design and provided guidance at every stage of the research. An undergraduate thesis student, Jessica Webber, assisted in the data collection and statistical analysis. Several undergraduate laboratory study students also assisted in the data collection: Tyler Czaniecki, Cecelia Dai, Adam Alic, Jenin El-Sayes, Shirley Ong, and Claudia Turco.

## Chapter 4

I was involved in all aspects of this modeling research: conceptualizing, programming, running simulations, collecting data, performing statistical analysis, and writing. Dr. Daniel Goldreich provided guidance at every stage, and made major contributions to the conceptualizing and programming. An undergraduate thesis student, Michael Wan, assisted in running simulations and collecting data.

## Acknowledgements

First and foremost, I would like to thank my graduate supervisor, Dr. Daniel Goldreich, for his guidance, support, and encouragement all these years. Dan is a wonderful mentor. His scientific enthusiasm is contagious. His devotion to research and education is inspiring. He is the type of researchers who find fulfillment in the purest pursuit of scientific discovery. He is also one of the nicest and most patient people I have met. I would like to extend my gratitude to my committee members, Drs. Deda Gillespie, Patrick Bennett, and David I. Shore, for their time, invaluable advice, and kindness that guide me through this rite of passage. I would also like to thank Dr. Jeffrey Min-in Yau, for his thoughtful feedback on this dissertation and his advice on finding the personal path in academia and science.

Some of my happiest moments in grad school were thanks to the company of my former lab mates, Drs. Andy Bhattacharjee, Jonathan Tong, Ryan Peters, and particularly, Mike Wong. I miss our laughter and little adventures together. I would also like to thank my current lab mates, Arnav Bharadwaj, Kyle Gauder, Akash Deep, and Nina Prodribaba, for continuing the merry lab spirit and their helpful comments on my manuscript. My experimental work would not have been possible without the assistance of many undergraduate students over the years, to whom I am grateful: Arielle Chan, Jessica Webber, Tyler Czaniecki, Shah Mehran Iqbal, Michael Wan, Soumya Saini, Cecelia Dai, Vy Ngo, Faiza Shafaqat, Hiral Patel, Adam Alic, Jenin El-Sayes, Kaitlyn Gonsalves, Shirley Ong, and Claudia Turco.

During my PhD and life journey in Canada, many friends have lent me an ear and perked me up when I felt down. Their emotional support helped me push through. In addition to my lab mates, I would like to give specific thanks to Savitri Jetoo and Alan Santinele Martino. There are too many other names to mention explicitly, but know that I thank you in my heart.

In the past a few years, the person who has been the closest to me, sharing both joy and tears with me, is my partner Trevor Copp. Trevor, thank you for having my back. You make me a better person, and you make these all possible. After being a foreigner in Canada for 11 years, you are where I call home. I'll extend my gratitude to Trevor's lovely family: You are my family in Canada.

I would like to dedicate this dissertation to my parents, Wang Jianmin and Li Zhencai, as well as my stepfather, Liang Hanzhen, for their love and support. Mom, although there were difficult times in the family as I grew up, I know that you love me deeply in the best way you know, and you did the best you could; for that I am infinitely grateful. Dad, thank you for giving me the freedom to explore what I want. Uncle Liang, thank you for being an incredible person and for your tremendous support for Mom and me.

# Table of Contents

# List of Figures

# List of Abbreviations and Symbols

**Abbreviations**

| | |
|---|---|
| 2IFC | Two-Interval (two-alternative) Forced-Choice |
| A or Adapt | Adaptation condition |
| A0, A3, A7 | Adaptation condition with 0, 3, or 7 seconds of top-ups in between trials |
| Anes | Anesthesia condition |
| CNS | Central Nervous System |
| DCML | Dorsal Column Medial Lemniscus |
| FA | Fast-Adapting |
| ips | Impulses per second (firing rate unit) |
| LLR | Log Likelihood-Ratio |
| LML | Log Maximum Likelihood |
| NA | No-Adaptation or No-Anesthesia (baseline) condition |
| PDF | Probability Distribution Function |
| PSE | Point of Subjective Equality |
| RA | Rapidly-Adapting (afferent) |
| RF | Receptive Field |
| RMSE | Root Mean Square Error |
| SD | Standard Deviation |
| SE | Standard Error |
| S1 | Primary somatosensory cortex |
| S2 | Secondary somatosensory cortex |
| SA | Slowly-Adapting |

| | |
|---|---|
| SA1 | Slowly-Adapting type 1 (afferent) |
| SA2 | Slowly-Adapting type 2 (afferent) |
| TAE | (Visual) Tilt After-Effect |
| V1 | Primary visual cortex |
| VPM | Ventral Posterior Medial nucleus (in the thalamus) |

**Symbols**

| | |
|---|---|
| $A$ | Amplitude of Gaussian function; expected spike count at the receptive field centre |
| $c$ | Expected (average) stimulus-evoked spike count |
| C | Comparison distance in a two-point distance-comparison task |
| $d$ | Distance between receptive field centre and a stimulus |
| $k$ | Actual spike count on a single trial |
| R | Reference distance in a two-point distance-comparison task |
| $s$ | Stimulus strength |
| $x$ | x-position in a simulated skin patch |
| $y$ | y-position in a simulated skin patch |
| $\Delta x$ | Distance between x-positions of two point-stimuli; two-point distance |
| $\alpha$ | Adaptation state |
| $\lambda$ | Total expected spike count |
| $\sigma$ | Standard deviation |
| $\Psi$ | Psychometric function |
| $\mu$ | Mean |
| $\gamma$ | y-intercept |
| $\delta$ | Lapse rate |

# CHAPTER 1

# GENERAL INTRODUCTION

## 1.1 An overview of neural mechanisms of tactile perception

Touch is essential in everyday life. It allows us to directly interact with the environment. It is through touch that we determine the surface properties of materials, manipulate and control objects, utilize tools to expand our reach and abilities, obtain accurate awareness of bodily position and movement, feel pleasure and pain, and establish connection and rapport with fellow humans by simple contact, such as a handshake or a pat on the shoulder.

We often take for granted our perception of the world through touch, but how does the somatosensory system accomplish this remarkable feat? The quick answer is we know very little. Despite its ubiquitous presence and immense importance, touch has been underinvestigated compared to vision and audition. Even though the history of research on touch can be dated back to Aristotle (Fulkerson, 2016), it was not until about 50 years ago that the fascinating neural mechanisms underlying somatosensation began to be unravelled (Morley, 1998).

Touch is more than skin deep. The somatosensory system comprises subsystems that are responsible for coding very different physical stimuli, such as pressure, vibration, temperature, pain, body position, and movement. This thesis is in the context of passive tactile perception, which mainly deals with the perception of light touch from stimuli imposed on the skin surface without active exploration. The lack of active exploration limits the proprioceptive and motor information. At first glance, passive tactile perception of simple stimulation such as point-pressure may appear to be a very basic task, but it is mediated by a complex and sophisticated system of neurons and pathways. Tactile perception begins with transduction in mechanoreceptors in the periphery, where the skin deformation caused by mechanical stimuli is converted into neural signals in the form of action potentials and transmitted by myelinated Aβ fibers (mechanoreceptive afferents), into the dorsal column medial lemniscus (DCML) pathway in the central nervous system (CNS) (Rustioni et al., 1979). Via this pathway and relayed by three orders of neurons, the signals travel through the dorsal column nuclei in the medulla, and the ventroposterior lateral nuclei in the thalamus, into the primary and secondary somatosensory cortices (S1 and S2, respectively). In addition to these thalamocortical projections of neural signals, there are extensive intracortical projections: S1 projects to S2, and both S1 and S2 project to downstream cortical areas (for reviews, see Iwamura, 1998; McGlone & Reilly, 2010; Bensmaia & Yau, 2011; Serino & Haggard, 2010). Ultimately, neural signals are translated into conscious perception.

An important component of tactile information processing is its spatial dimension. The extraction of information about many properties of an object, such as its size, shape, and surface texture, relies on identifying where and how the skin is stimulated. Simple spatial perception, such as locating a stimulus or determining the distance between two stimuli on the skin, is at the foundation of performing many complex tactile tasks. Here, the main research interest of the present thesis is tactile spatial perception. Specifically, this thesis examines how recent tactile experience influences tactile spatial perception.

Spatial information about a tactile stimulus is first conveyed by peripheral tactile receptors. Much of the knowledge about tactile receptors has come from research on the glabrous (i.e. hairless) skin of the fingertips. This is because the fingertips possess a plethora of tactile receptors and are important for a wide variety of tactile tasks. Neurophysiological studies have identified four major classes of primary afferents and their associated mechanoreceptors in the glabrous skin of the fingertips in humans, non-human primates, and other mammals. These primary afferents are categorized and named based on the adaptation properties of their responses and their receptive field (RF) sizes. They are: slowly-adapting type 1 (SA1) afferents, innervating Merkel cells; slowly-adapting type 2 (SA2) afferents, innervating Ruffini endings; rapidly-adapting (RA) afferents, innervating Meissner corpuscles; and PC afferents, innervating Pacinian corpuscles. RA and PC afferents are also called fast-adapting type 1 and type 2 (FA1 and FA2) afferents respectively in the literature (Johansson & Flanagan, 2009). The slowly-adapting afferents (SA1 and SA2) fire throughout a sustained indentation, whereas the fast-adapting afferents (RA and PC) fire only at the onset and offset of the indentation. The RFs of type 1 afferents (SA1 and RA) are small and well-defined, whereas the RFs of type 2 afferents (SA2 and PC) are large with borders that are difficult to delineate (for reviews, see Johnson, 2001; Johansson & Flanagan, 2009; Abraira & Ginty, 2013).

The current consensus in the tactile literature is that the four main types of primary afferents are optimal for different functions. SA1s have high spatial acuity to skin indentation, which makes them the best candidate for coding tactile spatial information, such as stimulus position and curvature. SA2s are sensitive to skin stretch, which allows them to signal motion direction, velocity, hand position and finger conformation through the pattern of skin stretch. RAs are sensitive to low-frequency vibration (i.e. flutter), which endows them with remarkable efficiency in signalling sudden motion on the skin and providing feedback for slip and grip control. PCs are extremely sensitive to high-frequency vibration, which enables them to transmit distant tactile information through objects held in the hand (Macefield, 1998; Johnson, 2001; Abraira & Ginty, 2013). Traditionally, the four afferent types have often been viewed as playing largely non-overlapping roles in mediating these functions (Ochoa & Torebjörk, 1983; Bolanowski et al. 1988; Johnson et el. 2000; Johnson, 2001). This view is supported by neurophysiological and neuroelectrical evidence suggesting that segregation of signals from different afferent types extends to S1 (e.g. Mountcastle, 1956; Sur et al., 1981; Romo et al., 2000). However, more recent evidence has suggested that individual S1

neurons receive convergent input from multiple afferent types, and that there may be a greater degree of functional interplay among the afferent types than traditionally believed (Pei et al., 2009; Saal & Bensmaia, 2014).

Because the present thesis focuses on tactile spatial perception, here we will give a more specific overview of SA1 afferents, which are generally viewed as the main afferents responsible for coding spatial detail. SA1s can transmit a highly precise spatial image of tactile stimuli. Several physiological properties equip SA1s with this remarkable ability. First, SA1s have small, well-defined RFs with points of maximum firing ("hot spots") within the fields. The hot spots correspond to individual branches of the afferent axon. When the stimulus is finer than the RF diameter (typically 2-3 mm on primate fingertips), an individual hot spot becomes dominant, allowing an individual SA1 afferent to resolve spatial detail as small as 0.5 mm (Phillips & Johnson, 1981; Phillips et al. 1992; Johnson, 2001). Second, SA1s innervate the skin with high density, about 1 afferent per $mm^2$ in monkey fingertips (Johnson et al., 2000) and 0.7 afferent per $mm^2$ in human fingertips (Johansson & Vallbo, 1979), and a single afferent can supply as many as 15 Merkel cells (Abraira & Ginty, 2013). Third, SA1s and Merkel cells are located close to the skin surface, in the basal layer of the epidermis (Halata et al., 2010); the shallow location facilitates their processing of tactile information on the skin surface. Fourth, SA1s are highly sensitive to points, edges, curvatures, and gaps, due to their selective sensitivity to local strain components on the skin (Phillips & Johnson, 1982; Sripati et al. 2006). Fifth, SA1s lack spontaneous firing. Sixth, SA1s are insensitive to skin displacement adjacent to their RFs or skin stretch (Johnson, 2001; Abraira & Ginty, 2013). These characteristics all contribute to SA1s' high-fidelity coding of fine spatial information.

The studies described in this thesis involved experimentation on human forearm skin, which belongs to the category of hairy skin. Microneurography studies have identified five classes of myelinated mechanoreceptive units in in human forearm skin (Vallbo et al., 1995; Olausson et al., 2000): two slowly-adapting types – SA1s and SA2s, and three fast-adapting types - hair units (also known as hair follicle afferents in the literature), field units, and Pacinian (PC) units. These mechanoreceptive units have also been identified in the hairy skin of a variety of mammals (for reviews, see Iggo & Andres, 1982; Zimmerman et al., 2014). Drawing from previous literature on mammalian hairy skin receptors, Vallbo et al. (1995) and Olausson et al. (2000) suggested that the end organs for SA1s, SA2s, hair units, and PC units in human forearm skin are Merkel cells, Ruffini endings, hair follicles, and Pacinian corpuscles, respectively; the end organs for field units are unclear.

Less is known about hairy skin mechanoreceptive afferents than glabrous skin ones; however, studies have suggested that the characteristics of hairy skin mechanoreceptive afferents are somewhat similar to their counterparts in glabrous skin. For example, SA1, SA2, and PC afferents can be classified based on their RF characteristics in a similar fashion to those in glabrous skin: SA1 RFs are small, well-defined, comprising 2-4 highly sensitive spots that presumably correspond to clusters of Merkel cells innervated by that

afferent, and lacking spontaneous firing; they are capable of signaling spatiotemporal information (Vallbo et al., 1995; Olausson et al., 2000). SA2 RFs are highly sensitive to skin stretch and display spontaneous background discharge; they play important roles in proprioception and kinesthesia (Edin, 1992; Olausson et al., 2000). PCs are sensitive to high-frequency vibration and remote taps, have large RFs, and are located deep down the tissues near bones and joints (Merzenich & Harrington, 1969; Sahai et al., 2006). Apart from these similarities, hairy skin afferents also exhibit some characteristics that differ from those in glabrous skin. For example, the innervation density of SA1s is much lower in human forearm skin (~4 per 100 $mm^2$; Vallbo et al. 1995) than in human fingertip (~100 per 100 $mm^2$; Johnson, 2001). The low density presumably contributes to the fact that the forearm has a much poorer spatial resolution than the fingertip (Stevens & Choo, 1996), because receptor innervation density is one of the determinants for spatial acuity (Peters et al. 2009). Moreover, human forearm skin seems to lack the most abundant mechanoreceptive afferents observed in glabrous skin – RA afferents (Johnson et al. 2000) – but instead has two other types of fast-adapting afferents in addition to PCs: hair units and field units. Hair units exhibit some properties similar to those of RA afferents: they are fast adapting, with the peak of sensitivity to flutter around 20-50 Hz, and are efficient in detecting motion or air puffs on the skin surface. Unlike RA afferents, however, hair units in human forearm have large RFs, roughly an order of a magnitude larger than SA1 RFs in human forearm. Field unit RFs bear some resemblance to hair unit RFs, although the functional roles of field units are unclear (Vallbo et al., 1995). The large RFs of hair units and field units in human forearm skin presumably limit their contribution to the perception of fine spatial detail.

The peripheral signals generated by these receptors and afferents then ascend the arm through the median and ulnar nerves, enter the spinal cord through the dorsal root ganglia, travel through the DCML pathway, and project onto S1 and S2. In S1, neurons encode tactile information within a spatial map. S1 of each hemisphere represents tactile sensations from the contralateral body parts in a topographically organized manner. In this "somatosensory homunculus", adjacent neurons tend to have adjacent RFs on the body. The somatotopic mapping between peripheral RFs and S1 representations have been clearly demonstrated by neurophysiological experiments: tactile stimulation of a specific body part elicits neural response in the S1 region that is responsible for that body part; conversely, direct stimulation of the S1 region induces a tactile sensation localized in the corresponding body part, even though no actual tactile stimulus is delivered to that body part (for a review, see Serino & Haggard, 2010). S1 comprises Brodmann areas 3a, 3b, 1, and 2. Area 3a responds primarily to proprioceptive stimulation. Areas 3b and 1 respond primarily to cutaneous stimulation; they are responsible for coding many elementary features of tactile stimuli, such as location, orientation, edge, and motion direction. The majority of area 3b neurons have single-locus RFs, whereas area 1 neurons have larger RFs and more composite response properties. Area 2 responds to both cutaneous and proprioceptive stimulation; it integrates input from areas 3b and 1 to code more complex spatial features, such as contour curvature. The components of S1 project to S2, which further integrates tactile information and extracts higher-order, more

complex stimulus features. For example, S2 neurons exhibit tuning for curvature direction and play important roles in two-dimensional shape perception. S2 neurons typically have very large RFs; some of them span across the midline of the body and receive bilateral input. In general, as tactile signals travel from earlier cortical processing areas to downstream areas (S1 area 3b -> area 1 -> area 2 -> S2 -> further downstream), neural responses reflect increasingly complex and integrated stimulus features, and neural RFs encompass increasingly larger and more composite body regions. Similar to neurons in earlier processing areas, some neurons in downstream areas are tuned to some elementary stimulus features, but over much larger RFs. For example, similar to some neurons in S1 areas 3b and 1, some neurons in S1 area 2 and S2 are tuned to orientation, but over much larger skin regions, e.g. covering multiple digits or even both hands. For these higher-order neurons, orientation tuning tends to be consistent across their very large RFs, suggesting that orientation tuning becomes position-invariant (for reviews, see Iwamura, 1998; Bensmaia & Yau, 2011; Yau et al., 2016).

Within this peripheral and central processing system, tactile spatial perception is mediated by the population response of groups of neurons, which is subject to the influence of sensory history and context. In other words, tactile spatial perception arises from the dynamic interplay among neuronal properties and sensory history. Sensory history mediates neuronal response properties and can substantially affect tactile spatial perception.

### 1.2 Adaptation and perceptual illusions

The present thesis aims to investigate how tactile spatial perception is influenced by recent sensory history – specifically, sensory adaptation. Our sensory systems continuously adjust to the sensory environment. When we are exposed to a sustained sensory stimulus – for example, light, noise, a scent, or clothes that touch our skin, our sensory systems adjust neural responses to reserve energy and efficiently represent the environment. This phenomenon, known as adaptation, is ubiquitous in all sensory modalities. Adaptation influences perception; for example, the same stimulus often feels less intense after prolonged exposure because of adaptation.

In tactile research, the term “adaptation” is usually used in two related but different contexts. The context that is used *less* is the general context as described in the previous paragraph: adaptation refers to the progressive changes in neural responses resulting from sustained stimulation, or the application of sustained stimulation to induce such changes. The other context, which is used much more frequently, is to classify mechanoreceptive afferents based on their response to sustained indentation, such as “slowly-adapting” (SA) or “rapidly-adapting” (RA) as described in Chapter 1.1. The same scheme has been used to classify somatosensory cortical neurons. For example, an S1 neuron that fires throughout a sustained stimulation on the skin, or receives input primarily from SA

afferents, is classified as an SA neuron. Even though response adaptation is one of the bases on which tactile receptors and, to a lesser extent, somatosensory cortical neurons are classified, the perceptual effects of tactile adaptation in the more general context have not been well studied.

The present thesis drew inspiration from the rich literature on visual adaptation. Unlike in touch, the perceptual effects of adaptation in vision have been studied extensively. A topic of interest in the visual adaptation literature is adaptation-induced aftereffects, particularly perceptual illusions, because illusions provide clues as to how the visual system normally encodes and interprets stimuli. Adaptation is often used as a tool in perceptual studies to induce aftereffects or illusions, thereby probing neural selectivity and neural computations in information processing (for reviews, see Webster, 2012; Solomon & Kohn, 2014).

A well-known adaptation-induced visual illusion is the tilt aftereffect (TAE) illusion: prolonged viewing of tilted lines causes subsequently viewed lines of a nearby orientation to appear tilted away from the adapted orientation (Gibson & Radner, 1937; Magnussen & Johnsen, 1986; Dragoi et al., 2000). The TAE has been studied extensively to probe the selectivity and functional organization of orientation-tuned neurons in the primary visual cortex (V1). The TAE is an example of a perceptual repulsion illusion: following focal adaptation, the subsequently viewed orientation appears to be "repelled" from the adapted orientation. In other words, focal adaptation induces a repulsive shift in the percept of the subsequent nearby orientation. Here, *focal* adaptation means to selectively adapt to a narrow, specific stimulus characteristic (in this example, a specific orientation); the degree of adaptation is likely to be graded as a function of distance from the adaptor value: neurons tuned to the adaptor orientation adapts the most, and neurons tuned to nearby orientations also adapts but to a lesser extent.

The adaptation-induced repulsive shift has perceptual benefits: it effectively magnifies the perceived difference between the subsequent nearby orientation and the adaptor orientation, thus enhancing perceptual resolution around the adaptor orientation, as evidenced by reduced discrimination threshold (Schwartz et al., 2007). Adaptation-induced perceptual repulsion has been well documented for a wide variety of visual properties, including orientation, motion direction, position, curvature, size, contrast, spatial frequency, and even high-level features such as facial properties (for reviews, see Clifford et al., 2007; Kohn, 2007; Webster, 2012). The common existence of this phenomenon across categories of visual perception may point to a fundamental computational strategy in the visual system for information processing. It has been proposed that, following lengthy exposure to a sustained stimulus, the visual system adapts by recalibrating neural responses to match the new baseline, in order to preserve energy and increase sensitivity to changes; the repulsive aftereffect is a consequence and by-product of this recalibration. Despite having general functional benefits, the adaptation process can manifest as seemingly non-beneficial perceptual illusions under unusual physical conditions such as those experimentally manipulated (Stocker & Simoncelli,

2006; Kohn, 2007; Seriès et al., 2009; Fischer & Whitney, 2014).

In light of the visual literature, an interesting question arises: Does adaptation induce an analogous repulsive effect in tactile perception? Touch and vision share many similarities in their perceptual goals and functional organizations; for example, both systems need to extract information from two-dimensional receptor sheets, both systems have analogous sensory channels optimized for coding certain spatial or temporal features, and both systems exhibit neural tuning to location and orientation. Although the physiological substrates of sensory transduction are by necessity different in these two systems, it has long been speculated that touch and vision have similar functional mechanisms for coding and representing information, especially spatial information (for a review, see Hsiao, 1998). Therefore, it is plausible that focal adaptation causes the tactile system to undergo similar changes as in the visual system, which leads to a perceptual repulsion for subsequent stimuli whose properties (e.g. orientation, position, frequency) are close to the adaptor value. A manifestation of the repulsive effect would be that discriminability around the adaptor value is enhanced following adaptation. Indeed, both the repulsive effect and enhanced discriminability following adaptation have been observed in tactile perception. Tactile psychophysical studies have reported that focal adaptation leads to perceptual repulsion aftereffects in motion direction (McIntyre et al., 2016a), speed (McIntyre et al., 2016a, 2016b), orientation (Silver, 1969), and distance between two simultaneous stimuli (Day & Singer, 1964; Calzolari et al. 2017), as well as improving discrimination performance in vibrotactile frequency (Goble & Hollins, 1994; Tommerdahl et al., 2005; Tannan et al., 2007), amplitude (Goble & Hollins, 1993; Delemos & Hollins, 1996), and spatial localization (Tannan et al., 2006).

Of these effects, the impact of adaptation on tactile spatial perception (e.g. position, distance) is the least studied and the most inconclusive. The very few existing studies on this topic have yielded somewhat contradictory results. For example, an early study on human forearm skin reported that adaptation altered the perceived separation between parallel bars placed on adjacent skin areas in a direction consistent with perceptual repulsion (Day & Singer, 1964). A follow-up study suggested, however, that the observed effects may not be adaptation-induced aftereffects, but rather estimation artifacts induced by the particular sets of comparison stimuli to which the participants were exposed (Gilbert, 1967).

In the present thesis, we revisited the question of whether adaptation induces spatial repulsion in touch. Specifically, we examined whether focal vibratory adaptation on the forearm induces a spatial repulsion illusion affecting the perceived distance between two points of contact straddling the adapted region. Punctate point-stimuli are commonly used to measure tactile spatial processing. Locating point-stimuli and determining the distance between them are the basis of many tactile spatial tasks. The present thesis provides one of the first studies investigating adaptation effects on tactile spatial perception, a topic that has rarely been documented in the literature.

### 1.3 Modeling perception as probabilistic inference

How do nervous systems transform raw sensory information into perception? Neurophysiological and psychophysical studies, among other empirical research, have helped to shed light on this question by revealing bits and pieces of the puzzle. However, there lacks a unifying theory on how nervous systems code, represent, and store sensory information, and how perception arises from these procedures. A promising complement to the empirical research is computational modeling, which aims to tackle the overarching coding principles that theoretically govern perception. The present thesis implements a computational framework known as Bayesian inference, which views perception as a probabilistic inference.

The idea of perception as a problem of inference can be dated back to Aristotle. In the 19$^{th}$ century, Hermann von Helmholtz systematically developed the concept of perception as an unconscious inference; he used the visual illusion of the sun rotating around the earth as an example to illustrate this inference. The task of perception is to infer the properties of the external environment from the patterns of sensorineural responses. A fundamental challenge faced by perception is the inherent uncertainty at every stage of processing. Sources of uncertainty include ambiguous stimuli, low receptor density, stochasticity in neural firing, and the multitude of hypothetical scenarios that are consistent with the available sensory data. The inherent uncertainty and noise in perception is best described in probabilistic terms. Over the past several decades, researchers have rigorously applied concepts from probability theory and information theory to investigate problems in perception and other neuroscience topics. One of the powerful probabilistic frameworks they have applied is Bayesian inference (Rao et al., 2002; Knill & Pouget, 2004).

The present thesis implements computational modeling with Bayesian inference. The Bayesian models treat perception as a statistical inference consisting of two information-processing stages: encoding and decoding. Encoding is the forward-processing, data-generative stage, in which stimulus properties are transformed into sensory data (e.g. firing rates) in the form of probabilistic measurements (i.e. likelihood probabilities). Decoding deals with the inverse problem; a Bayesian observer interprets the noisy sensory data in light of sensory experience or expectation (i.e. prior probabilities) to provide probabilistic estimates (i.e. posterior probabilities) for the stimulus properties (Knill & Pouget, 2004; Goldreich, 2007). Thus, Bayesian inference allows the model observer to quantify uncertainty in different stages of perception in a unified and well-controlled manner.

With Bayesian modeling, we aimed to better understand the perceptual effects that we empirically observed. The Bayesian model yielded psychometric functions that allowed us to quantitatively compare the model performance with the psychophysically measured human performance. Moreover, it allowed us to explore the factors that plausibly contributed to the empirical observations in a simulated environment, where we could

specifically define parameters, directly manipulate constraints and information available, and precisely measure responses. Our goal was not only to *replicate* human performance – which we did – but also to *predict* human performance given different constraints, and to shed light on the possible neural response properties and computations that underlie tactile spatial perception and adaption-induced repulsion illusions.

## 1.4 Overview of studies

The present thesis investigated the effects of adaptation on tactile spatial perception, using a combination of psychophysical experimentation and computational modeling. With psychophysical testing in human participants, we showed that tactile spatial perception is subject to an adaptation-induced repulsion illusion that expands the perceived distance between points on the skin (Chapter 2). This illusion, however, was not observed when the intervening skin between points was desensitized with topical anesthesia instead of vibrotactile adaptation (Chapter 3). With Bayesian perceptual models, we showed that the repulsion illusion empirically observed was consistent with the hypothesis that the brain decodes the tactile spatial input without awareness of the adaptation state in the nervous system (Chapter 4).

In Chapter 2, we examined the effects of vibrotactile adaptation on two-point distance perception. In a series of experiments involving a two-interval forced-choice (2IFC) task, participants compared the perceived separation between two point-stimuli applied on the forearms successively. Separation distance was constant on one arm (the reference) and varied on the other arm (the comparison). Experiment 1 applied repeated baseline measurements, and verified that participants' distance perception was unbiased across arms and stable across experimental blocks. Experiment 2 implemented a monofilament-detection task, and showed that vibration of the skin between the two stimulus points on the reference arm focally reduced tactile sensitivity, verifying the efficacy of the vibrotactile protocol in inducing adaptation. Experiment 3 repeated the distance-comparison task in Experiment 1 with the adaptation protocol from Experiment 2, and showed that adaptation significantly increased the perceived distance between the reference points, causing a repulsion illusion. The results are consistent with findings in the visual and auditory perception literature that reported repulsion illusions following focal adaptation.

In Chapter 3, we conducted the battery of tests from Chapter 2 in a different group of participants, but applied a topical anesthetic (a mixture of lidocaine and prilocaine) instead of vibration to the intervening skin between the reference points. Anesthesia focally reduced tactile sensitivity but caused little to no increase in perceived two-point distance. We discussed possible explanations for the discrepancy between the adaptation and anesthesia results. A possibility is that mere desensitization of peripheral receptors is

not sufficient to cause the repulsion illusion observed in Chapter 2, and that adaptation in the central nervous system is also required.

In Chapter 4, we implemented Bayesian perceptual models to investigate adaptation effects on tactile spatial perception on a theoretical and computational basis. The model has two major components: a generative model (the encoder) and a Bayesian decoder. The generative model simulated somatosensory neural firing patterns evoked by point-stimuli. It incorporated response properties of somatosensory cortical neurons, including the spacing and size of their receptive fields, firing rate variability, and adaptation state. The Bayesian decoder interpreted the simulated neural data from the generative model to perform 2IFC tasks (two-point distance comparison, monofilament detection). With specific sub-optimal constraints, such as sparse receptive fields and Poisson firing noise, the Bayesian observer performed quantitatively similarly to human participants. It exhibited a repulsion illusion following adaptation in the two-point distance comparison task, which was comparable to the repulsion illusion we empirically observed in Chapter 2. In general, this illusion emerged when the decoder was unaware of the adaptation in the encoding stage. We speculated on the plausibility of this assumption, as well as other implications from the model performance, in the context of human tactile perception and its underlying neural computations.

Taken together, this thesis provides one of the first combined psychophysical and computational studies on the effects of adaptation on tactile spatial perception. Its main findings are consistent with the adaptation-induced repulsion illusions reported in vision and audition, suggesting that tactile perception shares common processing features with visual and auditory perception. It sheds light on possible mechanisms and functional organizations underlying dynamic tactile spatial processing as the somatosensory system adjusts to the external environment.

## 1.5 References

Abraira, V., & Ginty, D. (2013). The sensory neurons of touch. *Neuron*, *79*(4), 618–639. https://doi.org/10.1016/j.neuron.2013.07.051

Bolanowski, S. J., Gescheider, G. a, Verrillo, R. T., & Checkosky, C. M. (1988). Four channels mediate the mechanical aspects of touch. *The Journal of the Acoustical Society of America*, *84*(5), 1680–1694. https://doi.org/10.1121/1.397184

Calzolari, E., Azanon, E., Danvers, M., Vallar, G., & Longo, M. R. (2017). Adaptation aftereffects reveal that tactile distance is a basic somatosensory feature. *Proc Natl Acad Sci USA*, *114*(17), 4555–4560.

Clifford, C. W. G., Webster, M. A., Stanley, G. B., Stocker, A. A., Kohn, A., Sharpee, T. O., & Schwartz, O. (2007). Visual adaptation: Neural, psychological and computational aspects. *Vision Research*, *47*(25), 3125–3131.

https://doi.org/10.1016/j.visres.2007.08.023
Day, R. H., & Singer, G. (1964). A tactile spatial aftereffect. *Australian Journal of Psychology*, *16*(I), 33–37.
Delemos, K. a, & Hollins, M. (1996). Adaptation-induced enhancement of vibrotactile amplitude discrimination: the role of adapting frequency. *The Journal of the Acoustical Society of America*, *99*(1), 508–16. https://doi.org/10.1121/1.414509
Dragoi, V., Sharma, J., & Sur, M. (2000). Adaptation-induced plasticity of orientation tuning in adult visual cortex. *Neuron*, *28*(1), 287–298. https://doi.org/10.1016/S0896-6273(00)00103-3
Edin, B. B. (1992). Quantitative analysis of static strain sensitivity in human mechanoreceptors from hairy skin. *Journal of Neurophysiology*, *67*(5), 1105–1113. https://doi.org/10.1152/jn.00628.2004.
Fischer, J., & Whitney, D. (2014). Serial dependence in visual perception. *Nature Publishing Group*, *17*(5), 738–743. https://doi.org/10.1038/nn.3689
Fulkerson, M. (2016). "Touch". The Stanford Encyclopedia of Philosophy. (Spring 201). Stanford University. Retrieved from https://plato.stanford.edu/entries/touch/
Gibson, J. J., & Radner, M. (1937). Adaptation, After-Effect and Constrast in the Perception of Tilted Lines. *Journal of Experimental Psychology*, *20*(5), 453–467. https://doi.org/10.1037/h0059826
Gilbert, A. J. (1967). Tactile spatial aftereffect or adaptation level? *Journal of Experimental Psychology*, *73*(3), 450–455.
Goble, A. K., & Hollins, M. (1993). Vibrotactile adaptation enhances amplitude discrimination. *The Journal of the Acoustical Society of America*, *93*(1), 771–780. https://doi.org/10.1121/1.410314
Goble, A. K., & Hollins, M. (1994). Vibrotactile adaptation enhances frequency discrimination. *The Journal of the Acoustical Society of America*, *96*(2), 771–780. https://doi.org/10.1121/1.410314
Goldreich, D. (2007). A Bayesian perceptual model replicates the cutaneous rabbit and other tactile spatiotemporal illusions. *PLoS ONE*, *2*(3). https://doi.org/10.1371/journal.pone.0000333
Halata, Z., Baumann, K. I., & Grim, M. (2010). Merkel Cells. *The Senses: A Comprehensive Reference*, *6*, 33–38. https://doi.org/10.1016/B978-012370880-9.00341-8
Hsiao, S. S. (1998). Similarities between touch and vision. In J. W. Morley (Ed.), *Neural computation* (pp. 131–165). Amsterdam ; New York: Elsevier.
Iggo, A., & Andres, K. H. (1982). Morphology of Cutaneous Receptors. *Ann. Rev. Neurosci.*, (5), 1–31.
Iwamura, Y. (1998). Representation of tactile functions in the somatosensory cortex. In J. W. Morley (Ed.), *Neural Aspects of Tactile Sensation* (pp. 195–238). Elsevier B.V.
Johansson, R. S., & Flanagan, J. R. (2009). Coding and use of tactile signals from the fingertips in object manipulation tasks. *Nature Reviews Neuroscience*, *10*(5), 345–359. https://doi.org/10.1038/nrn2621
Johansson, R., & Vallbo, A. (1979). Tactile sensibility in the human hand: relative and absolute densities of four types of mechanoreceptive units in glabrous skin. *The*

*Journal of Physiology*, (286), 283–300. https://doi.org/10.1113/jphysiol.1979.sp012619

Johnson, K. O. (2001). The Roles and Functions of cutaneous mechanoreceptors. *Current Opinion in Neurobiology*, *11*, 455–461. Retrieved from papers3://publication/uuid/5F042AE7-BBCB-4A6C-B1BA-B6480F271B1B

Johnson, K. O., & Hsiao, S. S. (1992). Neural mechanisms of tactile form and texture perception. *Ann. Rev. Neurosci.*, *15*, 227–250. https://doi.org/10.1016/j.cub.2014.02.049

Johnson, K. O., Yoshioka, T., & Vega-Bermudez, F. (2000). Tactile functions of mechanoreceptive afferents innervating the hand. *Journal of Clinical Neurophysiology : Official Publication of the American Electroencephalographic Society*, *17*(6), 539–558. https://doi.org/10.1097/00004691-200011000-00002

Knill, D. C., & Pouget, A. (2004). The Bayesian brain: The role of uncertainty in neural coding and computation. *Trends in Neurosciences*, *27*(12), 712–719. https://doi.org/10.1016/j.tins.2004.10.007

Kohn, A. (2007). Visual Adaptation: Physiology, Mechanisms, and Functional Benefits. *Journal of Neurophysiology*, *97*(5), 3155–3164. https://doi.org/10.1152/jn.00086.2007

Macefield, V. G. (1998). The signalling touch, movement and manipulation by mechanoreceptors in human skin. In J. W. Morley (Ed.), *Neural Aspects of Tactile Sensation* (pp. 89–130). Amsterdam: Elsevier.

Magnussen, S., & Johnsen, T. (1986). Temporal aspects of spatial adaptation. A study of the tilt aftereffect. *Vision Research*, *26*(4), 661–672. https://doi.org/10.1016/0042-6989(86)90014-3

McGlone, F., & Reilly, D. (2010). The cutaneous sensory system. *Neuroscience and Biobehavioral Reviews*, *34*(2), 148–159. https://doi.org/10.1016/j.neubiorev.2009.08.004

McIntyre, S., Birznieks, I., Vickery, R. M., Holcombe, A. O., & Seizova-Cajic, T. (2016). The tactile motion aftereffect suggests an intensive code for speed in neurons sensitive to both speed and direction of motion. *Journal of Neurophysiology*, *115*(3), 1703–1712. https://doi.org/10.1152/jn.00460.2015

McIntyre, S., Seizova-Cajic, T., & Holcombe, A. O. (2016). The tactile speed aftereffect depends on the speed of adapting motion across the skin rather than other spatiotemporal features. *Journal of Neurophysiology*, *115*(3), 1112–1121. https://doi.org/10.1152/jn.00821.2014

Morley, J. W. (Ed.). (1998). *Neural aspects in tactile sensation / edited by J.W. Morley*. Amsterdam ; New York: Elsevier. Retrieved from http://www.loc.gov/catdir/enhancements/fy0602/98209962-t.html

Mountcastle, V. (1957). Modality and topographic properties neurons of cat's somatic sensory. *Journal of Neurophysiology*, *20*(4), 408–434.

Ochoa, J., & Torebjörk, E. (1983). Sensations evoked by intraneural microstimulation of single mechanoreceptor units innervating the human hand. *The Journal of Physiology*, *342*, 633–54. https://doi.org/10.1016/0304-3959(85)90304-5

Olausson, H., Wessberg, J., & Kakuda, N. (2000). Tactile directional sensibility:

Peripheral neural mechanisms in man. *Brain Research*, *866*(1–2), 178–187. https://doi.org/10.1016/S0006-8993(00)02278-2

Pei, Y.-C., Denchev, P. V, Hsiao, S. S., Craig, J. C., & Bensmaia, S. J. (2009). Convergence of submodality-specific input onto neurons in primary somatosensory cortex. *Journal of Neurophysiology*, *102*(3), 1843–1853. https://doi.org/10.1152/jn.00235.2009

Peters, R. M., Hackeman, E., & Goldreich, D. (2009). Diminutive Digits Discern Delicate Details: Fingertip Size and the Sex Difference in Tactile Spatial Acuity. *Journal of Neuroscience*, *29*(50), 15756–15761. https://doi.org/10.1523/JNEUROSCI.3684-09.2009

Phillips, J. R., & Johnson, K. O. (1981). Tactile spatial resolution. III. A continuum mechanics model of skin predicting mechanoreceptor responses to bars, edges, and gratings. *Journal of Neurophysiology*, *46*(6), 1204–1225. https://doi.org/10.1152/jn.00955.2003

Romo, R., Hernández, a, Zainos, a, Brody, C. D., & Lemus, L. (2000). Sensing without touching: psychophysical performance based on cortical microstimulation. *Neuron*, *26*(1), 273–278. https://doi.org/10.1016/S0896-6273(00)81156-3

Rustioni, A., Hayes, N. L., & O'Neill, S. (1979). Dorsal column nuclei and ascending spinal afferents in macaques. *Brain : A Journal of Neurology*, *102*(1), 95–125. https://doi.org/https://doi.org/10.1093/brain/102.1.95

Saal, H. P., & Bensmaia, S. J. (2014). Touch is a team effort: Interplay of submodalities in cutaneous sensibility. *Trends in Neurosciences*, *37*(12), 689–697. https://doi.org/10.1016/j.tins.2014.08.012

Schwartz, O., Hsu, A., & Dayan, P. (2007). Space and time in visual context. *Nature Reviews. Neuroscience*, *8*(7), 522–535. https://doi.org/10.1038/nrn2155

Seriès, P., Stocker, A. A., & Simoncelli, E. P. (2009). Is the homunculus "aware" of sensory adaptation? *Neural Computation*, *21*(12), 3271–304. https://doi.org/10.1162/neco.2009.09-08-869

Serino, A., & Haggard, P. (2010). Touch and the body. *Neuroscience and Biobehavioral Reviews*, *34*(2), 224–236. https://doi.org/10.1016/j.neubiorev.2009.04.004

Silver, R. J. (1969). *Tilt after-effects in touch*. Brandeis University.

Solomon, S. G., & Kohn, A. (2014). Moving sensory adaptation beyond suppressive effects in single neurons. *Current Biology*, *24*(20), R1012–R1022. https://doi.org/10.1016/j.cub.2014.09.001

Sripati, A. P., Bensmaia, S. J., & Johnson, K. O. (2006). A Continuum Mechanical Model of Mechanoreceptive Afferent Responses to Indented Spatial Patterns. *Journal of Neurophysiology*, *95*(6), 3852–3864. https://doi.org/10.1152/jn.01240.2005

Stevens, J. C., & Choo, K. K. (1996). Spatial Acuity of the Body Surface over the Life Span. *Somatosensory & Motor Research*, *13*(2), 153–166. https://doi.org/10.3109/08990229609051403

Stocker, A. a, & Simoncelli, E. P. (2006). Noise characteristics and prior expectations in human visual speed perception. *Nature Neuroscience*, *9*(4), 578–585. https://doi.org/10.1038/nn1669

Sur, M., Wall, J. T., & Kaas, J. H. (1981). Modular segregation of functional cell classes

within the postcentral somatosensory cortex of monkeys. *Science (New York, N.Y.)*, *212*(4498), 1059–1061. https://doi.org/10.1126/science.7233199

Sur, M., Wall, J. T., & Kaas, J. H. (1984). Modular distribution of neurons with slowly adapting and rapidly adapting responses in area 3b of somatosensory cortex in monkeys. *Journal of Neurophysiology*, *51*(4), 724–744.

Tannan, V., Simons, S., Dennis, R. G., & Tommerdahl, M. (2007). Effects of adaptation on the capacity to differentiate simultaneously delivered dual-site vibrotactile stimuli. *Brain Research*, *1186*(1), 164–170. https://doi.org/10.1016/j.brainres.2007.10.024

Tannan, V., Whitsel, B. L., & Tommerdahl, M. A. (2006). Vibrotactile adaptation enhances spatial localization. *Brain Research*, *1102*(1), 109–116. https://doi.org/10.1016/j.brainres.2006.05.037

Tommerdahl, M., Hester, K. D., Felix, E. R., Hollins, M., Favorov, O. V., Quibrera, P. M., & Whitsel, B. L. (2005). Human vibrotactile frequency discriminative capacity after adaptation to 25 Hz or 200 Hz stimulation. *Brain Research*, *1057*(1–2), 1–9. https://doi.org/10.1016/j.brainres.2005.04.031

Vallbo, A. B., Olausson, H., Wessberg, J., & Kakuda, N. (1995). Receptive field characteristics of tactile units with myelinated afferents in hairy skin of human subjects. *The Journal of Physiology*, *483*, 783–95. https://doi.org/10.1113/jphysiol.1995.sp020622

Webster, M. (2012). Evolving concepts of sensory adaptation. *F1000 Biology Reports*, *4*(November), 1–7. https://doi.org/10.3410/B4-21

Yau, J. M., Kim, S. S., Thakur, P. H., & Bensmaia, S. J. (2016). Feeling form: the neural basis of haptic shape perception. *Journal of Neurophysiology*, *115*(2), 631–642. https://doi.org/10.1152/jn.00598.2015

Zimmerman, A., Bai, L., & Ginty, D. D. (2014). The gentle touch receptors of mammalian skin. *Science (New York, N.Y.)*, *346*(6212), 950–4. https://doi.org/10.1126/science.1254229

# CHAPTER 2

# ADAPTATION

## 2.1 Preface

The perceptual effects of sensory adaptation are well documented in vision and audition, but have been much less studied in touch. In this chapter, we investigated the effects of adaptation on tactile spatial perception. With psychophysical testing involving two-interval forced-choice (2IFC) tasks in human participants, we measured tactile sensitivity and the perceived distance between point-stimuli on the forearm skin with and without vibratory adaptation.

We found that adaptation significantly reduced tactile sensitivity and induced a repulsion illusion in tactile spatial perception that expands the perceived distance between points on the skin. This study is one of the first to provide evidence for adaptation-induced spatial repulsion illusions in touch. The results are consistent with adaptation-induced repulsion illusions reported in vision and audition, and may point to common processing features and computational principles across the sensory modalities.

frontiers in Human Neuroscience

ORIGINAL RESEARCH
published: 28 June 2017
doi: 10.3389/fnhum.2017.00331

# An Adaptation-Induced Repulsion Illusion in Tactile Spatial Perception

*Lux Li[1], Arielle Chan[1], Shah M. Iqbal[1] and Daniel Goldreich[1,2]**

[1]*Department of Psychology, Neuroscience and Behaviour, McMaster University, Hamilton, ON, Canada,* [2]*McMaster Integrative Neuroscience Discovery and Study, McMaster University, Hamilton, ON, Canada*

Following focal sensory adaptation, the perceived separation between visual stimuli that straddle the adapted region is often exaggerated. For instance, in the tilt aftereffect illusion, adaptation to tilted lines causes subsequently viewed lines with nearby orientations to be perceptually repelled from the adapted orientation. Repulsion illusions in the nonvisual senses have been less studied. Here, we investigated whether adaptation induces a repulsion illusion in tactile spatial perception. In a two-interval forced-choice task, participants compared the perceived separation between two point-stimuli applied on the forearms successively. Separation distance was constant on one arm (the reference) and varied on the other arm (the comparison). In Experiment 1, we took three consecutive baseline measurements, verifying that in the absence of manipulation, participants' distance perception was unbiased across arms and stable across experimental blocks. In Experiment 2, we vibrated a region of skin on the reference arm, verifying that this focally reduced tactile sensitivity, as indicated by elevated monofilament detection thresholds. In Experiment 3, we applied vibration between the two reference points in our distance perception protocol and discovered that this caused an illusory increase in the separation between the points. We conclude that focal adaptation induces a repulsion aftereffect illusion in tactile spatial perception. The illusion provides clues as to how the tactile system represents spatial information. The analogous repulsion aftereffects caused by adaptation in different stimulus domains and sensory systems may point to fundamentally similar strategies for dynamic sensory coding.

**Keywords: somatosensory, psychophysics, sensory adaptation, perceptual inference, tactile illusion, two-point perception, human, aftereffect**

OPEN ACCESS

***Edited by:***
*Christoph Braun, University of Tübingen, Germany*

***Reviewed by:***
*Alessandro Farne, Institut National de la Santé et de la Recherche Médicale (INSERM), France*
*Matthew R. Longo, Birkbeck University of London, United Kingdom*

***Correspondence:***
*Daniel Goldreich*
*goldrd@mcmaster.ca*

***Received:*** *09 February 2017*
***Accepted:*** *08 June 2017*
***Published:*** *28 June 2017*

***Citation:***
*Li L, Chan A, Iqbal SM and Goldreich D (2017) An Adaptation-Induced Repulsion Illusion in Tactile Spatial Perception. Front. Hum. Neurosci. 11:331. doi: 10.3389/fnhum.2017.00331*

## INTRODUCTION

Prolonged exposure to stimulation causes a reduction in neuronal firing rate. For reasons that have yet to be elucidated, this phenomenon, adaptation, is ubiquitous in neural sensory systems (Wark et al., 2007; Sato and Aihara, 2011). Adaptation may have several beneficial consequences: it may support perceptual constancy, increase the salience of novel stimuli, improve discrimination and improve coding efficiency (for review see Webster, 2012).

A seemingly non-beneficial consequence of focal adaptation is that it produces illusions. For instance, following focal adaptation, the perceived separation between stimuli that straddle the adapted region is often exaggerated. A well-known example of this is the visual tilt after effect

illusion: adaptation to tilted lines causes subsequently viewed lines with nearby orientations to appear tilted away, i.e., repelled, from the adapted orientation (Gibson and Radner, 1937; Magnussen and Johnsen, 1986; Dragoi et al., 2000, 2001; He and MacLeod, 2001).

In vision, adaptation-induced repulsion illusions have been reported to affect perception of a wide variety of stimulus features, including luminance, contrast, spatial frequency, temporal frequency, color, contour, shape, size, orientation, motion direction, contingent visual properties (e.g., color and orientation, as in the McCollough effect) and high-level features such as the gender, ethnicity and emotion of faces (for reviews, see Clifford et al., 2007; Kohn, 2007; Webster, 2012). Adaptation-induced repulsive aftereffects have also been reported in auditory perception and audio-visual perception, including aftereffects in sound localization (Thurlow and Jack, 1973; Kashino and Nishida, 1998; Carlile et al., 2001), duration (Walker et al., 1981; Heron et al., 2012), loudness (Kitagawa and Ichihara, 2002), and high-level auditory perception such as action sounds (Barraclough et al., 2017).

The present study concerns a particular type of adaptation-induced repulsion illusion, *spatial* repulsion, in which the positions of stimuli are perceptually repelled away from an adapted area. Spatial repulsion illusions have been well documented in vision (Clifford et al., 2007; Kohn, 2007; Schwartz et al., 2007) and to a lesser extent in audition (Kashino and Nishida, 1998; Carlile et al., 2001) but have rarely been reported in touch. An early tactile study reported that prolonged static pressure on the forearm altered the perceived separation between parallel bars placed on adjacent skin areas in a direction consistent with perceptual repulsion (Day and Singer, 1964). A follow-up study suggested, however, that the observed effects may not have been aftereffects but rather perceptual recalibrations induced by the particular sets of comparison stimuli to which the participants were exposed (Gilbert, 1967). Here, we revisited the question of whether adaptation-induced spatial repulsion occurs in touch. Specifically, we investigated whether focal vibratory adaptation on the forearm induces a spatial repulsion illusion affecting the perceived distance between two points of contact straddling the adapted region. We hypothesized that adaptation of the mechanoreceptors in the intervening skin would decrease the overlap between the neuronal population responses elicited by the two points. Consequently, the brain would infer a greater distance between the points: a repulsion illusion.

# MATERIALS AND METHODS

## Participants

Sixty-nine participants were recruited from the McMaster University community. By self-report, all participants were free of conditions that are known to impair tactile sensitivity (e.g., calluses, scars, or injuries on tested skin areas, carpel tunnel syndrome, diabetes) or perceptual processing (e.g., neurological disorders, attention deficit disorders, dyslexia). All participants had normal or corrected-to-normal vision. Of the 69 recruits, 60 passed the perceptual qualification criteria (see below). Of the 60 qualified participants, 20 took part in Experiment 1 (13 women, 7 men; 17 right-handed, 2 left-handed, 1 ambidextrous; aged 18.7–30.5 years, median age 20.7 years), 20 in Experiment 2A (13 women, 7 men; 19 right-handed, 1 left-handed; aged 18.5–22.6 years, median age 19.9 years), and 20 in Experiments 2B and 3 (12 women, 8 men; all right-handed; aged 19.1–28.8 years, median age 20.8 years). Handedness was assessed by a modified Edinburgh Handedness Inventory (Oldfield, 1971). Participants provided signed informed consent and received monetary compensation and/or course credits for their participation. This study was carried out in accordance with the recommendations of the McMaster Research Ethics Board. All subjects gave written informed consent in accordance with the Declaration of Helsinki. The protocol was approved by the McMaster Research Ethics Board.

# EXPERIMENT 1

Experiment 1 assessed whether the baseline perception of two-point distance was stable across experimental blocks and unbiased across arms. We tested participants on a two-interval forced-choice (2IFC) two-point distance comparison task to measure their baseline two-point distance perception.

## Preparation and Skin Sites Tested

The participant sat in front of a table with the experimental apparatus concealed by an opaque black curtain. The participant's forearms, inserted under the curtain, rested comfortably on a padded surface, with the wrists (palm side up) resting stably on concave foam supports. To assist the experimenters in positioning the stimuli, the participant's forearms were demarcated with a fine-tipped pen. A pair of small dots 30 mm apart was drawn on each volar forearm to guide the application of the two-point test stimuli. On each arm, the dots were symmetrical about the midpoint between the wrist and the elbow, aligned with the proximal-distal axis of the forearm, and slightly laterally offset from midline (**Figure 1A**, left). The slightly lateral-to-midline skin surface was parallel to the ground when participants rested their forearms in a supine position as they naturally tended to rotate the forearms slightly inward when relaxed; the choice of this skin surface thereby facilitated the application of the test stimuli perpendicularly to participants' forearms.

## Psychophysical Procedure

A two-point stimulus was applied onto the participant's volar forearm with the two points simultaneously indenting the skin. Approximately 1 s later, another two-point stimulus was applied to the other volar forearm. The participant compared the distance between the first pair of points with the distance between the second pair of points, and reported which distance felt greater (**Figure 1A**). The participants verbalized their answers by saying "first" or "second", and the experimenter recorded the answers into a computer by pressing one of two response keys. The two-point distance was fixed at 30 mm on the right forearm (the reference) and variable

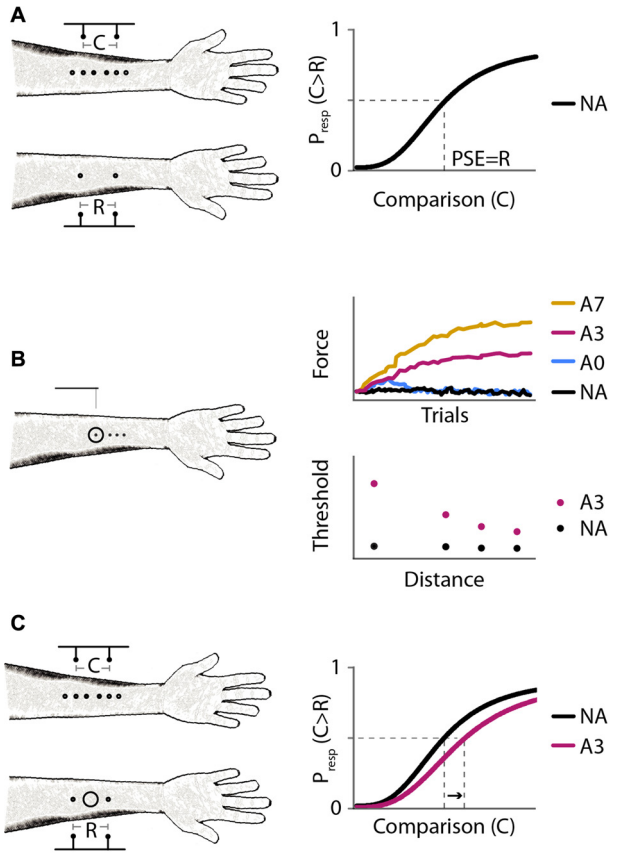


**FIGURE 1 |** Experimental protocols and expected results. **(A)** Experiment 1: baseline distance comparison. Left: participants compared the perceived distance between two-point stimuli applied on the forearms successively. On the right arm, the points were separated by a fixed reference distance (*R* = 30 mm); on the left arm, the points were separated by a variable comparison distance (*C* = 6, 12, 18, 24, 30, 36, 42, 48, or 54 mm). Right: expected psychometric function. Horizontal axis: comparison distance, C. Vertical axis: proportion of trials in which the participant responds that C is greater than R, $P_{resp}(C > R)$. The point of subjective equality (PSE; vertical dashed line) is the value of C for which $P_{resp}(C > R) = 0.5$ (horizontal dashed line); the expected PSE is equal to R. **(B)** Experiment 2: effect of adaptation on tactile sensitivity. Left: participants reported in which of two intervals they felt a monofilament stimulus on the right forearm. Circle: site of vibratory stimulus. Experiment 2A measured reduction in tactile sensitivity at the center of the vibration site under different adaptation protocols. Experiment 2B measured reduction in tactile sensitivity as a function of distance from the center of vibration. Right: expected results from Experiments 2A (top) and 2B (bottom). Monofilaments applied in a 2-down 1-up staircase procedure. Black, no adaptation (NA); blue, 40 s adaptation with no top-ups (A0); magenta, 40 s adaptation with 3 s top-ups (A3); yellow, 40 s adaptation with 7 s top-ups (A7). **(C)** Experiment 3: distance comparison, as in Experiment 1, but with and without adaptation. Left: circle: skin site that received vibratory adaptation. Right: expected psychometric functions. Horizontal and vertical axes as in **(A)**. Black, NA; magenta, 40 s adaptation with 3 s top-ups (A3). A rightward shift upon adaptation (arrow) indicates increased perceived distance between points straddling the adapted skin site.

from 6 mm to 54 mm in increments of 6 mm on the left forearm (the comparison; nine comparison distances in total). The application order of the reference and comparison points was counter balanced across participants: half of the participants received the reference points first and comparison second in all trials, and the other half of the participants received the comparison points first and reference second in all trials.

Each participant completed a practice block followed by three identical testing blocks. The practice block consisted of 16 trials with auditory feedback to indicate whether the response was correct (two trials were presented for each of the eight comparison distances not equal to the reference distance of 30 mm). Each testing block consisted of 90 trials without feedback, 10 trials at each of the nine comparison distances, randomly sampled without replacement. A custom computer program (LabVIEW 2011 for Macintosh, National Instruments) instructed the experimenter as to which comparison distance to apply. The participant took a 5 min break after the practice and a 20 min break between testing blocks. During each testing block, the participant took a 1-min break upon completing each quarter of the 90 trials (i.e., after completing trials 22, 45, 67).

## Force-Controlled Two-Point Stimuli

A custom-made lever system (**Figure 2**) was used to apply two-point stimuli in alignment with the proximal-distal axis of the forearm, and with force control. Each two-point applicator was made of two plastic pins attached to one face of the shaft of a wood pencil of hexagonal cross-section. The uniform size and weight of the pencils facilitated force control of the test stimuli, and the hexagonal cross-section helped align the two pins. The heights by which the pins protruded from the pencils were carefully adjusted such that they were equal for a given two-point applicator and across all applicators. The stimulus surfaces were spherical pinheads of diameter 1.5 mm. Separation distances between the centers of the pinheads were 6, 12, 18, 24, 30, 36, 42, 48 and 54 mm.

The lever system consisted of two acetal plastic arms attached via a metal rod that passed through a ball bearing. The metal rod rotated with little friction, allowing the arms to swivel smoothly. A magnet was attached to the end of each arm, and two magnets were attached to each applicator. The applicator could be easily attached to and removed from the swivel arms via the magnets, which allowed the experimenter to quickly change the applicator from trial to trial. To apply a test stimulus, the experimenter first attached the applicator to the swivel arms. Supporting the swivel arms with both hands from below, the experimenter gently lowered the swivel arms such that the two pinheads contacted the forearm simultaneously and perpendicular to the skin surface. The pinheads contacted the skin with a total force determined by the combined weight of the swivel arms, which measured 80–82 g when the pinheads were applied with this method to a scale. The pinheads were in contact with the skin for ∼0.5 s before the experimenter raised the swivel arms to end the stimulus.

Two identical lever apparatuses were used to apply the test stimuli, one for each forearm. Two experimenters were needed to conduct the experiment, each operating one lever apparatus. The order of the forearms receiving the test stimuli in each trial (either reference first or comparison first) was consistent for a given participant but counterbalanced across

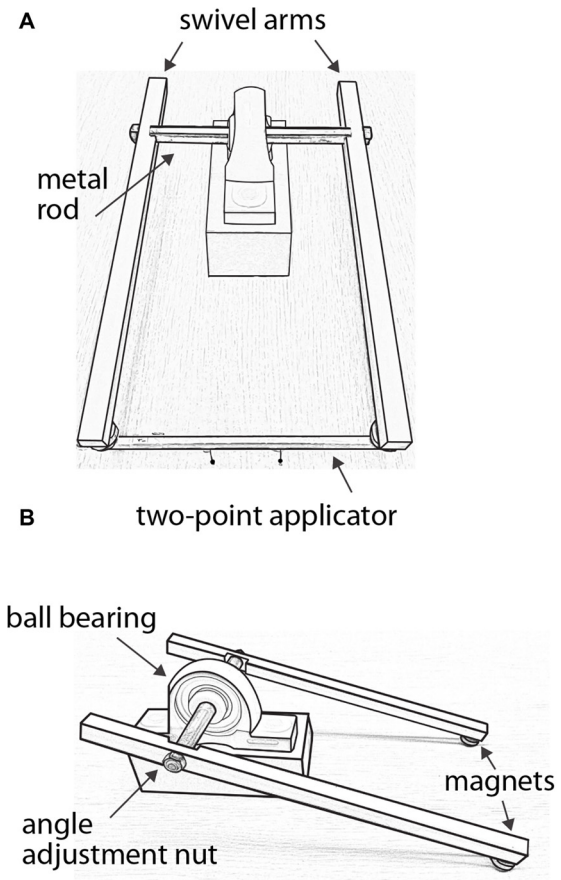


**FIGURE 2 |** Force-controlled two-point stimulus apparatus. **(A)** Front view with a two-point applicator attached to magnets at the ends of the swivel arms. In this illustration, the applicator's pinheads are separated by 42 mm. **(B)** Side view without applicator, illustrating the angle adjustment nut on one of the swivel arms.

participants. Regardless of the order, in each trial, the stimuli were applied to the forearms sequentially. As one experimenter completed the first stimulus and raised the swivel arms away from the skin, the second experimenter initiated the stimulus to the other forearm. The inter-stimulus interval was ∼1 s. The two experimenters were trained to keep the application pace consistent between stimuli and across trials.

The precise angles of the swivel arms were individually adjustable in order to match the slight change in thickness (and therefore height above the table) of the forearm along the proximal-distal axis. The experimenters adjusted the angles of the two swivel arms within each apparatus in order to ensure that the two pinheads contacted the skin simultaneously and with equal force, as reported by the participant.

## Qualification Criteria

To ensure that participants' baseline two-point distance perception was sufficiently accurate to perform the two-point distance comparison task, we compared participants' baseline performance in the first testing block to two qualification criteria: the proportion of "comparison is longer" responses at the longest comparison distance (54 mm) should be $\geq$0.7, and at the shortest comparison distance (6 mm) should be $\leq$0.3. If a participant failed to meet either criterion, then we considered their baseline performance as unreliable. In this case, the participant did not proceed with the experiment, and their data were excluded from analysis.

## Psychometric Function Parameterization and Estimation of Point of Subjective Equality (PSE)

For each of the three testing blocks for each participant, we fit to the data a sigmoidal cumulative normal function, which describes the proportion of trials at which the comparison distance, $x$, was reported as being longer than the reference distance:

$$\Psi(x) = \frac{\delta}{2} + (1-\delta)\left[\gamma + (1-\gamma)\frac{1}{\sigma\sqrt{2\pi}}\int_{-\infty}^{x} e^{-(t-\mu)^2/2\sigma^2}\,dt\right]$$

This function has four free parameters: the mean ($\mu$) and standard deviation ($\sigma$) of the cumulative normal curve, a lapse rate ($\delta$), and a y-intercept ($\gamma$). We allowed $\gamma$ to take on non-zero values, because the psychometric function for many participants did not fall completely to zero at the left tail. Using Bayesian parameter estimation, beginning with uniform prior probabilities over the four parameters, we calculated the joint ($\mu$, $\sigma$, $\gamma$, and $\delta$) posterior density. We marginalized this over $\delta$ and read out the mode of the ($\mu$, $\sigma$, $\gamma$) posterior as the best-estimate of the participant's psychometric function. We then extracted the comparison distance at which the psychometric function crossed 50% as the perceptual equivalent of the reference distance, i.e., the point of subjective equality (PSE).

# EXPERIMENT 2

In Experiment 2, we assessed the extent to which vibratory adaptation changed tactile sensitivity, by measuring participants' 2IFC detection of force-calibrated Semmes-Weinstein monofilaments (a.k.a von Frey hairs; Timely Neuropathy Testing, LLC and Texas Medical Design, Inc., Dallas, TX, USA). We individually measured the application force produced by each filament with an analytical balance (model AB54-S/FACT, Mettler Toledo).

## Vibrotactile Adaptation Procedure

The participant was seated in front of a table with the experimental apparatus concealed by an opaque black curtain. The participant's right forearm rested comfortably in a supine position on a padded surface; the wrist was secured to a concave foam support. To mark the skin site for receiving vibratory adaptation, a circle of 19 mm diameter (the size of the adapting probe surface) was drawn with a fine-tipped pen on the volar forearm midway between the wrist and the elbow, and slightly

lateral to the proximal-distal midline; the center of the circle was at approximately the midpoint between the two reference points in Experiment 1.

The adapting vibration was delivered via the plastic hemispherical surface of a JVP dome (Stoelting Co., Wood Dale, IL, USA; 19 mm diameter, 0.35 mm groove width). A mechanical arm holding the JVP dome was vibrated via the rotation of an attached eccentric motor (a NexxTech 1.98A DC motor whose axle we asymmetrically weighted, powered at 7.5V by DC power supply 1621A, BK Precision). A force sensor (Honeywell FSG15N1A) in contact with the end of the JVP dome shaft passed a voltage signal proportional to the contact force to an iMac computer via a USB board (NI USB-6210, 16-bit, National Instruments). A custom LabVIEW program monitored the force trace at 5000 samples/s. The program displayed the baseline indentation force and recorded the force waveform during vibration.

To apply the adapting stimulus, the experimenter lowered the mechanical arm and pressed the JVP dome against the participant's volar forearm at a perpendicular angle. Prior to and during the vibration, the experimenter adjusted the baseline indentation force to approximately 250 g. Post-experiment analysis on the force sensor data showed that the probe vibrated at 122 $\pm$ 5 Hz with a peak-to-peak force fluctuation of 125 $\pm$ 34 g (mean $\pm$ 1 SD; baseline force 245 $\pm$ 14 g). As soon as the adapting vibration ceased, the experimenter retracted the mechanical arm to remove the probe from the forearm. The experimenter then applied the monofilament test stimuli. The time between the offset of the adapting vibration and the application of the test stimuli was $\sim$3 s.

## Experiment 2A

To assess the strength of adaptation as a function of vibration duration, we measured participants' ability to detect Semmes-Weinstein monofilament stimuli applied at the center of the adapted skin site in different adaptation conditions: (a) no-adaptation (NA); (b) 40 s initial adaptation without top-ups (A0); (c) 40 s initial adaptation plus a 3 s top-up vibration prior to each subsequent trial (A3); and (d) 40 s initial adaptation plus a 7 s top-up vibration prior to each subsequent trial (A7). The purpose of the top-ups was to prevent the adaptation effect from waning.

After 20 practice trials with auditory feedback, participants completed the four testing blocks without feedback. Half of the participants completed the four blocks in the order NA-A0-A3-A7, and the other half in the order NA-A7-A3-A0. In the NA-A0-A3-A7 situation, participants took a 10 min break after completing NA, a 10 min break after completing A0, and a 15–20 min break after completing A3. In the NA-A7-A3-A0 situation, participants took a 10 min break after completing NA, a 15–20 min break after completing A7, and a 15–20 min break after completing A3. The breaks after A3 and A7 were longer than after NA or A0, because the A3 and A7 blocks lasted much longer due to the top-ups. The longer breaks were designed to allow participants to recuperate and their nervous systems to recover from possible long-lasting effects of adaptation.

Each testing block had 100 2IFC trials. Each trial consisted of two intervals, separated by $\sim$1.25 s and demarcated by beeps. Simultaneously with one of the beeps, the skin was stimulated with a monofilament for $\sim$0.5 s. By pressing one of two response keys with the left hand, the participant reported whether the stimulus occurred with the first or second beep. Monofilament force began at 0.07 g and was adaptively adjusted via a 2-down 1-up staircase procedure: If the participant answered correctly for two consecutive trials, the monofilament with the next-lower force was applied; if the participant answered incorrectly on any trial, the monofilament with the next-higher force was applied. This procedure converges towards the participant's 71% correct detection threshold (Levitt, 1971).

At the beginning of each adaptation block (A0, A3 and A7), the circled skin site received a 40 s vibration. Additionally, in the adaptation blocks with top-ups (A3 and A7), the circled site received a 40 s vibration when the participant returned from a break. Within each block, participants took a break after trials 33 and 66. For blocks NA and A0, which occurred relatively quickly, the break duration was 10 s. For blocks A3 and A7, which took much longer because of the top-ups, the break duration was 5 min to allow participants to recuperate.

For each testing block, the participant's 71% threshold was estimated by averaging the staircase reversal points in the last 50 of the 100 trials. In the rare circumstances in which the last 50 trials contained no reversal points and the participant consistently gave correct responses, so the staircase dropped to and continued at the lowest filament force, we used that force (0.008 g) as the estimated threshold.

## Experiment 2B

To assess the spatial spread of vibrotactile adaptation, we used 40 s adaptation plus 3 s top-ups (protocol A3) and measured 2IFC monofilament detection at four distances from the center of adaptation. In addition to the circle drawn on the participant's right volar forearm to indicate the site for vibrotactile adaptation, four dots were drawn at 0, 10, 15 and 20 mm from the center of the circle to mark the monofilament test sites. The dots were aligned along the proximal-distal axis of the forearm (**Figure 1B**). For half of the participants, the dots extended proximally, from the center of the circle towards the elbow; for the other half of the participants, the dots extended distally, from the center of the circle towards the wrist.

Using interleaved 2-down 1-up staircases, we tested the four sites in consecutive trials in the order 0, 10, 15 and 20 mm from the center of the circle. For example, the 0 mm site was tested on trial 1, the 10 mm site on trial 2, the 15 mm site on trial 3, the 20 mm site on trial 4, and the 0 mm site again on trial 5. For all sites, the first trial used the 0.07 g monofilament. The force of the monofilament applied at each test site on subsequent trials followed the staircase procedure based on the participant's responses at that site. For example, if the participant responded correctly on trials 1 and 5 on which the 0 mm site was tested, then the monofilament applied on

the next trial at that site (trial 9) went down to the next-lower force.

After 20 practice trials with auditory feedback, each participant completed two testing blocks without feedback: a NA block and an adaptation (A3) block. Half of the participants completed the NA block first; the other half completed the A3 block first. Each block consisted of 200 trials (i.e., 50 trials at each of the four test sites). In the A3 block, prior to the first trial and every time the participant returned from a break, the circled skin site received a 40 s vibration. To prevent the adaptation effect from waning, the circled skin site received a 3 s top-up vibration prior to each of the subsequent trials. Participants took a 20 min break between testing blocks; within each block, they took a break after completing trials 33, 66, 100, 133 and 166 (break durations: NA block, 10 s after trials 33, 66, 133, 166, 5 min after trial 100; A3 block, 5 min after trials 33, 66, 133, 166, 10 min after trial 100).

For each testing block, the participant's 71% threshold at each test site was estimated by averaging the staircase reversal points in the last 25 of 50 trials at that site. In the rare circumstances in which the last 25 trials contained no reversal points and the participant consistently gave correct responses, so the staircase dropped to and continued at the lowest filament force, we used that force (0.008 g) as the estimated threshold.

## EXPERIMENT 3

In Experiment 3, we investigated the effects of vibratory adaptation on two-point distance perception. We applied the A3 vibrotactile adaptation protocol to the same 20 participants tested in Experiment 2B but on a different day. The participants compared two-point distances on the two forearms, as in Experiment 1, but with or without vibratory adaptation to the intervening skin between the reference points (**Figure 1C**).

The test skin sites, exclusion criteria, and PSE estimation procedure were as described in Experiment 1. After practice, participants completed three testing blocks, a pre-adaptation (Pre) block without adapting vibration, an adaptation (A3) block, and a post-adaptation (Post) block without adapting vibration. The Pre and Post blocks were identical to the baseline testing blocks in Experiment 1. Participants took a 5 min break after the practice block and a 20 min break between testing blocks. During the Pre and Post blocks, participants took a 1-min break—and during the A3 block, a 5-min break—upon completing each quarter of the 90 trials (i.e., after completing trials 22, 45, 67).

In the A3 block, prior to the first trial and every time the participant returned from a 5 min break, the skin midway between the two reference points (30 mm apart) on the right forearm received a 40 s adapting vibration. In addition, the same skin site received a 3 s vibration as a top-up adaptation prior to each subsequent trial, to prevent the adaptation effects from waning. The adapting probe was removed immediately from the skin when the adapting vibration ceased, and then the two pairs of test stimuli were applied to the forearms successively. The application order of the reference and comparison points was counterbalanced across participants: half of the participants received the reference points first in every trial, and the other half received the comparison points first in every trial. The time between the offset of the adapting vibration and the application of the reference points was ∼3 s for participants who received the reference points first, and ∼4 s for participants who received the comparison points first.

### Statistical Analyses

We performed ANOVAs with type III sum of squares (and Greenhouse-Geisser correction to the degrees of freedom and the *p*-values in case of violation of sphericity) and two-tailed *t*-tests using SPSS Statistics version 20 (IBM) for Macintosh with an alpha level of 0.05. We performed two-tailed binomial proportion tests in R version 3.0.3. We used R version 3.0.3, companion to applied regression (car) package for *post hoc* one-way repeated-measures ANOVAs. For multiple *post hoc* pairwise comparisons, we used Bonferroni correction and reported *p*-values multiplied by the number of comparisons.

## RESULTS

We undertook a series of three experiments to test for the presence of a tactile adaptation-induced repulsion illusion on the forearm. In a 2IFC task, participants compared the distances of two pairs of point-stimuli (reference vs. comparison) applied on their forearms successively, reporting which distance felt greater. The reference distance was fixed at 30 mm, and the comparison distance varied from 6 mm to 54 mm. The order of the reference and comparison distances was counterbalanced across participants. The PSE (i.e., the comparison distance reported as being greater than the reference distance 50% of the time) was extracted as a measure of participants' perceived distance between the reference points. We measured baseline PSEs (Experiment 1) and PSEs following vibrotactile adaptation (Experiment 3). We used force-calibrated Semmes-Weinstein monofilaments to assess the efficacy of the adaptation protocol in reducing tactile sensitivity (Experiment 2).

### Baseline Distance Perception Was Unbiased and Stable

In Experiment 1, we assessed the accuracy and stability of participants' baseline two-point distance perception. Experiment 1 consisted of three identical testing blocks of the 2IFC distance-comparison test without adaptation.

One participant reported that all comparison distances (6–54 mm) were greater than the reference distance (30 mm) in the third testing block; consequently, we could not reliably measure his psychometric curve or PSE for that block. We therefore excluded his data from all three blocks and analyzed the remaining 19 participants' data. The average psychometric curves and estimated PSEs are shown in **Figure 3** (**Figure 3A**: raw data. **Figure 3B**: psychometric function fits).

The raw psychometric curves for some participants were noisy and crossed the $y = 0.5$ line multiple times, making it difficult

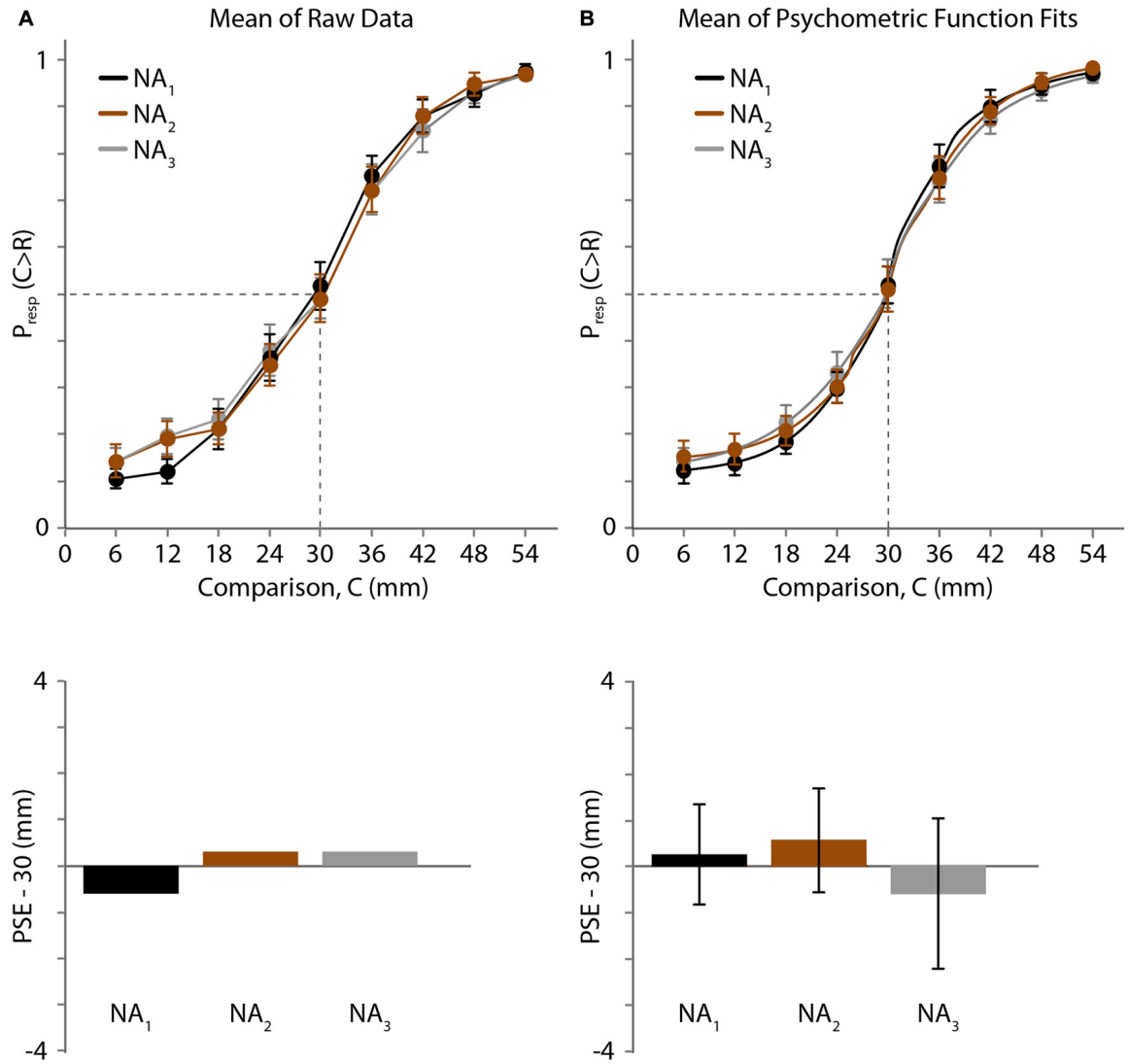


**FIGURE 3 |** Experiment 1 results. **(A)** Top: mean of raw data ($N$ = 19 participants) for three NA blocks. Black, 1st block; brown, 2nd block; gray, 3rd block. Horizontal axis: comparison distance (mm). Vertical axis: proportion of trials in which the comparison distance (C) was perceived as greater than the reference distance ($R$ = 30 mm). Dashed lines: $P_{resp}(C > R) = 0.5$ and C = 30 mm. Error bars: ±1 SE (when error bars are not visible, it is because they are smaller than the data point circles). Bottom: for each testing block, the difference between 30 mm and the mean PSE, estimated by linear interpolation of the mean data (top). **(B)** Top: mean of the participants' individual best-fitting psychometric functions. Error bars: ±1 SE. Bottom: difference between 30 mm and the mean of the PSEs extracted from the participants' individual best-fitting psychometric functions. Error bars: ±1 SE.

to extract individual PSEs directly from the raw data. Therefore, using the raw data we estimated only the across-participant mean PSE by linearly interpolating the mean response proportions (**Figure 3A**, top). The mean PSEs obtained in this fashion for the three baseline NA blocks were 29.38, 30.27 and 30.27 mm (**Figure 3A**, bottom). Binomial tests revealed that the proportion of trials in which participants judged the 30 mm comparison distance as longer than the 30 mm reference distance did not differ significantly from 0.5 for any block ($p$ = 0.717, 0.828 and 0.828, for blocks 1, 2 and 3, respectively).

Next, we used Bayesian curve fitting to estimate the psychometric functions and extract the PSEs of the individual participants. Each of the curves shown in **Figure 3B** (top) is an average of 19 individual best-fitting psychometric curves; the similarity of these three curves to those shown in **Figure 3A** (top) suggests that our curve fitting procedure provided a valid estimate of participant performance. The means (±1 SE) of the PSEs extracted from the participants' individual best-fitting psychometric functions for the three blocks were 30.25 ± 1.08, 30.56 ± 1.13 and 29.39 ± 1.62 mm (**Figure 3B**, bottom). One-sample $t$-tests indicated that none of the PSEs differed significantly from the reference distance of 30 mm (block 1: $t_{(18)} = 0.227$, $p = 0.823$; block 2: $t_{(18)} = 0.493$, $p = 0.628$; block 3: $t_{(18)} = -0.373$, $p = 0.713$), and a one-way repeated-measures

ANOVA indicated that the PSEs did not differ across blocks ($F_{(1.485,26.727)}$ = 0.458, $p$ = 0.580). These results indicate that baseline two-point distance perception was unbiased and stable across testing blocks.

## Focal Vibration Caused a Reduction in Tactile Sensitivity

Having found that participants' baseline two-point distance comparison judgments were reliable, we next asked whether we could induce focal adaptation between the two reference points. In Experiment 2, we applied prolonged vibration locally to the skin on the reference arm, and we measured 2IFC monofilament detection thresholds as a function of vibration duration and distance from vibration center.

In Experiment 2A, we found that vibration caused an elevation of monofilament detection thresholds (i.e., a reduction in tactile sensitivity) that increased with the duration of vibration. 71% correct detection thresholds (mean ± 1 SE) at the center of the vibration site were 0.16 ± 0.05 g, 0.20 ± 0.07 g, 0.52 ± 0.12 g and 0.80 ± 0.17 g for the NA, 40 s adaptation, 40 s adaptation with 3 s top-ups, and 40 s adaptation with 7 s top-ups conditions (**Figure 4A**). A one-way repeated-measures ANOVA indicated a highly significant effect of adaptation duration ($F_{(1.860,35.345)}$ = 9.894, $p$ < 0.001, partial $\eta^2$ = 0.342). *Post hoc* paired-sample $t$-tests comparing each condition to the others revealed that 40 s adaptation alone did not cause significantly different thresholds from the NA baseline condition ($p$ = 1.000); however, the addition of a top-up vibration prior to each trial significantly increased detection thresholds. Detection thresholds in the adaptation conditions with 3 s and 7 s top-ups both differed significantly from the NA baseline threshold (3 s top-ups, $p$ = 0.015, Cohen's $d$ = 0.676; 7 s top-ups, $p$ = 0.006, Cohen's $d$ = 1.182) but did not differ significantly from each other ($p$ = 0.608). Thus, 40 s adaptation with 3 s top-ups was sufficient to reduce tactile sensitivity considerably, and the efficacy of this adaptation protocol was comparable to that of a protocol with much longer top-up duration. We therefore chose 40 s adaptation with 3 s top-ups as the protocol to employ in Experiments 2B and 3.

In Experiment 2B, using 40 s adaptation with 3 s top-ups, we found that the threshold elevation was greatest under the adapting probe and diminished as a function of distance (**Figure 4B**). Seventy-one percent correct detection thresholds (mean ± 1 SE) at the test sites 0, 10, 15 and 20 mm from the center of adaptation were 0.07 ± 0.01 g, 0.08 ± 0.02 g, 0.06 ± 0.01 g and 0.06 ± 0.01 g for the baseline condition, and 0.47 ± 0.11 g, 0.38 ± 0.10 g, 0.15 ± 0.02 g and 0.26 ± 0.07 g for the adaptation condition. A 2 × 4 repeated-measures ANOVA with condition (baseline, adaptation) and distance (0, 10, 15, 20 mm from center of adaptation) as factors indicated a highly significant effect of condition ($F_{(1,19)}$ = 24.552, $p$ < 0.001, partial $\eta^2$ = 0.564), a significant effect of distance ($F_{(3,57)}$ = 3.316, $p$ = 0.026, partial $\eta^2$ = 0.149), and a significant condition × distance interaction ($F_{(2.186,41.542)}$ = 3.341, $p$ = 0.041, partial $\eta^2$ = 0.150). *Post hoc* one-way repeated-measures ANOVAs indicated that the baseline (NA) detection thresholds did not differ across the four distances ($F_{(3,57)}$ = 0.854, $p$ = 0.470), whereas the detection thresholds in the adaptation condition differed significantly at different distances ($F_{(3,57)}$ = 3.381, $p$ = 0.024, partial $\eta^2$ = 0.151). These results indicate that baseline tactile sensitivity was stable across the forearm test area and that vibratory adaptation effectively reduced tactile sensitivity in a manner that diminished with distance from the center of vibration.

## Focal Adaptation Caused an Illusory Increase in Two-Point Distance

Having established that the adaptation protocol significantly reduced focal tactile sensitivity, we next investigated the effect of focal adaptation on two-point distance perception. In Experiment 3, we measured perceived distance with or without vibrotactile adaptation of the intervening skin between the two reference points.

The average psychometric curves and estimated PSEs are shown in **Figure 5** (**Figure 5A**: raw data. **Figure 5B**: psychometric function fits). As in Experiment 1, we first linearly interpolated the across-participant average of the raw psychometric curves. The mean PSEs obtained in this fashion for the pre-adaptation (Pre), adaptation (A3), and post-adaptation (Post) blocks were 28.59, 31.88 and 30.86 mm, respectively (**Figure 5A**, bottom). Binomial tests revealed that the proportion of trials in which participants judged the 30 mm comparison distance as longer than the 30 mm reference distance did not differ significantly from 0.5 for the Pre ($p$ = 0.104) and Post blocks ($p$ = 0.229). In contrast, this proportion did differ from 0.5 for the A3 block (mean proportion, 0.425; $p$ = 0.040). These results are consistent with a rightward shift of the psychometric curve.

Next, we used Bayesian curve fitting to estimate the psychometric functions and extract the PSEs of the individual participants. Each of the curves shown in **Figure 5B** (top) is an average of 20 individual best-fitting psychometric curves; the similarity of these three curves to those shown in **Figure 5A** (top) suggests that our curve fitting procedure provided a valid estimate of participant performance. The means (±1 SE) of the PSEs extracted from the participants' individual best-fitting psychometric functions for the Pre, A3, and Post blocks were 28.98 ± 1.00, 32.85 ± 1.23, and 30.51 ± 1.10 mm (**Figure 5B**, bottom). One-sample $t$-tests indicated that the A3 PSE was significantly greater than the reference distance of 30 mm ($t_{(19)}$ = 2.322, $p$ = 0.031, Cohen's $d$ = 0.519). By contrast, neither the Pre PSE nor the Post PSE differed significantly from 30 mm (Pre PSE: $t_{(19)}$ = −1.024, $p$ = 0.319; Post PSE: $t_{(19)}$ = 0.461, $p$ = 0.650). A one-way repeated-measures ANOVA indicated that the PSEs differed significantly across conditions ($F_{(1.412,26.835)}$ = 5.643, $p$ = 0.016, partial $\eta^2$ = 0.229). *Post hoc* paired-samples $t$-tests indicated that the A PSE differed from the Pre PSE ($p$ = 0.021, Cohen's $d$ = 0.886), whereas the Post PSE did not differ from the Pre PSE ($p$ = 0.129) or from the A PSE ($p$ = 0.319). These results indicate that focal vibrotactile adaptation increased the perceived

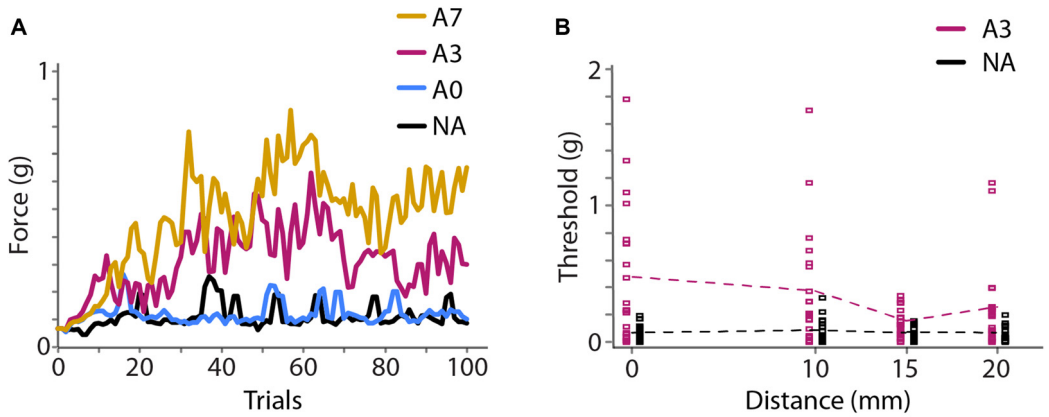


**FIGURE 4 |** Experiment 2 results. **(A)** Experiment 2A. Mean (*N* = 20 participants) monofilament force applied during 100 trials of a 2IFC detection task following a 2-down 1-up staircase procedure that converges to 71% correct detection. Colors represent different adaptation conditions. Black, NA; blue, 40 s adaptation with no top-ups (A0); magenta, 40 s adaptation with 3 s top-ups (A3); yellow, 40 s adaptation with 7 s top-ups (A7). **(B)** Experiment 2B (*N* = 20 participants). Seventy-one percent correct detection thresholds at four distances from the center of adaptation. Black, NA; magenta, 40 s adaptation with 3 s top-ups (A3). Squares show thresholds of individual participants. Data points from the NA and A3 conditions are slightly offset horizontally for clarity. Dashed lines: mean thresholds.

distance between two points straddling the adapted skin area.

## DISCUSSION

We have reported an adaptation-induced tactile spatial repulsion illusion: vibrotactile stimulation focally reduced tactile sensitivity and increased the perceived separation between points straddling the adapted region. Whereas adaptation-induced spatial illusions have been well studied in vision, and to a lesser extent in audition, such illusions have rarely been reported in touch. Our finding suggests that adaptation plays a central role in calibrating spatial perception in multiple sensory modalities.

### Comparison to Previous Tactile Adaptation Studies

Previous studies have characterized the effects of tactile adaptation on amplitude detection threshold, intensity estimation, amplitude and frequency discrimination, and motion direction and speed perception (Hahn, 1966, 1968; Gescheider and Wright, 1968; Berglund and Berglund, 1970; Hollins et al., 1990; Goble and Hollins, 1993, 1994; Tommerdahl et al., 2005; Tannan et al., 2007; McIntyre et al., 2016a,b). By contrast, the effects of adaptation on tactile spatial perception have been rarely studied. In one of the few modern studies in this area, Tannan et al. (2006) tested participants' ability to identify which of two skin locations on the dorsal hand was tapped. Following 5 s of 25 Hz sinusoidal skin displacement to one of the stimulus sites, participants' accuracy improved. Tannan et al. (2006) interpreted their finding to indicate that the adaptation caused an improvement in spatial acuity, perhaps because it resulted in more clearly defined loci of activation in the primary somatosensory cortex (SI). However, a plausible alternative hypothesis is that a test stimulus applied to the adapted site felt weaker than one applied to the non-adapted site, and that this intensity cue caused the increased accuracy on the task. Very recently, Calzolari et al. (2017) reported that adaptation to specific tactile distances can lead to spatial aftereffects. The authors repeatedly applied 2-point stimuli separated by short distances to one hand and 2-point stimuli separated by long distances to the other hand. Exposure to short-distance stimuli caused subsequent stimuli on that hand to appear longer, and exposure to long-distance stimuli caused subsequent stimuli to appear shorter. This interesting perceptual repulsion phenomenon may be of a different nature than the adaptation-induced repulsion that we have observed, as the adapting stimuli in Calzolari et al. (2017) were themselves two-point stimuli, and the authors intentionally varied the stimulus positions on each hand from trial to trial in order to avoid adapting specific skin locations. In contrast, we applied a vibratory stimulus to the intervening skin region between two points precisely in order to adapt that specific area.

In an early study of adaptation-induced tactile repulsion, Silver (1969) reported a tactile equivalent of the visual tilt aftereffect illusion. In the visual tilt aftereffect illusion, prolonged viewing of oriented bars causes subsequently viewed bars of nearby orientation to appear tilted away from the adapting orientation (Gibson and Radner, 1937; Blakemore, 1973). Silver (1969) reported that 1 min of static indentation or active scanning of a tilted bar resulted in an analogous repulsive aftereffect in tactile orientation perception. This study was reported in a doctoral dissertation; unfortunately, to the best of our knowledge, the study did not appear in any later peer-reviewed report.

Two other early studies (Day and Singer, 1964; Gilbert, 1967) had strong similarities to the present study. In both studies, participants compared the perceived distance between two parallel bars pressed transversely against one forearm (the reference arm) with two similar bars pressed against the

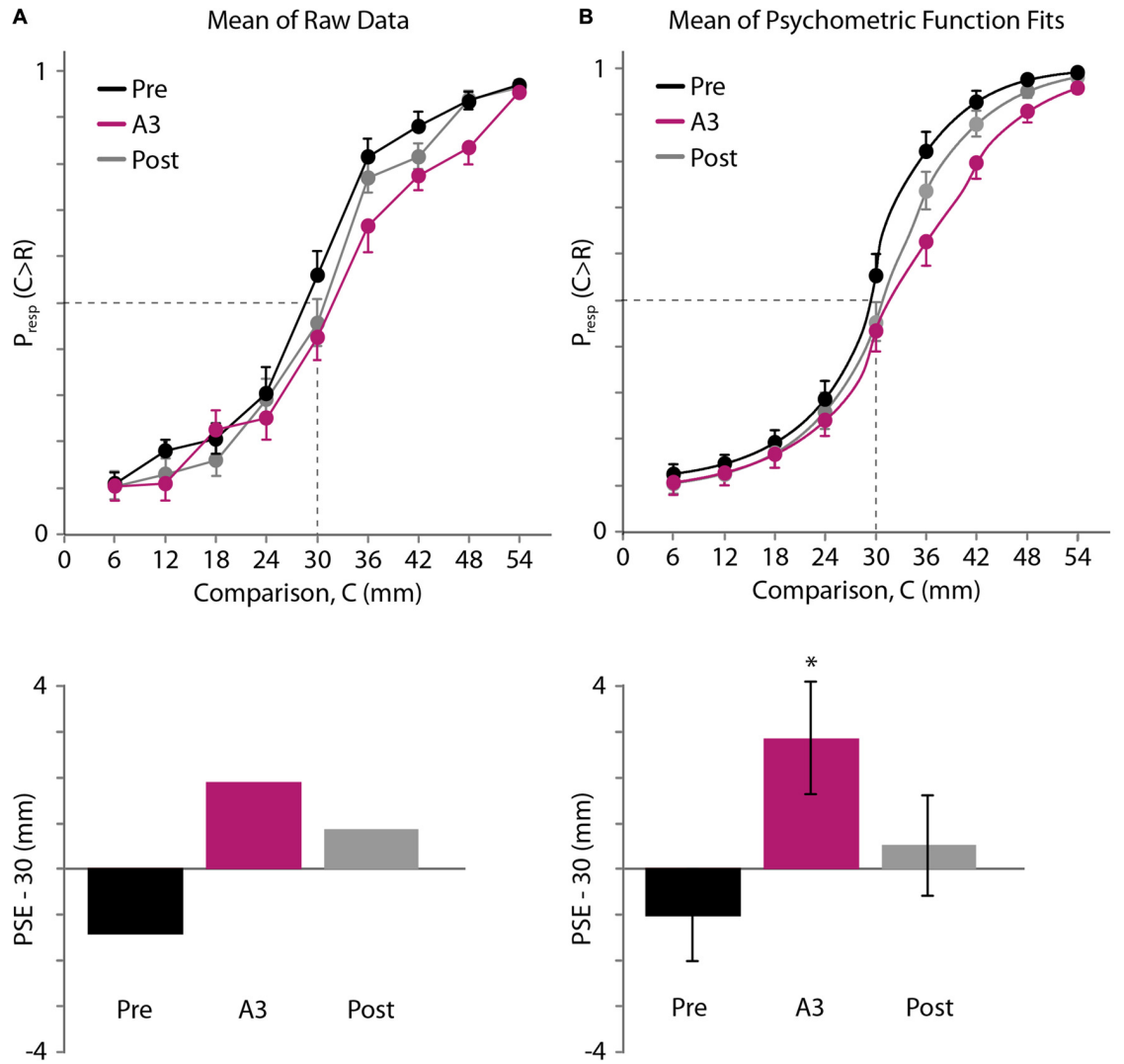


**FIGURE 5 |** Experiment 3 results. **(A)** Top: mean of raw data ($N$ = 20 participants). Black, pre-adaptation (Pre); magenta, adaptation (A3); gray, post-adaptation (Post). Horizontal axis: comparison distance, C. Vertical axis: proportion of trials in which C was perceived to be greater than $R$ = 30 mm. Dashed lines: $P_{resp}(C > R) = 0.5$ and C = 30 mm. For visual clarity, error bars show +1 SE, −1 SE and ±1 SE for the highest, lowest, and middle points at each comparison distance, respectively. Bottom: for each testing block, the difference between 30 mm and the mean PSE, estimated by linear interpolation of the mean data (top). **(B)** Top: mean of the participants' individual best-fitting psychometric functions. Error bars displayed as in **(A)**. Bottom: difference between 30 mm and the mean of the PSEs extracted from the participants' individual best-fitting psychometric functions. Error bars: ±1 SE. *Significant difference ($p < 0.05$) from 0 mm.

other forearm. In the adaptation conditions, static pressure was applied for 90 s before the first trial with a 10 s top-up before each of the subsequent trials. The adapting stimulus was applied either on the intervening skin between the reference bars ("inside adaptation") or on the adjacent skin outside the reference bars ("outside adaptation"). The perceived distance between the reference bars increased following adaptation of the intervening skin (Day and Singer, 1964) and decreased following adaptation of the adjacent outside skin (Day and Singer, 1964; Gilbert, 1967). Both results indicated that the bars were perceptually shifted away from the adapted skin regions, a repulsion illusion consistent with our findings. However, the proper interpretation of these studies' results is somewhat unclear. Gilbert (1967) argued that the apparent repulsion effect reported by Day and Singer (1964) owed primarily to the authors' use of different ranges of comparison distances for the "inside" and "outside" adaptation conditions, ranges that were not symmetrically distributed about the reference separation; the exposure to particular distributions of comparison distances may have resulted in a recalibration of the perception of distance, a sort of statistical adaptation described previously by Helson (1947). Gilbert (1967) suggested that, when this factor was taken into account, little evidence remained for a true repulsion effect in either study.

In light of this controversy, we revisited the question of whether adaptation-induced spatial repulsion occurs on

the forearm. We used comparison separations that were symmetrically distributed around the reference separation and found clear evidence for tactile repulsion similar to the "inside adaptation" repulsion effect reported by Day and Singer (1964). The adapting and test parameters used in our study differed from those used by Day and Singer (1964) and Gilbert (1967). Specifically, in our study, the adapting stimulus was a vibration rather than static pressure; the duration of the adapting stimulus was shorter; our test stimuli were much smaller in size (1.5 mm diameter spherical points instead of 30 × 1.5 mm bars); and our test stimuli were much closer together (30 mm instead of 110 mm). The similar perceptual effects observed in our study and these two early studies suggest that adaptation-induced tactile spatial repulsion is robust to variability in adapting and test parameters.

Additional research is needed to determine the duration of the adaptation-induced repulsion effect. A curious aspect of our Experiment 3 is that the post-adaptation psychometric function appeared not to fully recover to the baseline state. This result was not statistically significant, as the post-adaptation PSE did not differ significantly from 30 mm (**Figures 5A,B**). Nevertheless, the possibility exists that our participants experienced some residual adaptation effect 20 min after the adaptation phase ended. To the best of our knowledge, no psychophysical or neurophysiological studies have reported such a long recovery time following merely tens of seconds of vibrotactile adaptation and seconds of top-ups. For instance, Hahn (1966) reported that, after 25 min of continuous vibrotactile adaptation at 200 μm peak-to-peak amplitude and 60 Hz, recovery largely occurred (as measured by psychophysical threshold or amplitude matching) within the first 1–2 min and fully completed after 8–12 min. A possible explanation for the discrepancy is that we used an intense adapting stimulus (125 g peak-to-peak force) that likely adapted multiple types of tactile channels (Bensmaia et al., 2005; Leung et al., 2005). Future studies are needed to characterize the time course of the adaptation-induced spatial repulsion effect and how it is affected by characteristics of the adapting stimulus.

## At What Level(s) of the Somatosensory System does Focal Adaptation Act to Cause the Repulsion Illusion?

Where in the somatosensory processing pathway does the adaptation take place that leads to the perceptual repulsion observed in the present study? A difficulty in discerning the relevant neural locus of adaptation is that neuronal responses will reflect changes in the driving input from earlier processing levels. Indeed, a general conclusion from the visual literature is that adaptation can exert effects—either direct or indirect—at multiple processing stages (Kohn and Movshon, 2003, 2004; Kohn, 2007; Dhruv and Carandini, 2014). For instance, under a variety of stimulus scenarios, adaptation results in changes in both subcortical and cortical neural responses. Similarly, in the tactile system, exposure to sustained vibration leads to lasting reduction in neural responsivity in the PNS (Bensmaia et al., 2005; Leung et al., 2005) and CNS (Bystrzycka et al., 1977; O'Mara et al., 1988; Whitsel et al., 2001).

A few somatosensory studies have provided convincing evidence for a strong central contribution to adaptation by comparing the degree of adaptation that occurs at multiple levels of the processing hierarchy. O'Mara et al. (1988) recorded extracellular responses of PC afferents and cuneate neurons to 300 Hz sustained vibration in decerebrated or anesthetized cats. It was found that: (1) afferent-induced inhibition was too brief to account for the long-lasting response depression in cuneate neurons; and (2) for cuneate neurons that received excitatory input from multiple skin sites, following 300 Hz adapting vibration on one site, the neurons displayed lasting response depression to 30 Hz test vibration on an unadapted site. O'Mara et al. (1988) concluded that peripheral factors make little contribution to the lasting adaptation effects observed in central neurons, and therefore presumably little contribution to adaptation effects at a perceptual level. Support for a central locus of vibrotactile adaptation was similarly provided by Whitsel et al. (2003). These investigators recorded responses of rapidly adapting (RA) afferents and SI RA neurons to sustained 10–50 Hz flutter stimulation in anesthetized monkeys and cats. Under the same stimulus condition, RA cortical neuron responses declined to a much greater extent than RA afferent responses. Finally, Chung et al. (2002) recorded simultaneously from neurons in the rat somatosensory thalamus and barrel cortex in response to repetitive brief whisker deflection, and found that the cortical responses declined more strongly, more quickly, and recovered more slowly than the thalamic responses. Chung et al. (2002) concluded that both subcortical and cortical mechanisms contributed to adaptation, and they suggested that rapid depression of thalamocortical synapses played a key role in cortical adaptation.

Intrinsic signal optical imaging studies in SI have shown that 1–10 s of flutter stimulation on the skin increased the absorbance of regions in areas 3b and 1 that received input from the stimulated skin site and decreased the absorbance of surrounding regions (Tommerdahl et al., 2002; Simons et al., 2005, 2007). The altered activities did not return to baseline levels until 10–15 s after stimulus offset. The results indicated that flutter adaptation narrows the spatial extent of SI response to a sustained stimulus; this sharpening has been proposed to underlie the enhancement of spatial discrimination following flutter adaptation (Tommerdahl et al., 2002, 2005). Another intrinsic signal optical imaging study showed that, in response to sustained 200 Hz vibration, SI initially exhibited a transient increase in absorbance that dropped to below-background level after 1 s, whereas the secondary somatosensory cortex (SII) exhibited a vigorous and well-maintained increase in absorbance (Tommerdahl et al., 1999). Although the perceptual consequences of such responses of SI and SII to vibrotactile adaptation are unknown, the results suggest that vibrotactile adaptation shapes cortical response dynamics. Last but not least, a functional MRI study in humans showed that the number of activated voxels in SI and SII exponentially reduced over time in response to 15 s of static pressure on the fingertip (Chung et al., 2015). Chung et al. (2015) interpreted the results as suggesting that cortical activation is refined during tactile adaptation. The converging evidence of substantial cortical

changes during prolonged tactile stimulation suggests a cortical locus of adaptation; however, it is important to keep in mind the caveat that observed cortical changes could reflect subcortical adaptation.

In contrast to the above studies, a recent, intriguing perceptual study in humans reported that vibrotactile adaptation occurs predominantly at the peripheral level. Klocker et al. (2016) performed experiments with either vibrotactile stimulation or transcutaneous electrical stimulation. They assumed electrical stimulation would bypass peripheral mechanoreceptor transduction and activate primary afferent axons directly. Klocker et al. (2016) reasoned that, if vibrotactile adaptation induced changes at a central level, then prolonged mechanical vibration on the fingertip would affect the ability to detect not only vibration but also electrical impulses on the fingertip. Contrary to this prediction, they found that vibrotactile adaptation of the fingertip impaired only vibration detection, leaving electrical detection intact. Similarly, prolonged electrical stimulation of the median nerve—which should have induced central adaptation—did not affect subsequent vibration detection on the fingertip. Klocker et al. (2016) concluded that somatosensory adaptation occurs predominantly in peripheral mechanoreceptors. Unfortunately, the authors did not report whether electrical adaptation of the median nerve impaired electrical detection on the fingertip. A plausible alternative hypothesis is that the vibratory and electrical stimuli activated different cutaneous channels, and adaptation of one channel did not affect perception via the other.

If peripheral adaptation contributes to the illusion we have reported, a second question of interest is: which mechanoreceptive afferents are involved? Five mechanoreceptive channels that convey action potentials via fast-conducting Aβ fibers have been identified in human forearm skin: slowly-adapting type 1 afferents (SA1), slowly-adapting type 2 afferents (SA2), and three fast-adapting types: hair units, field units, and Pacinian (PC) units (Vallbo et al., 1995; Olausson et al., 2000). Our intense adapting vibration (peak-to-peak amplitude ∼125 g, frequency ∼122 Hz) and strong test stimuli (point static pressure, ∼80 g) likely activated multiple types of afferents (Bolanowski et al., 1988; Abraira and Ginty, 2013) and caused adaptation in them as well (Bensmaia et al., 2005; Leung et al., 2005). Evidence suggests that, as in glabrous skin (Johnson, 2001; Abraira and Ginty, 2013), in forearm skin only SA1s have the characteristics that are needed to convey fine spatial information. SA1s innervate the human forearm close to the skin surface and are highly responsive to light skin indentation; they have small, distinctive receptive fields and high distribution density compared to the forearm's fast-adapting afferents (Vallbo et al., 1995; Olausson et al., 2000). These characteristics suggest that the spatial pattern of SA1 firing rates encodes the spatial structure of stimuli pressed against the skin. Like SA1s, SA2 afferents are sensitive to local skin strain, and some microneurography studies have estimated that in human forearm skin the size and distribution density of SA2 receptive fields are comparable to those of SA1s (Vallbo et al., 1995; Olausson et al., 2000). However, SA2s are characterized by continuous spontaneous firing, pronounced enlargement in receptive field size with stronger stimulation, and high sensitivity to directional horizontal skin stretch (Chambers et al., 1972; Edin, 1992; Vallbo et al., 1995; Olausson et al., 2000). Interestingly, intraneural activation of individual SA2 afferents, unlike stimulation of other afferent types, did not evoke conscious sensation (Ochoa and Torebjörk, 1983). Given their response characteristics, SA2s are presumably better suited for proprioceptive signaling than for conveying fine spatial information. The fast-adapting afferent types (hair units, field units, and PCs) presumably do not contribute significantly to fine spatial coding, as they have large receptive fields with diffuse borders and low distribution density (Bolanowski et al., 1994; Vallbo et al., 1995). As SA1s have the requisite properties to serve fine spatial perception on the forearm, it is likely that the perception of two-point distance relies largely on SA1 input, and it is plausible that adaptation in the SA1 population contributes to the repulsion illusion reported here.

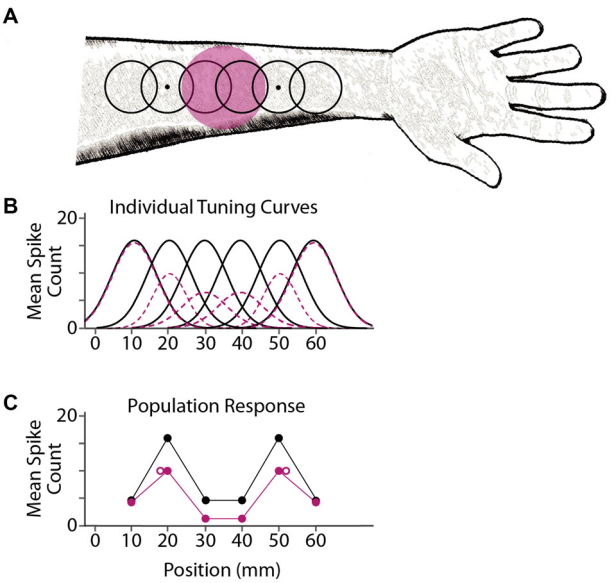


**FIGURE 6 |** A model for adaptation-induced tactile spatial aftereffects. **(A)** Black open circles depict receptive fields of six simulated cortical neurons, with centers at 10, 20, 30, 40, 50 and 60 mm on the arm. Dots depict two point-stimuli delivered simultaneously at 20 and 50 mm. Magenta circle depicts the area adapted by prolonged tactile stimulation (e.g., vibration). **(B)** Mean firing (spike counts) expected from the six individual neurons in response to a point stimulus at each location on the *x*-axis, before adaptation (black solid curves) or following adaptation (magenta dashed curves). For illustration purposes, these simulated tuning curves are Gaussian functions; the actual shapes, sizes, and activity profiles of cortical receptive fields are much more variable than shown here (Peters et al., 2015). **(C)** Simulated population response from the six neurons. Each solid circle depicts a neuron's mean firing rate (vertical axis) plotted against the neuron's receptive field center location (horizontal axis). Black, NA; magenta, adaptation. The two point-stimuli evoke two mounds of activity in the population response. Open magenta circles: focal adaptation shifts the perceived locations of the stimuli (e.g., the average of the receptive field center locations in each mound, weighted by the firing rates of the neurons) away from the adapted area. The brain consequently misattributes the focal reduction in firing to a greater distance between stimulus points.

## A Model for Tactile Spatial Localization and Adaptation-Induced Aftereffects

We propose that tactile stimulus localization is based on responses from a population of neurons with overlapping receptive fields. Prolonged exposure to a focal stimulus reduces the responsiveness of nearby neurons, via either fatigue (Köhler and Wallach, 1944; Sutherland, 1961; Barlow and Hill, 1963) or lingering inhibition (Ganz, 1966; Tolhurst and Thompson, 1975; Magnussen and Kurtenbach, 1980), resulting in a shift in perceived location (**Figure 6**). Inherent in this model is the hypothesis that the brain interprets stimulus-evoked neural activity without accounting for the fact that the neurons are in a state of adaptation.

From an information processing perspective, perception in touch as in other modalities can be viewed as consisting of two fundamental stages: encoding and decoding (Pouget et al., 2000; Paninski et al., 2007; Peters et al., 2015). The encoding stage samples sensory stimuli from the environment and converts these into spatiotemporal patterns of action potentials. This forward processing or data generative stage is stochastic, both because natural sensory stimuli are samples from an environmental stimulus distribution and because individual neurons respond stochastically (e.g., with Poisson variability; Sripati et al., 2006). The decoding stage interprets the observed action potential pattern in an attempt to infer the stimulus that caused it. The decoder is thus undertaking the notoriously difficult inverse problem of inferring a cause from its stochastically generated effects (Pizlo, 2001). As a consequence, perceptual inference is inherently uncertain.

An ideal Bayesian observer would decode by interpreting the observed action potential pattern in light of the actual generative model; that is, optimal perceptual inference requires that the observer's prior probability distribution match the actual stimulus distribution and that the observer's likelihood function correctly represent the statistical mapping from stimuli to observation (Ma, 2012). We propose that violation of the second of these conditions underlies adaptation-induced repulsion illusions such as the one reported in the present study. Specifically, in keeping with similar suggestions from the visual and multisensory literature, we propose that focal adaptation leads the brain to mistakenly infer that a subsequently presented stimulus is shifted away from the adapted region, because the brain decodes without taking into account that the sensory system is focally adapted (Schwartz et al., 2007; Series et al., 2009; Crommett et al., 2017; **Figure 6**). Future research will apply Bayesian modeling to further investigate the tactile repulsion illusion reported here.

## CONCLUSION

The current study supports the similarity of spatial processing in touch, vision and audition. Previous studies have revealed similarities between tactile and visual processing for perception of spatial properties such as orientation, shape and form (Phillips et al., 1983; Hsiao, 1998; Bensmaia et al., 2008; Yau et al., 2009). The study of spatial illusions has also revealed similar processing across sensory modalities. Notably, tactile, visual and auditory perception all are prone to perceptual length contraction illusions (e.g., sensory saltation) that occur in response to discrete stimuli delivered in rapid succession (Geldard, 1982; Goldreich, 2007; Getzmann, 2009; Khuu et al., 2011; Goldreich and Tong, 2013; Tong et al., 2016). In the current study, we have verified that another type of spatial illusion, adaptation-induced spatial repulsion, which has been demonstrated previously in vision and audition (Thurlow and Jack, 1973; Kashino and Nishida, 1998; Carlile et al., 2001; Clifford et al., 2007; Kohn, 2007; Schwartz et al., 2007), occurs also in touch. Collectively, these observations suggest that spatial processing operates via fundamentally similar mechanisms in different sensory modalities.

## AUTHOR CONTRIBUTIONS

LL and DG designed the study. LL, AC and SMI conducted the experiments. AC and SMI contributed to preliminary data analysis and draft reports. LL and DG performed the final data analyses and wrote the article with feedback from AC and SMI.

## FUNDING

This work was funded by a Discovery Grant to DG from the Natural Sciences and Engineering Research Council of Canada (NSERC).

## ACKNOWLEDGMENTS

We thank Cecelia Dai, Kyle Gauder, Kaitlyn Gonsalves, Vy Ngo, Hiral Patel, Soumya Saini and Faiza Shafaqat for assistance with data collection. We thank Keon Allen, Arnav Bharadwaj, Umang Bharaj, Akash Deep, Kyle Gauder, Farah Hasan, Gabriel Herman, Nina Prodribaba, Rebecca Voth and Michael Wong for their thoughtful comments on the manuscript.

## REFERENCES

Abraira, V. E., and Ginty, D. D. (2013). The sensory neurons of touch. *Neuron* 79, 618–639. doi: 10.1016/j.neuron.2013.07.051

Barlow, H. B., and Hill, R. M. (1963). Evidence for a physiological explanation of the waterfall phenomenon and figural after-effects. *Nature* 200, 1345–1347. doi: 10.1038/2001345a0

Barraclough, N. E., Page, S. A., and Keefe, B. D. (2017). Visual adaptation enhances action sound discrimination. *Atten. Percept. Psychophys.* 79, 320–332. doi: 10.3758/s13414-016-1199-z

Bensmaia, S. J., Denchev, P. V., Dammann, J. F. III, Craig, J. C., and Hsiao, S. S. (2008). The representation of stimulus orientation in the early stages of somatosensory processing. *J. Neurosci.* 28, 776–786. doi: 10.1523/jneurosci.4162-07.2008

Bensmaia, S. J., Leung, Y. Y., Hsiao, S. S., and Johnson, K. O. (2005). Vibratory adaptation of cutaneous mechanoreceptive afferents. *J. Neurophysiol.* 94, 3023–3036. doi: 10.1152/jn.00002.2005

Berglund, U., and Berglund, B. (1970). Adaptation and recovery in vibrotactile perception. *Percept. Mot. Skills* 30, 843–853. doi: 10.2466/pms.1970.30.3.843

Blakemore, C. (1973). "The baffled brain," in *Illusion in Nature and Art*, eds R. L. Gregory and E. H. Gombrich (London: Duckworth), 8–47.

Bolanowski, S. J., Gescheider, G. A., and Verrillo, R. T. (1994). Hairy skin: psychophysical channels and their physiological substrates. *Somatosens. Mot. Res.* 11, 279–290. doi: 10.3109/08990229409051395

Bolanowski, S. J. Jr., Gescheider, G. A., Verrillo, R. T., and Checkosky, C. M. (1988). Four channels mediate the mechanical aspects of touch. *J. Acoust. Soc. Am.* 84, 1680–1694. doi: 10.1121/1.397184

Bystrzycka, E., Nail, B. S., and Rowe, M. (1977). Inhibition of cuneate neurones: its afferent source and influence on dynamically sensitive "tactile" neurones. *J. Physiol.* 268, 251–270. doi: 10.1113/jphysiol.1977.sp011856

Calzolari, E., Azanon, E., Danvers, M., Vallar, G., and Longo, M. R. (2017). Adaptation aftereffects reveal that tactile distance is a basic somatosensory feature. *Proc. Natl. Acad. Sci. U S A* 114, 4555–4560. doi: 10.1073/pnas.1614979114

Carlile, S., Hyams, S., and Delaney, S. (2001). Systematic distortions of auditory space perception following prolonged exposure to broadband noise. *J. Acoust. Soc. Am.* 110, 416–424. doi: 10.1121/1.1375843

Chambers, M. R., Andres, K. H., von Duering, M., and Iggo, A. (1972). The structure and function of the slowly adapting type II mechanoreceptor in hairy skin. *Q. J. Exp. Physiol. Cogn. Med. Sci.* 57, 417–445. doi: 10.1113/expphysiol.1972.sp002177

Chung, Y. G., Han, S. W., Kim, H. S., Chung, S. C., Park, J. Y., Wallraven, C., et al. (2015). Adaptation of cortical activity to sustained pressure stimulation on the fingertip. *BMC Neurosci.* 16:71. doi: 10.1186/s12868-015-0207-x

Chung, S., Li, X., and Nelson, S. B. (2002). Short-term depression at thalamocortical synapses contributes to rapid adaptation of cortical sensory responses *in vivo*. *Neuron* 34, 437–446. doi: 10.1016/s0896-6273(02)00659-1

Clifford, C. W., Webster, M. A., Stanley, G. B., Stocker, A. A., Kohn, A., Sharpee, T. O., et al. (2007). Visual adaptation: neural, psychological and computational aspects. *Vision Res.* 47, 3125–3131. doi: 10.1016/j.visres.2007.08.023

Crommett, L. E., Perez-Bellido, A., and Yau, J. M. (2017). Auditory adaptation improves tactile frequency perception. *J. Neurophysiol.* 117, 1352–1362. doi: 10.1152/jn.00783.2016

Day, R. H., and Singer, G. (1964). A tactile spatial aftereffect. *Aust. J. Psychol.* 16, 33–37. doi: 10.1080/00049536408255500

Dhruv, N. T., and Carandini, M. (2014). Cascaded effects of spatial adaptation in the early visual system. *Neuron* 81, 529–535. doi: 10.1016/j.neuron.2013.11.025

Dragoi, V., Rivadulla, C., and Sur, M. (2001). Foci of orientation plasticity in visual cortex. *Nature* 411, 80–86. doi: 10.1038/35075070

Dragoi, V., Sharma, J., and Sur, M. (2000). Adaptation-induced plasticity of orientation tuning in adult visual cortex. *Neuron* 28, 287–298. doi: 10.1016/s0896-6273(00)00103-3

Edin, B. B. (1992). Quantitative analysis of static strain sensitivity in human mechanoreceptors from hairy skin. *J. Neurophysiol.* 67, 1105–1113.

Ganz, L. (1966). Mechanism of the figural aftereffects. *Psychol. Rev.* 73, 128–150. doi: 10.1037/h0022952

Geldard, F. A. (1982). Saltation in somesthesis. *Psychol. Bull.* 92, 136–175. doi: 10.1037/0033-2909.92.1.136

Gescheider, G. A., and Wright, J. H. (1968). Effects of sensory adaptation on the form of the psychophysical magnitude function for cutaneous vibration. *J. Exp. Psychol.* 77, 308–313. doi: 10.1037/h0025746

Getzmann, S. (2009). Exploring auditory saltation using the "reduced-rabbit" paradigm. *J. Exp. Psychol. Hum. Percept. Perform.* 35, 289–304. doi: 10.1037/a0013026

Gibson, J. J., and Radner, M. (1937). Adaptation, after-effect and contrast in the perception of tilted lines. I. Quantitative studies. *J. Exp. Psychol.* 20, 453–467. doi: 10.1037/h0059826

Gilbert, A. J. (1967). Tactile spatial aftereffect or adaptation level? *J. Exp. Psychol.* 73, 450–455. doi: 10.1037/h0024258

Goble, A. K., and Hollins, M. (1993). Vibrotactile adaptation enhances amplitude discrimination. *J. Acoust. Soc. Am.* 93, 418–424. doi: 10.1121/1.405621

Goble, A. K., and Hollins, M. (1994). Vibrotactile adaptation enhances frequency discrimination. *J. Acoust. Soc. Am.* 96, 771–780. doi: 10.1121/1.410314

Goldreich, D. (2007). A Bayesian perceptual model replicates the cutaneous rabbit and other tactile spatiotemporal illusions. *PLoS One* 2:e333. doi: 10.1371/journal.pone.0000333

Goldreich, D., and Tong, J. (2013). Prediction, postdiction and perceptual length contraction: a Bayesian low-speed prior captures the cutaneous rabbit and related illusions. *Front. Psychol.* 4:221. doi: 10.3389/fpsyg.2013.00221

Hahn, J. F. (1966). Vibrotactile adaptation and recovery measured by two methods. *J. Exp. Psychol.* 71, 655–658. doi: 10.1037/h0023094

Hahn, J. F. (1968). Low-frequency vibrotactile adaptation. *J. Exp. Psychol.* 78, 655–659. doi: 10.1037/h0026621

He, S., and MacLeod, D. I. (2001). Orientation-selective adaptation and tilt after-effect from invisible patterns. *Nature* 411, 473–476. doi: 10.1038/35078072

Helson, H. (1947). Adaptation-level as frame of reference for prediction of psychophysical data. *Am. J. Psychol.* 60, 1–29. doi: 10.2307/1417326

Heron, J., Aaen-Stockdale, C., Hotchkiss, J., Roach, N. W., McGraw, P. V., and Whitaker, D. (2012). Duration channels mediate human time perception. *Proc. Biol. Sci.* 279, 690–698. doi: 10.1098/rspb.2011.1131

Hollins, M., Goble, A. K., Whitsel, B. L., and Tommerdahl, M. (1990). Time course and action spectrum of vibrotactile adaptation. *Somatosens. Mot. Res.* 7, 205–221. doi: 10.3109/08990229009144707

Hsiao, S. S. (1998). Similarities between touch and vision. *Adv. Psychol.* 127, 131–165. doi: 10.1016/s0166-4115(98)80066-6

Johnson, K. O. (2001). The roles and functions of cutaneous mechanoreceptors. *Curr. Opin. Neurobiol.* 11, 455–461. doi: 10.1016/s0959-4388(00)00234-8

Kashino, M., and Nishida, S. (1998). Adaptation in the processing of interaural time differences revealed by the auditory localization aftereffect. *J. Acoust. Soc. Am.* 103, 3597–3604. doi: 10.1121/1.423064

Khuu, S. K., Kidd, J. C., and Badcock, D. R. (2011). The influence of spatial orientation on the perceived path of visual saltatory motion. *J. Vis.* 11:5. doi: 10.1167/11.9.5

Kitagawa, N., and Ichihara, S. (2002). Hearing visual motion in depth. *Nature* 416, 172–174. doi: 10.1038/416172a

Klocker, A., Gueorguiev, D., Thonnard, J. L., and Mouraux, A. (2016). Peripheral vs. central determinants of vibrotactile adaptation. *J. Neurophysiol.* 115, 685–691. doi: 10.1152/jn.00519.2015

Köhler, W., and Wallach, H. (1944). Figural after-effects. an investigation of visual processes. *Proc. Am. Philos. Soc.* 88, 269–357.

Kohn, A. (2007). Visual adaptation: physiology, mechanisms and functional benefits. *J. Neurophysiol.* 97, 3155–3164. doi: 10.1152/jn.00086.2007

Kohn, A., and Movshon, J. A. (2003). Neuronal adaptation to visual motion in area MT of the macaque. *Neuron* 39, 681–691. doi: 10.1016/s0896-6273(03)00438-0

Kohn, A., and Movshon, J. A. (2004). Adaptation changes the direction tuning of macaque MT neurons. *Nat. Neurosci.* 7, 764–772. doi: 10.1038/nn1267

Leung, Y. Y., Bensmaia, S. J., Hsiao, S. S., and Johnson, K. O. (2005). Time-course of vibratory adaptation and recovery in cutaneous mechanoreceptive afferents. *J. Neurophysiol.* 94, 3037–3045. doi: 10.1152/jn.00001.2005

Levitt, H. (1971). Transformed up-down methods in psychoacoustics. *J. Acoust. Soc. Am.* 49, 467–477. doi: 10.1121/1.1912375

Ma, W. J. (2012). Organizing probabilistic models of perception. *Trends Cogn. Sci.* 16, 511–518. doi: 10.1016/j.tics.2012.08.010

Magnussen, S., and Johnsen, T. (1986). Temporal aspects of spatial adaptation. A study of the tilt aftereffect. *Vision Res.* 26, 661–672. doi: 10.1016/0042-6989(86)90014-3

Magnussen, S., and Kurtenbach, W. (1980). Adapting to two orientations: disinhibition in a visual aftereffect. *Science* 207, 908–909. doi: 10.1126/science.7355271

McIntyre, S., Birznieks, I., Vickery, R. M., Holcombe, A. O., and Seizova-Cajic, T. (2016a). The tactile motion aftereffect suggests an intensive code for speed in neurons sensitive to both speed and direction of motion. *J. Neurophysiol.* 115, 1703–1712. doi: 10.1152/jn.00460.2015

McIntyre, S., Seizova-Cajic, T., and Holcombe, A. O. (2016b). The tactile speed aftereffect depends on the speed of adapting motion across the skin rather than other spatiotemporal features. *J. Neurophysiol.* 115, 1112–1121. doi: 10.1152/jn.00821.2014

Ochoa, J., and Torebjörk, E. (1983). Sensations evoked by intraneural microstimulation of single mechanoreceptor units innervating the human hand. *J. Physiol.* 342, 633–654. doi: 10.1113/jphysiol.1983.sp014873

Olausson, H., Wessberg, J., and Kakuda, N. (2000). Tactile directional sensibility: peripheral neural mechanisms in man. *Brain Res.* 866, 178–187. doi: 10.1016/s0006-8993(00)02278-2

Oldfield, R. C. (1971). The assessment and analysis of handedness: the Edinburgh inventory. *Neuropsychologia* 9, 97–113. doi: 10.1016/0028-3932(71)90067-4

O'Mara, S., Rowe, M. J., and Tarvin, R. P. (1988). Neural mechanisms in vibrotactile adaptation. *J. Neurophysiol.* 59, 607–622.

Paninski, L., Pillow, J., and Lewi, J. (2007). "Statistical models for neural encoding, decoding, and optimal stimulus design," in *Progress in Brain Research*, eds T. D. Paul Cisek and F. K. John (Amsterdam: Elsevier), 493–507.

Peters, R. M., Staibano, P., and Goldreich, D. (2015). Tactile orientation perception: an ideal observer analysis of human psychophysical performance in relation to macaque area 3b receptive fields. *J. Neurophysiol.* 114, 3076–3096. doi: 10.1152/jn.00631.2015

Phillips, J. R., Johnson, K. O., and Browne, H. M. (1983). A comparison of visual and two modes of tactual letter resolution. *Percept. Psychophys.* 34, 243–249. doi: 10.3758/bf03202952

Pizlo, Z. (2001). Perception viewed as an inverse problem. *Vision Res.* 41, 3145–3161. doi: 10.1016/s0042-6989(01)00173-0

Pouget, A., Dayan, P., and Zemel, R. (2000). Information processing with population codes. *Nat. Rev. Neurosci.* 1, 125–132. doi: 10.1038/35039062

Sato, Y., and Aihara, K. (2011). A bayesian model of sensory adaptation. *PLoS One* 6:e19377. doi: 10.1371/journal.pone.0019377

Schwartz, O., Hsu, A., and Dayan, P. (2007). Space and time in visual context. *Nat. Rev. Neurosci.* 8, 522–535. doi: 10.1038/nrn2259

Series, P., Stocker, A. A., and Simoncelli, E. P. (2009). Is the homunculus "aware" of sensory adaptation? *Neural Comput.* 21, 3271–3304. doi: 10.1162/neco.2009.09-08-869

Silver, R. J. (1969). *Tilt After-Effects in Touch*. Doctoral Dissertation. Waltham, MA: Brandeis University. Database: ProQuest/UMI Dissertations Publishing. Order no.: 2-700248141.

Simons, S. B., Chiu, J., Favorov, O. V., Whitsel, B. L., and Tommerdahl, M. (2007). Duration-dependent response of SI to vibrotactile stimulation in squirrel monkey. *J. Neurophysiol.* 97, 2121–2129. doi: 10.1152/jn.00513.2006

Simons, S. B., Tannan, V., Chiu, J., Favorov, O. V., Whitsel, B. L., and Tommerdahl, M. (2005). Amplitude-dependency of response of SI cortex to flutter stimulation. *BMC Neurosci.* 6:43. doi: 10.1186/1471-2202-6-43

Sripati, A. P., Yoshioka, T., Denchev, P., Hsiao, S. S., and Johnson, K. O. (2006). Spatiotemporal receptive fields of peripheral afferents and cortical area 3b and 1 neurons in the primate somatosensory system. *J. Neurosci.* 26, 2101–2114. doi: 10.1523/JNEUROSCI.3720-05.2006

Sutherland, N. (1961). Figural after-effects and apparent size. *Q. J. Exp. Psychol.* 13, 222–228. doi: 10.1080/17470216108416498

Tannan, V., Simons, S., Dennis, R. G., and Tommerdahl, M. (2007). Effects of adaptation on the capacity to differentiate simultaneously delivered dual-site vibrotactile stimuli. *Brain Res.* 1186, 164–170. doi: 10.1016/j.brainres.2007.10.024

Tannan, V., Whitsel, B. L., and Tommerdahl, M. A. (2006). Vibrotactile adaptation enhances spatial localization. *Brain Res.* 1102, 109–116. doi: 10.1016/j.brainres.2006.05.037

Thurlow, W. R., and Jack, C. E. (1973). Some determinants of localization-adaptation effects for successive auditory stimuli. *J. Acoust. Soc. Am.* 53, 1573–1577. doi: 10.1121/1.1913505

Tolhurst, D. J., and Thompson, P. G. (1975). Orientation illusions and after-effects: inhibition between channels. *Vision Res.* 15, 967–972. doi: 10.1016/0042-6989(75)90238-2

Tommerdahl, M., Favorov, O., and Whitsel, B. L. (2002). Optical imaging of intrinsic signals in somatosensory cortex. *Behav. Brain Res.* 135, 83–91. doi: 10.1016/s0166-4328(02)00159-6

Tommerdahl, M., Hester, K. D., Felix, E. R., Hollins, M., Favorov, O. V., Quibrera, P. M., et al. (2005). Human vibrotactile frequency discriminative capacity after adaptation to 25 Hz or 200 Hz stimulation. *Brain Res.* 1057, 1–9. doi: 10.1016/j.brainres.2005.04.031

Tommerdahl, M., Whitsel, B. L., Favorov, O. V., Metz, C. B., and O'Quinn, B. L. (1999). Responses of contralateral SI and SII in cat to same-site cutaneous flutter versus vibration. *J. Neurophysiol.* 82, 1982–1992.

Tong, J., Ngo, V., and Goldreich, D. (2016). Tactile length contraction as Bayesian inference. *J. Neurophysiol.* 116, 369–379. doi: 10.1152/jn.00029.2016

Vallbo, A. B., Olausson, H., Wessberg, J., and Kakuda, N. (1995). Receptive field characteristics of tactile units with myelinated afferents in hairy skin of human subjects. *J. Physiol.* 483, 783–795. doi: 10.1113/jphysiol.1995.sp020622

Walker, J. T., Irion, A. L., and Gordon, D. G. (1981). Simple and contingent aftereffects of perceived duration in vision and audition. *Percept. Psychophys.* 29, 475–486. doi: 10.3758/bf03207361

Wark, B., Lundstrom, B. N., and Fairhall, A. (2007). Sensory adaptation. *Curr. Opin. Neurobiol.* 17, 423–429. doi: 10.1016/j.conb.2007.07.00

Webster, M. A. (2012). Evolving concepts of sensory adaptation. *F1000 Biol Rep* 4:21. doi: 10.3410/B4-21

Whitsel, B. L., Kelly, E. F., Quibrera, M., Tommerdahl, M., Li, Y., Favorov, O. V., et al. (2003). Time-dependence of SI RA neuron response to cutaneous flutter stimulation. *Somatosens. Mot. Res.* 20, 45–69. doi: 10.1080/0899022031000083834

Whitsel, B. L., Kelly, E. F., Xu, M., Tommerdahl, M., and Quibrera, M. (2001). Frequency-dependent response of SI RA-class neurons to vibrotactile stimulation of the receptive field. *Somatosens. Mot. Res.* 18, 263–285. doi: 10.1080/01421590120089659

Yau, J. M., Pasupathy, A., Fitzgerald, P. J., Hsiao, S. S., and Connor, C. E. (2009). Analogous intermediate shape coding in vision and touch. *Proc. Natl. Acad. Sci. U S A* 106, 16457–16462. doi: 10.1073/pnas.0904186106

**Conflict of Interest Statement**: The authors declare that the research was conducted in the absence of any commercial or financial relationships that could be construed as a potential conflict of interest.

# CHAPTER 3

# ANESTHESIA

## 3.1 Preface

In Chapter 2, we reported an adaptation-induced repulsion illusion in perceived two-point distance. Here, we further investigated this repulsion illusion by using topical anesthesia instead of vibrotactile adaptation to induce focal peripheral desensitization. We tested the same psychophysical tasks (monofilament detection, distance discrimination) as those applied in Chapter 2, without or with topical anesthesia of the forearm skin.

Like vibrotactile adaptation, topical anesthesia focally reduced tactile sensitivity. Unlike adaptation, however, anesthesia did not significantly increase the perceived separation between points straddling the anesthetized region. These results suggest that peripheral desensitization is not sufficient to induce the tactile spatial repulsion illusion previously observed.

## 3.2 Abstract

In Chapter 2, we reported an adaptation-induced repulsion illusion: prolonged vibration focally reduced tactile sensitivity and significantly increased the perceived separation between points straddling the adapted region. Here, we investigated whether peripheral desensitization was sufficient to induce the repulsion illusion, by applying topical anesthesia instead of vibrotactile adaptation to reduce tactile sensitivity more thoroughly. We applied the same battery of psychophysical tests used in Chapter 2. In a two-interval forced-choice task, participants compared the perceived separation between two point-stimuli applied on the forearms successively. Separation distance was constant on one arm (the reference) and varied on the other arm (the comparison). On day 1, we measured two-point distance comparison without or with topical anesthesia of the skin between the two reference points. In addition, we measured the degree of desensitization at the reference points, as indicated by elevated monofilament detection thresholds. On day 2, we applied the same anesthesia protocol on the same 20 participants from day 1, and measured the degree of desensitization as a function of distance from the centre of anesthesia. Anesthesia reduced tactile sensitivity to a greater extent than adaptation did, and the relative desensitization pattern as a function of distance was similar between anesthesia and adaptation. However, anesthesia caused little to no shift in the perceived separation between the reference points. We discuss possible explanations for the discrepancy between the anesthesia and adaptation effects, including plausible different consequences in the central nervous system. We conclude that peripheral desensitization is not sufficient to induce the spatial repulsion illusion, and central adaptation is presumably required for the illusion to occur.

## 3.3 Introduction

Previously, we reported an adaptation-induced tactile spatial repulsion illusion: prolonged vibrotactile stimulation significantly increased the perceived separation between points straddling the adapted skin region. In the previous study, the vibrotactile protocol was found to focally reduce tactile sensitivity, as indicated by elevation in detection thresholds of monofilaments (aka von Frey hairs) that diminished with distance from centre of adaptation. Thus, a logical hypothesis is that vibrotactile adaptation causes focal peripheral desensitization, which in turn induces the repulsion illusion we observed.

Desensitization is a well-documented effect of sensory adaptation. In psychophysical research, characterization of vibrotactile adaptation typically emphasizes two main effects: increase in detection threshold, and decrease in subjective magnitude of suprathreshold stimuli whose attributes are similar to those of the adapting stimulus (e.g. Hahn, 1966; Berglund & Berglund, 1970; Hollins et al., 1990; Gescheider et al., 2004); both effects have been interpreted as forms or results of desensitization. In primate and

human neurophysiological research, it has been found that seconds to a few minutes of vibration temporarily increases firing threshold (Bensmaia et al., 2005; Leung et al., 2005) and reduces nerve volley amplitude (a measurement of axon excitability; Applegate & Burke, 1989) of mechanoreceptive afferents. Accordingly, it has been suggested that desensitization caused by vibrotactile adaptation is due to the subsequent period of peripheral axonal hypoexcitability (Applegate & Burke, 1989). Mechanistically, axonal hypoexcitability following repetitive activation has been linked to intracellular hyperpolarization (e.g. Barrett & Barrett, 1982). It is plausible that vibrotactile adaptation shifts the afferent membrane potential away from the threshold required for spike generation, thereby reducing firing and desensitizing the afferents.

If afferent desensitization is the primary cause of the adaptation-induced repulsion illusion reported previously, then a greater degree of afferent desensitization would plausibly lead to a more prominent perceptual repulsion between points straddling the desensitized skin region. Here, we tested this hypothesis by desensitizing the skin site more thoroughly using a local anesthetic instead of prolonged vibration. The local anesthetic (EMLA, a mixture of lidocaine and prilocaine) inactivates or reduces spike generation by blocking voltage-gated sodium channels (Attal & Bouhassira, 2006). Although the anesthetic likely desensitizes afferents via different mechanisms than prolonged vibration does, presumably both procedures result in peripheral response reduction. We tracked the extent of desensitization by measuring changes in tactile sensitivity using a monofilament-detection task, and we measured distance perception using a two-point distance-comparison task. We predicted that anesthesia would cause a greater loss of tactile sensitivity and thus induce a more prominent repulsion illusion than did adaptation.

### 3.4 Methods

We tested tactile spatial perception with a two-interval forced-choice (2IFC) two-point distance-comparison task, and tracked changes in tactile sensitivity with a 2IFC monofilament-detection task. The two tasks followed basic protocols that were almost identical to their counterparts in Chapter 2, except that topical anesthesia instead of vibrotactile adaptation was applied to reduce skin sensitivity. In this section, we will recapitulate the test procedures. A more detailed description can be found in Chapter 2, under Materials and Methods.

*Participants.* Twenty-six participants were recruited from the McMaster University community. By self-report, all participants were free of conditions that are known to impair tactile sensitivity (e.g., calluses, scars, or injuries on tested skin areas, carpel tunnel syndrome, diabetes) or perceptual processing (e.g., neurological disorders, attention deficit disorders, dyslexia). All participants had normal or corrected-to-normal vision. Of the 26 recruits, 20 passed the perceptual *qualification criteria* (see below).

Data are reported from these 20 qualified participants (all women; 19 right-handed, 1 left-handed; ages 18.2-29.9 years, median age 20.1 years). Handedness was assessed by a modified Edinburgh Handedness Inventory (Oldfield, 1971). Participants provided signed informed consent and received monetary compensation and/or course credits for their participation. The McMaster University Research Ethics Board approved all procedures.

**Day 1**

Participants were tested with two tasks on day 1: 2IFC two-point distance comparison and 2IFC monofilament detection. In the distance-comparison task, participants compared the perceived separation between two point-stimuli applied on the forearms successively. Separation distance was constant between the reference points on the right arm (reference distance, R), and varied between the comparison points on the left arm (comparison distance, C) (Fig. 1A). In addition, tactile sensitivity of skin sites at the two reference points was measured with the monofilament-detection task (Fig. 1B). Monofilament detection and distance comparison were tested before and following topical anesthesia of the skin area between and extending slightly beyond the reference points. The order of the tasks was: monofilament detection, no anesthesia (NA) -> distance comparison, NA -> distance comparison, following anesthesia (Anes) -> monofilament detection, Anes.

*Preparation and skin sites tested.* Prior to the experiment, the participant washed her volar forearms with soap and lukewarm water. The participant sat in front of a table with the experimental apparatus concealed by an opaque black curtain. The participant's forearms, inserted under the curtain, rested comfortably on a padded surface, with the wrists (palm side up) resting stably on concave foam supports. To assist the experimenters in positioning the stimuli, the participant's forearms were demarcated with a fine-tipped pen. A pair of small dots 30 mm apart was drawn on each volar forearm to guide the application of the two-point test stimuli. On each arm, the dots were symmetrical about the midpoint between the wrist and the elbow, aligned with the proximal-distal axis of the forearm, and slightly laterally offset from midline (Fig. 1A). The slightly lateral-to-midline skin surface was parallel to the ground when participants rested their forearms in a supine position as they naturally tended to rotate the forearms slightly inward when relaxed; the choice of this skin surface thereby facilitated the application of the test stimuli perpendicularly to participants' forearms. In addition, a circle of 34 mm diameter was drawn on the reference forearm to mark the skin patch to receive topical anesthetic later. The center of the circle coincided with the midpoint between the reference points. The diameter value 34 mm was chosen based on pilot experiments (see Discussion for detail).

*Two-point distance comparison*. On the first interval of each trial, a pair of point-stimuli was applied onto the participant's volar forearm with the two points simultaneously indenting the skin; the points aligned along the proximal-distal axis of the forearm. Approximately 1 s later, on the second interval, another pair of point-stimuli was applied

to the other volar forearm in the same manner. The participant compared the distance between the first pair of points with the distance between the second pair of points, and reported which distance felt greater (Fig. 1A). The participants verbalized their answers by saying "first" or "second", and the experimenter recorded the answers into a computer by pressing one of two response keys. The two-point distance was fixed at 30 mm on the right forearm (the reference) and variable from 6 to 54 mm in increments of 6 mm on the left forearm (the comparison; nine comparison distances in total). The application order of the reference and comparison points was counterbalanced across participants: half of the participants received the reference points first and comparison second on all trials, and the other half of the participants received the comparison points first and reference second on all trials.

A custom-made lever system was implemented to apply the two-point stimuli with force control. A detailed description of the lever system is in Chapter 2 under *Force-controlled two-point stimuli* (illustrated in Fig. 2, Chapter 2). To recapitulate briefly, the lever system consisted of two plastic arms attached via a metal rod that passed through a ball bearing. The metal rod rotated with little friction, allowing the arms to swivel smoothly. Each two-point applicator was made of two plastic pins attached to a wood pencil. The stimulus surfaces that contacted the skin were spherical pinheads of diameter 1.5 mm. Separation distances between the centres of the pinheads were 6, 12, 18, 24, 30, 36, 42, 48, and 54 mm. The two-point applicator could be easily attached to and removed from the swivel arms of the lever via magnets; this allowed the experimenter to quickly change the two-point stimulus from trial to trial.

To apply a test stimulus, the experimenter first attached the two-point applicator to the swivel arms of the lever and lifted the swivel arms to a horizontal position over the participant's forearm. The experimenter then gently lowered the swivel arms from the horizontal position, allowing the two pinheads to gently fall and contact the forearm simultaneously and perpendicularly to the skin surface. The pinheads indented the skin with a total force determined by the combined weight of the swivel arms, which measured 80 - 82 g when the pinheads were applied with this method to a scale (40 - 41 g exerted via each pinhead). The pinheads were in contact with the skin for ~ 0.5 s before the experimenter raised the swivel arms to end the stimulus. Two identical lever apparatuses were used, one for each forearm. Two experimenters conducted the experiment, each operating one lever apparatus. On each trial, the test stimuli were applied to the forearms sequentially. As one experimenter completed the first two-point stimulus and raised the swivel arms away from the skin, the second experimenter initiated the stimulus to the other forearm. The inter-stimulus interval was ~ 1 s. The two experimenters were trained to keep the application pace consistent between stimuli and across trials.

Each participant completed a practice block of 16 trials with auditory feedback; two practice trials were presented for each of the eight comparison distances that were different from the reference distance 30 mm. The participant then completed a testing block of 90 trials with no feedback. Ten trials were present at each of the nine comparison

distances; the order of the trials was randomized. A custom computer program (LabVIEW 2011 for Macintosh, National Instruments) randomly sampled the comparison distances without replacement, and instructed the experimenter as to which comparison distance to apply. The participant took a 1-min break upon completing roughly each quarter of the 90 trials (i.e., after trials 22, 45, 67).

*Qualification criteria.* To ensure that participants' baseline two-point distance perception was sufficiently accurate to perform the two-point distance comparison task, we compared participants' baseline performance (before anesthesia) to two qualification criteria: the proportion of "comparison is greater" responses at the longest comparison distance (54 mm) should be $\geq 0.7$, and at the shortest comparison distance (6 mm) should be $\leq 0.3$. If a participant failed to meet either criterion, then we considered her baseline performance to be unreliable. In this case, the participant did not proceed with the experiment, and her data were excluded from analysis.

*Psychometric function parameterization and estimation of point of subjective equality (PSE).* For each participant, we fit to the data a sigmoidal cumulative normal function, which describes the proportion of trials at which the comparison distance, $x$, was reported as being longer than the reference distance:

$$\psi(x) = \frac{\delta}{2} + (1-\delta)\left[\gamma + (1-\gamma)\frac{1}{\sigma\sqrt{2\pi}}\int_{-\infty}^{x} e^{-(t-\mu)^2/2\sigma^2}dt\right]$$

This function has four free parameters: the mean ($\mu$) and standard deviation ($\sigma$) of the cumulative normal curve, a lapse rate ($\delta$), and a y-intercept ($\gamma$). We allowed $\gamma$ to take on non-zero values, because the psychometric function for many participants did not fall completely to zero at the left tail. Using Bayesian parameter estimation, beginning with uniform prior probabilities over the four parameters, we calculated the joint ($\mu$, $\sigma$, $\gamma$, and $\delta$) posterior density. We marginalized this over $\delta$ and read out the mode of the ($\mu$, $\sigma$, $\gamma$) posterior as the best-estimate of the participant's psychometric function. We then extracted the comparison distance at which the psychometric function crossed 50% as the perceptual equivalent of the reference distance, i.e. the PSE.

*Monofilament detection at two points (M2pts).* We assessed tactile sensitivity by measuring participants' 2IFC detection of force-calibrated Semmes-Weinstein monofilaments (Timely Neuropathy Testing, LLC and Texas Medical Design, Inc.). Monofilament detection was tested on the skin sites at the two reference points. As described above, the reference points were symmetrical about the midpoint between the wrist and the elbow, and were 30 mm apart. In other words, either point was 15 mm away from the midpoint, which was the centre of anesthesia later applied. We denote the more proximal point (i.e. closer to elbow) of the two reference points "proximal point", and the more distal point (i.e. closer to wrist) "distal point". We refer to this task as *M2pts*, short

for “monofilament detection at two points”, later in the chapter where we compare it with another monofilament-detection task on day 2, to distinguish the two tasks.

Each trial consisted of two intervals, separated by ~ 1.25 s and indicated by beeps. Simultaneously with one of the beeps, the skin was stimulated with a monofilament for ~ 0.5 s. The participant reported whether the stimulus occurred with the first or second beep, by pressing one of two response keys with the left hand. Monofilament force began at 0.07 g and was adaptively adjusted via a 2-down 1-up staircase procedure: If the participant answered correctly for two consecutive trials, the monofilament with the next-lower force was applied; if the participant answered incorrectly on any trial, the monofilament with the next-higher force was applied. This procedure converges towards the participant's 71% correct detection threshold (Levitt, 1971).

Using interleaved 2-down 1-up staircases, we tested the two skin sites in consecutive trials. For example, the proximal point was tested on trial 1, the distal point on trial 2, the proximal point again on trial 3, the distal point again on trial 4, and so on. The order was counterbalanced across participants. For both sites, the first trial began with the 0.07 g monofilament. On a subsequent trial, the monofilament applied at either test site was determined by the staircase procedure based on previous responses at that skin site. For example, if the participant responded correctly on trials 1 and 3 on which the proximal point was tested, then the monofilament applied on the next trial at that site (trial 5) went down to the next-lower force.

After a practice block of 20 trials with auditory feedback, each participant completed a testing block without feedback. The testing block consisted of 100 trials, 50 trials for each test site. The participant took a 10-s break upon completing roughly each third of the 100 trials (i.e. after trials 33 and 66). The participant's 71% correct threshold at each test site was estimated by averaging the staircase reversal points in the last 25 of 50 trials at that site. In the circumstances in which the last 25 trials contained no reversal points and the participant consistently gave correct responses, so the staircase dropped to and continued at the lowest filament force, we used that force (0.008 g) as the estimated threshold.

*Anesthesia protocol.* Upon completion of the baseline blocks for monofilament detection and distance comparison, the circular patch of skin marked on the participant’s reference forearm (Fig. 1A) was treated with a topical anesthetic cream, EMLA (AstraZeneca Inc.). EMLA is an mixture of 2.5% of lidocaine and 2.5% of prilocaine, and is an over-the-counter local anesthetic commonly used prior to painful minor procedures, such as hair removal. The experimenter applied 1.4 ml of EMLA cream topically to the encircled skin area, and gently spread the cream with the tip of a syringe so that the cream covered the encircled area evenly but did not spread beyond the circle. Then, a small piece of plastic dressing was placed on top of the cream. To prevent the cream from spreading, the perimeter of the plastic dressing was sealed with four pieces of medical tape enclosing the treated skin area. The anesthetic was left on the participant’s skin for 2 hours, as EMLA consumer information advised that approximately 2 hours of application will allow the

anesthetic to exert optimal numbing effect that will last at least 2 hours after removal of the anesthetic. During the 2 hours, the participant remained in the laboratory and was instructed to avoid vigorous movements of her reference forearm or rubbing the treated skin area. At the end of 2 hours, the cream was partly absorbed by the participant's skin. The experimenter removed the medical tape and the plastic dressing, and carefully wiped off the residual cream with a tissue paper. Although the anesthetized skin area felt numb to all participants, none of them reported irritation or discomfort caused by the anesthetic treatment.

The participant was then tested with the two psychophysical tasks again: this time, two-point distance comparison first, and monofilament detection second. The procedure for each task was identical to that prior to anesthesia.

**Day 2**

To assess the spatial spread of the sensitivity-reducing effect of anesthesia, on a different day we applied the anesthesia protocol to the same 20 participants, and measured 2IFC monofilament detection at four distances from the centre of anesthesia. We will henceforth refer to this task as *M4pts*, short for "monofilament detection at four points", to distinguish it from the monofilament detection task on day 1 (M2pts).

The experimental setup was similar to M2pts, except that four skin sites instead of two were tested (Fig. 1C). On the participant's right volar forearm (the reference arm), a circle of 34 mm diameter was demarcated to indicate the skin area for anesthesia. The position of the circle was identical to that on day 1: midway between the wrist and the elbow, and the centre of the circle was at where the midpoint of the reference points in the distance-comparison task would be. In addition, four dots were drawn at 0, 10, 15, and 20 mm from the centre of the circle to indicate the monofilament test sites. The dots were aligned along the proximal-distal axis of the forearm, and slightly laterally offset from midline. For half of the participants, the dots extended distally, from the centre of the circle towards the wrist; for the other half of the participants, the dots extended proximally, from the centre of the circle towards the elbow.

Using interleaved 2-down 1-up staircases, we tested the four skin sites in consecutive trials in the order 0, 10, 15, and 20 mm from the centre of the circle. For example, the 0 mm site was tested on trial 1, the 10 mm site on trial 2, the 15 mm site on trial 3, the 20 mm site on trial 4, and the 0 mm site again on trial 5. For all test sites, the first trial used the 0.07 g monofilament. On subsequent trials, the monofilament applied at each test site was determined by the staircase procedure based on previous responses at that site. For example, if the participant responded correctly on trials 1 and 5 on which the 0 mm site was tested, then the monofilament applied on the next trial at that site (trial 9) went down to the next-lower force.

After 20 practice trials with auditory feedback, each participant completed two testing blocks with no feedback: a no-anesthesia (NA) baseline block, and a block following 2 hours of topical anesthesia (Anes). The anesthesia protocol was identical to that used on day 1. Each testing block consisted of 200 trials, 50 trials at each of the four test sites. Within each block, participants took a break after completing trials 33, 66, 100, 133, and 166 (break durations: 10 s after trials 33, 66, 133, 166, 5 min after trial 100). For each testing block and each of the test sites, the participant's 71% correct threshold was estimated by averaging the staircase reversal points in the last 25 of 50 trials at that site. In the rare circumstances in which the last 25 trials contained no reversal points and the participant consistently gave correct responses, so the staircase dropped to and continued at the lowest filament force, we used that force (0.008 g) as the estimated threshold.

**Statistical analyses**

We performed ANOVAs with type III sum of squares and two-tailed t-tests using SPSS Statistics version 20 (IBM) for Macintosh. For post-hoc one-way repeated-measures ANOVAs, we used R version 3.3.2 and the companion to applied regression (car) package. For ANOVAs, in case of violation of sphericity, we applied Greenhouse-Geisser correction to the degrees of freedom and the p-values. For multiple post-hoc pairwise comparisons, we used Bonferroni correction and reported p-values multiplied by the number of comparisons. We performed two-tailed binomial proportion tests in LabVIEW 2011 for Macintosh (National Instruments). We performed power analysis on two-tailed t-tests using G*Power (Faul et al., 2007). All statistical tests used an alpha level of 0.05.

## 3.5 Results

We tested for the presence of a tactile repulsion illusion on the forearm following focal skin anesthesia. In a 2IFC task, participants compared the distances of two pairs of point-stimuli (reference vs. comparison) applied on their forearms successively, reporting which distance felt greater. The reference distance was fixed at 30 mm, and the comparison distance varied from 6 to 54 mm. The PSE was extracted as a measure of participants' perceived distance between the reference points. We measured baseline PSEs and PSEs following topical anesthesia. In addition, we used force-calibrated Semmes-Weinstein monofilaments to assess the extent of the tactile sensitivity reduction by the anesthesia protocol.

**Topical anesthesia greatly reduced tactile sensitivity**

Using 2IFC monofilament-detection tasks (M2pts and M4pts), we assessed the extent and spatial spread of tactile sensitivity reduction caused by topical anesthesia. We applied a

topical anesthetic focally to the skin on the reference arm, and measured detection threshold to track the reduction in tactile sensitivity.

For M2pts, we found that anesthesia elevated detection thresholds on the skin sites at the reference points involved in the distance-comparison task (Fig. 2A). 71% correct detection thresholds (mean ± 1 SE) at the proximal point and the distal point, respectively, were 0.064 ± 0.012 g and 0.127 ± 0.057 g for the NA (baseline) condition, and 1.304± 0.237 g and 1.347 ± 0.230 g for the Anes condition (Fig. 2A). A 2 x 2 repeated-measures ANOVA with condition (NA, Anes) and position (proximal, distal) as factors indicated a highly significant effect of condition ($F(1, 19)=41.705$, $p<0.001$, partial $\eta^2=0.687$), but no effect of position ($F(1, 19)=0.192$, $p=0.666$) or condition x position interaction ($F(1, 19)=0.002$, $p=0.962$). These results indicate that baseline tactile sensitivity was similar at the skin sites of the reference points, and that topical anesthesia reduced tactile sensitivity at these skin sites.

For M4pts, we found that the threshold elevation was greatest at the centre of anesthesia and diminished as a function of distance (Fig. 2B). 71% correct detection thresholds (mean ± 1 SE) at the test sites 0, 10, 15, and 20 mm from the centre of anesthesia were 0.068 ± 0.013 g, 0.050 ± 0.012 g, 0.052 ± 0.011 g, and 0.048 ± 0.011 g for baseline (NA), and 4.085 ± 0.765 g, 2.856 ± 0.453 g, 1.850 ± 0.317 g, and 0.205 ± 0.077 g following anesthesia (Anes). A 2 x 4 repeated-measures ANOVA with condition (NA, Anes) and distance (0, 10, 15, 20 mm from centre of anesthesia) as factors indicated highly significant effects of condition ($F(1.000, 19.000)=56.282$, $p<0.001$, partial $\eta^2=0.748$), distance ($F(1.611, 30.616)=14.903$, $p<0.001$, partial $\eta^2=0.440$), and condition x distance interaction ($F(1.602, 30.430)=14.931$, $p<0.001$, partial $\eta^2=0.440$). Post-hoc one-way repeated-measures ANOVAs indicated that the baseline thresholds did not differ across distances ($F(3, 57)=1.058$, $p=0.374$), whereas the Anes thresholds differed significantly across distances ($F(1.606, 30.517)=14.924$, $p<0.001$, partial $\eta^2=0.440$). At 15-mm distance from the centre of anesthesia (i.e. the skin sites corresponding to the reference points), the Anes threshold was still significantly different from baseline ($t(19)=5.750$, $p<0.001$, Cohen's $d = 1.286$), but the difference became non-significant at 20-mm distance ($t(19)=2.028$, $p=0.057$). These results indicate that baseline tactile sensitivity was similar across the forearm test area, and topical anesthesia greatly reduced tactile sensitivity. Furthermore, the anesthesia effect diminished with distance from the centre of anesthesia; however, there was still a considerable loss of tactile sensitivity at the skin sites of the reference points.

In addition, to assess whether detection thresholds and anesthesia effects were stable across days and tests, we compared thresholds at the test site 15 mm from the centre of anesthesia in M4pts (day 2) with thresholds at the reference points in M2pts (day 1); these sites coincided in position because the reference points were 15 mm from the centre of anesthesia. In M2pts (day 1), the threshold (mean ± 1 SE) averaged across the reference points (proximal, distal) was 0.095 ± 0.028 g for NA, and 1.326 ± 0.204 g for Anes. In M4pts (day 2), the threshold (mean ± 1 SE) at the test site 15 mm from the centre of

anesthesia was 0.052 ± 0.011 g for NA, and 1.850 ± 0.317 g for Anes (Fig. 2C). Paired t-tests indicated that neither the NA nor the Anes thresholds differed significantly across days and tests (NA: t(19)=-1.893, p=0.074; Anes: t(19)=1.958, p=0.065). The results indicate that the measured thresholds and anesthesia effects were quite stable across days and tests.

**Topical anesthesia did not cause a significant shift in perceived distance**

We applied a topical anesthetic focally to the skin on the reference forearm, and investigated the effect of anesthesia on two-point distance perception using a 2IFC distance-comparison task. The average psychometric curves and estimated PSEs are shown in Fig. 3 (Fig. 3A: raw data. Fig. 3B: best-fitting data).

The raw psychometric curves for many participants were noisy and crossed the y = 0.5 line multiple times, making it difficult to extract individual PSEs directly from the raw data. Therefore, for the raw data, we estimated only the across-participant mean PSE by linearly interpolating the mean response proportions (Fig. 3A, top). The mean PSEs obtained in this fashion for the NA and Anes blocks were 29.10 mm and 31.77 mm, respectively (Fig. 3A, bottom). Binomial tests revealed that the proportion of trials in which participants judged the 30-mm comparison distance as longer than the 30-mm reference distance did not differ significantly from 0.5 for either block (p = 0.724 and 0.077 for NA and Anes, respectively).

Next, we used Bayesian curve fitting to estimate the psychometric functions and extract the PSEs of the individual participants. Each of the curves shown in Figure 3B (top) is an average of 20 individual best-fitting psychometric curves; the similarity of the curves to those shown in Figure 3A (top) suggests that our curve fitting procedure provided a valid estimate of participant performance. The means (± 1 SE) of the PSEs extracted from the participants' individual best-fitting psychometric functions for the NA and Anes blocks were 29.19±1.53 mm and 31.54±1.47 mm, respectively (Fig. 3B, bottom). One-sample t-tests indicated that neither PSE differed significantly from the reference distance of 30 mm (NA: t(19)=-0.529, p=0.603; Anes: t(19)=1.041, p=0.311). A two-tailed paired t-test indicated that the Anes PSE did not differ significantly from the NA PSE (t(19)=1.866, p=0.078). These results indicate the absence of a significant shift in the perceived two-point distance following anesthesia. Nevertheless, the data suggest a nonsignificant trend for PSE to increase in the Anes condition. These statistically nonsignificant results may indicate no true PSE shift, or that the PSE shift was too small to be detectable in our experimental setup. Power analysis on (Anes PSE - 30 mm) suggested that, for a sample size N = 20, a PSE shift would need to be at least 3.71 mm to be detectable with 80% power; in the present experiment, the observed average difference between Anes PSE and 30 mm was 1.54 mm, which was smaller than 3.71 mm. Moreover, power analysis on (Anes PSE – NA PSE) suggested that a PSE shift would need to be at least 4.35 mm to be

detectable with 80% power; the observed average difference between Anes PSE and NA PSE was only 2.34 mm.

## 3.6 Discussion

To investigate whether peripheral desensitization was sufficient to cause the adaptation-induced tactile repulsion illusion reported in the previous chapter, we applied topical anesthesia instead of vibratory adaptation to focally desensitize the test skin site more thoroughly, and measured the perceived distance between points straddling the anesthetized site using a 2IFC distance-comparison task. In addition, to assess the extent of desensitization and the reliability of the anesthesia protocol, we tracked the changes in tactile sensitivity using a 2IFC monofilament-detection task at a variety of skin sites on different days. As we predicted, loss of tactile sensitivity was greater following topical anesthesia than vibrotactile adaptation. Interestingly, however, and contrary to our prediction, anesthesia caused little to no increase in the perceived two-point distance.

### Anesthesia versus adaptation for focally reducing tactile sensitivity

In pilot experiments when we developed the anesthesia protocol, our goal was to thoroughly anesthetize the skin region between the reference points while somewhat reducing sensitivity at the reference points, thus replicating the pattern of relative threshold elevation at different distances caused by adaptation (Fig. 4B in Chapter 2) but with greater overall absolute elevation. The application area of the anesthetic, namely, the anesthesia area, was determined via pilot experiments on 17 participants[3]. Anesthesia areas in the pilot experiments were 19, 25, 30, and 34 mm in diameter; 19 mm was the diameter of the adapting probe used in the adaptation experiments in Chapter 2. Pilot results suggested that an anesthesia area up to 30 mm in diameter (i.e. up to the reference points) did not achieve the desired effect for about half of the participants: the anesthetization effect fell sharply before or at the reference points, and did not elevate detection thresholds at these points. Extending the anesthesia area to 34 mm seemed to produce slightly better results. Therefore, we used 34-mm anesthesia area for the official experiments with 20 participants.

[3] Data from the last three of the 17 participants, for whom 34-mm anesthesia area was applied, were used as part of the official experimental data. In other words, these three participants were counted as three of the 20 participants in the official experiments. The experimental protocol they received was identical to the protocol used in the official experiments.

As expected, the anesthesia protocol reduced tactile sensitivity to a much greater extent than the adaptation protocol, as indicated by the amount of threshold elevation in Fig. 2 of this chapter compared to Fig. 4B in Chapter 2. Lidocaine has been shown to inactivate hair units in human forearm skin, which are a type of fast-adapting unit (Mahns, 2006), and on glabrous skin the responsivity of fast-adapting units (both type 1 and type 2) determines monofilament detection threshold (Strzalkowski et al., 2015). Despite the difference in the absolute amount of threshold elevation, the patterns of relative desensitization were similar between the two protocols. The relative threshold elevation caused by anesthesia versus adaptation as a function of distance is shown in Fig. 4. Each point depicts the elevation of the mean 71% correct monofilament-detection threshold at that distance by adaptation or anesthesia, normalized by the maximum threshold elevation in each condition. In other words, each point depicts

$$mean(thres_A - thres_{NA})/\max\left(mean(thres_A - thres_{NA})\right)$$

where $thres_A$ is the threshold in the anesthesia or adaptation condition, and $thres_{NA}$ is the threshold in the corresponding no-anesthesia or no-adaptation (baseline) condition, at that distance. The anesthesia protocol is as described in this chapter, with 34-mm application area of 1.4 ml EMLA for 2 hours. The adaptation protocol is the A3 protocol described in Chapter 2 (40 s adaptation with 3 s top-ups). Maximum threshold elevation in either condition occurred at the centre of anesthesia or adaptation (distance = 0). The normalized curves indicate that the relative threshold elevation at the four distances was similar between anesthesia and adaptation, suggesting that the anesthesia and adaptation protocols reduced tactile sensitivity differentially at the test sites in similar spatial patterns: tactile sensitivity reduction (i.e. threshold elevation) was greater between the centre of anesthesia or adaptation and the site of the reference point (15 mm away), than at the site of the reference point or beyond, and as a general trend the reduction diminished with distance.

**Was the lack of a significant PSE shift due to too much desensitization?**

Whether topical anesthesia could cause a repulsion illusion in tactile spatial perception is inconclusive. Results from the distance-comparison experiment (Fig. 3) seemed to suggest a trend of a PSE increase following anesthesia, but the shift compared to baseline was statistically non-significant based on a two-tailed paired t-test ($p=0.078$); furthermore, the Anes PSE did not differ from the reference distance 30 mm ($p=0.311$). It is tempting to speculate that our anesthesia protocol desensitized too broad a skin region, and anesthesia would have caused a significant PSE increase had the desensitization effect been more focal. The application area of EMLA, 34 mm in diameter, covered the reference points, which were 30 mm apart and symmetric about the centre of the anesthesia circle. Results from the monofilament-detection experiments (Fig. 2) indicated that anesthesia elevated detection thresholds at the reference points by ~ 1 – 2 g, a 10 – 35-fold increase from baseline. Compared to the threshold elevation at the same distance

caused by vibrotactile adaptation (0.09 g elevation, a 1.5-fold increase from baseline), desensitization of skin sites at the reference points was substantially greater following anesthesia. Consequently, it is possible that receptive fields (RFs) under and near the reference points might be too desensitized to generate sufficient spikes to convey even a vague spatial profile of the two reference points, and therefore the spatial repulsion that could have manifested was blurred.

Nevertheless, this explanation cannot account for the fact that following anesthesia, participants performed distance discrimination almost as well as without anesthesia, as indicated by the comparable slopes of the Anes and NA psychometric functions (Fig. 3 top panels). Anesthesia presumably reduced the perceived intensity of the reference points much more than adaptation did, but the subjective weakness of the stimuli did not necessarily result in poorer performance in spatial discrimination. A more plausible explanation is needed for the discrepancy between effects of adaptation and anesthesia on two-point distance perception.

**Was the lack of a significant PSE shift due to different central consequences?**

Earlier studies on tactile adaptation tended to emphasize various forms of peripheral desensitization, such as receptor fatigue and afferent hypoexcitability (e.g. Wedell & Cummings, 1938; Gescheider & Wright, 1969; Barker et al. 1982; Pubols, 1982; Lundstrom, 1986). However, it has been shown that exposure to sustained vibration suppresses neural responsivity not only in the periphery (Bensmaia et al., 2005; Leung et al., 2005) but also in the central nervous system (CNS; e.g. Bystrzycka et al., 1977; O'Mara et al., 1988; Lee & Whitsel, 1992; Whitsel et al., 2001; Chung et al., 2002; Whitsel et al., 2003; Chung et al., 2013). Some of these studies compared the degree of adaptation that occurs at multiple levels of the processing hierarchy, providing convincing evidence for a strong central contribution to adaptation. For example, O'Mara et al. (1988) recorded extracellular responses of PC afferents and cuneate neurons (i.e. second-order relay neurons) to 300 Hz sustained vibration in decerebrated or anesthetized cats. It was found that 1) response depression of cuneate neurons lasted much longer than that of afferents, and 2) in cuneate neurons that received convergent excitatory input from multiple skin sites, adaptation of one site caused lasting response depression to a test stimulus on an unadapted site, even when the test stimulus was of a different vibration frequency. O'Mara et al. suggested that central factors contribute more than peripheral factors to adaptation effects at the perceptual level. Furthermore, studies comparing response depression of cortical neurons and primary afferents have also supported a greater central than peripheral contribution to adaptation. For instance, Whitsel et al. (2003) recorded extracellular responses of rapidly-adapting (RA) afferents and RA neurons in the primary somatosensory cortex (S1) in monkeys and cats to sustained 10-50 Hz flutter stimulation; they found that S1 RA neuronal responses displayed large and systematic dynamic changes including response depression, whereas RA afferents displayed only minor response depression and little to no other dynamic changes.

Consistent with this result, a human study recording cerebral evoked potentials over the sensorimotor cortex found that the cortical response evoked by a test stimulus to the fingertip decreased for as long as 25 min after a 200 Hz adapting vibration was delivered for 10 min to the same RF or RFs of adjacent afferents; in comparison, the reduction in the magnitude of the afferent volley was small. Furthermore, even when the reduced magnitude of the afferent volley was compensated on-line by increasing test stimulus intensity, the cortical response still declined sharply with adaptation (Macefield & Burke, 1991). These results indicate that modifications of cortical neural response by sustained stimulation are mainly due to adaptation in the CNS. It has been suggested that short-term plasticity in synaptic transmission at the cuneate nucleus and/or thalamocortical levels, as well as intracortical mechanisms, play key roles in cortical adaptation (Macefield & Burke, 1991; Chung et al., 2002).

In light of these findings that suggest an important role of central adaptation in perception, we propose a simple schematic model that provides a parsimonious plausible explanation for anesthesia versus adaptation effects on tactile spatial perception (Fig. 5). In Fig. 5, the top panels illustrate a scenario that represents our original hypothesis, which is not supported by our empirical results, whereas the bottom panels illustrate a scenario that could account for the observed discrepancy between adaptation and anesthesia effects.

In Fig. 5 top panels (A-C), convergence and divergence of afferent input are negligible. In the baseline (NA) condition (Fig. 5A), the two-point stimulus evokes stronger responses in the lateral afferents and weaker response in the middle afferent. Based on the pattern in the population activity of the cortical neurons, the brain infers that the skin is stimulated at two points. Adaptation (Fig. 5B) or anesthesia (Fig. 5C) of the intervening skin between the points primarily reduces the middle afferent's responsivity, and the reduction is greater by anesthesia than by adaptation. This reduced afferent responsivity results in reduced responsivity in the cortical neuron to which the afferent projects. Similarly, the cortical response is reduced further by anesthesia than by adaptation. In the case of vibrotactile adaptation, the cortical neuron's reduced responsivity could be due to intrinsic mechanisms within the CNS, such as short-term depression in thalamocortical synapses. Thus, response depression is plausibly more pronounced in the cortical neuron than in the afferent. In the case of topical anesthesia, the cortical neuron's reduced responsivity presumably reflects reduced afferent input and does not involve intrinsic suppression within the CNS circuitry. Thus, response depression is plausibly similar in the cortical neuron and in the afferent. Despite the different mechanisms and different degrees of responsivity reduction, the consequences of adaptation and anesthesia in the CNS are functionally similar: they both lead to focal responsivity reduction. Consequently, the largely intact responsivity of the adjacent cortical RFs contributes to two mounds of activity in cortical population response, thus shifting the perceived locations of the points away from the desensitized region. In this scenario, following anesthesia, we would observe a repulsion illusion in the perceived separation between point-stimuli that straddle the anesthetized region compared to baseline. However, our

empirical finding of a lack of a significant PSE shift suggests that the scenario in Fig. 5A-C is unlikely to be the case.

By contrast, in Fig. 5 bottom panels (D-F), afferent input converges and diverges to different cortical neurons, and the overlap of cortical RFs is considerably greater than the overlap of afferent RFs. This scenario is more realistic than that in Fig. 5A-C, as convergence and divergence of afferent input has been shown to occur at multiple levels of the processing pathway in the CNS, for example, in the dorsal column nuclei (Pubols & Pubols, 1973), the ventral posterior nucleus in the thalamus (Mountcastle et al., 1969; Sinclair et al., 1991), and in areas 3b and 1 in S1 (Iwamura, 1998; Pei et al., 2009). In the baseline (NA) condition (Fig. 5D), the two-point stimulus evokes slightly stronger response in the lateral cortical neurons than in the middle one. Due to input convergence and divergence, the cortical population activity is less distinctly differential that that in Fig. 5A, but the brain can infer the possibility of the existence of two points and their distance, versus one point only. In addition, this scenario is consistent with the general finding that when two simultaneous point-stimuli are separately by a small distance, it is difficult to perceptually distinguish them from a single point. Following focal adaptation, however, the cortical population activity becomes more distinctively differential (Fig. 5E). Prolonged vibration to the middle afferent RF adapts the central cortical neuron it primarily projects to. It also depresses the adjacent neurons but to a lesser extent. The RFs of these differentially depressed cortical neurons are subsequently activated to different extents by afferent input. The polarized distribution of population activity then gives rise to a repulsion in the perceived separation between the points that straddle the adapted afferent RF. In comparison, the peripheral desensitization effect of topical anesthesia is compensated by input convergence and divergence, and thus fails to result in a significant PSE shift (Fig. 5F). Anesthesia of the middle afferent RF reduces its input to the cortical neurons. However, these cortical neurons are not adapted, and are subsequently activated by the convergent and divergent input from the adjacent unanesthetized afferent RFs. Although the cortical neurons may fire slightly less following anesthesia. The relative distribution of activity in the population response profile is similar to that in baseline. This plausibly contributes to the lack of an observable repulsion illusion following anesthesia.

In addition, focal peripheral anesthesia could have other central consequences, such as unmasking. Neurophysiological studies have found that focal temporal deafferentation by intradermal injection of lidocaine produces immediate and reversible reorganization of sensory maps at all levels of the somatosensory pathway, including the thalamus and the cortex (e.g. Calford, 1991; Nicolelis et al., 1993; Shin et al., 1995; Faggin et al., 2017). This phenomenon is a form of unmasking, as new RFs emerge (i.e. are “unmasked”) around the temporarily deafferented region. The downstream area that used to receive input from the deafferented region expands its RF to cover the surrounding intact peripheral regions. The anesthesia hypothesis illustrated in Fig. 5F could be modified to take into account the general effect of unmasking, for example, by expanding the central cortical RF (central circle in the top row) and strengthening its responsivity to input from

the lateral afferent RFs. These changes, however, would be more likely to result in a perceptual attraction instead of a repulsion, as the distribution of population activity would be more centralized. A perceptual attraction would manifest as a leftward shift in the psychometric function and a decrease in PSE, which were not observed in our study. However, it is plausible that multiple mechanisms of opposing perceptual effects were at play, thus blurring any of the effects from becoming observable. For example, anesthesia might trigger immediate modifications of the balance between excitation and inhibition at multiple levels of the pathway, and this dynamic might interact with any other changes induced by anesthesia in the population response.

Alternatively, the anesthesia protocol in our study might induce negligible amount of unmasking or any central consequence. Studies reporting central effects of local anesthetic typically inject the anesthetic subcutaneously. In our study, a small amount of anesthetic was applied topically to a small skin area. Therefore, it is plausible that the lack of any significant central consequence accounts for the lack of a significant PSE shift following focal anesthesia.

## 3.7 Conclusion

In the current study, we found that focal topical anesthesia did not significantly increase the perceived separation between points straddling the anesthetized skin region. This result is in contrast with the adaptation-induced tactile repulsion illusion reported in the previous chapter, and indicates that peripheral desensitization was not sufficient to induce the spatial repulsion illusion. We suggest that focal adaptation in the CNS is required for the illusion to occur. This is consistent with findings from somatosensory studies that support a strong central contribution to tactile adaptation. This intriguing but inconclusive result calls for future research to systematically assess the effects of focal anesthesia on tactile spatial perception. For example, future research could systematically vary the area of anesthesia and measure the resulting two-point distance perception, or compare topical application with intradermal injection of a local anesthetic to investigate the possible impact of unmasking on tactile spatial perception.

## 3.8 References

Applegate, C., & Burke, D. (1989). Changes in excitability of human cutaneous afferents following prolonged high-frequency stimulation. *Brain*, *112*(1), 147–164. https://doi.org/10.1093/brain/112.1.147

Attal, N., & Bouhassira, D. (2006). Translating basic research on sodium channels in human neuropathic pain. *J Pain*, *7*(1 Suppl 1), S31-7.

https://doi.org/10.1016/j.jpain.2005.09.005
Barker, D. J., Shepard, P. D., & McDermott, K. L. (1982). Fatigue in cat facial mechanoreceptors. *Neuroscience Letters*, *30*, 117–122.
Barrett, E. F., & Barrett, J. N. (1982). Intracellular recording from vertebrate myelinated axons: mechanism of the depolarizing afterpotential. *The Journal of Physiology*, *323*, 117–44. https://doi.org/10.1002/mus.21496.Conduction
Berglund, U., & Berglund, B. (1970). Conditions of Adaptation and recovery in vibrotactile perception. *Perceptual and Motor Skills*, *30*(3), 843–853.
Bystrzycka, B. Y. E., Nail, B. S., & Rowe, M. (1977). Inhibition of cuneate neurons: Its afferent source and influence on dynamically sensitive "tactile" neurons. *J Physiol*, *268*, 251–270.
Calford, M. (1991). Curious cortical change. *Nature*, *352*, 759–760.
Chung, S., Li, X., Nelson, S. B., & Street, S. (2002). Short-Term Depression at Thalamocortical Synapses Contributes to Rapid Adaptation of Cortical Sensory Responses In Vivo. *Neuron*, *34*, 437–446.
Chung, Y. G., Kim, J., Han, S. W., Kim, H. S., Choi, M. H., Chung, S. C., … Kim, S. P. (2013). Frequency-dependent patterns of somatosensory cortical responses to vibrotactile stimulation in humans: A fMRI study. *Brain Research*, *1504*, 47–57. https://doi.org/10.1016/j.brainres.2013.02.003
Faggin, B. M., Nguyen, K. T. R. I., & Nicolelis, M. A. L. (2017). Immediate and Simultaneous Sensory Reorganization at Cortical and Subcortical Levels of the Somatosensory System. *Proceedings of the National Academy of Sciences*, *94*(17), 9428–9433.
Faul, F., Erdfelder, E., Lang, A.-G., & Buchner, A. (2007). G*Power: A flexible statistical power analysis program for the social, behavioral, and biomedical sciences. *Behavior Research Methods*, *39*(2), 175–191. https://doi.org/10.3758/BF03193146
Gescheider, G. A., Bolanowski, S. J., & Verrillo, R. T. (2004). Some characteristics of tactile channels. *Behavioural Brain Research*, *148*(1–2), 35–40. https://doi.org/10.1016/S0166-4328(03)00177-3
Gescheider, G. A., & Wright, J. H. (1969). Effects of vibrotactile adaptation on perception of stimuli of varied intensity. *Journal of Experimental Psychology*, *81*(3), 449–453.
Hahn, J. F. (1966). Vibrotactile adaptation and recovery measured by two methods. *Journal of Experimental Psychology*, *71*(5), 655–658. https://doi.org/10.1037/h0023094
Hollins, M., Goble, a K., Whitsel, B. L., & Tommerdahl, M. (1990). Time course and action spectrum of vibrotactile adaptation. *Somatosensory & Motor Research*, *7*(2), 205–221.
Iwamura, Y. (1998). Representation of tactile functions in the somatosensory cortex. In J. W. Morley (Ed.), *Neural Aspects of Tactile Sensation* (pp. 195–238). Elsevier B.V.
Lee, C. J., & Whitsel, B. L. (1992). Mechanisms underlying somatosensory cortical dynamics: I. In vivo studies. *Cerebral Cortex (New York, N.Y. : 1991)*, *2*(2), 81–106.
Lundstrom, J. (1986). Responses of mechanoreceptive afferent units in the glabrous skin of the human hand to vibration. *Scandinavian Journal of Work, Environment &*

*Health*, *12*(4), 413–416.
Macefield, G., & Burke, D. (1991). Long-lasting depression of central synaptic transmission following prolonged high-frequency stimulation of cutaneous afferents: a mechanism for post-vibratory hypaesthesia. *Electroencephalography and Clinical Neurophysiology*, *78*, 150–158.
Mahns, D. A. (2006). Vibrotactile frequency discrimination in human hairy skin. *Journal of Neurophysiology*, *95*(3), 1442–1450. https://doi.org/10.1152/jn.00483.2005
Mountcastle, V. B., Talbot, W. H., Sakata, H., & Hyvärinen, J. (1969). Cortical neuronal mechanisms in flutter-vibration studied in unanesthetized monkeys. Neuronal periodicity and frequency discrimination. *Journal of Neurophysiology*, *32*(3), 452–484.
Nicolelis, M. A. L., Lin, R. C. S., Woodward, D. J., & Chapin, J. K. (1993). Induction of immediate spatiotemporal changes in thalamic networks by peripheral block of ascending cutaneous information. *Nature Letters*, *361*, 533–536.
O'Mara, S., Rowe, M. J., & Tarvin, R. P. (1988). Neural mechanisms in vibrotactile adaptation. *Journal of Neurophysiology*, *59*(2), 607–622.
Oldfield, R. C. (1971). The assessment and analysis of handedness: the Edinburgh inventory. *Neuropsychologia*, *9*(1), 97–113.
Pei, Y.-C., Denchev, P. V, Hsiao, S. S., Craig, J. C., & Bensmaia, S. J. (2009). Convergence of submodality-specific input onto neurons in primary somatosensory cortex. *Journal of Neurophysiology*, *102*(3), 1843–1853. https://doi.org/10.1152/jn.00235.2009
Pubols, B. H. (1982). Factors affecting cutaneous mechanoreceptor response. I. Constant-force versus constant-displacement stimulation. *Journal of Neurophysiology*, *47*(3), 515–529.
Pubols, L. M., & Pubols Jr, B. H. (1973). Modality composition and functional characteristics of dorsal column mechanoreceptive afferent fibers innervating the raccoon's forepaw. *Journal of Neurophysiology*, *36*(6), 1023–1037. Retrieved from http://www.scopus.com/inward/record.url?eid=2-s2.0-0015734004&partnerID=40&md5=33538e01482d93f406b7663ffaf09e61
Shin, H., Park, S., Son, J., & Sohn, J. (1995). Responses from new RF of VPL neurons following deafferation (anesthesia vs amputation, rat).pdf. *Neuroreport*, *7*, 33–36.
Sinclair, R. J., Sathian, K., & Burton, H. (1991). Neuronal responses in ventroposterolateral nucleus of thalamus in monkeys (Macaca mulatta) during active touch of gratings. *Somatosensory & Motor Research*, *8*(4), 293–300. https://doi.org/10.3109/08990229109144753
Strzalkowski, N. D. J., Mildren, R. L., & Bent, L. R. (2015). Thresholds of cutaneous afferents related to perceptual threshold across the human foot sole. *Journal of Neurophysiology*, *114*(4), 2144–2151. https://doi.org/10.1152/jn.00524.2015
Wedell, C. H., & Cummings, S. B. . J. (1938). Fatigue of the vibratory sense. *Journal of Experimental Psychology*, *22*(5), 429–438. https://doi.org/10.1037/h0059105
Whitsel, B. L., Kelly, E. F., Quibrera, M., Tommerdahl, M., Li, Y., Favorov, O. V, … Metz, C. B. (2003). Time-dependence of SI RA neuron response to cutaneous flutter stimulation. *Somatosensory & Motor Research*, *20*(1), 45–69.

https://doi.org/10.1080/0899022031000083834

Whitsel, B. L., Kelly, E. F., Xu, M., Tommerdahl, M., & Quibrera, M. (2001). Frequency-dependent response of SI RA-class neurons to vibrotactile stimulation of the receptive field. *Somatosensory & Motor Research*, *18*(4), 263–285. https://doi.org/10.1080/01421590120089 65

Whitsel, D. L., Favorov, O. V, Kelly, D. G., & Tommerdahl, M. (1991). Mechanisms of Dynamic Peri- and Intra-columnar Interactions in Somatosensory Cortex: Stimulus-specific Contrast Enhancement by NMDA Receptor Activation. In O. Franzén & J. Westman (Eds.), *Information Processing in the Somatosensory System: Proceedings of an International Symposium at the Wenner-Gren Center, Stockholm, 3-5 July, 1989* (pp. 353–369). London: Macmillan Education UK. https://doi.org/10.1007/978-1-349-11597-6_26

### 3.9 Figures and Captions

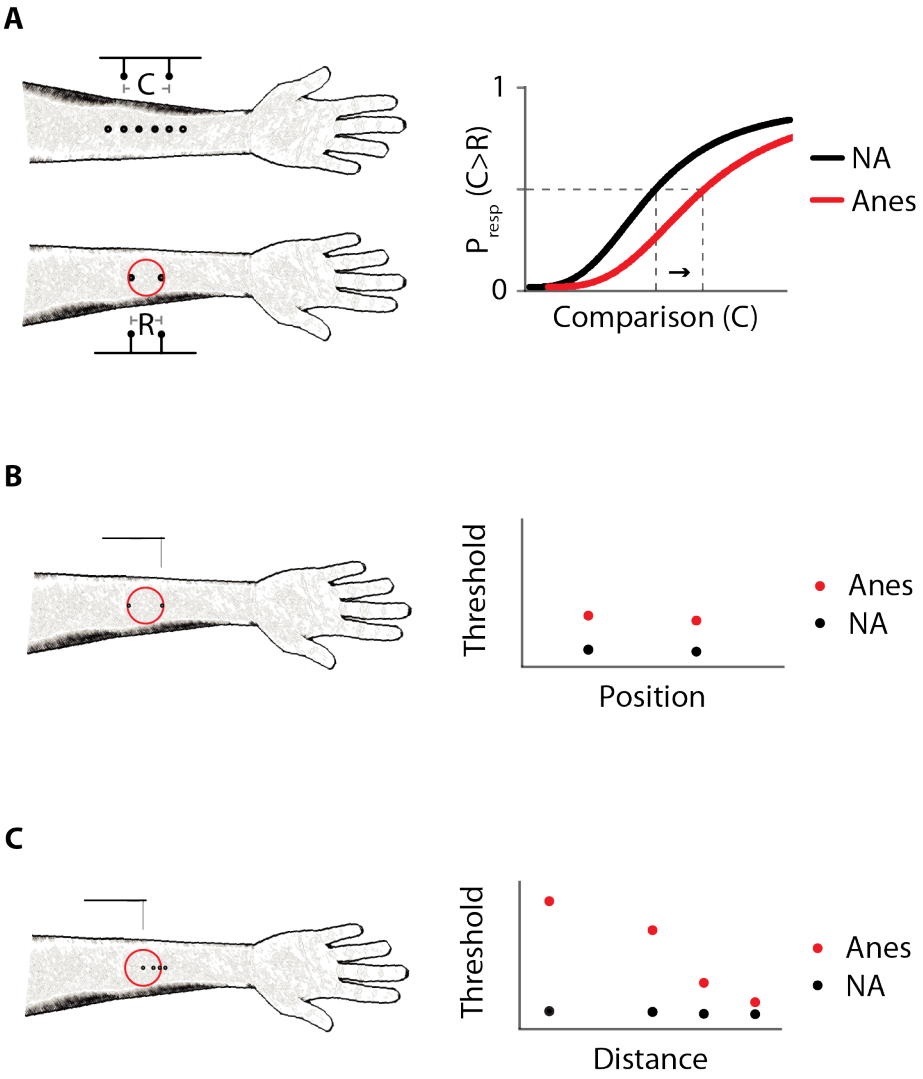


**Figure 1**. Experimental protocols (left) and expected results (right). Black: no anesthesia (NA). Red: anesthesia (Anes). Red circle: area of anesthesia. (**A**) Two-point distance comparison (day 1). Left: Participants compared the perceived distance between two point-stimuli applied on the forearms successively. On the right arm, the points were separated by a fixed reference distance (R = 30 mm); on the left arm, the points were separated by a variable comparison distance (C = 6, 12, 18, 24, 30, 36, 42, 48, or 54 mm). Right: expected psychometric function. Horizontal axis: comparison distance, C. Vertical axis: proportion of trials in which the participant responds that C is greater than R,

$P_{resp}(C>R)$. The point of subjective equality (PSE; vertical dashed line) is the value of C for which $P_{resp}(C>R) = 0.5$ (horizontal dashed line); the expected PSE is equal to R without anesthesia, and increases following anesthesia. (**B**) Monofilament detection at two reference points (day 1, "M2pts"). Left: Participants reported in which of two intervals they felt a monofilament stimulus on the right forearm. Detection threshold was measured at two skin sites (small dots) equidistant from centre of anesthesia; these sites coincided in position with the reference points in the distance-comparison task. Right: moderate threshold elevation (sensitivity reduction) expected at positions of reference points caused by anesthesia. (**C**) Monofilament detection at four points (day 2, "M4pts"). Similar to M2pts on day 1, but measured thresholds at a variety of distances from centre of anesthesia. Left: four test sites 0, 10, 15, and 20 mm from centre of anesthesia. Right: expected tactile sensitivity reduction as a function of distance. All tasks were tested on the same 20 participants (within-subjects design).

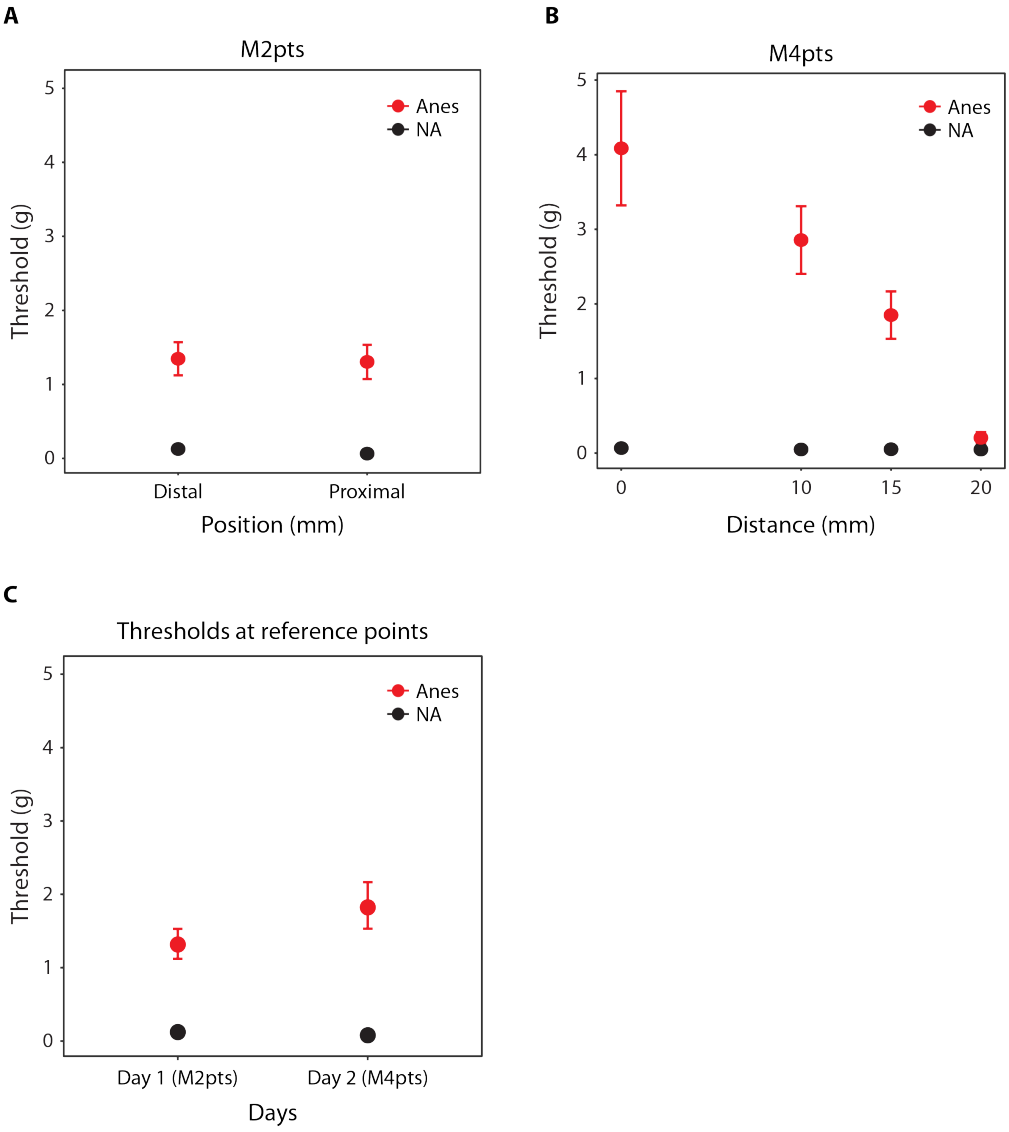


**Figure 2**. Monofilament detection results. Vertical axis: Mean 71% correct 2IFC detection threshold (in gram force) measured via a 2-down 1-up staircase procedure; values were calculated by averaging the reversal points in the last half of trials. Black: no anesthesia. Red: anesthesia. (**A**) M2pts (day 1). Thresholds at two reference points symmetric about and equidistant (15 mm) from centre of anesthesia; one point was proximal and the other distal to the centre. (**B**) M4pts (day 2). Thresholds at four distances from centre of anesthesia. (**C**) Thresholds at the reference points, day 1 vs. day 2. Average results from M2pts (day 1) were compared to results at 15-mm distance from M4pts (day 2). N=20 participants. Error bars: ±1 SE (when error bars are not visible, it is because they are smaller than the data point circles).

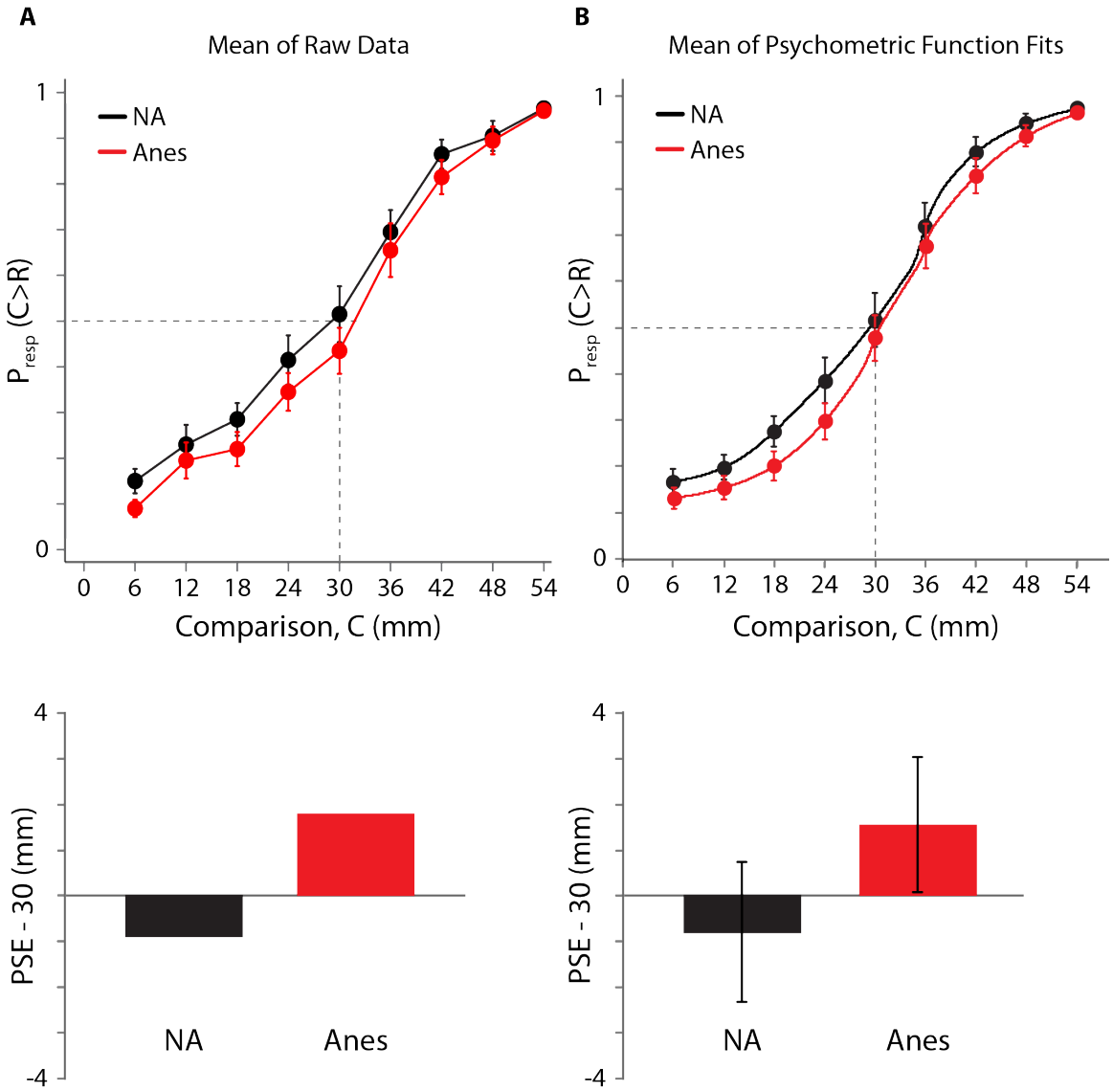


**Figure 3**. Two-point distance comparison results. Black: no anesthesia. Red: anesthesia. (**A**) Top: Mean of raw data. Horizontal axis: comparison distance (mm). Vertical axis: proportion of trials on which the comparison distance (C) was perceived as greater than the reference distance (R = 30 mm). Dashed lines: $P_{resp}(C>R) = 0.5$ and C = 30 mm. Bottom: For each testing block, the difference between 30 mm and the mean PSE, estimated by linear interpolation of the mean data (top). (**B**) Top: Mean of the participants' individual best-fitting psychometric functions. Bottom: Difference between 30 mm and the mean of the PSEs extracted from the participants' individual best-fitting psychometric functions. N=20 participants. Error bars: ±1 SE (when error bars are not visible, it is because they are smaller than the data point circles).

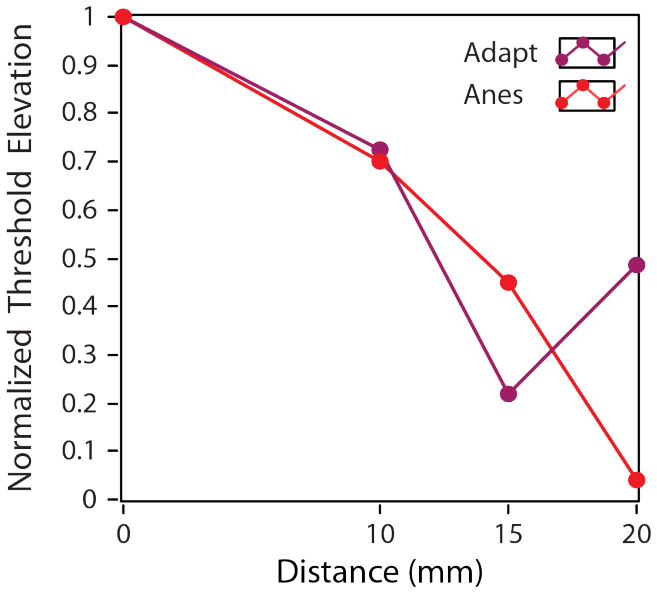


**Figure 4**. Normalized threshold elevation by anesthesia vs. adaptation as a function of distance from centre of anesthesia or adaptation. Data points depict the mean elevation of 71% correct detection threshold at each distance, (Anes – NA) or (Adapt – NA), normalized by the maximum mean elevation in the corresponding experiment. Anes: experiment M4pts described in this chapter. Adapt: experiment 2B in Chapter 2, using 40 s adaptation plus 3 s top-ups (i.e. "A3") as the adaptation protocol. N = 20 participants in each experiment.

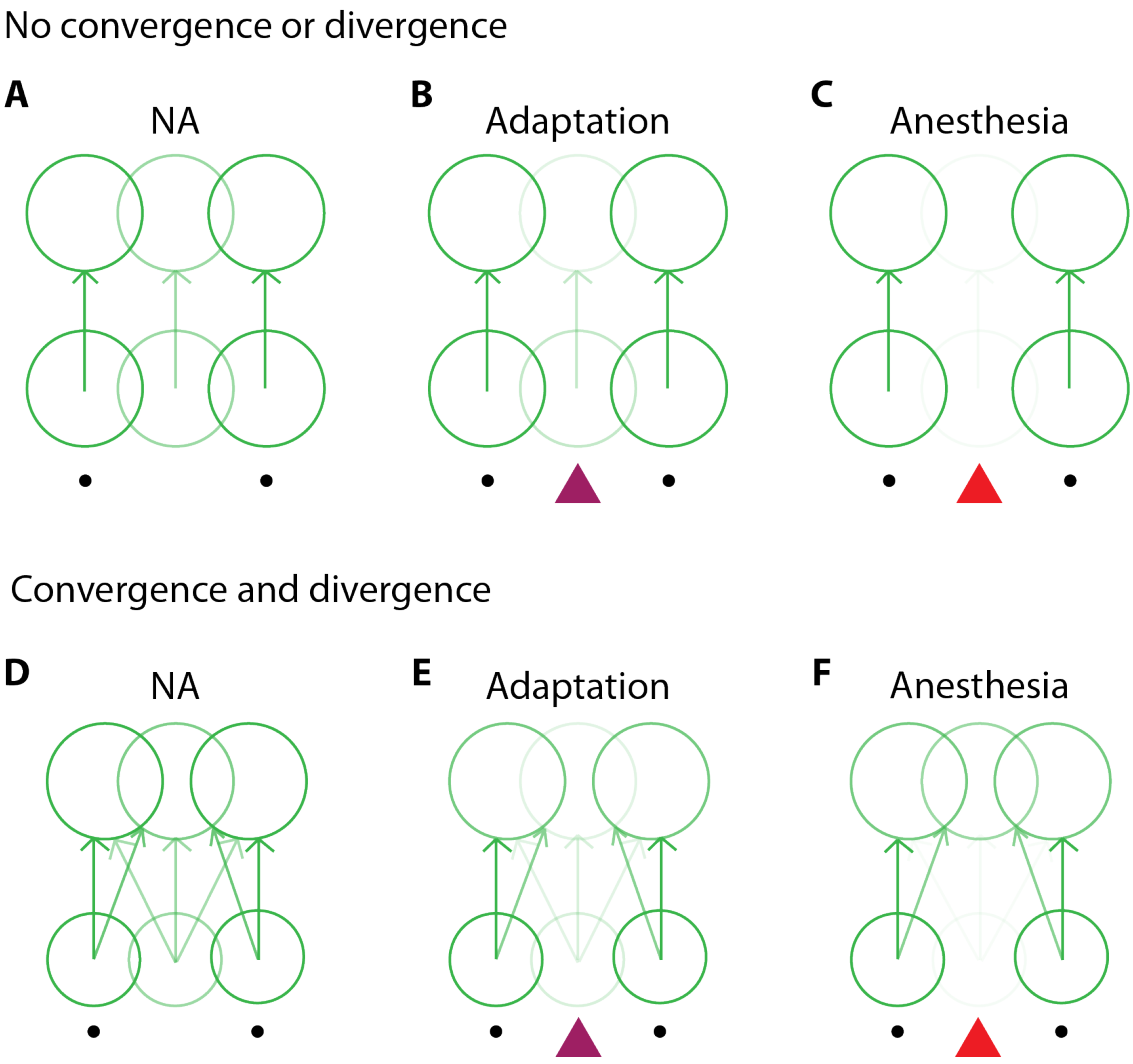


**Figure 5**. A simple schematic model for adaptation vs. anesthesia effects on tactile spatial perception. Circles in bottom row: afferent RFs. Circles in top row: cortical neuronal RFs. Arrows: input of afferent responses evoked by a two-point stimulus (black dots). Colour saturation: strength of response to the two-point stimulus. For visual clarity of illustration, the perimeter of each circle represents the contour of half-maximal firing instead of the full RF to reduce appearance of overlap, and the two-point stimulus is depicted beneath the afferent RFs. **Top panels**: scenario consistent with our original hypothesis. (**A**) Baseline (no-adaptation or no-anesthesia). (**B**) Vibrotactile adaptation. (**C**) Topical anesthesia. In the absence of convergence or divergence of peripheral input, either adaptation (magenta triangle) or anesthesia (red triangle) of an afferent RF (middle dim circle in bottom row) leads to reduced responsivity in the RF of the cortical neuron it projects to (middle dim circle in top row). The stronger response of the lateral cortical RFs (bright circles in top row) would result in a repulsion in perceived separation

between points straddling the desensitized skin region. **Bottom panels**: scenarios that hypothetically account for the observed discrepancy between adaptation and anesthesia on two-point distance perception. Peripheral input converges and diverges to different cortical neurons, causing cortical RFs to be larger and overlap more than afferent RFs. (**D**) Baseline. (**E**) Vibrotactile adaptation. Repetitive firing of an afferent RF caused by vibration adapts the cortical neuron it primarily projects to. The adapted cortical neuron responds less to the subsequent two-point stimulus. Responses of the lateral cortical neurons that receive input from the adapted afferent are slightly suppressed but stronger than the middle cortical neuron's response. The polarized distribution of cortical population activity gives rise to a repulsion illusion. (**F**) Topical anesthesia. The middle afferent's firing is reduced, but the cortical neurons are not adapted, and are subsequently activated by input from the adjacent unanesthetized afferents. The relative distribution of cortical population activity is similar to that in baseline and thus does not result in a repulsion illusion.

# CHAPTER 4

# COMPUTATIONAL MODELING

## 4.1 Preface

In previous chapters, with psychophysical testing in human participants, we showed that tactile spatial perception is subject to an adaptation-induced repulsion illusion that expands the perceived distance between points on the skin (Chapter 2). This illusion, however, was not observed when the intervening skin was desensitized with topical anesthesia instead of vibrotactile adaptation (Chapter 3). These empirical findings raised the question: What possible mechanisms underlie the spatial repulsion illusion or lack thereof? In this chapter, we investigated this question on a theoretical and computational basis. We constructed Bayesian perceptual models that simulated the responses of somatosensory cortical neurons and performed the psychophysical tasks with which we tested human participants.

We showed that with specific sub-optimal constraints, the Bayesian observer quantitatively replicated human performance. The Bayesian observer exhibited a repulsion illusion following adaptation in the two-point distance comparison task, which was comparable to the spatial repulsion illusion empirically observed in Chapter 2. In general, this illusion emerged when the observer decoded the spatial input without awareness of the adaptation in the encoding stage.

## 4.2 Abstract

We take for granted our ability to perceive the external world via touch, but how does the somatosensory system accomplish this feat, and how does adaptation change tactile perception? In this chapter, we investigated these questions from an information-processing perspective using computational simulations. We constructed a Bayesian perceptual model that characterized tactile perception as comprising two information-processing stages: encoding and decoding. The encoder (the generative model) simulated the responses of somatosensory cortical neurons to point-stimuli on the skin. It incorporated receptive field properties such as spacing, size, and firing variability. In addition, it simulated adaptation as graded firing reduction in the population of neurons at the encoding stage. The decoder applied Bayesian inference to interpret the simulated neural data from the encoder, and made probabilistic estimates of the stimulus attributes, such as the distance between two point-stimuli and the indentation strength of a point-stimulus. It then used the probabilistic estimates to perform two-point distance discrimination or monofilament detection, psychophysical tasks with which we tested human participants. The model replicated human performance without or with adaptation. In simulations, adaptation elevated detection thresholds and induced a repulsion illusion in the perceived two-point distance; these effects were consistent with the empirical observations. Different combinations of receptive field properties could give rise to similar results, suggesting that neurons with a diversity of receptive field properties are similarly susceptible to the general adaptation effects. Moreover, the model suggested that the repulsion illusion emerged via a suboptimal decoder that was unaware of the adaptive changes at the encoding stage. We discuss possible neural substrates underlying the model performances, as well as assumptions and alternative constructions of the model. The adaptation effect on tactile spatial perception is consistent with computational and empirical findings in the visual adaptation literature, which may point to common or similar mechanisms for spatial processing and for focal adaptation effects between touch and vision.

## 4.3 Introduction

How does the somatosensory system translate raw tactile information into perception, and how is this process subject to the influence of recent sensory experience, such as adaptation? These unsolved questions carry fundamental importance to the understanding of touch. Neurophysiological and psychophysical studies, among other empirical research, have helped to shed light on these questions by revealing bits and pieces of the puzzle. However, it remains largely unknown how the somatosensory system represents tactile features and what computational principles plausibly link these representations to perception. It is difficult to directly address these questions via experiments on humans or non-human animals. A promising alternative to the empirical research is computational

modeling, which uses mathematical principles and stimulations to tackle neural coding and perceptual strategies.

In a perceptual task, an observer's performance is limited by the uncertainty inherent in various stages of information processing. Sources of uncertainty include ambiguous stimuli, low receptor density, sensory neural noise, and variability in the decoding circuits. This omnipresent uncertainty makes probabilistic frameworks attractive for modeling perception (Rao et al. , 2002; Geisler, 2011). A powerful probabilistic framework is *Bayesian inference*. Bayesian inference provides a unified, coherent framework for optimally quantifying uncertainty and the interplay between uncertainty at different processing stages. Bayesian perceptual models can quantitatively characterize information constraints for a given perceptual task, thereby generating testable predictions for human performance (Rao et al., 2002).

A Bayesian observer represents information in probability mass functions or probability density functions. A probability mass function represents information among a distinct or discretized set of possible scenarios, such as categories of stimuli. A probability density function represents information from a continuous stimulus property, such as motion velocity. In this chapter and the rest of the thesis, we will refer to both probability mass function and probability density function with the general term probability distribution function, or PDF for short. Three major components of PDFs in Bayesian computations are prior, likelihood, and posterior. To illustrate the basic structure of these components, consider as an example the simple tactile task of localizing a point-stimulus on the skin. A Bayesian observer would represent the perceived *stimulus* position not as a simple value *S*, but as a conditional PDF, p($\boldsymbol{S}|\boldsymbol{R}$), where $\boldsymbol{R}$ represents the *responses* evoked in the sensory neurons. This PDF, p($\boldsymbol{S}|\boldsymbol{R}$), is known as posterior probabilities. Loosely speaking, p($\boldsymbol{S}|\boldsymbol{R}$) specifies the probabilities that the stimulus is at different positons, given the observed sensory neural data. The observer's task is to estimate the stimulus position based on the sensory neural data $\boldsymbol{R}$. It would choose the position value $\hat{S}$, among all possible values $\boldsymbol{S}$, that gives the highest posterior probability as its estimate for the stimulus position:

$$\hat{S} = argmax[p(\boldsymbol{S}|\boldsymbol{R})]$$

Here, arg max[*f(x)*] denotes the procedure of finding the value of *x* (the argument) for which *f(x)* reaches its maximum value (regular letters denote single values, whereas boldfaced letters denote vectors).

To compute the posterior probability for a stimulus position $S_i$, the observer uses Bayes' formula:

$$p(S_i|\boldsymbol{R}) = \frac{p(\boldsymbol{R}|S_i)p(S_i)}{p(\boldsymbol{R})}$$

where the conditional probability $p(\boldsymbol{R}|S_i)$ is the likelihood function, and $p(S_i)$ is the prior probability for $S_i$. The likelihood function represents the sensory neural measurement of the stimulus position. The prior probabilities represent the statistical properties of the sensory environment and the stimulus, as well as the observer's knowledge, experience, or expectation regarding these properties. The probability in the denominator, $p(\boldsymbol{R})$, is a sum of joint probabilities and represents all possible scenarios that could lead to the observed sensory neural data $\boldsymbol{R}$:

$$p(\boldsymbol{R}) = \sum_{j=1}^{n} p(\boldsymbol{R}|S_j)p(S_j)$$

This term is a constant that is the same for all $S_i$, and therefore does not affect the perceptual estimate. Its role is to normalize the posterior distribution so that the distribution represents the relative probabilities for different stimulus positions, and the relative probabilities sum to one. Combining the likelihood functions and the prior probabilities, the Bayesian observer optimally estimates the stimulus property under given constraints.

A growing body of research in theoretical neuroscience and psychophysics has suggested that humans perform perceptual tasks in a Bayesian or Bayesian-like fashion (for reviews, see Rao et al., 2002; Knill & Pouget, 2004; Doya et al., 2007; Colombo & Seriès, 2012). Specifically, human observers take into account information uncertainty in a manner that is predictable by Bayesian inference. Bayesian modeling has proven fruitful in research on visual perception, cue combination, and sensorimotor control. In the past several years, studies from our laboratory have applied Bayesian modeling to investigate passive tactile perception. The Bayesian models proposed by our laboratory have successfully replicated human performance in tactile orientation perception (Peters et al., 2015) and tactile spatiotemporal perception (Goldreich, 2007; Goldreich & Tong, 2013; Tong et al., 2016). In addition, the spatiotemporal models have helped explain a variety of tactile spatiotemporal illusions, including the cutaneous rabbit illusion (Geldard & Sherrick, 1972), where the perceived distance between rapidly succeeding point-stimuli is distorted.

Inspired by the literature, in this chapter we applied Bayesian perceptual modeling to explore factors that may contribute to adaptation-induced effects in tactile perception. We modeled tactile perception as a probabilistic inference consisting of two information-processing stages: encoding and decoding. The encoding models generated firing for a population of simulated somatosensory cortical neurons in response to simulated tactile stimuli. These models incorporated receptive field (RF) characteristics of neurons in the primary somatosensory cortex (S1), such as RF spacing, size, and maximum responsivity, and accounted for response variability with realistic neuronal noise. The decoding models interpreted the noisy population response to infer the task-relevant stimulus attributes, and performed the perceptual tasks described in previous chapters (two-point distance comparison, monofilament detection). We manipulated the constraints imposed on the

Bayesian observer, which have anatomical and physiological bases, and compared the model performance with the psychophysically measured human performance. We thereby investigated how different factors individually or collectively affected perception and yielded human-like performance.

## 4.4 Methods

We constructed Bayesian perceptual models that performed psychophysical tasks under different adaptation conditions. Each model comprised two components: encoder and decoder. The encoder simulated population response of S1 neurons to point-stimuli on the forearm skin. This forward-processing stage was stochastic: noise was added to the spike counts to simulate the response variability in the cortex (Poisson-like, high variability). The decoder was a Bayesian observer that calculated the most probable stimulus attributes that gave rise to the population response, such as the stimulus indentation depth or the two-point distance.

### 4.4.1 Encoding models

The goal of the encoding models was to transform the physical attributes of simulated tactile stimuli into simulated spiking patterns, based on the structural and response properties of modeled RFs. For simplicity, we simulated only the *cortical* neurons with RFs on the forearm, and we used a single layer of RFs. We did not model the anatomical connectivity from periphery to cortex.

#### 4.4.1.1 Modeling cortical RF response to point stimulation on the forearm

We modeled RFs of S1 neurons in a 150 x 10 mm patch of simulated forearm skin. The RF centre of a neuron $i$ was determined two-dimensionally by its position ($x_i$, $y_i$) on the skin patch. The x-axis (150 mm) was defined as the longitudinal axis along the forearm, and the y-axis (10 mm) was the transverse short axis across the forearm. There was always an RF centre located at the centre of the 150 x 10 mm patch, i.e. at the position (75, 5). The other RF centres were arranged symmetrically to this central RF and within the size of the skin patch. By default, we used a single line of evenly distributed Gaussian RFs along the midline (y = 5 mm) of the patch width (Fig. 1A). The spacing between two adjacent cortical RF centres, namely, *RF spacing* (Fig. 1B), was a free parameter for data fitting, with a range of 5 - 75 mm (see 2.6 Discussion for the rationale for choosing these default settings, and for impact on model performance from alternative settings).

A point stimulus was defined by its position ($x$, $y$) on the skin patch and its indentation strength, $s$. The default stimulus duration was 200 ms. The evoked spike count, $c$, was modeled as a Gaussian function of distance from the neuron's RF centre:

$$c_i = Ae^{\frac{-d_i^2}{2\sigma^2}} \tag{1}$$

where $c_i$ was the expected spike count of a neuron $i$ in response to a point stimulus with a Euclidean distance $d_i$ to the neuron's RF centre; $d_i = \sqrt{(x - x_i)^2 + (y - y_i)^2}$ , where ($x$, $y$) was the point stimulus' position, and ($x_i$, $y_i$) was neuron $i$'s RF centre position.

This Gaussian function was centred at $d = 0$ and had two free parameters, $\sigma$ and $A$. $\sigma$ was the standard deviation (SD) of the Gaussian function, and was a free parameter ranging 5 - 70 mm for data fitting (Fig. 1C). $A$ was the Gaussian amplitude, which was the expected spike count at the RF centre (i.e. at $d = 0$). $A$ was described as a power function of the stimulus strength $s$:

$$A = K(s)^n \tag{2}$$

where $K$ was a constant of proportionality, and n was the slope of the fitted straight line for the A-s relation in log-log coordinates. This was based on Werner & Mountcastle (1965), which studied the stimulus-response relation of mechanoreceptive afferents in the hairy skin of monkeys and cats. The authors reported that for the majority of the afferents studied, the increase in firing rate negatively accelerated with increasing stimulus strength, a trend that could be nicely fitted with a power function with $n < 1$.

Because the values for $K$ and $n$ varied from neuron to neuron, we used the normalized version of Equation (Eq.) (2), adapted from Werner & Mountcastle (1965):

$$\frac{A}{A_{max}} \propto (\frac{s}{s_{max}})^n \tag{3}$$

where each of $A$ and $s$ was expressed as percentage of its corresponding maximum value used in the simulations. For Gaussian amplitude $A$ (i.e. the expected spike count at RF centre), the maximum value $A_{max}$ was a free parameter for data fitting (Fig. 1D). For stimulus strength $s$, the maximum value $s_{max}$ was specified by the human psychophysics experiment: for the two-point distance-comparison task, the force was constant at 40 g for each point; for the monofilament-detection task, the biggest monofilament used was 10 g for the adaptation experiment (Chapter 2).

We simplified Eq. (3) using the best-fitting parameter values estimated by Werner & Mountcastle (1965) based on pooled data from 10 mechanoreceptive afferents. The best-fitting version of Eq. (3) was:

$$\frac{A}{A_{max}} = 1.0(\frac{s}{s_{max}})^{0.52} \quad (4)^4$$

where $A$ and $s$ were each normalized by their corresponding maximum value. For a given $A_{max}$ , $s$, *and* $s_{max}$, we used Eq. (4) to determine $A$, and substituted $A$ into Eq. (1) to calculate the evoked spike count.

Next, we added cortical spontaneous activity to the evoked spike count. The median spontaneous firing rate in S1 has been reported to be 10 spikes per second by Romo and colleagues (Vázquez et al 2013). Accordingly, because our default stimulus duration was 200 ms (1/5 of 1 s), we added 2 spikes (1/5 of 10 spikes) to the expected evoked spike count, $c$, to obtain the total expected spike count, $\lambda$.

When the simulated perceptual task involved a single point-stimulus, the expected spike count $\lambda$ was determined as described above. When the task involved two simultaneous point-stimuli, the default was to simply sum the numbers of expected spikes:

$$\lambda = \lambda_1 + \lambda_2 \quad (5)$$

where $\lambda_1, \lambda_2$ were the expected spike counts evoked by the first and second point, respectively. Here, we assumed there was no inter-stimulus interaction that suppressed the firing.

Cortical response is highly variable; therefore, we added noise to the expected spike count to simulate cortical response variability. Johnson and colleagues reported that S1 area 3b neuronal noise is Poisson-like (Sripati et al. 2006). That is, the variance of the firing rate is roughly equal to the mean of the firing rate. Accordingly, we added Poisson noise by sampling from a Poisson distribution whose mean and variance equaled the expected spike count. The probability of neuron $i$ firing $k_i$ number of spikes, given the expected spike count $\lambda_i$, was

$$p(k_i|\lambda_i) = \frac{\lambda_i^{k_i}\, e^{-\lambda_i}}{k_i!} \quad (6)$$

Put in other words, for a neuron $i$ on a trial, the encoder randomly drew a spike count, $k_i$, from a Poisson distribution with a probability defined by the above formula. $k_i$ therefore

[4] Owing to what may have been rounding errors in Werner & Mountcastle (1965), the actual value used in our simulations for the constant 1.0 in Eq. (4) was 1.03. However, it should have very little effect on the simulation results.

varied stochastically from trial to trial even for the same underlying $\lambda_i$. Here, we assumed that the responses were conditionally independent across neurons and across trials. Finally, the encoder passed the collection of noisy spike counts from all neurons, $\boldsymbol{k}$, to the decoder. $\boldsymbol{k}$ represents the noisy population response in the sensory system.

#### 4.4.1.2 Modeling adaptation

We modeled adaptation as a reduction in the spike count of neurons that were affected by the adapting stimulus. The reduction was partly determined by the degree of adaptation, which we called *adaptation state*, and denoted $\alpha$. Following adaptation, the expected spike count for neuron *i* to a 200-ms *test* stimulus was

$$c_{i,test,adapted} = c_{i,test,unadapted}\left(1 - \frac{c_{i,adaptor(d)}}{c_{i,adaptor(0)}} * \alpha\right) \tag{7}$$

where $c_{i,test,unadapted}$ was neuron *i*'s unadapted expected spike count to the *test* stimulus, as defined in Eq. ((1)). $c_{i,adaptor(d)}$ was the neuron's unadapted expected spike count to the *adapting* stimulus (i.e. the adaptor). $c_{i,adaptor(0)}$ was the expected spike count if the adapting stimulus had occurred at the neuron's RF centre, which was the neuron's maximum expected spike count to the adapting stimulus. $\alpha$ ranged from 0 to 1, with 0 meaning completely unadapted, and 1 meaning completely adapted.

In the psychophysical experiments, the adapting probe surface was hemispherical with a radius of 9.5 mm (JVP dome, Stoelting Co.). The adapting probe was quite large compared to the test stimulus, which has a spherical surface with a radius of 0.75 mm. The adapting probe's gently curved surface likely caused an approximately even deformation in the skin it contacted, thus eliminating stronger activation that would have been caused by the perimeter or edge of a flat probe (Phillips & Johnson, 1981). Accordingly, the model by default assumed that any skin region under the hemispherical probe surface (radius = 9.5 mm) was uniformly adapted; in other words, all RFs whose centres fell within the circular area with an origin at the adaptation centre and a radius of 9.5 mm were assumed to adapt to the same extent (Fig. 1A). $c_{i,adaptor(d)}$ for RFs outside this circular area was calculated based on the distance from the RF centre to the circumference (instead of the origin) of the circle, with a modified version of Eq. ((1)):

$$c_{i,adaptor(d)} = Ae^{\frac{-(d_i-9.5)^2}{2\sigma^2}} \tag{8}$$

In other words, the expected activation by the adapting stimulus of a RF outside the circular area was a Gaussian function as a distance from the RF centre to the

circumference of the circle (Fig. 1A). We then substituted $c_{i,adaptor(d)}$ into Eq. (7). Another term in Eq. (7), $c_{i,adaptor(0)}$, was calculated using the original Eq. ((1)) for RFs outside as well as inside the circle, because by definition $c_{i,adaptor(0)}$ represented the expected spike count to a stimulus that occurred at the RF centre. The $A$ parameter in $c_{i,adaptor(d)}$ and $c_{i,adaptor(0)}$ was calculated using Eq. (4) with the assumption that the adapting stimulus strength equaled the maximum test stimulus force used in the corresponding task (40 g for each point stimulus in the distance-comparison task, 10 g for the filament-detection task). However, the exact value of the adapting stimulus strength had no impact on the simulation results, because it was present in both $c_{i,adaptor(d)}$ and $c_{i,adaptor(0)}$ in Eq. (7) and therefore cancelled out; in our model, only the relative adaptation states affected the perception. The strength of adaptation was modeled not by specifying the vibrotactile adaptation magnitude or duration, but simply by specifying the adaptation state.

In Eq. (7), both the adaptation state, $\alpha$, and the spike count evoked (previously) by the adaptor, $c_{i,adaptor(d)}$, served as scaling factors for the amount of reduction in spike count. $\alpha$ represented the general state of adaptation in the system; it scaled the responsivity of the entire system. $c_{i,adaptor(d)}$ represented how strongly the specific neuron was affected by adaptation; it scaled the impact of $\alpha$ for each neuron individually. The rationale for $c_{i,adaptor(d)}$ was that the more strongly the neuron was previously activated by the adapting stimulus, the greater reduction in firing would occur following adaptation. $c_{i,adaptor(d)}$ was normalized by $c_{i,adaptor(0)}$, the maximum response of the neuron to the adaptor. The greater the distance between the neuron's RF centre and the adaptor, the smaller the ratio of $c_{i,adaptor(d)}$ to $c_{i,adaptor(0)}$ was. Taken together, these three terms in Eq. (7) specified how adaptation selectively affected individual neurons: the general adaptation state in the system ($\alpha$) was scaled by each neuron's response to the adapting stimulus ($c_{i,adaptor(d)}$) relative to its maximum response that would have resulted if the adapting stimulus had occurred at the neuron's RF centre ($c_{i,adaptor(0)}$). For simplicity, we assumed that $\alpha$ was invariant across time.

### 4.4.2 The Bayesian decoders

The decoding models were Bayesian observers that inferred the task-relevant stimulus parameters (two-point distance, point position, indentation strength) from the simulated neural data. A Bayesian decoder took in the noisy population response from the encoder, hypothesized about the task-relevant stimulus parameters, calculated each neuron's likelihood of generating a certain number of spikes, pooled the likelihoods from all neurons to generate the joint likelihood for the population response, interpreted the joint likelihood in light of prior expectations, and estimated the relative probabilities (posterior PDF) for different hypothesized stimulus parameters. The decoder then used the posterior

PDF to perform simulated perceptual tasks, such as comparing two-point distances or detecting a stimulus.

We assumed that the decoder knew the following parameters from the encoding stage: 1) RF properties, such as the x- and y-positions of the RFs, RF spacing, and shape; 2) the Gaussian response function (Eq. ((1))), the standard deviation ($\sigma$), and the expected firing rate at the RF centre ($A$); 3) in the case of two simultaneous point-stimuli, how the RFs combined the spikes from the points (summation by default, Eq. (5)); 4) the structure of the firing noise was Poisson (Eq. (6)). Furthermore, like the encoder, the decoder assumed that the spike counts were conditionally independent across neurons and across trials given a stimulus.

#### 4.4.2.1 Task 1: two-point distance comparison

This task assessed tactile perception of distance between point-stimuli without or with adaptation to the intervening skin between the points. In a two-interval forced-choice (2IFC) task, the simulated forearm skin was "tapped" twice, each time with a pair of simultaneous point-stimuli, and the Bayesian observer had to determine which pair of point-stimuli had the greater separation distance. One of the distances was fixed at 30 mm (reference), and the other distance was variable from 6 to 54 mm in increments of 6 mm (comparison). Each point-stimulus exerted a simulated force of 40 g. These settings were identical to the 2IFC distance-comparison psychophysical experiments described in Chapters 2 and 3. To perform the task, the Bayesian observer first calculated the posterior PDF for each of the distances. It then compared the two posterior PDFs to determine which distance was greater.

Specifically, the Bayesian observer began by hypothesizing about the two-point distance, $\Delta x$, with the simplifying assumption that the points were symmetrical to a fixed midpoint. In the psychophysical experiments, we applied two-point stimuli symmetrically to a fixed midpoint marked on either forearm. Here, we chose the midpoint of the RF line, 75 mm, to be the fixed midpoint. Let us denote the x-positions of the first and second point stimulus as $x_1$ and $x_2$, respectively; then $x_1$ = 75 - (1/2)$\Delta x$, and $x_2$= 75 + (1/2)$\Delta x$. The observer considered a discrete set of hypotheses for $\Delta x$ with intervals of 1 mm, for example, $\Delta x$ = 1, 2, 3, …,150 mm, and assumed uniform priors over $\Delta x$. For a particular hypothesized distance, $\Delta x_m$, due to taps at ($x_{1m}$, $x_{2m}$), the likelihood of observing spike count $k_i$ from neuron $i$ is given by the Poisson formula:

$$p(k_i|\Delta x_m) = p(k_i|x_{1m}, x_{2m}: \lambda_i) = \frac{\lambda_i^{k_i}\, e^{-\lambda_i}}{k_i!} \tag{9}$$

where $\lambda_i$ was calculated using Eqs. (1), (4), and (5); the value of $\Delta x$ affected $\lambda_i$ via affecting the distance between the stimuli and RF centres. Next, the joint likelihood of

observing a set of spike counts, $\boldsymbol{k}$, from the neural population was equal to the product of the likelihoods from individual neurons:

$$p(\boldsymbol{k}|\Delta x_m) = \prod_i p(k_i|x_{1m}, x_{2m}: \lambda_i) = \prod_i \frac{\lambda_i^{k_i} e^{-\lambda_i}}{k_i!} \tag{10}$$

Here, $\boldsymbol{k}$ is the observed population response. An example of the population response on a random trial is shown in Fig. 2B.

The Bayesian observer then combined the likelihoods with prior probabilities over the hypothesized distance. By default, the observer assumed uniform priors for both the reference and comparison distances. It applied Bayes' formula to calculate the posterior PDF over $\Delta x$, given the population response $\boldsymbol{k}$:

$$p(\Delta x_m|\boldsymbol{k}) = \frac{p(\boldsymbol{k}|\Delta x_m)p(\Delta x_m)}{\sum_{\Delta x} p(\boldsymbol{k}|\Delta x)p(\Delta x)} \tag{11}$$

With the posterior PDF, the observer had not only a single best estimate for $\Delta x$ (the mode of the posterior PDF), but also a full probability distribution that reflected the relative levels of confidence for a range of estimates (Fig. 2C). Thus, the observer was able to calculate the probability that a given comparison distance was greater than the reference distance, by comparing the posterior PDFs for the comparison and the reference. To simplify the notation, let us denote the posterior PDF for the comparison distance, $p(\Delta x_{comp}|\boldsymbol{k})$, as $p(comp)$ for short, and the posterior PDF for the reference distance, $p(\Delta x_{ref}|\boldsymbol{k})$, as $p(ref)$. The probability that the comparison was perceived to be greater than the reference was represented by the area of the comparison PDF that was to the right of the reference PDF, which could be calculated as

$$p(comp > ref) = \int_{ref=0}^{\infty} p(ref) \left( \int_{comp=ref}^{\infty} p(comp) d_{comp} \right) d_{ref} \tag{12}$$

Conversely, the probability that the comparison was smaller than the reference was

$$p(comp < ref) = \int_{comp=0}^{\infty} p(comp) \left( \int_{ref=comp}^{\infty} p(ref) d_{ref} \right) d_{comp} \tag{13}$$

The observer then compared these two probabilities to make a perceptual decision. If

$p(comp > ref) > p(comp < ref)$, then the observer determined that the comparison was the greater distance of the two; if $p(comp > ref) < p(comp < ref)$, then it determined that the reference was the greater distance. In the case where the two probabilities were equal, the observer randomly picked one of the distances as the answer, with 50/50 probabilities (i.e. guessing).

On each trial, the observer compared the reference distance 30 mm with one of nine comparison distances: 6, 12, 18, 24, 30, 36, 42, 48, or 54 mm. There were 200 trials per comparison distance, and a total of 1800 trials, in each run of simulation. In the end of each simulation, we obtained a psychometric function which showed the proportion of "comparison is longer" responses at different comparison distances. We used the psychometric functions to compare the model performance with human performance.

#### 4.4.2.2 Task 2: single-point detection

We assessed the extent to which adaptation reduced tactile sensitivity by simulating a 2IFC detection task equivalent to the monofilament-detection task in Chapters 2 and 3. On each trial, the forearm skin was "tapped" with a single point-stimulus in one of two intervals, and the Bayesian observer had to determine which interval contained the stimulus. Each point-stimulus simulated a monofilament (also known as von Frey hair), which is force-calibrated to exert a constant force when applied. To simulate the stimulus forces, we mapped the whole set of monofilament forces applied in our psychophysical experiments into expected spike counts using Eqs. (1) and (4). Each monofilament force was translated into an expected spike count at the RF centre, i.e. the amplitude of the Gaussian response function, *A*. The *A* values for different monofilament forces are shown in Fig. 3A.

Four simulated skin sites were tested. They were 0, 10, 15, and 20 mm to the right of the midpoint of the line of RFs at the position (75, 5), and had the same y-position as the midpoint. In other words, the four sites were at the x-positions 75, 85, 90, and 95 mm, respectively, and their y-positions were all 5 mm (Fig. 3B). This setting was identical to that in our monofilament-detection experiments (Chapters 2 and 3). The four sites were tested consecutively in the order of 0, 10, 15, and 20 mm from the midpoint at x = 75 mm. An example of the population response on a random trial to a stimulus at x = 75 mm is shown in Fig. 3B.

To perform the task, on each trial the observer calculated the posterior PDF for each of the two intervals (stimulus, no stimulus), and compared the PDFs to determine which interval was more likely to contain a stimulus. To do so, the observer started with hypotheses about two parameters: stimulus x-position, *x*, and stimulus strength (force), *s*. For each parameter, the observer assumed uniform priors. The hypothesized x values ranged from 75 to 150 mm in intervals of 1 mm. This range covered the midpoint of the RF line and the x-positions to the right of the midpoint, because the four test sites were

either on the midpoint or to the right of it. The hypothesized *s* values ranged from the smallest to the largest monofilament force used in the psychophysical experiments, with more hypotheses in the lower force range, to reflect the fact that monofilaments are force-calibrated on a logarithmic scale and cluster in the lower force range. We tried using different *s* hypotheses within the full force range to fit human data, and found that the exact values of the hypotheses or how they were discretized had little effect on the model performance; thus, we chose a set of *s* hypotheses that exactly matched the actual monofilament force values used in our psychophysical experiments.

On each interval of each trial, the likelihood of observing a set of spike counts, $\boldsymbol{k}$, from the RF population given a joint-hypothesis, $(s_j, x_m)$, equaled the product of likelihoods of observing spike count $k_i$ from neuron $i$ when $\lambda_i$ spike count was expected under the joint-hypothesis:

$$p(\boldsymbol{k}|s_j, x_m) = \prod_i p(k_i|s_j, x_m: \lambda_i) = \prod_i \frac{\lambda_i^{k_i} e^{-\lambda_i}}{k_i!} \tag{14}$$

where the expected spike count $\lambda_i$ was calculated using Eqs. (1), (4), and (5). The observer then calculated the joint-posteriors over ($s$, $x$):

$$p(s_j, x_m|\boldsymbol{k}) = \frac{p(\boldsymbol{k}|s_j, x_m)p(s_j, x_m)}{\sum_{s,x} p(\boldsymbol{k}|s, x)p(s, x)} \tag{15}$$

To determine which interval contained the stimulus, the observer needed to estimate the stimulus strength, *s*; the other parameter, stimulus x-position, was a nuisance parameter whose main utility was to inform the estimation of *s*. Thus, the observer marginalized the joint-posteriors over *x* to obtain a posterior PDF for *s*:

$$p(s|\boldsymbol{k}) = \sum_x p(s, x|\boldsymbol{k}) \tag{16}$$

An example of this posterior PDF on a random trial is shown in Fig. 3C.

Due to spontaneous firing, some spikes were observed even in the interval where the stimulus was absent. On each trial, the observer calculated the posterior PDF for *s* for both intervals, and then compared the two PDFs to determine which interval was more likely to contain a stimulus. Let us denote the posterior PDF $p(s|\boldsymbol{k})$ as $p(S)$ for the interval with a stimulus, and as $p(NS)$ for the interval without a stimulus; *S* and *NS* represented the observed stimulus strength in the intervals respectively. Then, the area of the *S*-PDF that was to the right of the *NS*-PDF could be calculated as

$$p(S > NS) = \int_{NS=0}^{\infty} p(NS) \left( \int_{S=NS}^{\infty} p(S) d_S \right) d_{NS} \tag{17}$$

This represented the probability that the observer perceived a stronger stimulus in the interval that contained a stimulus than in the interval that did not. Conversely, the area of the *S*-PDF that was to the left of the *NS*-PDF could be calculated as

$$p(S < NS) = \int_{S=0}^{\infty} p(S) \left( \int_{NS=S}^{\infty} p(NS) d_{NS} \right) d_S \tag{18}$$

The observer then compared these two probabilities to make a perceptual decision. If $p(S > NS) > p(S < NS)$, then the observer answered correctly; if $p(S > NS) < p(S < NS)$, then it answered incorrectly. In the case where the two probabilities were equal, the observer randomly picked either interval as the answer, with 50/50 probabilities (i.e. guessing).

The stimulus force applied on each trial was adaptively adjusted based on whether the observer answered correctly on previous trials. We applied a 2-down 1-up staircase procedure: If the observer answered correctly for two consecutive trials, then the force applied on the next trial went down to the next-lower force. If the observer answered incorrectly on any trial, then on the next trial the next-higher force was applied. The 2-down 1-up staircase converges towards the observer's 71% correct detection threshold (Levitt, 1971). Furthermore, we used interleaved 2-down 1-up staircases to test the four skin sites on consecutive trials. For all sites, the first trial used a 0.07 g stimulus. The stimulus force applied at each test site on subsequent trials followed the staircase procedure based on the observer's responses at that site. For example, if the observer responded correctly for two consecutive trials on which the 0 mm site was tested, then the force applied on the next trial at that site went down to the next-lower force.

There were 200 trials in each run of simulation, 50 trials for each of the four test skin sites. The 71% correct detection threshold for each site was estimated by averaging the staircase reversal points in the last 25 of the 50 trials. If the last 50 trials contained no reversal points and the observer consistently gave correct responses, so the staircase dropped to and continued at the lowest monofilament force, we used that force (0.008 g) as the estimated threshold. The staircase procedure and the threshold estimation method were identical to those used in the experiments (Chapters 2 and 3).

#### 4.4.1.3 Decoder being aware or unaware of adaptation

We modeled adaptation as changes in RF responses in the encoding stage. How would this affect the model performance differently for different decoders? Importantly, we manipulated the decoder to be either aware or unaware of the state of adaptation in the encoder. An aware (optimal) decoder had full knowledge of the adaptation-induced changes in the encoder, and dynamically adjusted itself to match those changes in order to maintain an optimal readout. This type of optimal decoder is common in the neural coding literature. Computationally, being "aware" of adaptation means that the decoder had access to the adaptation components in the encoder. Specifically, it knew the adaptation state $\alpha$, and it calculated the expected evoked spike count, $c$, from each point-stimulus using the adapted version of the spike-count formulae, Eqs. (7) and (8), instead of the unadapted formula, Eq. ((1)).

By contrast, an unaware (suboptimal) decoder did not have access to the adaptation-related information in the encoder. Specifically, it assumed that the adaptation state was zero, and calculated each expected evoked spike count as if it was unadapted. As a result, the decoder had a fixed readout procedure regardless of the adaptive changes in the encoder. This fixed readout procedure was optimized for estimating the stimulus attribute in an unadapted condition, but it became suboptimal when it could not account for adaptation-induced changes and thus became mismatched to the adapted encoder; this mismatch can give rise to perceptual biases (for a review, see Seriès et al., 2009). A schematic diagram of the aware versus unaware decoder is shown in Figs. 6A and 6B.

### 4.5 Results

First, we fit the model to average human performance in the no-adaptation (NA) condition, and found the best-fitting RF parameter values given the model constraints. Then, we fit the model to data from the adaptation experiments, and replicated the empirically observed effects of adaptation on tactile sensitivity and two-point distance perception (Chapter 2). Moreover, we investigated how adaptation affected the model's performance under different decoder settings.

#### 4.5.1 Best-fit RF parameters for two-point distance comparison without adaptation

For the distance-comparison task, given each set of parameter values and constraints, the model yielded a psychometric function, which depicted the proportion of "comparison distance (C) > reference distance (R)" responses, p(C>R), at each of the nine C values. We compared each function with the average human psychometric performance curve. We used the maximum log-likelihood to determine the best-fitting parameters. The binomial likelihood of observing the human data, given an underlying set of p(C>R) from

model performance at different C's, was

$$p_{binom} = \prod_{C} (p_C)^h (1 - p_C)^{(n-h)} \tag{19}$$

where $p_C$ was short for p(C>R) for a particular C from the model performance, $(1 - p_C)$ was the proportion of the opposite response (R>C); $n$ was the total number of trials for that C value from the human data, $h$ was the number of trials out of $n$ on which C was perceived by human participants to be greater than R, and ($n$ - $h$) was the number of trials on which R was perceived to be greater than C.

Because $n$ was large (on the order of hundreds), $p_{binom}$ was extremely small for certain parameter values. To avoid underflow problems, we log-transformed Eq. (19):

$$\log\ p_{binom} = \sum_{C} [(h) \log(p_C) + (n - h) \log\ (1 - p_C)] \tag{20}$$

We used log base 10. We found the maximum value of $log\ p_{binom}$, which we called the log maximum likelihood (LML), and the best-fitting model parameter values were the values that gave rise to LML. We then calculated the log likelihood-ratio (LLR) for all other parameter values in comparison to the best-fit, simply by subtracting LML from each corresponding log-likelihood, because log (B/A) = log B – log A. The maximum LLR was zero, which corresponded to the LML and the best-fit. In addition, for each model fit, we reported the coefficient of determination, $r^2$, with respect to the human data.

We fit the model to the average human performance in the NA condition (Experiment 1 in Chapter 2). The human data were averaged from 19 participants, three NA testing blocks per participant, and a total of 570 trials at each comparison distance. The top 12 best-fitting RF parameter sets, ranked by LLR, are shown in Fig. 4. The five numbers in the top-left corner of each plot are (from top to bottom): LLR, $r^2$, RF spacing, $\sigma$, and $A_{max}$, respectively. The results suggest that different combinations of spacing, $\sigma$, and $A_{max}$ values can give rise to similarly satisfactory fits. In the top 12 best-fitting values, spacing ranged from 15 to 65 mm, $\sigma$ was either 20 or 30 mm, and $A_{max}$ ranged from 12 to 22 spikes. A smaller spacing (i.e. more dense RFs) tended to pair with a larger $\sigma$ (i.e. broader RFs) to yield human-like performance.

### 4.5.2 Effects of adaptation on two-point distance perception

We modeled adaptation as changes in RF responses in the encoding stage. The adapting stimulus was applied to the midpoint of the RF line, x-position = 75 mm. It uniformly adapted a circular area with a radius of 9.5 mm (magenta circle in Fig. 1A); its effects on

RFs outside the circle were calculated with Eqs. (7) and (8). Fig. 5 demonstrates how adaptation changed the population response patterns. For illustration purpose, the examples in Fig. 5 used a denser RF line (spacing = 10 mm) than the best-fitting values. Each plot depicts three adaptation conditions: NA, adaptation with $\alpha = 0.1$, and adaptation with $\alpha = 0.5$. The two point-stimuli were either 54 mm apart or 30 mm apart. The plots on the left (Figs. 5A, 5C) depict the expected spike counts, $\boldsymbol{\lambda}$, and those on the right (Figs. 5B, 5D) depict the actual spike counts, $\boldsymbol{k}$. $\boldsymbol{\lambda}$ are theoretical averages over many repeated trials, and illustrate the general trends in the population response changes caused by adaptation. $\boldsymbol{k}$ are the stochastic noisy neural data observed on a random trial, and what the decoder later interprets to make a perceptual decision. Fig. 5 suggests that, following adaptation to the intervening skin between the point-stimuli, the overlapped area in the population response was reduced; a greater degree of adaptation (a larger $\alpha$) led to a greater reduction in the overlap. For the 54-mm stimulus, without adaptation, the separation between the two population response peaks was roughly 54 mm; following adaptation, the peaks became more separate. For the 30-mm stimulus, without adaptation, the population response was unimodal (Fig. 5C, $\lambda$) or almost unimodal (Fig. 5D, $k$); following adaptation, a bimodal pattern started to emerge in the population response, which plausibly made the two points more distinguishable.

How do these adaptation-induced changes in the encoder affect perception via different decoders? How may the spatial repulsion illusion we empirically observed (Chapter 2) arise from the encoding-decoding cascade? To answer these questions, we considered two types of decoders. One had access to the adaptation state in the encoder and adjusted its readout accordingly (the aware decoder, Fig. 6A). The other was unaware of the adaptation state in the encoder, and therefore had a fixed readout without accounting for adaptation (the unaware decoder, Fig. 6B).

Figs. 6C and 6D demonstrate that following adaptation, the two types of decoders generated different estimates for the same two-point distance ($\Delta x$), despite having comparable estimates without adaptation. Without adaptation, the posterior PDFs over $\Delta x$ from both decoders peaked at approximately the actual stimulus value (30 mm in this example). Adaptation reduced the certainty of the estimation for the aware decoder, reflected by the lowered PDF, but it did not shift the PDF. This suggests that for the aware decoder, adaptation made the two points appear weaker and more difficult to locate, but it did not bias the spatial estimate of the points. By contrast, for the unaware decoder, adaptation not only reduced the certainty but also induced a positive bias in the estimate, reflected by the lowered and rightward-shifted PDF. This suggests that, following adaptation, the unaware decoder estimated the points to be not only weaker but also more separate.

Consequentially, the differential adaptation-induced effects via the two types of decoders manifest in perception, as shown in the model's psychometric functions (Fig. 7). For the aware decoder, as the degree of adaptation ($\alpha$) increased from 0 (NA) to 0.8, the psychometric function became flatter, but the point of subjective equality (PSE) remained

at approximately the actual stimulus distance. In other words, distance perception remained largely unbiased (Fig. 7A). By contrast, as $\alpha$ increased, the psychometric function generated by an unaware decoder shifted more rightward and the PSE increased, indicating an increase in the perceived distance between points that straddled the adapted skin site (Fig. 7B).

Figs. 7A and 7B were generated with the best model fit (parameters in Fig. 4 top-left plot) to participants' average baseline distance-perception (Expt. 1 in Chapter 2), and made predictions for the general human performance under arbitrary $\alpha$ conditions. In the adaptation experiment (Expt. 3 in Chapter 2), we tested a different group of participants and fewer trials in each condition than those in Expt. 1. To account for the idiosyncrasies between groups of participants, we fit the model to the participants in the adaptation experiment (Expt. 3). We first found the best-fitting parameters for these participants' NA performance, and then used the same values but with added $\alpha$ to fit the participants' adapted performance. The results are shown in Fig. 7C. With an unaware decoder, the model's adapted performance (solid curves) matched the experimentally observed spatial repulsion illusion (dashed curves and squares). Moreover, the unaware decoder in Figs. 7B and 7C generated similar results indicating a spatial repulsion illusion, despite using different RF parameters. This suggests that a wide variety of RF configurations are susceptible to the illusion, and different adaptation conditions can induce the illusion to different extents.

### 4.5.3 Decoder awareness made little difference in adaptation-induced detection threshold elevation

For the single-point (monofilament) detection task, the model yielded eight (2 x 4) 71% correct thresholds: two experimental conditions (no-adaptation, adaptation), four test skin sites for each condition. The model calculated each threshold from the corresponding 2-down-1-up staircase in the same way we calculated the thresholds for human participants (by averaging the reversal points in the second-half of the staircase). For a given set of parameters, we compared the eight thresholds generated by the model with the average human thresholds, and used least-squares fit to determine the best-fitting parameters.

Fig. 8A shows the best-fitting model performances for adaptation-induced thresholds elevation (Expt. 2B in Chapter 2) ranked by the root mean square error (RMSE); the model used an unaware decoder. With the same best-fitting parameter values but an aware decoder, the model produced similar results (Fig. 8B). This suggests that the decoder's awareness of adaptation made little difference in its sensitivity to detect a point-stimulus. Adaptation reduced firing and thus increased the detection threshold, regardless of whether the decoder knew about the adaptation state in the encoder.

### 4.5.4 Best-fit RF properties for one task did not account for the other task

In the adaptation study in Chapter 2, we tested the same group of participants for the monofilament-detection task (Expt. 2B) and the two-point distance-comparison task (Expt. 3), with the same adaptation protocol. We hypothesized that adaptation-induced changes in neural responses underlying the observed effects in one task might also be responsible for those in the other task. However, empirically we found no correlation between the threshold elevation in Expt. 2B and the PSE shift in Expt. 3. Consistent with the lack of correlation in the experimental results, the simulation results indicated that the best-fitting RF and adaptation parameters for the two tasks were quite different from each other (monofilament detection: spacing = 65 mm, $\sigma$ = 40 mm, $A_{max}$ = 4 spikes, $\alpha$ = 0.7; distance comparison: spacing = 55 mm, $\sigma$ = 15 mm, $A_{max}$ = 11 spikes, $\alpha$ = 0.08). Does this suggest that different RF populations may be responsible for the perceptual effects in the two tasks, and that they may be adapted to different degrees by the same adapting stimulus? Here, we investigated this question by using the best-fitting parameters for the monofilament-detection task to perform the distance-comparison task, and vice versa.

The best-fitting RF properties for the monofilament-detection task (Fig. 9A, left) fit poorly for the distance-comparison task (Fig. 9A, right). Even without adaptation, this RF population could not distinguish between the distances; it performed the task at near chance level. This low spatial acuity is plausibly due to the RF population's low evoked spike counts combined with the sparse and broad RFs. Similarly, the best-fitting RF properties for the distance-comparison task (Fig. 9B, left) fit poorly for the monofilament-detection task (Fig. 9B, right). This RF population did not have enough sensitivity to detect the very light monofilaments, and therefore could not account for the very low baseline thresholds in humans. Moreover, it was not sufficiently adapted to account for the threshold elevation following adaptation. The discrepancies lend evidence to the possibility that different RF populations are responsible for the spatial discrimination versus detection task, and that they are adapted to different degrees by the same adapting stimulus.

## 4.6 Discussion

Here, we undertook a theoretical and computational investigation of tactile perception and adaptation. We parameterized the forearm RF properties of somatosensory cortical neurons, and used Bayesian perceptual models to perform psychophysical tasks under different adaptation conditions. We modeled adaptation as reduction in neural responsivity at the encoding stage, and examined what type of decoder readout of the neural population activity was consistent with experimentally observed perceptual effects. The simulation results are in general agreement with human performance. We found that adaptation reduced tactile sensitivity, as indicated by elevated thresholds for 2IFC monofilament-detection, and that adaptation increased the perceived distance between

point-stimuli that straddled the adapted area. The spatial repulsion illusion emerged when the decoder was unaware of the adaptation at the encoding stage.

### 4.6.1 Modeling adaptation

We modeled adaptation as response reduction in the neurons that are responsive to the adaptor. This is essentially a gain-reduction model. The notion *gain* can be understood in terms of input-output relations in neural response; more specifically, it can be represented in the response amplitude to a given stimulus attribute. Our primary hypothesis was that focal adaptation differentially reduces the gain of neurons coding the adaptor: neurons that are most responsive to the adaptor have the greatest reduction in response amplitude. Evidence for the differential response reduction has been observed at multiple levels of perceptual processing pathways across modalities (Yates et al., 1985; Baylis & Rolls, 1987; Saul & Cynader, 1989; Belin & Zatorre, 2003; Dragoi et al. 2000; Dragoi et al., 2001). The differential response reduction results in a shift in the population response distribution to a subsequent similar test stimulus. Because the neurons that were previously more activated are now more adapted and therefore respond less, the peak or the mean activity of the stimulus-response mapping now shifts away from the adaptor's attribute. This distribution-shift hypothesis has been proposed to explain adaptation as a self-calibrating mechanism of the sensory systems to adjust to changes in stimulus statistics and optimize information gain (Levinson & Sekuler, 1976; Mather, 1980; Clifford et al., 2000; Stocker & Simoncelli, 2006). A perceptual consequence of the adaptation-induced shift in population response is the occurrence of repulsive aftereffects (Clifford et al., 2000; Kohn, 2007; Seriès et al., 2009).

The notion of adaptation as stimulus-specific gain reduction has provided powerful explanations for many repulsive aftereffects observed in vision, for example, the tilt aftereffect illusion, motion aftereffect, and contrast adaptation (Dragoi et al., 2000, 2001; Kohn & Movshon, 2004; Jin et al., 2005; Clifford et al., 2007; Kohn, 2007; Seriès et al., 2009). Moreover, it is central to a number of proposals for the functional roles of adaptation (Webster, 2011, 2012). To add to the literature, our rather simplified model has successfully replicated the observed effects in tactile perception. It is important to acknowledge, however, that adaptation likely induces complex changes in addition to or other than a gain reduction. Recent physiological studies in vision have shown that adaptation can cause a variety of changes in the response properties of both peripheral receptors and cortical neurons. For example, in the periphery, adaptation can change the spatiotemporal RFs of retinal ganglion cells (Hosoya et al., 2005). In V1, adaptation can shift orientation tuning curves (Dragoi et al., 2000, 2001), change tuning curve widths (Dragoi et al., 2000; Kohn & Movshon, 2004), reduce surround inhibition (Webb, 2005; Wissig & Kohn, 2012), and modify noise correlation (Gutnisky & Dragoi, 2008). These effects of adaptation are intriguing but somewhat controversial (Adam Kohn, 2007; Seriès et al., 2009a); moreover, it is difficult to draw comparisons between the physiological data and human perception, because most of the physiological data came from monkey or

cat studies and were obtained using different stimuli than those used in human perceptual experiments. For our model, we chose to focus on the gain-reduction aspect of adaptation, because it is currently the simplest and least controversial account for adaptation effects with the most supporting evidence.

Our model is equivalent to a tuning curve model with firing rate reduction or response suppression for the tuning curves at or around the adaptor. It shows that a repulsive shift in the population response does not necessarily require shifts in individual tuning curves or changes in the tuning curve widths. However, these alternative effects have been reported in physiological studies of visual adaptation (e.g. Dragoi et al., 2000, 2001; Kohn & Movshon, 2004; Jin et al., 2005). Future modeling research can investigate changes at the level of tuning curves as alternative ways to model tactile adaptation effects. An incomplete list of possible models are as follows: (1) attractive shift of nearby tuning curves towards the adaptor; (2) repulsive shift of nearby tuning curves away from the adaptor; (3) sharpening of the tuning curves at or around the adaptor; (4) broadening of the tuning curves at or around the adaptor; (5) combinations of any of the effects above in various ways, for example, flank suppression, which could be modeled as a combination of response suppression and sharpening.

Modeling and empirical studies have indicated that (1), (3), or their combination with response suppression would lead to *repulsive* perceptual aftereffects observed for a variety of visual stimuli, whereas (2) or (4) would lead to *attractive* perceptual aftereffects, and have been observed in monkeys' medial temporal (MT) area for motion direction (Kohn & Movshon, 2004b; Jin et al., 2005; Schwartz et al., 2007; Seriès et al., 2009; Solomon & Kohn, 2014). Interestingly, an *attractive* shift of the nearby *tuning curves* towards the adaptor would lead to a *repulsive* shift in the *perception*, and vice versa. This seemingly reversed link has been observed both computationally and experimentally (e.g. Kohn & Movshon, 2004b; Jin et al., 2005). In addition, adaptation can cause simultaneous tuning curve changes that would have opposing effects (repulsive vs. attractive) on perception, and the perceptual outcome depends on the net results of these changes (e.g. Jin et al., 2005). Furthermore, it is important to point out that these adaptation effects may not be exclusionary with one another. Our model, as well as some of the modeling studies cited above, features a single layer of neurons or RFs, and is not a multi-layered network model. It is plausible that via certain convergence mechanisms, simple rate reduction or response suppression in the lower level of the processing hierarchy can lead to more complex tuning curve changes in the higher levels.

In short, although our model did not explore all the intriguing effects of adaptation or their myriad possible combinations, it nevertheless provides a satisfactory explanation from an information-processing perspective for the tactile spatial repulsion illusion we observed. It also provides a simple and useful scaffolding on which more sophisticated models can be built.

### 4.6.2 Decoding ambiguity

We modeled tactile perception as an encoding-decoding cascade. We showed that the spatial illusion arose from this cascade when the decoder was unaware of adaptation and thus produced a readout that was mismatched to the adapted encoder. This result is consistent with the computational work on visual adaptation that posits that adaptation-induced perceptual biases may arise from decoding ambiguity (Fairhall et al., 2001) or "coding catastrophe" (Schwartz et al., 2007): under circumstances that are still unknown or unclear in the literature, downstream decoding mechanisms operate blindly with respect to the adaptation states or tuning changes in the previous layer of processing hierarchy, in the short temporal context of adaptation.

The notion of decoding ambiguity or coding catastrophe raises important questions for computational work on dynamic sensory perception. It seems counterintuitive and even functionally detrimental that the decoding mechanisms would be oblivious to the adaptation state in the circuit. Although it is unclear whether or how decoding ambiguity is implemented in neural substrates, a few functional accounts have been proposed for possible roles of decoding ambiguity (for a review, see Schwartz et al., 2007). One of them is in terms of efficient coding. The efficient coding account proposes that the sensory system is concerned with stimulus local salience, change detection, or discrimination more than about precise estimation. In the case of a prolonged, unchanging stimulus, there is substantial information redundancy in the input. Adaptation occurs as a strategy to reduce response correlation and mitigate coding inefficiency. It accentuates responses to stimuli that embody changes or new relationships, and thus improves discriminability around the adaptor attribute. As a trade-off for the boosted salience and improved discriminability, however, the system is susceptible to estimation biases.

Another proposed account for decoding ambiguity is in terms of Gibson's notion of normalization (Gibson & Radner, 1937), recalibration, and error correction. Take the tilt aftereffect illusion for example (where prolonged exposure to slightly tilted lines leads to a repulsion illusion for subsequently viewed lines tilted at a similar orientation): it is proposed that the cardinal orientations are the norm in the visual system's long-run representation of stimulus statistics in the environment, but recent sensory experience favours the slightly off-cardinal tilt as the norm; therefore, the visual system needs to temporarily recalibrate to be consistent with the long-run norm regardless of the adaptation state. This recalibration is an error-correcting strategy that is functionally beneficial in general, but it can lead to temporary estimation biases. However, it would be difficult to apply this normalization account to explain the tactile spatial illusion we observed, as there are presumably no norms for the stimulus positions on the forearm, although a similar attempt has been made to explain a tactile orientation repulsion illusion akin to the visual tilt aftereffect (Silver, 1969).

Regardless of what functional benefits it may entail, a decoder that fails to account for adaptation at the encoding stage falls short of optimality. It is suboptimal in that it does

not have access to all the information available or does not utilize it, and it is mismatched to the generative model and to the stimulus attribute. This suboptimality can be nicely captured in a Bayesian framework. A Bayesian perceptual model does not have to be optimal. Indeed, Bayesian inference under a wrong assumption about the generative model usually produces suboptimal perceptual decisions. Optimal perceptual inference would require that the observer's prior probability distribution match the actual stimulus distribution and that the observer's likelihood function correctly represent the statistical mapping from stimuli to observation. In real-world scenarios, however, perceptual computations are likely to be suboptimal due to complexity of the generative models and limitations in neural circuitry (Ma, 2012).

In our simulations, whether the decoder was aware of adaptation or not made qualitative differences in two-point distance discrimination, but not in single-point detection: adaptation increased detection thresholds regardless of the decoder awareness setting (Fig. 8). It is tempting to link this finding to the experimental results in Chapter 3, where topical anesthesia reduced tactile sensitivity but caused little to no increase in the perceived two-point separation. We speculate that the discrepancies between the adaptation and anesthesia results may in part represent an unaware versus aware decoder in neural circuitry. This is a pure speculation, as the general neural substrates for perceptual decoding are still unknown, let alone how decoder awareness or lack thereof may be implemented in the circuitry. We speculate that the proposed different decoding strategies may be driven by a range of factors at different processing stages or their interactions, and vibrotactile adaptation and topical anesthesia may have different impacts on these factors. Alternatively, the discrepancies between the adaptation and anesthesia results may be due to different changes induced in the encoder and independent of the decoder. For example, perhaps the perceptual bias is primarily driven by focal response suppression in the CNS, whereas topical anesthesia weakens peripheral input but does not necessarily induce the pattern of central changes required for the perceptual repulsion to occur, due to compensation from convergent input from adjacent afferents (Fig. 5, Chapter 3).

In order to link adaptation-induced neurophysiological changes to psychophysical results, we need to understand how neural population responses are decoded to produce perceptual effects. Although some models proposed to explain the link have been partly validated by empirical studies - for example, the models about tuning changes described in section 2.6.1 – perceptual decisions involve processing in extensive and perhaps interactive networks of sensory circuits, the neural implementation of which is still largely unknown. Adaptation likely induces complex changes in neural circuits, and our model is clearly an oversimplification of its effects. Our model is not a mechanistic model attempting to explain the detailed neural mechanisms; instead, it is meant to offer a basic computational construct, from an information-processing perspective, of how perceptual consequences of focal adaptation may be linked to neural changes. Future research is needed to elucidate the computational principles and their neural substrates that translate the neurophysiological changes into perceptual effects.

### 4.6.3 Neural populations responsible for observed effects in spatial discrimination vs. monofilament detection

Based on the simulation results, the best-fitting RF properties and adaptation states for the two perceptual tasks were quite different from each other (distance comparison: spacing = 55 mm, $\sigma$ = 15 mm, $A_{max}$ = 11 spikes, $\alpha$ = 0.08; monofilament detection: spacing = 65 mm, $\sigma$ = 40 mm, $A_{max}$ = 4 spikes, $\alpha$ = 0.7). We applied the best-fitting parameters from one task to perform the other task and vice versa, and the resulting performances were poor (Fig. 9). This suggests that different neural populations may be primarily responsible for the perceptual effects in the two tasks, and that they may be adapted to different degrees by the same adapting stimulus.

The best-fitting RFs for two-point distance perception had smaller spacing, smaller $\sigma$, higher $A_{max}$, and smaller $\alpha$ than those for monofilament detection. In other words, these RFs had comparatively higher density, were smaller in size, fired more, and adapted less. These properties resemble the SA1 population. Among the primary mechanoreceptive afferents identified in human forearm hairy skin (two slowly-adapting types: SA1s and SA2s, and three fast-adapting types: hair units, field units, and PCs; Vallbo et al., 1995; Olausson et al., 2000), SA1s are the best candidates for encoding spatial detail. They have smaller and more densely distributed RFs than the fast-adapting afferent types in human forearm skin (Vallbo et al., 1995; Olausson et al., 2000). The fast-adapting afferent types presumably do not contribute significantly to fine spatial coding, as they have large receptive fields with diffuse borders and low distribution density (Bolanowski et al., 1994; Vallbo et al., 1995). The other slowly-adapting afferent type, SA2s, are presumably more responsible for proprioceptive signalling than for conveying fine spatial information (Chambers et al., 1972; Edin, 1992; Vallbo et al., 1995; Olausson et al., 2000). These findings suggest that, in human forearm skin, SA1s are the only primary mechanoreceptive afferents that have the requisite properties needed to convey fine spatial information. In addition, although research is needed to elucidate how human forearm skin receptors adapt to and recover from vibrotactile stimuli, neurophysiological research in monkey glabrous skin has shown that SA1s and the fast-adapting afferent types all adapt after being stimulated with seconds to tens of seconds of vibration, but SA1s recover faster from vibrotactile adaptation than the fast-adapting afferent types do (Leung et al., 2008), which may account for the smaller $\alpha$. Taken together, these pieces of evidence suggest that two-point distance perception relies largely on SA1 input, and it is plausible that adaptation in the SA1 population contributes to the spatial repulsion illusion we observed.

By contrast, when used to perform monofilament detection, the best-fitting RFs for two-point distance perception yielded poor fits for human data: their baseline thresholds were too high compared to human performance, indicating a lack of sufficient sensitivity (Fig. 9B, right). Microneurography research has suggested that monofilament-detection threshold is determined by fast-adapting, not slowly-adapting, afferent types; firing thresholds of slowly-adapting afferents are higher than the observed detection thresholds,

and thus unlikely to mediate the detection of very light monofilaments (Strzalkowski et al., 2015). Accordingly, it is plausible that the RF properties that resemble SA1 RFs would yield poor fits for the monofilament-detection data, and that the RFs best-fitting for monofilament detection may represent the fast-adapting afferent types in forearm skin: hair units, field units, and/or PCs. The fast-adapting afferent types have exquisite sensitivity but poor spatial acuity. Consistent with what would be predicted from poor spatial acuity, the best-fitting RFs for monofilament detection yielded poor fits for the distance-comparison data (Fig. 9A, right): they could not distinguish between the distances even without adaptation, and performed the task at near chance level. This poor spatial acuity is to be expected from sparse and broad RFs with low evoked spike counts, as indicated in these RFs' parameter values (Fig. 9A, numbers in the middle), which are characteristics of fast-adapting afferent types.

The different RF properties and functional roles discussed above belong to the primary afferents. Do they also manifest in the RFs of cortical neurons in S1, which were what our model simulated? Like the primary afferents, S1 neurons have been classified into slowly-adapting and fast-adapting types, based on whether they display sustained firing to static indentation or respond only at the stimulus onset and offset. Early studies in cats and monkeys suggested that slowly-adapting and fast-adapting S1 neurons are largely segregated in interleaved columns (Mountcastle, 1957; Dykes et al., 1980; Sur et al., 1981, 1984). Studies of S1 neurons with RFs in the glabrous skin have shown that low-, intermediate-, and high-frequency vibrations, which target SA1, RA, and PC afferents, respectively, activate different bands of S1 neurons separately (Chen et al., 2001; Friedman et al., 2004). Moreover, direct microstimulation of the cortical RA bands, but not of the SA1 bands, enables monkeys to perform frequency-discrimination task on flutter stimuli, a frequency range to which RA afferents are most sensitive (Romo et al., 1998, 2000). In addition, evidence has suggested that slowly-adapting and fast-adapting channels are segregated along the tactile pathway all the way to the ventroposterior nucleus of the thalamus, where the input is projected into the cortex (Jones, 1975; Jones et al., 1982). These findings have been interpreted to suggest that the slowly-adapting and fast-adapting properties of S1 neurons are driven by slowly-adapting and fast-adapting afferent input, respectively (Johansson & Vallbo, 1979; Iggo & Andres, 1982), and that they remain largely segregated in the early cortical processing area (area 3b). This is consistent with our hypothesis that different groups of cortical RFs are primarily responsible for distance perception versus monofilament detection, and is consistent with what our model fits seem to imply.

Several caveats are in order. First, the properties of cortical RFs are much more heterogeneous and mixed than those of afferent RFs, partly due to the complexities in input convergence and divergence (Pei et al., 2009), excitatory and inhibitory mechanisms (Hendry & Jones, 1981; Dykes et al., 1984; DiCarlo et al., 1998; DiCarlo & Johnson, 2002), and high response nonlinearity in general. Moreover, recent research has suggested that submodalities of S1 neurons are less segregated than traditionally thought. Most neurons receive input from more than one afferent type (Pei et al., 2009; Saal &

Bensmaia, 2014). According to a recent electrophysiological study of monkey S1 neurons with RFs in the glabrous skin of the fingers, approximately 50% of area 3b neurons and 40% of area 1 neurons exhibit a mixture of significant SA1- and RA-like response properties, and only 7% of area 3b neurons and 6% of area 1 neurons are predominately SA1-like (Pei et al., 2009). Tactile perception is likely to be a team effort that requires the collaboration of afferents and neurons of different types (Saal & Bensmaia, 2014). It is plausible that our different model fits for the different perceptual tasks reflect the average weighted mixtures of RF properties across submodalities of neurons.

A second caveat is the possibility of overfitting. A variety of combinations of RF parameters can lead to similarly satisfactory fits. For example, the top 12 best-fitting RF values for baseline distance perception ranged from 15 – 65 mm for spacing, 20 – 30 mm for $\sigma$, and 12 – 22 spikes for $A_{max}$ (Fig. 4). Small idiosyncrasies in the human data sets to which we fit the model performance could lead to considerable differences in the best-fitting values; for example, all other settings being equal, the best-fitting RF spacing for average baseline distance comparison was 35 mm if the human data were from Experiment 1, Chapter 2, and 55 mm if the human data were from Experiment 3, Chapter 2, which tested a different group of participants and different numbers of trials than those in Experiment 1. This may be partly due to the fact that in our model, the variation in spacing was confounded with the variation in RF positions relative to the stimuli/stimulus. When the RFs were sparse (for example, when spacing was 35 mm there were only five RFs in the simulated skin patch, and when spacing was 55 mm there were only three RFs), small changes in RF positions relative to the stimuli/stimulus had considerable impact on the spatial resolution of the population response. Indeed, primate research on tactile curvature perception has suggested that the relative positions of RFs to the curvature provide more critical information than does the overall afferent innervation density, especially when the RFs are sparse (Wheat & Goodwin, 2001). The considerable impact from RF positions relative to the stimulus may in part account for the different fits for small variations in human data. Furthermore, it may also contribute to the variations in monofilament-detection threshold elevation following adaptation, observed empirically (Fig. 8, dashed magenta curves) and in simulations (Fig. 8, solid magenta curves): the threshold elevation did not reduce monotonically for test sites that were more distant from the centre of adaptation; instead, it fluctuated. This fluctuation, as well as other idiosyncrasies in human or model performances, may reflect specific interactions of relative RF positions, firing stochasticity, and adaptation effects.

Related to the first and second caveats, a third caveat is that the model RF behaviours strongly depend on model assumptions on the underlying architecture and coding strategies, such as uniform distribution of RF centres, Gaussian response function, and spike count code. Under different assumptions, the model could have yielded different patterns regarding the best-fitting RF properties for distance comparison versus monofilament detection. Therefore, we cannot conclude based on the model performance that adaptation of SA1s and adaptation of fast-adapting afferents are primarily responsible for the results in distance comparison and monofilament detection, respectively. Future

empirical research is needed to test this model suggestion; a possible approach is to selectively adapt one or a few of the afferent types (e.g. Gescheider et al., 1979; Hollins et al., 2001).

Moreover, the model bases perceptual inferences on the decoded activity of neuronal responses in areas 3b and 1 of S1. This is reasonable, given that areas 3b and 1 neurons are responsible for coding the perceived location of a stimulus, even in the absence of an actual physical stimulus at that location (Chen et al., 2003; Friedman et al., 2008). However, we cannot rule out the potential role of other cortical areas, such as area 2 in S1, and the secondary somatosensory cortex (S2), both of which have larger and more complex RFs.

In addition, we did not incorporate a lapse term in the model when we fit it to human data; thus, the possibility of making mistakes at the largest stimulus values was extremely small for the model and yet non-negligible for humans. Consequently, the fits might have overcompensated for data points at the largest stimulus values, which would result in less accurate best-fitting values.

Considering these caveats and other limitations of our model, we do not claim that our model fits imply the realistic average values of cortical RF properties. Instead, the model performances are meant to capture the general trends in the human data for different perceptual tasks with or without adaptation.

### 4.6.4 Assumptions and variations: RF properties

We made many simplifying assumptions to constrain the simulated RF structures and response properties. In addition, we allowed some RF parameters to vary freely to fit model performance to experimental data; we chose the ranges of these parameters as realistically as possible based on literature. Here, we discuss the assumptions underlying these constraints and parameterization, and suggest some plausible alternative approaches to model construction.

*Homogeneity of RFs*. We assumed that the perception of a stimulus attribute was gated by a single-layered, homogeneous population of cortical RFs. Once a set of parameter values was specified, we applied it to all RFs in the population. Realistically, RF structures of S1 neurons are pronouncedly heterogeneous (DiCarlo et al., 1998; James J. DiCarlo & Johnson, 2002; Sripati et al., 2006; Foffani et al., 2008). They vary greatly in size, shape, the amount of overlap, and the excitatory and/or inhibitory regions. This heterogeneity is further complicated by the dependency of the RF properties on the nature of the stimulus. Nevertheless, we subscribe to the view that insights into brain function can be gained by characterizing the average RF properties and examining the general trend. Future research is needed to investigate inter-individual variation in tactile spatial perception and

associate it with individually assigned model RFs (e.g. Peters et al., 2015).

*Spike count as a Gaussian function of distance*. In our simulations, we needed to determine spike counts evoked by stimuli at various distances from the RF centre. Primate neurophysiological studies have suggested that evoked spike count gradually reduces as the stimulus moves away from the RF centre of primary afferents (e.g. Vega-Bermudez & Johnson, 1999) or cortical neurons (e.g. Gardner & Costanzo, 1980a, 1980b). We found that the cortical firing profiles documented by Gardner and Costanzo (1980a, 1980b) could be nicely fitted with Gaussian functions. Therefore, we characterized the simulated spike count as a Gaussian function of distance from the RF centre, as described in Eq. ((1)). Future research could explore other functions for characterizing the RF response, such as Gabor with inhibitory sidebands (e.g. Peters et al., 2015).

The SD of the Gaussian response function, $\sigma$, ranged from 5 - 70 mm for data fitting. It was roughly estimated from Gardner & Costanzo (1980a), which recorded rhesus monkeys' cortical neuronal responses to weak pressure on the forearm skin. Specifically, the study reported the average firing profiles of 37 neurons in areas 3b and 1 in response to air puffs to the forearm (peak pressure = 1.24 N/cm$^2$; the stimulus felt like a weak tap on the skin to human participants). The authors reported that the neurons recorded were either RA-like or mixed (both RA-like and SA-like), and were driven by rapidly-adapting hair units, Meissner's corpuscles, or mixed touch and hair cells. We fit Gaussian curves to the bell-shaped average firing profiles documented by the authors (Fig. 9 in Gardner and Costanzo, 1980a). The best-fitting $\sigma$ for the average response to a single air puff was 30.4 mm. We applied a broad range of $\sigma$ around this value to account for the fact our stimulus was stronger and sharper than air puffs, which might result in a different $\sigma$ value.

The maximum Gaussian amplitude, $A_{max}$ (i.e. the expected spike count at the RF centre evoked by the maximum stimulus), was estimated based on firing rate data from primate studies using extracellular recording. The firing rates reported in the literature vary greatly depending on factors such as the stimulus properties, the stimulated body site, the recording site, and the type of neurons or afferents recorded. For example, Gardner and Costanzo (1980a) reported that areas 3b and 1 neurons driven by rapidly-adapting receptors or mixed touch and hair cells in monkey forearm fired an average of 4-10 spikes per stimulus to an air puff to their RF centres. By contrast, Pei et al. (2009) applied point-stimuli to monkey fingertip with ~ 1 mm indentation, and reported much greater average firing rates: 113 ips for neurons in area 3b, 86 ips for neurons in area 1, 162 ips for SA1 afferents, and 174 ips for RA afferents. For data fitting, we used a range of 5 – 120 ips for the evoked firing rate. This range translated to 1 - 24 spikes for $A_{max}$ for a 200-ms stimulus.

*RF shape*. We used symmetric two-dimensional (2D) Gaussian RFs as default for simulations; namely, the RFs had circular iso-firing rate contours. Realistically,

somatosensory RFs tend to be elongated rather than symmetrical. Although there is very little research on forearm RF shape from which to draw inferences, studies on fingertip RFs have shown that both cortical and afferent RFs tend to be elongated (aspect ratio > 1.5) (DiCarlo et al. 1998; Sripati et al. 2006; Pruszynski and Johansson, 2014), and that the elongated shape tend to be more prevalent for cortical RFs than afferent RFs (Sripati et al. 2006), plausibly reflecting input convergence and orientation selectivity in cortical neurons. Nevertheless, in our simulations, because RF orientation was not factored in, changing symmetric RFs to elongated RFs would be equivalent in effect to increasing RF spacing and increasing the SD (broadness) of the response profile; both RF spacing and SD were already parameterized. Future research could use elongated RFs, and factor in RF orientation and anisotropy.

*RF spacing*. RF spacing ranged from 5 - 75 mm for data fitting. The lower end of this range reflected the innervation density of peripheral mechanoreceptive afferents. The upper end of the range reflects the sizes of cortical RFs in S1 areas 3b and 1, which are much larger than afferent RFs (DiCarlo et al., 1998; Sripati et al., 2006). This range reflects two hypothetical extreme situations. On one extreme, two cortical RFs are almost completely overlapped with each other, and each of them receives input from one of two adjacent receptors in the skin (Fig.10A, left). In this case, the spacing between the cortical RF centres is determined by the spacing between the peripheral RF centres. Microneurography studies have estimated that the average SA1 receptor density in human forearm skin is 4 SA1 units per 100 $mm^2$ (Vallbo et al. 1995; Olausson et al. 2000). This gives a 5-mm average spacing between SA1 receptors, hence we used 5 mm as the lower limit for RF spacing for data fitting. On the other extreme, two adjacent cortical RFs border each other with zero overlap, and each receives convergent and divergent input from multiple receptors so the influence of receptor spacing washes out. In this case, the spacing between the cortical RF centres is approximately the cortical RF diameter (Fig.10A, right). We did not consider the situation where adjacent cortical RFs are separated by a gap, as this situation is unlikely or at least uncommon based on neurophysiological literature. Studies using different experimental protocols have estimated drastically different values for cortical RF size. For example, the mean cortical RF area in area 3b layer 4 of owl monkeys, with RFs in the hairy skin of the forearm, has been reported to be 600 $mm^2$ in response to a light touch delivered by a fine glass probe (Sur et al., 1980). Assuming a circular RF shape, this would give a radius of ~14 mm. This value is possibly in the lower range of cortical RF sizes, as neurons in area 3b layer 4 have the smallest RFs compared to neurons in other laminae of area 3b or in area 1. For example, the RF area for the thumb is about 1.5 times larger in layers 2, 3, 5 and 6 of area 3b than in layer 4, and about 10-17 times larger in area 1 (Sur et al., 1985). Indeed, a different study estimated a very large cortical RF size: Gardner and Costanzo (1980a) recorded from pyramidal cells in rhesus monkeys' areas 3b and 1 with large cell bodies (which are likely to be in layers 3 and 5) in response to air puffs to the forearm. The authors reported that neurons with RFs on the forearm were activated by stimuli located as far as 90 mm from the RF centres; however, when the stimulus was farther than 45

mm, the firing rates dropped to fewer than 1-2 impulses per second (ips). This suggests that the radius of the RFs was roughly 45-90 mm, and accordingly, its diameter was 90-180 mm. However, the realistic spacing between two adjacent RFs is likely to be smaller than these values due to overlap. For our model simulation, we used 75 mm as the upper limit for the average spacing of forearm cortical RF centres. Because our simulated skin patch was 150 mm long, and the RFs were arranged symmetrically to a central RF at the midpoint of the patch at 75 mm, a RF spacing value greater than 75 mm would result in only one or zero RFs in the entire skin patch.

In our simulations, the RFs were at evenly distributed positions separated by equal spacing. Future modeling work can jitter the RF positions, for example, with Gaussian noise. In addition, only a single line of RFs along the x-axis (150 mm long) of the simulated skin patch (150 x 10 mm) was used. All RFs and the stimulated stimuli were delivered to the same line at y = 5 mm. In the psychophysical experiments with human participants (Chapters 2 and 3), the two point-stimuli were delivered along the longitudinal axis on the forearm (equivalent to the x-axis in the simulations), and participants were told that the two points always aligned longitudinally. Presumably, RFs beneath the line along the two points were the main contributors in determining the x-positions of the points, which in turn gave rise to the perceived two-point distance. RFs outside the line along the two points presumably contributed less information for the task performance. Based on this rationale, the simulation default was to use one line of RFs along the two point-stimuli. Indeed, we ran pilot simulations using three lines of RFs, where the y-positions of the top and bottom two RF lines were separate from the middle RF line by the RF spacing. The pilot simulations yielded results similar to the results using one line of RFs, but with slightly sharper psychometric functions. Thus, to reduce computational time, we proceeded with one line of RFs as the default.

*Lack of surround suppression*. When the simulated task involved two simultaneous point-stimuli, the default was to simply sum the number of spikes elicited by the two points individually (Eq. (5)). This was under the assumption that there was no inter-stimulus interaction. Empirically, the presence of a nearby second point indenting the skin can cause surround suppression and reduce firing rate. For example, Vega-Bermudez & Johnson (1999) showed that when two apposed points indented a monkey's fingertip, one point on top of the hot spot (i.e. the point of maximum response in the RF), and the other point 1 mm away, the evoked firing rate was lower than that evoked by the single point on the hot spot alone. This might be because the presence of the nearby second point distributes the stress on the skin surface and reduces local strain caused by the single point, thereby reducing the evoked firing rate, as SA1 and RA responses are sensitive to local strain (Sripati et al., 2006). Nevertheless, experiments using punctate stimuli comparable to those used in Vega-Bermudez & Johnson (1999) found that surround suppression ceased when the two-point separation was greater than 3 mm on the fingertip (Phillips & Johnson, 1981; Sripati et al, 2006). In our experiments, the smallest two-point separation was 6 mm on the volar forearm. Although the forearm has different receptor

types, sizes, and densities than the fingertip does, which makes it difficult to directly compare the two body sites, we assumed that skin compliance is similar between the forearm and the fingertip, and that two point-stimuli 6 mm apart do not significantly affect the local skin deformation caused by one another. Future modeling work could investigate the possible suppression of spike counts caused by the presence of the second point.

*Lack of inhibition*. We modeled the cortical RFs with Gaussian excitatory functions (as described above), and did not incorporate inhibitory surrounds, sidebands, intracortical connections, or any other inhibitory terms. In reality, however, complex inhibitory mechanisms shape cortical responses. S1 RF structures are diverse, and the prevalence and configuration of their inhibitory regions partly depend on the stimuli. For example, in response to rotating raised-dot stimuli on monkey fingertip, 90% of S1 area 3b neurons showed one or more inhibitory sidebands; the inhibitory sidebands often emerged in the direction of the moving stimulus (DiCarlo et al., 1998). It has been suggested that in some cases the inhibition might actually overlap with the excitatory RF but was temporarily lagged, thus giving the appearance of a spatial offset (DiCarlo & Johnson, 2000, 2002). Consistent with this hypothesis, another primate study using static point-stimuli instead of moving dots found that only 50% of the recorded area 3b neurons exhibited surround inhibition (Sripati et al., 2006). The inhibitory sidebands plausibly give rise to or enhance orientation selectivity in S1 (Hsiao et al., 2002). A primate study using indented bars showed that, of the area 3b and 1 neurons that exhibited significant bar-orientation selectivity (~ 50% of the recorded neurons), 67% had RFs that contained inhibitory sidebands and could be classified with Gabor spatial filters, and 33% had RFs that lacked inhibitory sidebands and could be classified with two-dimensional Gaussian spatial filters (Bensmaia et al., 2008). A modeling study from our laboratory linked the RFs containing inhibitory sidebands to higher performance in a bar orientation discrimination task, and the RFs lacking inhibitory sidebands to lower performance in the task (Ryan M. Peters et al., 2015). For our model RFs, incorporating inhibitory sidebands would likely improve spatial resolution and further reduce the number of RFs needed to replicate human performance. In addition, future modeling work can investigate adaptation effects in terms of inhibitory interactions. For example, adaptation has been shown to cause flank suppression of tuning curves of monkey's MT neurons (Adam Kohn & Movshon, 2004b); a possible way to model flank suppression is to use a combination of gain change, sharpening, and shift of the tuning curves (Seriès et al., 2009a).

### 4.6.5 Assumptions and variations: encoding and decoding

*Spike count code.* We modeled S1 neural coding using spike counts in a 200-ms duration, and characterized adaptation as spike count reduction. This assumes that the RFs convey information in their firing rates (i.e. rate code), and that the number of spikes fired in the first 200 ms since the firing onset conveys sufficient information for the task

performance. Firing rates or spike counts have long been characterized as an important code to convey stimulus information in the somatosensory system (e.g. Johnson & Hsiao, 1992; Craig & Rollman, 1999; Johnson et al., 2000; Goodwin & Wheat, 2004) as well as in other sensory systems. Spike rates or spike counts alone in models of primary afferents or somatosensory cortical neurons have provided satisfactory accounts for tactile coding of indented spatial patterns, such as distance between stimuli, edge, gratings, and bar orientation (Phillips & Johnson, 1981; Sripati et al., 2006; Peters et al., 2015). In addition to the strength of spiking, the timing of spiking provides important information (Johansson & Flanagan, 2009; Harvey et al. 2013; Saal et al., 2015), not only for the temporal aspects of tactile stimuli, e.g. frequency (Mackevicius et al., 2012), but also for the spatial aspects. For example, human microneurography research has demonstrated that the relative timing of the first spike elicited in the ensemble of tactile afferents upon contact with an object provides precise information about the shape of the contacted surface and the direction of force exerted on the fingertips (Johansson & Birznieks, 2004). Moreover, research on rodent S1 has shown that, even though spatial location discrimination can be achieved using a small population of neurons and spike counts only, additional information from the relative timing of the first spike elicited in the neural population significantly improves discrimination; first spike timing is especially informative for neurons with large RFs (Foffani et al., 2008). Inspired by these findings, future modeling work on tactile spatial perception and adaptation could investigate the role of spike timing in addition to spike count or rate.

*Adaptation state (α).* $\alpha$ was a free parameter ranging from 0 - 1 for data fitting, with 0 meaning no adaptation, and 1 meaning complete adaptation. This was an abstract parameter that was meant to capture the general degree of adaptation in the entire system. The impact of $\alpha$ was scaled for each neuron individually as described in Section 2.4.1.2. In the model, $\alpha$ was assumed to be time-invariant. However, results from our monofilament-detection experiment with different top-up adaptation durations suggest that the degree of adaptation increases with the duration of the adapting stimulus, and seems to eventually saturate (Expt. 2A, Chapter 2, Fig. 4A). Similar results have been reported in primate neurophysiological studies with vibrotactile adaptation by Kenneth Johnson and colleagues (Bensmaia et al., 2005; Leung et al., 2005). The authors continuously measured the degree of adaptation and recovery by tracking estimated changes in absolute thresholds and entrainment thresholds (K.O. Johnson, 1974) over time. They tracked the thresholds in SA1, RA, and PC afferents in response to vibrotactile adaptation of various frequencies and amplitudes; they found that for all three afferent types, adaptation and recovery followed an exponential time course. Future research could characterize $\alpha$ as a function of time.

*Small information-processing time window*. We chose 200 ms as the default stimulus duration. Primate electrophysiological research has suggested that the evoked sensorineural activity is not uniformly informative throughout the stimulus duration; the

somatosensory system may only need to integrate the evoked activity over a small time window in order to reach a perceptual decision. For example, Romo and colleagues reported that, for a frequency discrimination task with 750-ms vibratory stimuli, the first 250 ms of evoked S1 neuronal response was determinately informative; responses were significantly attenuated after 250 ms. They found that a coding method that was based on spike count integrated over a time window with the most weight in the first 230-250 ms replicated the behavioural data and accounted for trial-by-trial variability (Luna et al., 2005). The attenuation of neuronal responses after a short time window was also reported by Bensmaia and colleagues using static punctate stimuli (Pei et al., 2009). In light of these findings, we chose 200 ms as the default stimulus duration. In addition, this duration reflected the briefness of the actual test stimulus used in our human psychophysical experiments (Chapters 2 and 3), which was ~ 500 ms.

*Spontaneous firing*. To account for spontaneous firing of cortical neurons, for each neuron we added a default of two spikes to the expected spike count, even for the intervals in a 2IFC task where the stimulus was absent and the expected stimulus-evoked spike count was therefore zero. The value of 2 spikes per 200 ms was based on the median spontaneous firing rate of 76 slowly-adapting and fast-adapting neurons in S1 reported by Romo and colleagues, which was 10 spikes per second (Vázquez et al 2013). Future research could use a different spontaneous firing rate and investigate how it affects perception.

*Poisson cortical noise*. We added Poisson noise to the expected spike count to simulate cortical firing variability, as per Johnson and colleagues' finding that S1 area 3b neuronal noise is Poisson-like (Sripati et al. 2006). Because our encoder was a single layer of simulated cortical neurons, we did not take into account firing variability arising from earlier processing stages, such as SA1 afferent noise, which could be well-approximated as a narrow Gaussian distribution (Vega-Bermudez & Johnson, 1999). Cortical firing variability is greater than afferent firing variability, a trend that is reflected by the broader Poisson distribution compared to the narrow Gaussian distribution given the same mean. We assumed that Poisson noise occurred regardless of the adaptation state. Future research could model adaptation as changes in firing variability. Evidence for this effect has been observed in cat V1 for contrast adaptation. Future modeling work could, for example, modify the ratio of response variance to mean response (i.e. the Fano factor; it equals one for Poisson noise) as a function of distance from the adapting stimulus, instead of treating it as constant.

*Conditional independence.* We assumed that the neural responses were conditionally independent across neurons and across trials. That is, the probabilities of firing a certain number of spikes for different neurons were independent of one another; for each neuron, the probability of response on each trial was independent of responses on previous trials.

We characterized the firing variability as Poisson-like, and assumed that the noise corrupting the activity of individual neurons contains no correlations. This is a fair approximation to the noise found in S1 (Sripati et al. 2006) and in some other cortical sensory areas (e.g. Gershon et al., 1998). However, interneuronal and trial-by-trial response variabilities do exhibit some correlations (Zohary et al., 1994; Kohn & Smith, 2005); this implies that the accuracy of population code depends on the distribution of noise correlations (Abbott & Dayan, 1999; Pouget, Dayan, & Zemel, 2003). Moreover, it has been proposed that an important functional role of adaptation is to improve coding efficiency via reducing neuronal correlations and hence input redundancy (Barlow, 1990; Atick, 1992). The decorrelation effect of adaptation has been confirmed experimentally (Gutnisky & Dragoi, 2008), and computational models that characterize adaptation as temporal decorrelation have accounted for empirical findings of visual adaptation (e.g. Clifford et al., 2000; Wang et al., 2003). Future modeling work on tactile perception can factor in neuronal correlations and investigate the possible decorrelation effect of adaptation on perception.

*Decoder hypotheses.* In our model, for two-point distance perception, by default the decoder hypothesized about the distance (with respect to a fixed midpoint). An alternative approach would be to hypothesize about the points' positions. We explored this possibility and found that it produced similar results to our default approach. We set the decoder to know the y-positions of the points, as only one line of RFs was used, and it only needed to estimate the x-positions. Let us denote the x-positions of the first and second point stimulus as $x_1$ and $x_2$, respectively. For $x_1$, the decoder considered a discrete set of hypotheses with intervals of 1 mm, that started from the beginning of the skin patch length: $x_1$ = 0, 1, 2, …149 mm. For $x_2$, the decoder considered a discrete set of hypotheses with the constraint $x_2 > x_1$; namely, the second point was always to the right of the first point. The second point position was also discretized with intervals of 1 mm: $x_2$ = 1, 2, 3…150 mm. The possible separation between $x_1$ and $x_2$ ranged from 1 mm to 150 mm. The decoder assumed uniform priors over the two point positions $(x_1, x_2)$. Similar to Eq. (9), the likelihood of observing a set of spike counts, $\boldsymbol{k}$, from the RF population given a specific pair of hypotheses, $(x_{1m}, x_{2n})$, equaled the product of likelihoods from individual neurons:

$$p(\boldsymbol{k}|x_{1m}, x_{2n}) = \prod_i p(k_i|x_{1m}, x_{2n}: \lambda_i) = \prod_i \frac{\lambda_i^{k_i} e^{-\lambda_i}}{k_i!} \tag{21}$$

where $p(k_i|x_{1m}, x_{2n}: \lambda_i)$ was the likelihood of observing spike count $k_i$ from neuron $i$ when $\lambda_i$ spike count was expected under two point positions $(x_{1m}, x_{2n})$, and $\lambda_i$ was calculated using Eqs. (1), (4), and (5). The decoder then calculated the joint-posteriors over $(x_1, x_2)$:

$$p(x_{1m}, x_{2n}|\boldsymbol{k}) = \frac{p(\boldsymbol{k}|x_{1m}, x_{2n})p(x_{1m}, x_{2n})}{\sum_{m,n}(\boldsymbol{k}|x_1, x_2)p(x_1, x_2)} \tag{22}$$

An example of the joint-posteriors on a random trial is shown in Fig. 10B. The decoder then considered the fact that different pairs of $x_1$ and $x_2$ could result in the same two-point distance ($x_1 - x_2$), or $\Delta x$; for example, $x_1$ = 60 and $x_2$ = 90 would give a two-point distance of 30 mm, but so would $x_2$ = 70 and $x_2$ = 100. The decoder solved this problem by summing up the posterior probabilities over all $(x_1, x_2)$ pairs that resulted in the same $\Delta x$. In other words, it marginalized the joint-posteriors over the two point positions to obtain a posterior PDF for $\Delta x$:

$$p(\Delta x|\boldsymbol{k}) = \sum_{m,n} p(x_{1m}, x_{2n}|\boldsymbol{k}), \text{ for all } (m, n) \text{ such that } x_{2n} - x_{1m} = \Delta x \tag{23}$$

This posterior PDF for $\Delta x$ obtained via marginalization turned out to be similar to the posterior PDF for $\Delta x$ obtained in the default setting where the decoder hypothesized directly about $\Delta x$ (Fig. 2C). The decoder calculated the marginal posterior PDF for the reference distance and the comparison distance, respectively. It then compared the two PDFs to discriminate the two distances, in a manner described in Eqs. (12) and (13). Simulations using hypotheses about the two point positions yielded similar results to simulations using hypotheses about the two-point distance.

*Priors*. The decoder had no specific prior expectations for the task-relevant stimulus values. For distance comparison, the decoder assumed uniform priors either over the two-point distance with respect to a fixed midpoint (default) or over the two point positions. For monofilament detection, the decoder assumed uniform priors over the monofilament force and position. Alternatively, the decoder could assume non-uniform priors. Adaptation could be modeled as changes in the internal representation of a prior distribution. For example, for the distance-comparison task, adaptation of the intervening skin between the reference points could be characterized as increasing priors around the adapting stimulus, because the consistent stimulation presumably increases the expectation for a stimulus near this location. Nevertheless, theoretical research on visual adaptation has shown that increasing priors at and around the adaptor would lead to an attractive aftereffect in perception towards the adaptor value, not a repulsive one. To account for the commonly observed repulsive effects, the priors would have to decrease at the location of the adapting stimulus, which seems inconsistent with the notion of a prior distribution. Therefore, it has been suggested that adaptation likely manifests itself not as changes in the priors, but as changes in the likelihood function (Stocker & Simoncelli, 2006b). Indeed, we modeled adaptation as focal response reduction that affected the likelihood function, and replicated the tactile spatial repulsion we observed

psychophysically. It is possible, however, that adaptation does change the internal representation of priors but the changes are counteracted by the likelihood effect. Moreover, we modeled tactile perception as an encoding-decoding cascade, and the cascade could be expanded to form a feedforward-feedback loop of multiple processing stages. The estimate from the previous stage could inform the measurement of the current stage, and adaptation could potentially influence different components in this loop.

## 4.7 Conclusion

In this chapter, we took a computational and theoretical approach to investigate tactile perception and adaptation. We characterized tactile perception as comprising two information-processing stages: encoding and decoding. We presented a Bayesian perceptual model that simulated the RF properties of somatosensory cortical neurons. The model applied Bayesian inference to make probabilistic estimates, and performed psychophysical tasks with which we tested human participants. Although the model made many simplifying assumptions, it replicated human performance in two-point distance perception and monofilament detection, as well as the effects of adaptation on the performance. Following focal adaptation, the model exhibited a spatial repulsion illusion in the perceived two-point distance, a behavior that was comparable to the spatial repulsion illusion empirically observed in humans. Moreover, the model suggested that this repulsion illusion emerged via decoding ambiguity: a suboptimal decoder that was unaware of the adaptive changes in the encoding stage generated a biased estimate. These results are consistent with computational and empirical findings in the visual adaptation literature, which may point to common or similar mechanisms for spatial processing and for focal adaptation effects between touch and vision. Although our model did not explore all the intriguing effects of tactile adaptation or their myriad possible combinations, it nevertheless offered a basic scaffolding, upon which progressively more sophisticated and biologically realistic models of tactile perception can be built.

## 4.8 References

Abbott, L. F., & Dayan, P. (1999). The Effect of Correlated Variability on the Accuracy of a Population Code. *Neural Computation*, *11*(1), 91–101. https://doi.org/10.1162/089976699300016827

Atick, J. J. (1992). Could information theory provide an ecological theory of sensory processing? *Network : Computation in Neural Systems*, *3*(2), 213–251.

Barlow, H. (1990). Conditions for versatile learning, Helmholtz's unconscious inference, and the task of perception. *Vision Research*, *30*(11), 1561–1571. https://doi.org/10.1016/0042-6989(90)90144-A

Baylis, G. C., & Rolls, E. T. (1987). Responses of neurons in the inferior temporal cortex in short term and serial recognition memory tasks. *Experimental Brain Research*, *65*, 614–622.

Belin, P., & Zatorre, R. J. (2003). Adaptation to speaker's voice in right anterior temporal lobe. *Neuroreport*, *14*(16), 2105–2109. https://doi.org/10.1097/01.wnr.0000091689.94870.85

Bensmaia, S. J., Hsiao, S. S., Denchev, P. V., Killebrew, J. H., & Craig, J. C. (2008). The tactile perception of stimulus orientation. *Somatosensory & Motor Research*, *25*(1), 49–59. https://doi.org/10.1080/08990220701830662

Bensmaia, S. J., Leung, Y. Y., Hsiao, S. S., & Johnson, K. O. (2005). Vibratory Adaptation of Cutaneous Mechanoreceptive Afferents. *Journal of Neurophysiology*, *94*(5), 3023–3036. https://doi.org/10.1152/jn.00002.2005

Chen, L. M., Friedman, R. M., Ramsden, B. M., Lamotte, R. H., Roe, A. W., Stepniewska, I., … Motte, R. H. L. A. (2001). Fine-Scale Organization of SI ( Area 3b ) in the Squirrel Monkey Revealed With Intrinsic Optical Imaging Fine-Scale Organization of SI ( Area 3b ) in the Squirrel Monkey Revealed With Intrinsic Optical Imaging. *J Neurophysiol*, *86*, 3011–3029. Retrieved from http://www.nature.com/nature/journal/v392/n6674/full/392387a0.html%5Cnhttp://www.nature.com/nature/journal/v392/n6674/pdf/392387a0.pdf

Chen, L. M., Friedman, R. M., & Roe, A. W. (2003). Optical Imaging of a Tactile Illusion in Area 3b of the Primary Somatosensory Cortex. *Science*, *302*(5646), 881–885.

Clifford, C. W. G., Webster, M. A., Stanley, G. B., Stocker, A. A., Kohn, A., Sharpee, T. O., & Schwartz, O. (2007). Visual adaptation: Neural, psychological and computational aspects. *Vision Research*, *47*(25), 3125–3131. https://doi.org/10.1016/j.visres.2007.08.023

Clifford, C. W. G., Wenderoth, P., & Spehar, B. (2000). A functional angle on some after-effects in cortical vision. *Proceedings of the Royal Society B: Biological Sciences*, *267*(1454), 1705–1710. https://doi.org/10.1098/rspb.2000.1198

Colombo, M., & Seriès, P. (2012). Bayes in the brain - On Bayesian modelling in neuroscience. *British Journal for the Philosophy of Science*, *63*(3), 697–723. https://doi.org/10.1093/bjps/axr043

Craig, J. C., & Rollman, G. B. (1999). Somesthesis. *Annu. Rev. Psychol.*, *50*, 305–331.

DiCarlo, J. J., & Johnson, K. O. (2000). Spatial and temporal structure of receptive fields in primate somatosensory area 3b: effects of stimulus scanning direction and orientation. *J Neurosci*, *20*(1), 495–510.

DiCarlo, J. J., & Johnson, K. O. (2002). Receptive field structure in cortical area 3b of the alert monkey. *Behavioural Brain Research*, *135*(1–2), 167–178. https://doi.org/10.1016/S0166-4328(02)00162-6

DiCarlo, J. J., Johnson, K. O., & Hsiao, S. S. (1998). Structure of receptive fields in area 3b of primary somatosensory cortex in the alert monkey. *The Journal of Neuroscience : The Official Journal of the Society for Neuroscience*, *18*(7), 2626–45. Retrieved from http://www.ncbi.nlm.nih.gov/pubmed/9502821

Doya, K., Ishii, S., Pouget, A., & Rao, R. P. N. (Eds.). (2007). *Bayesian Brain*. MIT Press.

Dragoi, V., Rivadulla, C., & Sur, M. (2001). Foci of orientation plasticity in visual cortex.

*Nature*, *411*(6833), 80–86. https://doi.org/10.1038/35075070
Dragoi, V., Sharma, J., & Sur, M. (2000). Adaptation-induced plasticity of orientation tuning in adult visual cortex. *Neuron*, *28*(1), 287–298. https://doi.org/10.1016/S0896-6273(00)00103-3
Dykes, R. W., Landry, P., Metherate, R., & Hicks, T. P. (1984). Functional role of GABA in cat primary somatosensory cortex: shaping receptive fields of cortical neurons. *Journal of Neurophysiology*, *52*(6), 1066–1093.
Dykes, R. W., Rasmusson, D. D., & Hoeltzell, P. B. (1980). Organization of primary somatosensory cortex in the cat. *Journal of Neurophysiology*, *43*(6), 1527–1546.
Fairhall, A. L., Lewen, G. D., Bialek, W., & de Ruyter Van Steveninck, R. R. (2001). Efficiency and ambiguity in an adaptive neural code. *Nature*, *412*(6849), 787–92. https://doi.org/10.1038/35090500
Foffani, G., Chapin, J. K., & Moxon, K. A. (2008). Computational Role of Large Receptive Fields in the Primary Somatosensory Cortex. *Journal of Neurophysiology*, *100*(1), 268–280. https://doi.org/10.1152/jn.01015.2007
Friedman, R. M., Chen, L. M., & Roe, A. W. (2004). Modality maps within primate somatosensory cortex. *Proceedings of the National Academy of Sciences of the United States of America*, *101*(34), 12724–9. https://doi.org/10.1073/pnas.0404884101
Friedman, R. M., Chen, L. M., & Roe, A. W. (2008). Responses of areas 3b and 1 in anesthetized squirrel monkeys to single- and dual-site stimulation of the digits. *J Neurophysiol*, *100*(6), 3185–3196. https://doi.org/10.1152/jn.90278.2008
Gardner, E. P., & Costanzo, R. M. (1980a). Spatial Integration of Multiple-Point Stimuli in Primary Somatosensory Cortical Receptive Fields of Alert Monkeys. *J. Neurophysiol.*, *43*(2), 420–443.
Gardner, E. P., & Costanzo, R. M. (1980b). Temporal integration of multiple-point stimuli in primary somatosensory cortical receptive fields of alert monkeys. *Journal of Neurophysiology*, *43*(2), 444–68. Retrieved from http://www.ncbi.nlm.nih.gov/pubmed/6770054
Geisler, W. S. (2011). Contributions of ideal observer theory to vision research. *Vision Research*, *51*(7), 771–781. https://doi.org/10.1038/jid.2014.371
Geldard, F. A., & Sherrick, C. E. (1972). The Cutaneous " Rabbit ": A Perceptual Illusion. *Science*, *178*(4057), 178–179.
Gershon, E. D., Wiener, M. C., Latham, P. E., & Richmond, B. J. (1998). Coding strategies in monkey V1 and inferior temporal cortices. *Journal Of Neurophysiology*, *79*(3), 1135–1144. https://doi.org/9497396
Gibson, J. J., & Radner, M. (1937). Adaptation, After-Effect and Constrast in the Perception of Tilted Lines. *Journal of Experimental Psychology*, *20*(5), 453–467. https://doi.org/10.1037/h0059826
Goldreich, D. (2007). A Bayesian perceptual model replicates the cutaneous rabbit and other tactile spatiotemporal illusions. *PLoS ONE*, *2*(3). https://doi.org/10.1371/journal.pone.0000333
Goldreich, D., & Tong, J. (2013). Prediction, postdiction, and perceptual length contraction: A bayesian low-speed prior captures the cutaneous rabbit and related

illusions. *Frontiers in Psychology*, *4*(MAY), 1–26. https://doi.org/10.3389/fpsyg.2013.00221

Goodwin, A. W., & Wheat, H. E. (2004). Sensory Signals in Neural Populations Underlying Tactile Perception and Manipulation. *Annual Review of Neuroscience*, *27*(1), 53–77. https://doi.org/10.1146/annurev.neuro.26.041002.131032

Gutnisky, D. A., & Dragoi, V. (2008). Adaptive coding of visual information in neural populations. *Nature*, *452*(7184), 220–224. https://doi.org/10.1038/nature06563

Harvey, M. A., Saal, H. P., Dammann, J. F., & Bensmaia, S. J. (2013). Multiplexing Stimulus Information through Rate and Temporal Codes in Primate Somatosensory Cortex. *PLoS Biology*, *11*(5). https://doi.org/10.1371/journal.pbio.1001558

Hendry, S. H. C., & Jones, E. G. (1981). Sizes and Distributions Incorporating Tritiated Sensory-Motor of Intrinsic Neurons in Monkey Cortex. *The Journal of Neuroscience*, *1*(4), 390–408.

Hosoya, T., Baccus, S. A., & Meister, M. (2005). Dynamic predictive coding by the retina. *Nature*, *436*(7047), 71–77. https://doi.org/10.1038/nature03689

Hsiao, S. S., Lane, J., & Fitzgerald, P. (2002). Representation of orientation in the somatosensory system. *Behavioural Brain Research*, *135*, 93–103. https://doi.org/10.1152/jn.01190.2005

Iggo, A., & Andres, K. H. (1982). Morphology of Cutaneous Receptors. *Ann. Rev. Neurosci.*, (5), 1–31.

Jin, D. Z., Dragoi, V., Sur, M., & Seung, H. S. (2005). Tilt Aftereffect and Adaptation-Induced Changes in Orientation Tuning in Visual Cortex Tilt Aftereffect and Adaptation-Induced Changes in Orientation Tuning in Visual Cortex. *Journal of Neurophysiology*, *94*(6), 4038–4050. https://doi.org/10.1152/jn.00571.2004

Johansson, R. S., & Birznieks, I. (2004). First spikes in ensembles of human tactile afferents code complex spatial fingertip events. *Nature Neuroscience*, *7*(2), 170–177. https://doi.org/10.1038/nn1177

Johansson, R. S., & Flanagan, J. R. (2009). Coding and use of tactile signals from the fingertips in object manipulation tasks. *Nature Reviews Neuroscience*, *10*(5), 345–359. https://doi.org/10.1038/nrn2621

Johansson, R., & Vallbo, A. (1979). Tactile sensibility in the human hand: relative and absolute densities of four types of mechanoreceptive units in glabrous skin. *The Journal of Physiology*, (286), 283–300. https://doi.org/10.1113/jphysiol.1979.sp012619

Johnson, K. O. (1974). Reconstruction Stimulus Fiber Population. *J Neurophysiol*, *37*, 48–72.

Johnson, K. O., & Hsiao, S. S. (1992). Neural mechanisms of tactile form and texture perception. *Ann. Rev. Neurosci.*, *15*, 227–250. https://doi.org/10.1016/j.cub.2014.02.049

Johnson, K. O., Yoshioka, T., & Vega-Bermudez, F. (2000). Tactile functions of mechanoreceptive afferents innervating the hand. *Journal of Clinical Neurophysiology : Official Publication of the American Electroencephalographic Society*, *17*(6), 539–558. https://doi.org/10.1097/00004691-200011000-00002

Jones, E. G. (1975). Lamination and differential distribution of thalamic afferents within

the sensory motor cortex of the squirrel monkey. *Journal of Comparative Neurology*, *160*(2), 167–203. https://doi.org/10.1002/cne.901600203

Jones, E. G., Friedman, D. P., & Hendry, S. H. (1982). Thalamic basis of place- and modality-specific columns in monkey somatosensory cortex: a correlative anatomical and physiological study. *Journal of Neurophysiology*, *48*(2), 545–568.

Kohn, A. (2007). Visual Adaptation: Physiology, Mechanisms, and Functional Benefits. *Journal of Neurophysiology*, *97*(5), 3155–3164. https://doi.org/10.1152/jn.00086.2007

Kohn, A., & Movshon, J. A. (2004a). Adaptation changes the direction tuning of macaque MT neurons. *Nature Neuroscience*, *7*(7), 764–772. https://doi.org/10.1038/nn1267

Kohn, A., & Movshon, J. A. (2004b). Adaptation changes the direction tuning of macaque MT neurons. *Nature Neuroscience*, *7*(7), 764–72. https://doi.org/10.1038/nn1267

Kohn, A., & Smith, M. A. (2005). Stimulus Dependence of Neuronal Correlation in Primary Visual Cortex of the Macaque. *Journal of Neuroscience*, *25*(14), 3661–3673. https://doi.org/10.1523/JNEUROSCI.5106-04.2005

Leung, Y. Y., Bensmaia, S. J., Hsiao, S. S., & Johnson, K. O. (2005). Time-Course of Vibratory Adaptation and Recovery in Cutaneous Mechanoreceptive Afferents. *J. Neurophysiol.*, *94*(5), 3037–3045. https://doi.org/10.1152/jn.00001.2005

Levinson, E., & Sekuler, R. (1976). Adaptation alters perceived direction of motion. *Vision Research*, *16*, 779–781.

Luna, R., Hernández, A., Brody, C. D., & Romo, R. (2005). Neural codes for perceptual discrimination in primary somatosensory cortex. *Nature Neuroscience*, *8*(9), 1210–1219. https://doi.org/10.1038/nn1513

Ma, W. J. (2012). Organizing probabilistic models of perception. *Trends in Cognitive Sciences*, *16*(10), 511–518. https://doi.org/10.1016/j.tics.2012.08.010

Mackevicius, E. L., Best, M. D., Saal, H. P., & Bensmaia, S. J. (2012). Millisecond precision spike timing shapes tactile perception. *The Journal of Neuroscience : The Official Journal of the Society for Neuroscience*, *32*(44), 15309–17. https://doi.org/10.1523/JNEUROSCI.2161-12.2012

Mather, G. (1980). The movement aftereffect and a distribution-shift model for coding the direction of visual movement. *Perception*, *9*(4), 379–392. https://doi.org/10.1068/p090379

Mountcastle, V. (1957). Modality and topographic properties neurons of cat's somatic sensory. *Journal of Neurophysiology*, *20*(4), 408–434.

Pei, Y.-C., Denchev, P. V, Hsiao, S. S., Craig, J. C., & Bensmaia, S. J. (2009). Convergence of submodality-specific input onto neurons in primary somatosensory cortex. *Journal of Neurophysiology*, *102*(3), 1843–1853. https://doi.org/10.1152/jn.00235.2009

Peters, R. M., Staibano, P., & Goldreich, D. (2015). Tactile orientation perception: an ideal observer analysis of human psychophysical performance in relation to macaque area 3b receptive fields. *Journal of Neurophysiology*, *114*(6), 3076–3096. https://doi.org/10.1152/jn.00631.2015

Phillips, J. R., & Johnson, K. O. (1981). Tactile spatial resolution. III. A continuum

mechanics model of skin predicting mechanoreceptor responses to bars, edges, and gratings. *Journal of Neurophysiology*, *46*(6), 1204–1225. https://doi.org/10.1152/jn.00955.2003

Pouget, A., Dayan, P., & Zemel, R. S. (2003). Inference and computation with population codes. *Annual Review of Neuroscience*, *26*(1), 381–410. https://doi.org/10.1146/annurev.neuro.26.041002.131112

Rao, R. P. N., Olshausen, B. A., & Lewicki, M. S. (Eds.). (2002). *Probabilistic Models of the Brain*. MIT Press.

Romo, R., Hernández, A., Zainos, A., & Salinas, E. (1998). Somatosensory discrimination based on cortical microstimulation. *Nature*, *392*(6674), 387–390. https://doi.org/10.1038/32891

Romo, R., Hernández, a, Zainos, a, Brody, C. D., & Lemus, L. (2000). Sensing without touching: psychophysical performance based on cortical microstimulation. *Neuron*, *26*(1), 273–278. https://doi.org/10.1016/S0896-6273(00)81156-3

Saal, H. P., & Bensmaia, S. J. (2014). Touch is a team effort: Interplay of submodalities in cutaneous sensibility. *Trends in Neurosciences*, *37*(12), 689–697. https://doi.org/10.1016/j.tins.2014.08.012

Saal, H. P., Harvey, M. A., & Bensmaia, S. J. (2015). Rate and timing of cortical responses driven by separate sensory channels. *eLife*, *4*(DECEMBER2015), 1–16. https://doi.org/10.7554/eLife.10450

Saul, A., & Cynader, M. (1989). Adaptation in single units in visual cortex: The tuning of aftereffects in the spatial domain. *Visual Neuroscience*, *2*(6), 593–607. https://doi.org/10.1017/S0952523800003527

Schwartz, O., Hsu, A., & Dayan, P. (2007). Space and time in visual context. *Nature Reviews. Neuroscience*, *8*(7), 522–535. https://doi.org/10.1038/nrn2155

Seriès, P., Stocker, A. A., & Simoncelli, E. P. (2009a). Is the homunculus "aware" of sensory adaptation? *Neural Computation*, *21*(12), 3271–304. https://doi.org/10.1162/neco.2009.09-08-869

Solomon, S. G., & Kohn, A. (2014). Moving sensory adaptation beyond suppressive effects in single neurons. *Current Biology*, *24*(20), R1012–R1022. https://doi.org/10.1016/j.cub.2014.09.001

Sripati, A. P., Bensmaia, S. J., & Johnson, K. O. (2006). A Continuum Mechanical Model of Mechanoreceptive Afferent Responses to Indented Spatial Patterns. *Journal of Neurophysiology*, *95*(6), 3852–3864. https://doi.org/10.1152/jn.01240.2005

Sripati, A. P., Toshioka, T., Denchev, P., Hsiao, S. S., & Johnson, K. O. (2006). Spatiotemporal Receptive Fields of Peripheral Afferents and Cortical Area 3b and 1 Neurons in the Primate Somatosensory System. *Journal of Neuroscience*, *26*(7), 2101–2114. https://doi.org/10.1523/JNEUROSCI.3720-05.2006

Stocker, A. A., & Simoncelli, E. P. (2006b). Sensory Adaptation within a Bayesian Framework for Perception. *Advances in Neural Information Processing Systems*, *18*, 1291–1298.

Strzalkowski, N. D. J., Mildren, R. L., & Bent, L. R. (2015). Thresholds of cutaneous afferents related to perceptual threshold across the human foot sole. *Journal of Neurophysiology*, *114*(4), 2144–2151. https://doi.org/10.1152/jn.00524.2015

Sur, M., Garraghty, P. E., & Bruce, C. J. (1985). see last page ! Somatosensory cortex in macaque monkeys : laminar differences in receptive field size in areas 3b and I. *Brain Research*, *342*, 391–395.

Sur, M., Merzenich, M. M., & Kaas, J. H. (1980). Magnification, receptive-field area, and "hypercolumn" size in areas 3b and 1 of somatosensory cortex in owl monkeys. *Journal of Neurophysiology*, *44*(2), 295–311. Retrieved from http://www.ncbi.nlm.nih.gov/pubmed/7411189

Sur, M., Wall, J. T., & Kaas, J. H. (1981). Modular segregation of functional cell classes within the postcentral somatosensory cortex of monkeys. *Science (New York, N.Y.)*, *212*(4498), 1059–1061. https://doi.org/10.1126/science.7233199

Sur, M., Wall, J. T., & Kaas, J. H. (1984). Modular distribution of neurons with slowly adapting and rapidly adapting responses in area 3b of somatosensory cortex in monkeys. *Journal of Neurophysiology*, *51*(4), 724–744.

Tong, J., Ngo, V., & Goldreich, D. (2016). Tactile length contraction as Bayesian inference. *Journal of Neurophysiology*, *116*(2), 369–379. https://doi.org/10.1152/jn.00029.2016

Vega-Bermudez, F., & Johnson, K. O. (1999). SA1 and RA receptive fields, response variability, and population responses mapped with a probe array. *Journal of Neurophysiology*, *81*(6), 2701–2710.

Wang, X.-J. (2003). Adaptation and Temporal Decorrelation by Single Neurons in the Primary Visual Cortex. *Journal of Neurophysiology*, *89*(6), 3279–3293. https://doi.org/10.1152/jn.00242.2003

Webb, B. S. (2005). Early and Late Mechanisms of Surround Suppression in Striate Cortex of Macaque. *Journal of Neuroscience*, *25*(50), 11666–11675. https://doi.org/10.1523/JNEUROSCI.3414-05.2005

Webster, M. (2012). Evolving concepts of sensory adaptation. *F1000 Biology Reports*, *4*(November), 1–7. https://doi.org/10.3410/B4-21

Webster, M. A. (2011). Adaptation and visual coding. *Journal of Vision*, *11*(5), 3–3. https://doi.org/10.1167/11.5.3

Werner, G., & Mountcastle, V. B. (1965). Neural activity in mechanoreceptive cutaneous afferents : stimulus-response relations, Weber functions, and information transmission. *J. Neurophysiol.*, *Mar*(28), 359–397.

Wheat, H. E., & Goodwin, a W. (2001). Tactile discrimination of edge shape: limits on spatial resolution imposed by parameters of the peripheral neural population. *The Journal of Neuroscience*, *21*(19), 7751–7763. https://doi.org/21/19/7751 [pii]

Wissig, S. C., & Kohn, A. (2012). The influence of surround suppression on adaptation effects in primary visual cortex. *Journal of Neurophysiology*, *107*(12), 3370–3384. https://doi.org/10.1152/jn.00739.2011

Yates, G. K., Robertson, D., & Johnstone, B. M. (1985). Very rapid adaptation in the guinea pig auditory nerve. *Hearing Research*, *17*(1), 1–12.

Zohary, E., Shadlen, M. N., & Newsome, W. T. (1994). Correlated neuronal discharge rate and its implications for psychophysical performance. *Nature*. https://doi.org/10.1038/370140a0

### 4.9 Figures and Captions

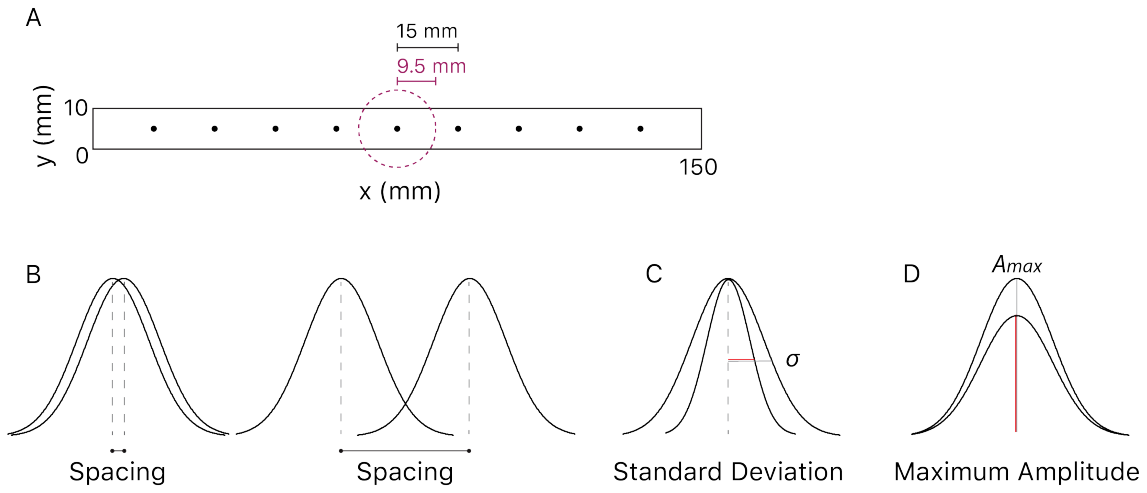


**Figure 1**. Simulated RFs and adapting stimulus. (**A**) A 150 x 10 mm patch of forearm skin with a line of cortical RFs along y = 5 mm. Black dot: RF centres. The spacing between adjacent RF centres (i.e. RF spacing) is a free parameter for data fitting. In this illustration, the spacing is 15 mm. Magenta dashed circle depicts site of adapting stimulus with a fixed radius of 9.5 mm. By default, areas covered by the circle are assumed to adapt uniformly; responses of RFs outside the circle are determined by the distance between the RF centre and the circumference of the circle. (**B**)(**C**)(**D**) Parameters of RF properties. (**B**) RF spacing. Left: small spacing, a great amount of overlap. Right: large spacing, little overlap. Same standard deviations and amplitudes. (**C**) Standard deviation ($\sigma$) of Gaussian RF response function. Wider curve and grey horizontal line: larger $\sigma$. Narrower curve and red horizontal line: smaller $\sigma$. Same amplitudes. (**D**) Maximum amplitude ($A_{max}$) of Gaussian RF response functions. Taller curve and grey vertical line: larger $A_{max}$. Shorter curve and red vertical line: smaller $A_{max}$. Same standard deviations.

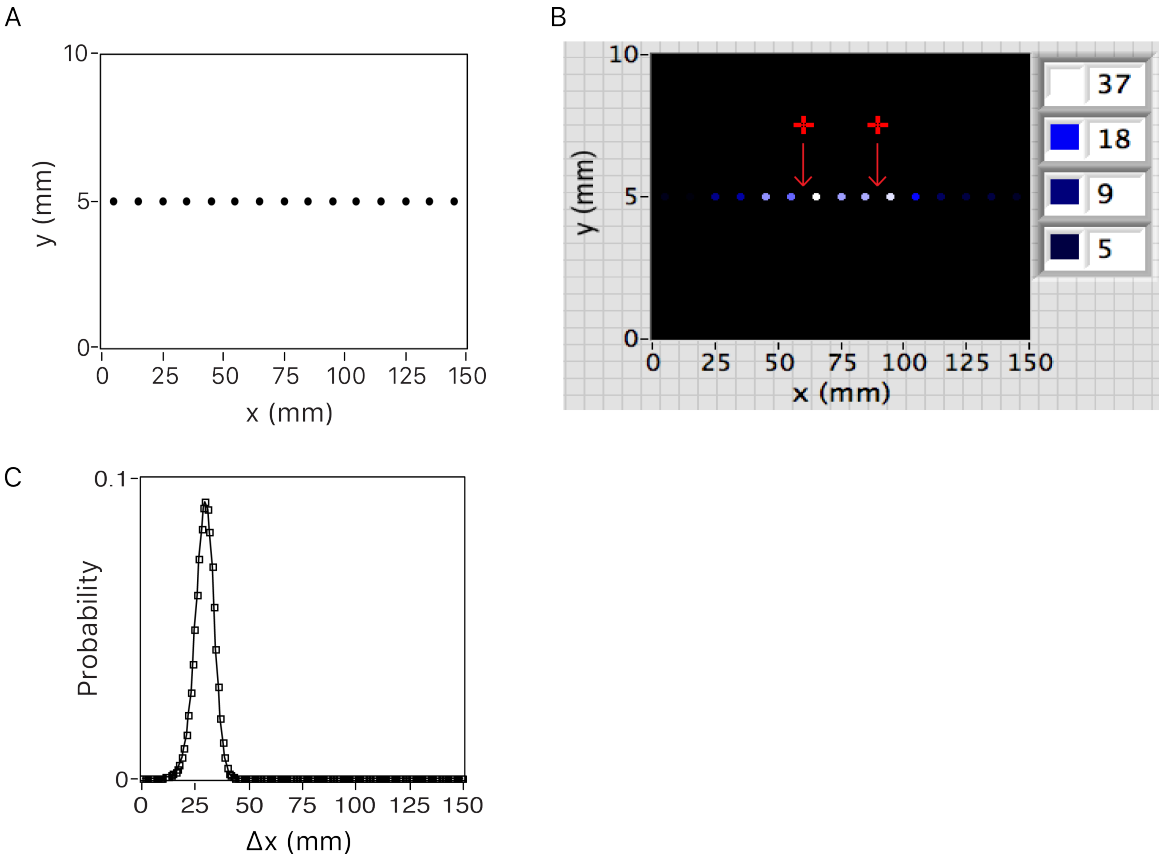


**Figure 2**. Modeling two-point distance comparison. (**A**) Simulated skin patch of RFs, with the axes rescaled for visual comparison with the population response plot. Parameters in the illustration: spacing = 10 mm, $\sigma$ = 20 mm, $A$ = 24 spikes. (**B**)(**C**) Example performance of the RFs in (A) on a random trial. (**B**) Population response to two simultaneous point-stimuli (red crosses) 30 mm apart. The point-stimuli are applied onto the same y-position (5 mm) as the RF centres; the red crosses are plotted above the RF line only for visual clarification. The arrows point to the x-positions of the two point-stimuli (60 mm, 90 mm); the points are asymmetric to the centre of the RF grid, (75 mm, 5 mm). Intensity scale bar on the right shows the actual number of spikes ($k$) each neuron fired, with lighter colours indicating greater numbers of spikes. (**C**) Posterior probability distribution over candidate two-point distances, $\Delta x$.

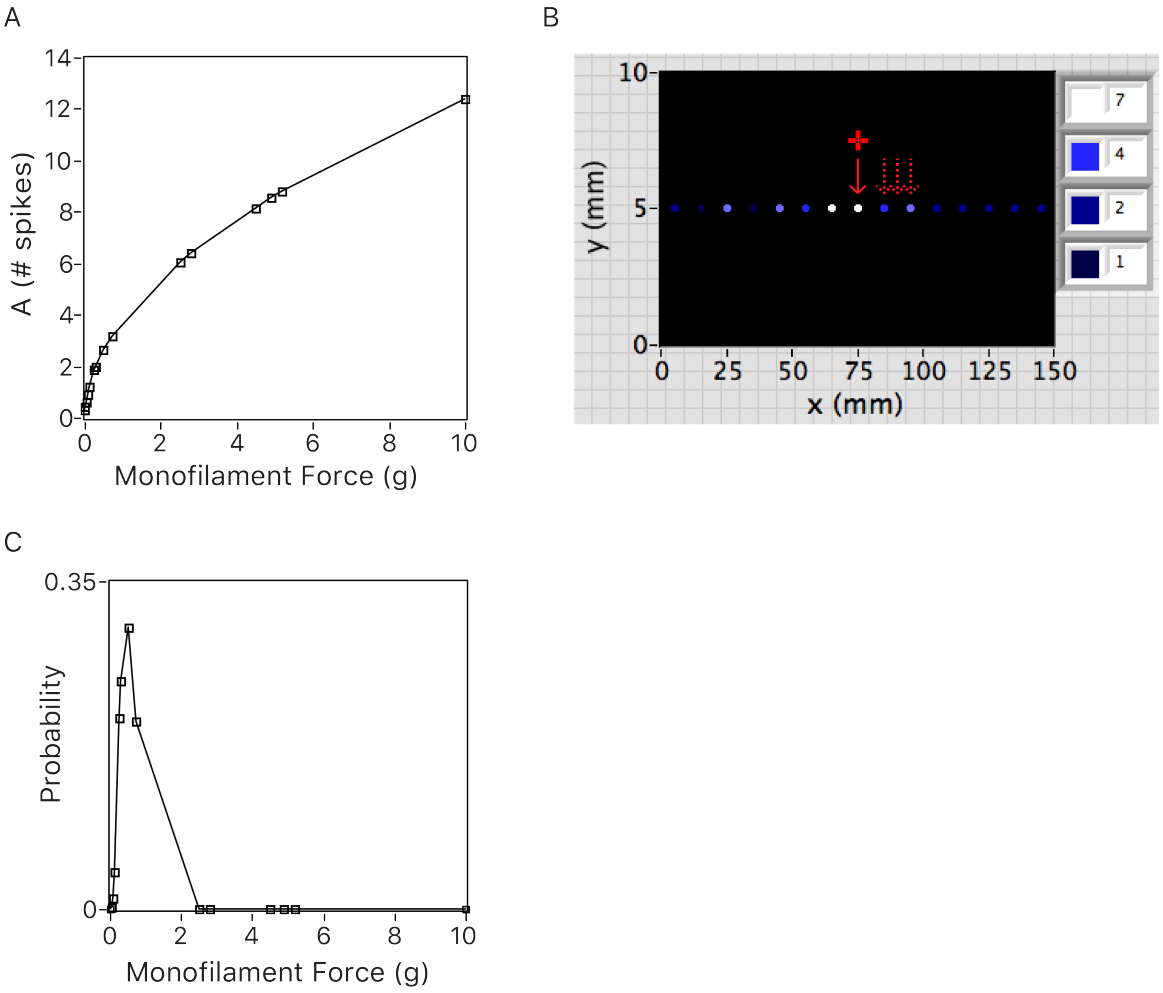


**Figure 3**. Modeling monofilament detection. (**A**) Amplitude (*A*) of the Gaussian response function, i.e. the expected spike count evoked at the RF centre, for different monofilament forces applied in the simulations and in empirical studies, calculated using Equations (1) and (4). (**B**) Population response on a random trial to a 0.5 g simulated monofilament (red cross) delivered at x = 75 mm (solid arrow). Intensity scale bar on the right: actual number of spikes (*k*) each neuron fired; lighter colours indicate greater numbers of spikes. Dashed arrows: the other three test sites 10, 15, and 20 mm to the right of x = 75 mm, respectively. The four sites are tested in consecutive trials. (**C**) Posterior probability distribution over candidate stimulus force.

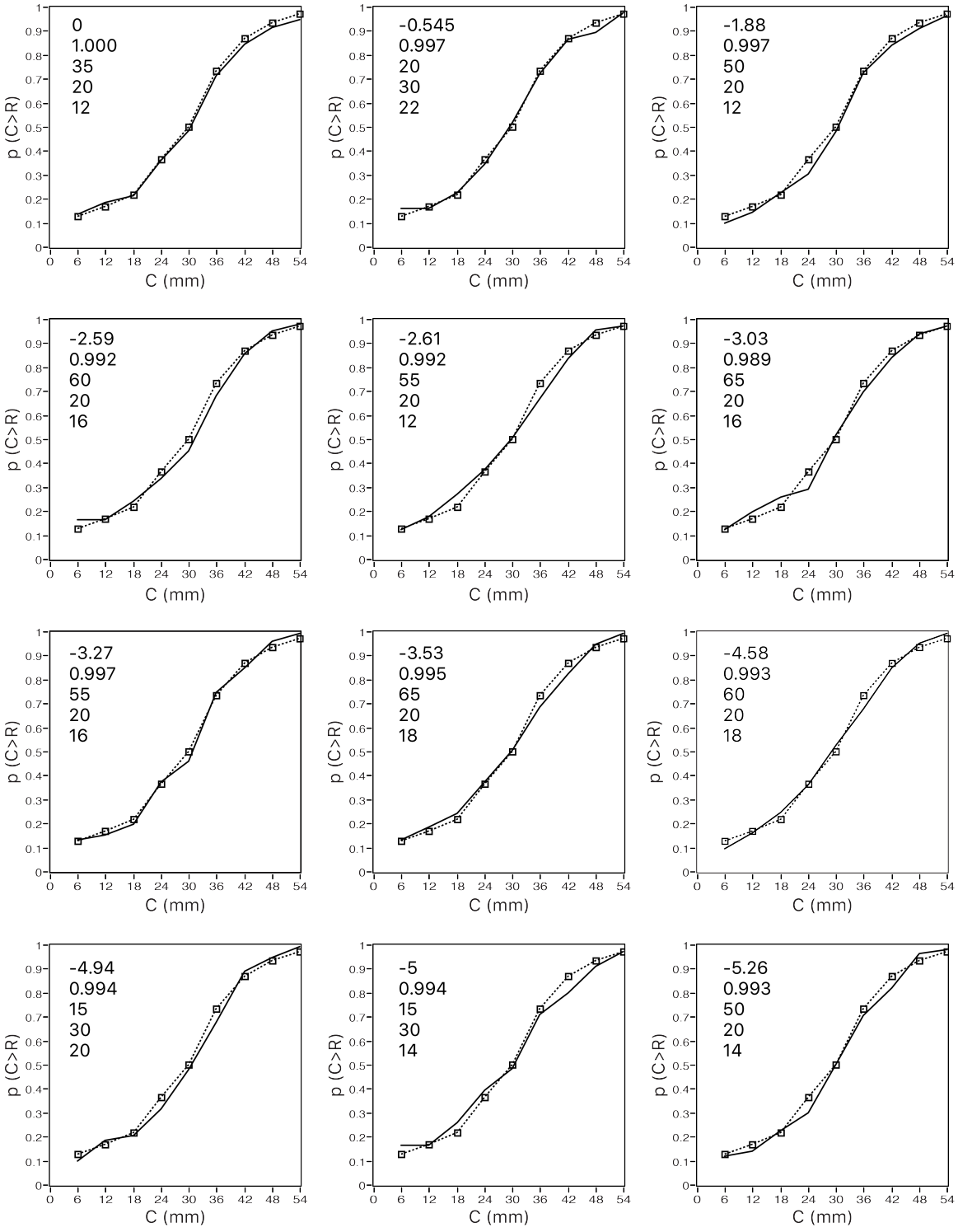


**Figure 4**. Top 12 best-fitting model performances (solid curves) in the no-adaptation (NA) condition, arranged in order of the highest (top left) to lowest (bottom right) log-

likelihood. Dashed curves and squares: average NA performance of 19 participants from Expt. 1 in Chapter 2; each square is the mean of 570 trials. Horizontal axis: comparison distance, C. Vertical axis: proportion of trials on which the comparison distance was perceived to be greater than the reference distance, p(C>R). The five numbers on the top-left corner in each sub-figure are (from top to bottom): the corresponding model fit's log likelihood-ratio (LLR; log base 10) relative to the top best-fit, $r^2$ (with respect to human data), RF spacing (mm), $\sigma$ (mm), and $A_{max}$ (spikes), respectively.

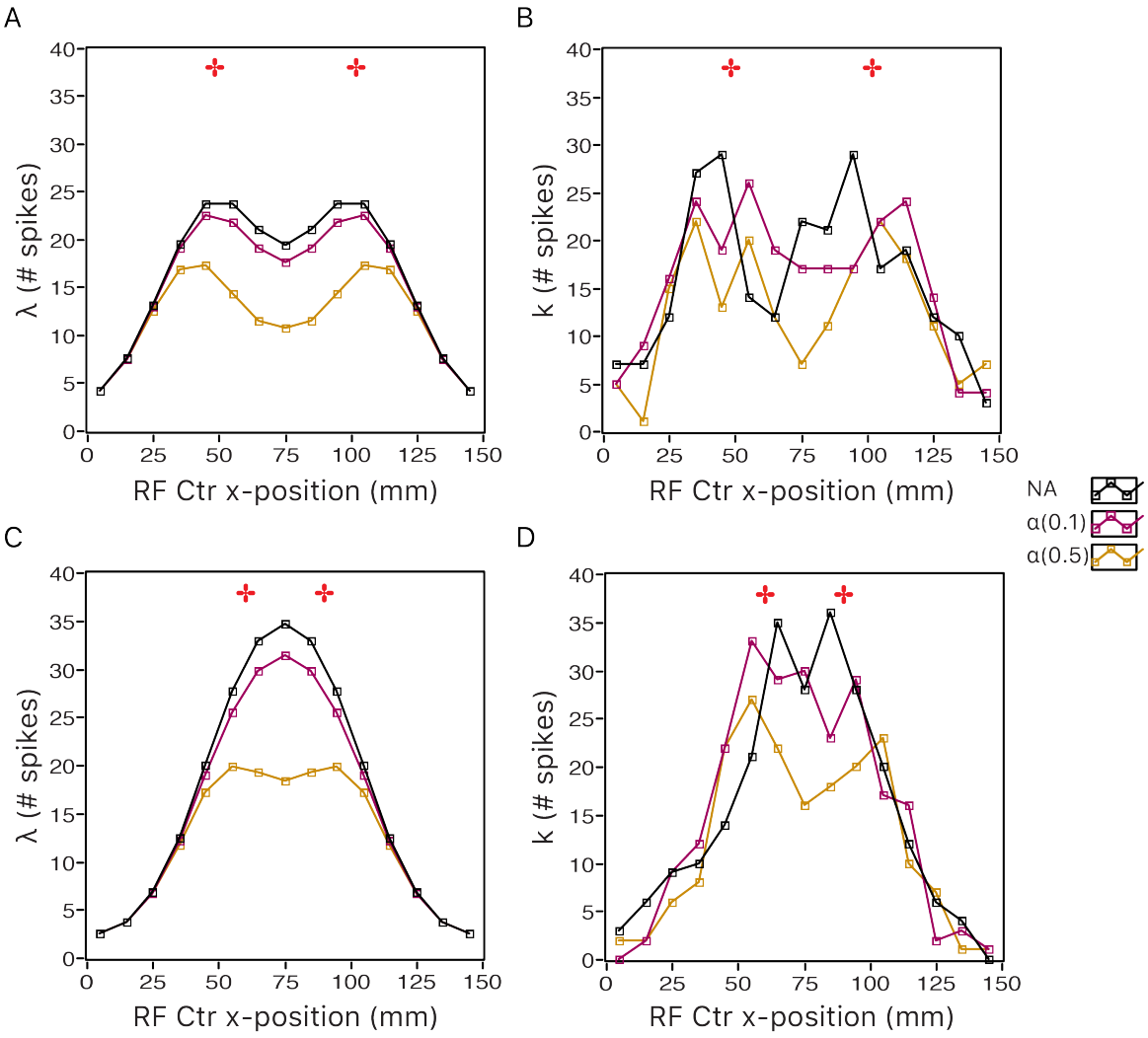


**Figure 5**. Effects of adaptation on neural population response in the encoder. Adapting stimulus was applied to the midpoint of the RF line (x-position = 75 mm) and adapted a circular area with a radius of 9.5 mm. Colours depict different adaptation conditions. Black: no adaptation (NA). Magenta: adaptation with the adaptation state $\alpha = 0.1$. Orange: adaptation with $\alpha = 0.5$. Squares on the curves: number of spikes fired by neurons with the corresponding RF centre x-positions (horizontal axis). (**A**)(**B**) Population response to two simultaneous point-stimuli 54-mm apart; x-positions for the stimuli were 48 mm and 102 mm (red crosses). (**C**)(**D**) Population response to two simultaneous point-stimuli 30-mm apart; x-positions for the stimuli were 60 mm and 90 mm (red crosses). (A)(C) depict the expected spike counts, $\boldsymbol{\lambda}$, which are the theoretical averages over many repeated trials. (B)(D) depict the actual spike counts, $\boldsymbol{k}$, observed on a random trial. The noisy neural data in (B) or (D) are what the encoder passes to the decoder, and they differ from trial to trial. RF parameters used for the illustrations: spacing = 10 mm, $\sigma = 20$ mm, $A_{max} = 22$ spikes.

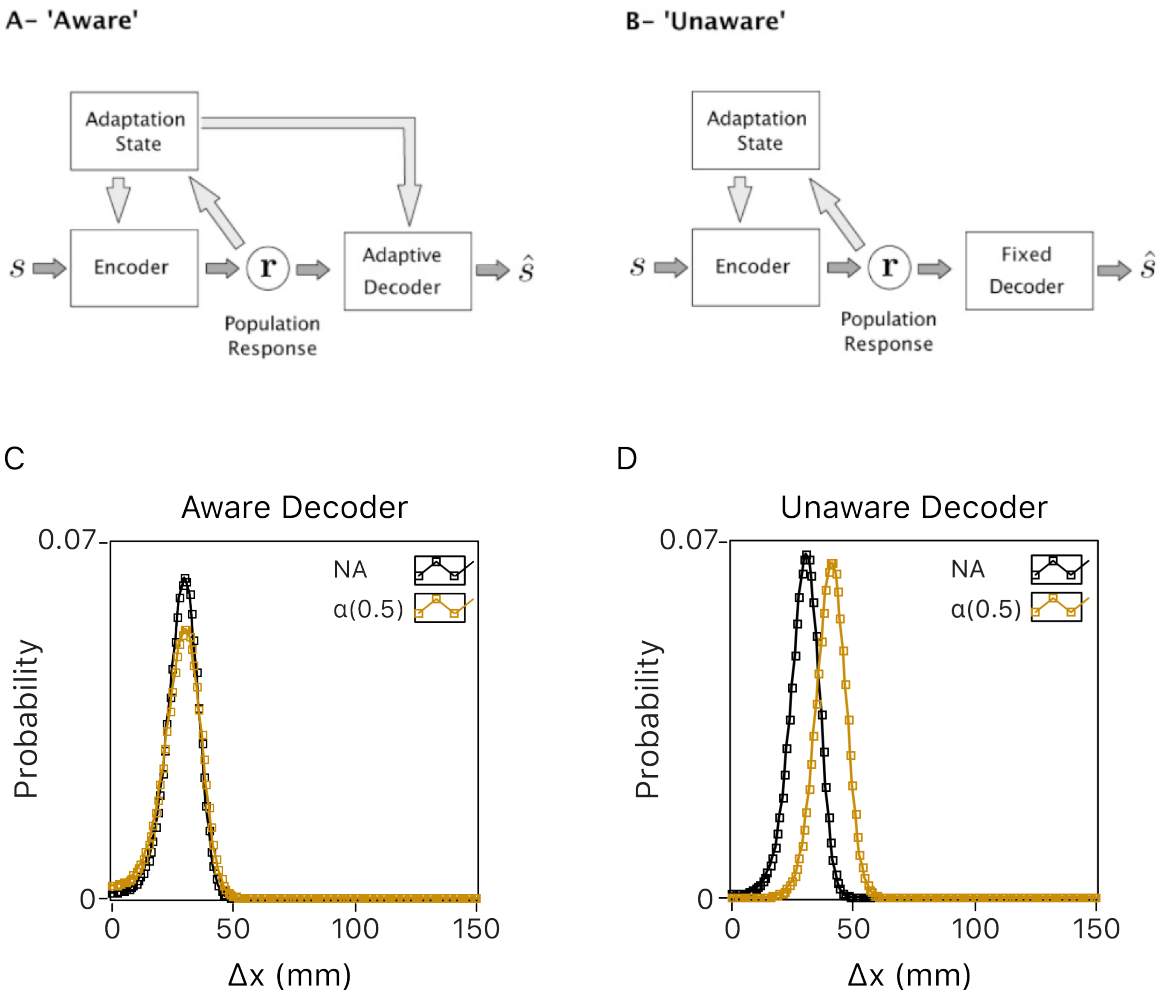


**Figure 6**. Effects of adaptation via an aware vs. unaware decoder. (**A**)(**B**) A general framework for adaptation proposed by Seriès et al. (2009). Stimulus attribute (S) is mapped into stochastic neural population response (r) by the encoder. The adaptation state affects this mapping. The response also affects the adaptation state; this is reflected in our model via the scaling of the general adaptation state for individual neurons based on their pre-adapted activation by the adaptor. The population response is then interpreted by a decoder to generate an estimate for the stimulus attribute ($\hat{S}$). Two types of decoders are considered. (**A**) An aware decoder knows about the adaptation state and adjusts its calculation accordingly. (**B**) An unaware decoder has a fixed readout procedure and does not have access to the adaptation state. Seriès et al. suggested that perceptual repulsion arises from an unaware decoder (figures are reused from Seriès et al. 2009 Fig. 1, with publisher permission for this dissertation only; copyright © 2009, MIT). (**C**)(**D**) Our model's estimates (posterior PDFs) for two-point distance ($\Delta x$) via different decoders. Actual distance: 30 mm. Black curves: NA. Orange curves: adaptation with $\alpha$ = 0.5. (**C**) Aware decoder. (**D**) Unaware decoder.

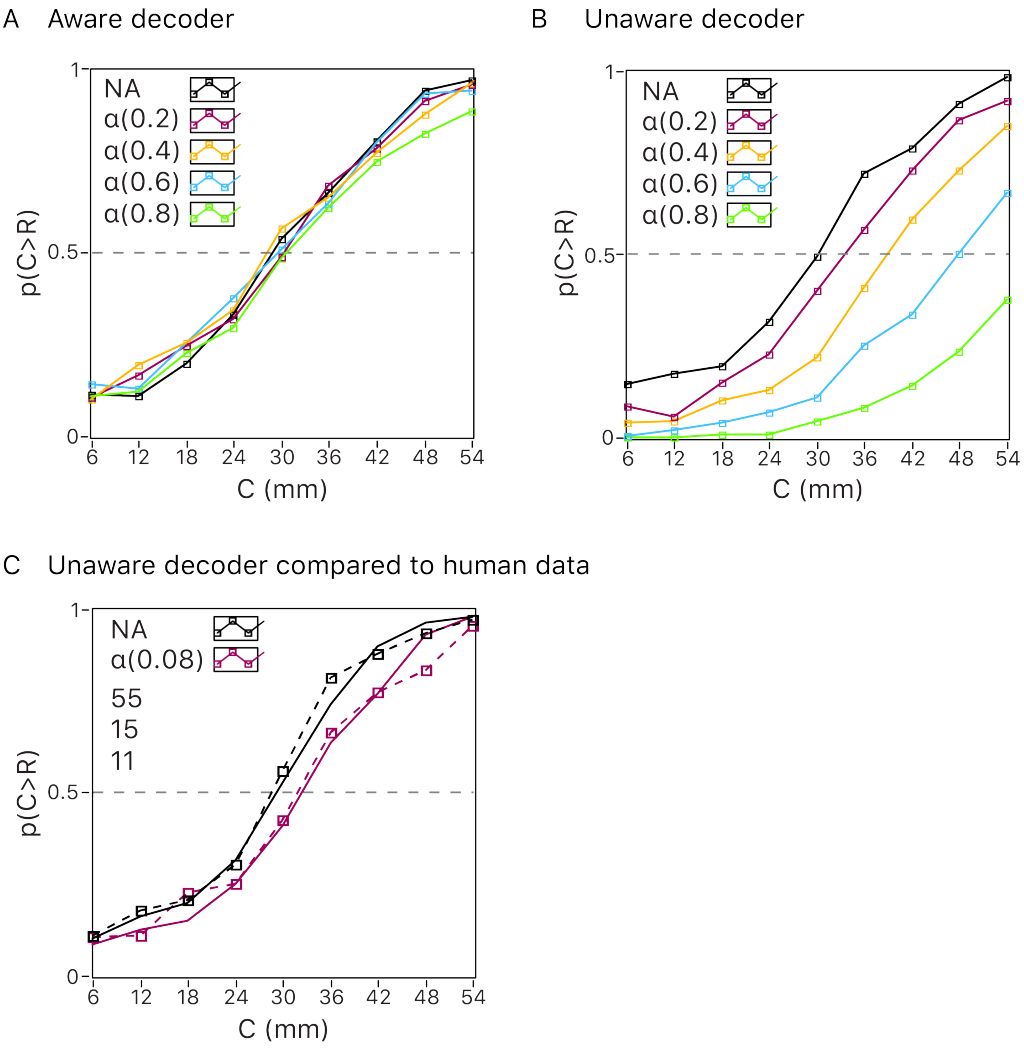


**Figure 7**. Effects of adaptation on two-point distance perception indicated by psychometric function and PSE. Colours depict different adaptation states indicated by $\alpha$ values (NA: $\alpha = 0$). (**A**)(**B**) Predictions using RF parameters best-fit to average baseline human data (Expt. 1 in Chapter 2) to perform under different adaptation states and decoder strategies. Parameters: RF spacing = 35 mm, $\sigma = 20$ mm, $A_{max} = 12$ spikes (same values as shown in top-left sub-figure of Fig. 4). (**A**) Aware decoder: adaptation does not induce a bias in the perceived distance. (**B**) Unaware decoder: increasing adaptation state causes a greater rightward shift of the psychometric function and increasing PSE, indicating an increasing perceived two-point separation. (**C**) Comparison of model performance to adaptation experimental data. The unaware decoder output is consistent with the spatial repulsion illusion observed empirically. Model performance was fit to data of Expt. 3 (adaptation experiment) in Chapter 2. Dashed curves and squares: human data averaged from 20 participants; each square is the mean of 200 trials. Solid curves: model fits averaged from 200 trials. Parameters: RF spacing = 55 mm, $\sigma = 15$ mm, $A_{max} = 11$ spikes, $\alpha = 0.08$.

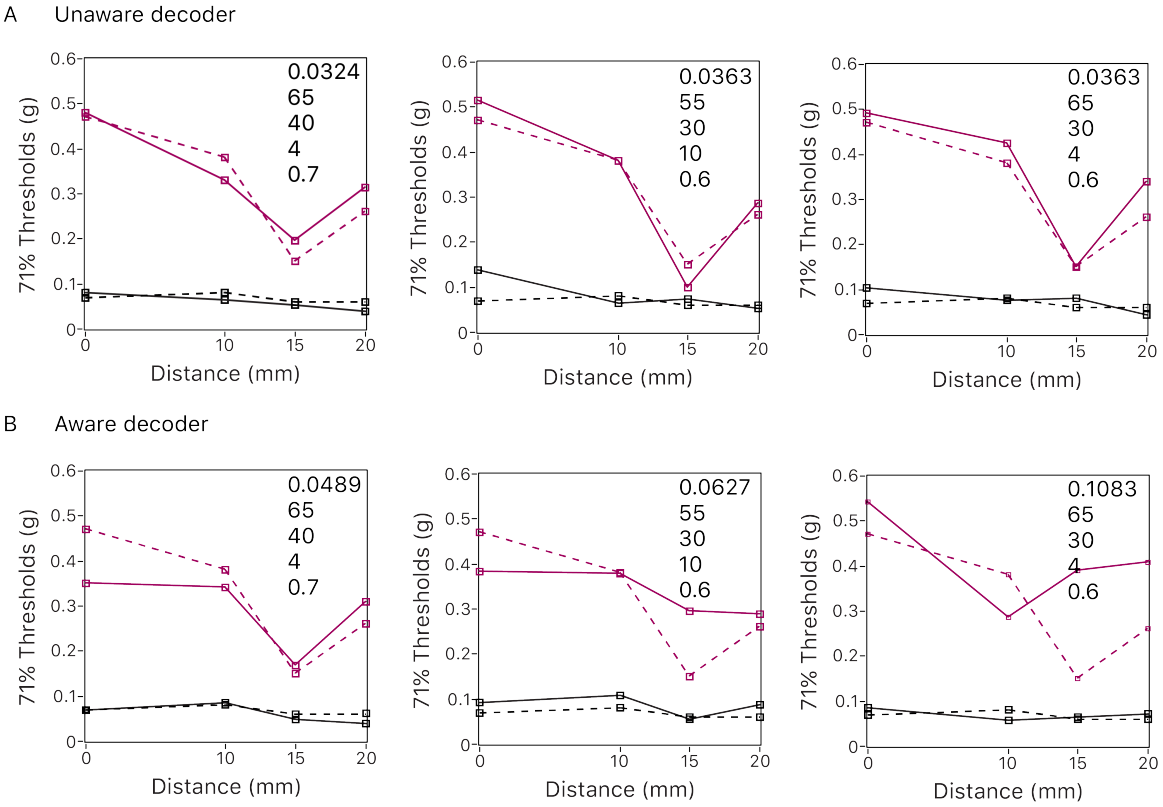


**Figure 8**. Effects of adaptation on single-point detection. Each sub-figure depicts the 71% correct detection thresholds at four test skin sites. Dashed curves: human performance averaged from 20 participants (Expt. 2B, Chapter 2). Solid curves: model performance averaged from 20 runs. Black: NA. Magenta: adaptation with $\alpha$ as the fit value. The five numbers on the top-right corner of each sub-figure are (from top to bottom): root mean square error (RMSE) of the fit, RF spacing, $\sigma$, $A_{max}$, and $\alpha$, respectively. (**A**) Top 3 model fits with an unaware decoder, ranked by RMSE. (**B**) Model performances using the same best-fitting parameters from (A) but with an aware decoder.

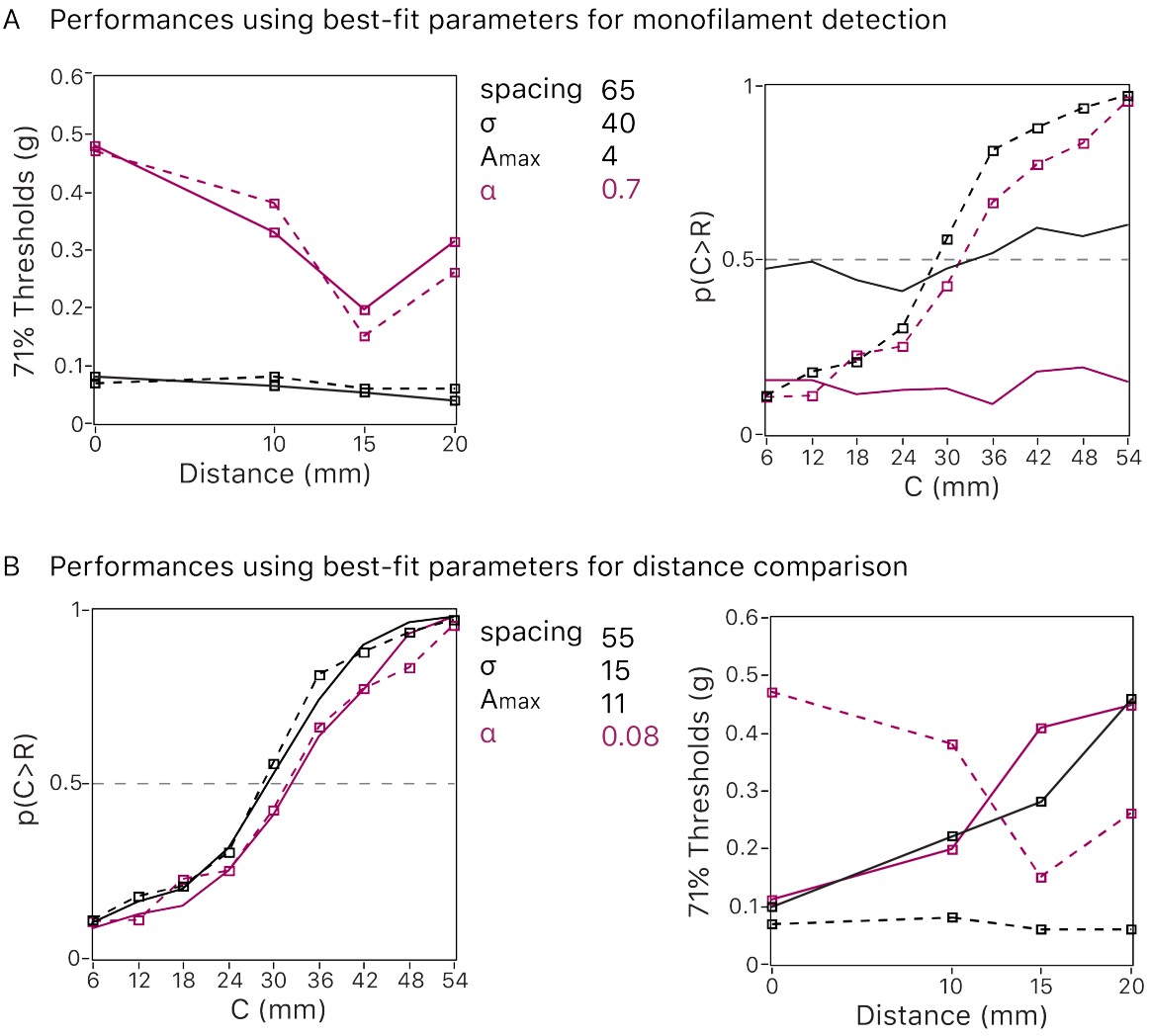


**Figure 9**. Model performance on either perceptual task using the best-fitting parameters from the other task. Dashed curves: average human performances. Solid curves: model performances. Black: NA. Magenta: adaptation with $\alpha$ as the fit value. (**A**) Model using best-fitting parameters (values in the middle) for monofilament detection (left; same figure as Fig. 8A left) performs poorly in two-point distance comparison (right). (**B**) Model using best-fitting parameters (values in the middle) for two-point distance comparison (left; same figure as Fig. 7C) performs poorly in monofilament detection (right). Monofilament-detection fits: RMSE = 0.0324 for (A) left, and 0.2483 for (B) right. Distance-comparison fits: $r^2$ NA = 0.992 and $r^2$ Adapt = 0.987 for (B) left, and $r^2$ NA = 0.694 and $r^2$ Adapt = 0.073 for (A) right.

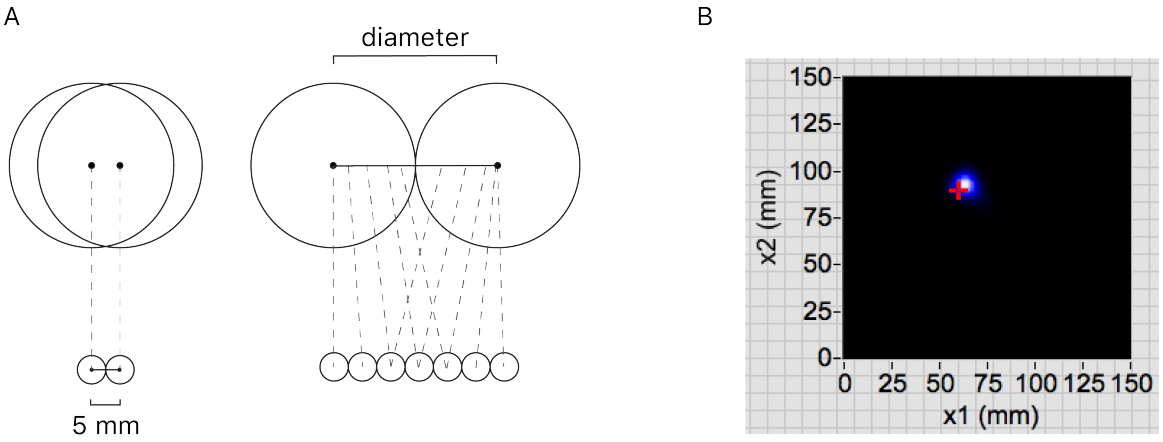


**Figure 10**. Illustrations for Discussion. (**A**) Range of cortical RF spacing for data fitting. Large circles: cortical neurons in S1. Small circles: peripheral receptors. Dashed lines: projection (convergence and divergence) of afferent input to the cortex. Left: adjacent cortical RFs are almost completely overlapped, and each receives input from one of two adjacent receptors; in this case, the cortical RF spacing is approximately determined by the receptor spacing. Right: adjacent cortical RFs border each other with zero overlap, and each receives convergent and divergent input from multiple receptors; in this case, the cortical RF spacing is approximately the average diameter of cortical RFs. (**B**) Joint (two-dimensional) posterior probability distribution over candidate two-point x-positions. For the distance-comparison task, if the model hypothesizes about the two-point positions ($x_1$, $x_2$), it first calculates these joint-posteriors for the two positions. It then marginalizes them over ($x_2 - x_1$) to generate the posterior distribution over $\Delta x$, similar to the one shown in Fig. 2C.

# CHAPTER 5

# GENERAL DISCUSSION

## 5.1 Summary of studies

The empirical and theoretical work presented in this thesis demonstrates that tactile spatial perception is subject to an adaptation-induced illusion that expands the perceived distance between points on the skin. We measured two-point distance perception using a two-interval forced–choice (2IFC) task: participants compared the distances of two pairs of point-stimuli (reference vs. comparison) applied on their forearms successively, reporting which distance felt greater. The reference distance was fixed, and the comparison distance varied. The point of subjective equality (PSE), i.e. the comparison distance reported as being greater than the reference distance 50% of the time, was extracted as a measure of the perceived distance between the reference points. The 2IFC comparison procedure and the use of PSE are robust against potential biases in participants' subjective estimates of the two-point distance or locations, because any possible biases would presumably be present on both forearms and thus canceled out via comparison. In addition, we tracked changes in tactile sensitivity using a 2IFC monofilament-detection task.

In Chapter 2, we investigated the effects of vibrotactile adaptation on two-point distance perception. First, we verified that baseline PSE was unbiased across arms and stable across experimental blocks. Then, we verified that prolonged vibration of a region of skin on the reference forearm focally reduced tactile sensitivity (i.e. adaptation), as indicated by elevated monofilament detection thresholds. Finally, we applied vibratory adaptation on the skin between the two reference points, and discovered that this caused an illusory increase in the perceived separation between the points (i.e. a repulsion illusion), as indicated by an increased PSE and a rightward shift of the psychometric function.

In Chapter 3, we investigated whether peripheral desensitization was sufficient to induce the repulsion illusion, by applying topical anesthesia instead of vibrotactile adaptation to reduce tactile sensitivity more thoroughly. We found that topical anesthesia focally reduced tactile sensitivity but caused little to no shift in the PSE. The results suggest that mere desensitization of peripheral receptors is not sufficient to induce the repulsion illusion, and central adaptation is required for the illusion to occur.

In Chapter 4, we applied Bayesian perceptual modeling to investigate adaptation effects on tactile perception on a theoretical and computational basis. The model parameterized receptive field (RF) properties of somatosensory cortical neurons, and simulated neural firing patterns evoked by point-stimuli. It then applied Bayesian inference to decode the

simulated neural data and make probabilistic estimates of the stimulus attributes, thereby performing simulated psychophysical tasks equivalent to those used to test human participants. With specific sub-optimal constraints, such as sparse RFs and Poisson firing noise, the model replicated human performance in two-point distance comparison and monofilament detection. Moreover, following focal adaptation, it exhibited a repulsion illusion that was comparable to the repulsion illusion empirically observed in Chapter 2. Interestingly, the illusion emerged only when the decoder was unaware of adaptation in the encoding stage. These results are consistent with the finding in computational research on visual perception that adaptation-induced illusions result from the brain's decoding of sensory input without awareness of the adaptation state of the nervous system.

To our knowledge, the current thesis provides the first combined psychophysical and computational study on the effects of adaptation on tactile spatial perception. Its main findings are consistent with the adaptation-induced repulsion illusions reported in vision and audition, suggesting that tactile perception shares common processing features with visual and auditory perception. It sheds light on possible mechanisms and functional organizations underlying dynamic tactile spatial processing as the somatosensory system adjusts to the external environment.

## 5.2 Possible cellular and synaptic mechanisms underlying tactile adaptation

Although adaptation to sustained or repetitive stimulation has been found to occur at multiple levels along the somatosensory pathway, the cellular and synaptic mechanisms underlying the effects of adaption on tactile perception are largely unknown. Nevertheless, *in vitro* and *in vivo* studies of rodent somatosensory cortex have shed some light on the neural mechanisms. *In vitro* studies have found that adaptation operates over several time scales, ranging from tens of milliseconds to tens of seconds (Rauch et al., 2003; La Camera et al., 2006). Using current clamp and injecting long-lasting episodes of step-like and noisy, in-vivo-like current to pyramidal neurons and fast-spiking interneurons from rat somatosensory cortex, Rauch et al. (2003) and La Camera et al. (2006) found that the neurons displayed a combination of several adaptive processes. Some of the processes were transient and disappeared in less than 10 ms (initial adaptation, pyramidal neurons only) or a few hundred milliseconds (fast adaptation); others were long-lasting and slowly decaying on the order of seconds to a minute (slow adaptation). Moreover, a slow afterhyperpolarization (AHP) was observed in the fast-spiking interneurons. Slow AHP has been associated with slow adaptation in this type of neurons in ferret visual cortex, and the duration of the AHP significantly correlates with the time constant of the adaptation (Descalzo et al., 2005). Although Rauch et al. (2003) and La Camera et al. (2006) did not explicitly speculate on presynaptic versus postsynaptic contributions, they suggested that slow inactivation of $Na^+$ or other ionic channels responsible for spike generation might be associated with the slow adaptation.

Interestingly, the timescale over which $Na^+$ channels recover from inactivation depends on the duration of the previous depolarization (Toib et al., 1998), which is consistent which the perceptual finding of a longer-lasting adaptation effect following a longer-lasting adapting stimulus.

Studies of the cellular mechanisms of adaptation in somatosensory cortical neurons have drawn inspiration from research in visual contrast adaptation. Of all adaptation effects, the cellular mechanisms underlying changes in visual contrast sensitivity are perhaps the best understood (A. Kohn, 2007). In the retina, $Na^+$ channel inactivation in ganglion cells contributes to changes in contrast sensitivity (Kim & Rieke, 2003). In the primary visual cortex (V1), whole cell recordings have shown that 30 s to several minutes of exposure to high contrast stimuli results in a tonic AHP but little change in synaptic input (Carandini & Ferster, 1997). This AHP is due primarily to activation of $Na^+$-activated $K^+$ channels, triggered by $Na^+$ influx that occurs with synaptic input (Sanchez-Vives et al., 2000a, 2000b). $Ca^{2+}$-activated $K^+$ currents also contribute to contrast adaptation but are presumably not the primary driving cause: blocking transmembrane $Ca^{2+}$ conductance does not reduce the slow AHP, but reducing $Na^+$ reduces the slow AHP even in the presence of pronounced $Ca^{2+}$ spikes (Sanchez-Vives et al., 2000b). Although these findings concern visual contrast adaptation, similar mechanisms may contribute to other adaptation effects in non-visual sensory systems.

Another mechanism plausibly underlying adaptation is short-term synaptic depression. During repeated stimulation, synaptic depression often decreases postsynaptic current amplitude, which can take seconds to minutes to recover after the stimulation. Activity-dependent synaptic depression is commonly attributed to depletion of presynaptic vesicles. In addition, depression of transmitter release can arise from the release of modulatory substances from the activated presynaptic terminals, postsynaptic cells, or neighbouring cells (for a review, see Zucker & Regehr, 2002). Theoretical studies have suggested how synaptic depression could explain certain neural aftereffects that could give rise to perceptual aftereffects (e.g. Chance et al., 1998).

An *in vivo* study of the rat whisker barrel cortex has suggested that short-term synaptic depression of thalamic input to the cortex, as well as intracortical mechanisms, plays a key role in rapid somatosensory cortical adaptation (Chung et al., 2002). Chung et al. performed *in vivo* whole-cell recording from neurons in the barrel cortex and measured synaptic responses to repetitive 4 or 8 Hz whisker deflection or electrical stimulation of the ventral posterior medial nucleus (VPM) of the thalamus. In addition, extracellular recording was performed simultaneously from the VPM and the barrel cortex. It was found that thalamic and cortical neurons both adapted within hundreds of milliseconds of deflections, but cortical neurons adapted faster and much more strongly, and recovered much more slowly than thalamic neurons. The thalamic neurons recovered immediately

after adaptation, whereas the recovery time of evoked excitatory postsynaptic potentials (EPSPs) in the cortex was ~ 10 s for 4 Hz deflection and ~ 20 s for 8 Hz deflection, which matched the recovery time course of cortical responsivity. These findings suggest that both subcortical adaptation and cortical mechanisms contribute to the observed rapid cortical adaptation. However, rapid adaptation did not alter the cortical neurons' intrinsic membrane properties, including resting membrane potential, input resistance, and current-evoked firing; this suggests that postsynaptic factors, such as AHP or accumulating GABAergic inhibition, was unlikely to account for the drastic response reduction observed during rapid cortical adaptation. Furthermore, rapid adaptation did not alter intracortically evoked EPSPs, which suggests that reduction in intracortical recurrent excitation or the degree of intracortical amplification could not account for the rapid cortical adaptation. Taken together, these results strongly suggest that synaptic depression of thalamic input to the cortex is responsible for the rapid adaptive modification of somatosensory cortical neuronal sensitivity.

In our study, 40 s of vibration at the beginning of a testing block plus a 3-s top-up in between trials was sufficient to induce changes in tactile spatial perception that appeared to partly linger >20 min after the cessation of vibration (Chapter 2, Fig. 5, Post vs. Pre). This result is consistent with the finding of Macefield & Burke (1991) in human participants that the cortical response evoked by a test stimulus to the fingertip decreased for as long as 25 min after a 10-min 200 Hz adapting vibration delivered to the same or adjacent digital nerves. The mechanisms described above plausibly contributed to changes in the somatosensory system that gave rise to the perceptual effects during vibrotactile adaptation and shortly after; however, the timescales over which these mechanisms operate (milliseconds to a few minutes) may be too short to account for the apparent lingering effect after 20 min. Mechanisms that function on longer timescales plausibly contribute to the long-lasting component of the effect.

Two candidates for such mechanisms are long-term depression (LTD) of excitatory synapses and long-term potentiation (LTP) of inhibitory synapses. LTD and LTP refer to activity-dependent long-lasting decrease or increase, respectively, in the efficacy of synaptic transmission. LTD consists of an initial phase lasting for ~ 10 min and a subsequent later phase that lasts hours or longer that can be reliably recorded (Ito, 1989). LTP lasts for hours *in vitro* and can persist *in vivo* for weeks or months (Cooke & Bliss, 2006). LTD and LTP occur in different types of neurons at many areas of the CNS via a variety of mechanisms and neurotransmitters. The most common neurotransmitter involved is glutamate, and a common glutamate receptor is the N-methyl-D-asparate (NMDA) receptor. *In vitro* research using rat somatosensory cortical slice and *in vivo* research on monkey S1 have shown that during repetitive stimulation, $K^+$ increasingly accumulates in the restrictive extracellular space of the cortical region (Lee & Whitsel, 1992; Lee et al., 1992). Comparable levels of $K^+$ accumulation have been shown to facilitate the activation of NMDA receptors (Poolos & Kocsis, 1990). Furthermore,

NMDA receptor antagonists attenuate the stimulus-evoked response changes in somatosensory cortical neuronal populations *in vitro* and *in vivo* in a dose-dependent manner (Duncan et al., 1982; Lee & Whitsel, 1992). Accordingly, it has been proposed that interactions among neuronal columns, mediated by NMDA receptors during adaptation, underlie the stimulus-specific modifications in the spatio-intensive pattern of somatosensory cortical activity (Whitsel et al., 1991; Lee & Whitsel, 1992). Future research is needed to elucidate how long these effects persist after the adapting stimulus.

In short, a variety of mechanisms at the level of single neurons or neuronal populations, especially mechanisms involving synaptic plasticity, could contribute to adaptive changes in the somatosensory system that might underlie the adaptation-induced tactile perceptual effects reported in the present thesis.

### 5.3 Functional benefits of adaptation

Earlier studies of tactile adaptation tended to emphasize various forms of receptor fatigue (e.g. Wedell & Cummings, 1938; Gescheider & Wright, 1969; Barker et al. 1982; Pubols, 1982; Lundstrom, 1986). However, more recent research has begun to unravel more complex consequences of adaptation in the somatosensory system and on tactile perception. Adaptation has been shown to induce profound changes along the somatosensory pathway in the CNS. For example, it can suppress neuronal response in the cuneate nucleus (Bystrzycka et al., 1977; O'Mara et al., 1988), thalamus (Chung et al., 2002), and S1 (Laskin & Spencer, 1979; Macefield & Burke, 1991; Whitsel et al., 2003). Furthermore, it can refine the spatial and temporal patterns of initial cortical activation, effectively fine-tuning cortical responses (Lee & Whitsel, 1992; Tommerdahl et al., 2002; Simons et al., 2005; Simons et al. 2007; Chung et al., 2015). Adaptation also leads to perceptual aftereffects more than just decreased sensitivity. An adaptation-induced perceptual aftereffect well-documented in vision and audition is known as perceptual repulsion: following focal adaptation, the perceived attribute of a subsequent stimulus similar to that of the adapting stimulus often shifts away from the adapting attribute. A well-known example of this is the visual tilt aftereffect illusion: Adaptation to tilted lines causes subsequently viewed lines with nearby orientations to appear tilted away from the adapted orientation (J. J. Gibson & Radner, 1937). Perceptual repulsion has been reported for a wide variety of visual (for reviews, see Clifford et al., 2007; Webster, 2012) and auditory (e.g. Carlile et al., 2001; Heron et al., 2012) stimulus features, including simple features such as location or direction, and more complex features such as contingent properties (e.g. contingent colour and orientation, as in the McCollough effect). Moreover, adaptation in vision can lead to perceptual repulsion in auditory perception (e.g. Kitagawa & Ichihara, 2002; Barraclough et al., 2017).

Adaptation presumably manifests differently in different sensory modalities and parts of the nervous system, but it is plausible that these different forms of adaptation share some common functional roles or computational principles. In the present thesis, we propose a general model that can apply to focal adaptation in any mosaic of neurons tuned to similar stimulus attributes. Adaptation is characterized as temporal response reduction of neurons that are selectively coding the adapting stimulus attribute. In other neurons, the degree of response reduction diminishes as a function of distance or dissimilarity between the adapting attribute and the attributes to which the neurons are tuned. This stimulus-specific response reduction has been observed at multiple levels of perceptual processing pathways across modalities (Yates et al., 1985; Baylis & Rolls, 1987; Saul & Cynader, 1989; Belin & Zatorre, 2003; Dragoi et al. 2000; Dragoi et al., 2001). We propose that this differential effect results in a shift in the distribution of neuronal population activity evoked by a subsequent similar stimulus, thus contributing to repulsive perceptual aftereffects following focal adaptation.

A prediction of this general model is that focal adaptation can selectively enhance discrimination around the adapting stimulus attribute. Because the differential response modifications magnify differences between the adapting attribute and the attributes in vicinity to it, the minimal differences required to distinguish between these attributes should decrease following adaptation. Indeed, vibrotactile adaptation has been found to improve frequency and amplitude discrimination around the adapting value (Goble & Hollins, 1993, 1994; Tommerdahl et al., 2005; Tannan et al., 2007). In the present thesis, the adaptation-induced spatial repulsion illusion indicates an increased discriminability between point-stimuli straddling the adapted skin region.

In our studies, some participants reported that the two reference points, separated by 30 mm on their forearm, felt like a single large point instead of two points. This was to be expected because the forearm has poor spatial acuity. The two-point limen (i.e. the minimal two-point separation required to reliably distinguish two points from a single point) has been reported to be ~ 39 mm on human forearm (Weinstein, 1968). The 30-mm reference distance was below this two-point limen. A recent study (Tong et al., 2013) applied two simultaneous point-stimuli diagonally to the volar forearm (i.e. at ±45 degrees relative to the cardinal axes of the arm) and measured participants' ability to distinguish them from a single point in a 2IFC task. The study found that 30-mm separation corresponded to ~ 85% correct discrimination. The discrimination performance would possibly have been worse in our studies due to anisotropy: RFs tend to be elongated and oriented longitudinally with respect to the arm, so the same two-point stimulus is likely to activate fewer RFs when applied longitudinally (as in our studies) than transversely or obliquely. Therefore, a proportion of our participants presumably could not perceive the reference points as two separate points. This is consistent with the performance of our computational model that generated a unimodal population response to a two-point stimulus when largely overlapped RFs were activated, a phenomenon that is evidenced in neurophysiological studies of the somatosensory cortical response to brief multi-point stimuli applied to adjacent loci of the skin surface (Dewson, 1964; Gardner &

Spencer, 1972a, 1972b; Chen et al. 2003). It is also consistent with psychophysical studies reporting that distance between simultaneous points on the forearm is underestimated, and the perceived point locations are biased towards their midpoint (Green, 1982). Nevertheless, the 2IFC distance-comparison task used in our studies was designed such that the perception of the reference distance was not with respect to the actual distance, but with respect to the comparison distance on the other arm. This design was robust against influence from potential underestimation bias or subjective criterion on what felt like two points versus one point, because an individual participant presumably had the same bias and criterion regarding both arms and thus the influence canceled. Consequently, the PSE shift was with respect to the baseline: following adaptation, the points were perceived as farther apart compared to without adaptation, not compared to the actual distance. We suggest that this PSE shift resulted from a more distinguishable spatial pattern in the neuronal population response caused by focal adaptation, as demonstrated in our model simulation (Chapter 4, Fig. 5).

The effect of enhanced discriminability around the adaptor is aligned with the general functional benefits proposed for adaptation. From an information-processing perspective, it has been proposed that adaptation is a self-calibrating mechanism of the sensory system to adjust to stimulus statistics and optimize information gain (for reviews, see Clifford et al., 2000; Stocker & Simoncelli, 2006; Kohn, 2007; Webster, 2012). Presumably, reducing neural responsivity to a sustained or repetitive stimulus (the adaptor) saves metabolic energy and reallocates the limited sensory resources for efficient coding. At the expense of overall sensitivity, adaptation improves differential sensitivity, facilitating detection of changes and discrimination of small differences around the adaptor (Barlow, 1990; Barraclough et al., 2017). At the single-cell level, adaptation can modify the spatiotemporal RF (Hosoya et al., 2005) or tuning curve (Dragoi et al., 2000, 2001; Kohn & Movshon, 2004; Jin et al., 2005). At the population level, adaptation can reduce neuronal correlations and hence coding redundancy (Gutnisky & Dragoi, 2008), and refine the spatial and temporal patterns of initial cortical activation (Lee & Whitsel, 1992; Tommerdahl et al., 2002; Simons et al., 2005; Simons et al. 2007; Chung et al., 2015). These effects presumably optimize the utility of the limited dynamic range of neuronal response. Therefore, adaptation serves the functionally beneficial role of facilitating neural coding efficiency for ongoing and subsequent stimuli.

### 5.4 Implications and future directions

Adaptation has a rich history of being utilized as a tool to probe the mechanisms of sensory perception. In tactile research, adaptation has commonly been used to classify mechanoreceptive afferents and S1 neurons. It has also been implemented to dissect the contribution of specific types of afferents on cortical responses or perception by selectively "adapting out" these afferents (e.g. Tommerdahl et al., 2002; Hollins et al., 2001; Bensmaia et al., 2006). In the present thesis, we used adaptation to probe tactile

spatial processing in the context of recent sensory history. The adaption-induced spatial repulsion illusion we observed provides a window into how spatial information is normally processed and interpreted by the somatosensory system as it adjusts to the sensory environment. Locating stimuli on the skin and determining the distance between them are the basis of many tactile spatial tasks; thus, the findings of this thesis have implications on tactile and haptic perception of more complex stimuli.

The spatial illusion we reported adds to the mounting evidence that the perception of space in touch rests on a rather pliable foundation and is influenced by its temporal context. The perceived distance between successive points and the perceived locations of successive points on the skin are both dependent on the timing between the points. This phenomenon manifests in several spatiotemporal illusions; the best-known of them is the cutaneous rabbit illusion, where three or more successive taps delivered rapidly to two skin sites appear to hop progressively along the skin from the first site to the second, although the intervening skin region received no actual taps. Previous work from our laboratory provided Bayesian perceptual models that nicely replicated the cutaneous rabbit and related spatiotemporal illusions. The models demonstrated how stimulus timing can distort spatial perception when the brain interprets noisy sensorineural data under a simple perceptual assumption: a low-speed prior (Goldreich, 2007; Goldreich & Tong, 2013; Tong et al., 2016). In the present thesis, we explored tactile spatial perception in a different form of temporal context, which affects perception not via the prior but by changing the likelihood function. We showed that a Bayesian decoder that is unaware of the adaptation-induced likelihood changes exhibits a repulsion illusion in the perceived two-point distance that is comparable to the illusion observed in human performance. This work contributes to the increasing evidence that the brain perceives in a probabilistic manner, and perception is subject to the influence of sensory history and the brain's expectations.

Moreover, the increased spatial resolution around the adapting stimulus raises interesting possibilities in plasticity and perceptual learning. It has been shown that many minutes to hours of repetitive stimulation on the fingertip, either mechanically or electrically by a wearable device, improved two-point discrimination performance for almost 24 hours after the removal of the device, indicating improved spatial acuity (e.g. Godde et al., 2000). This suggests that perceptual learning can be induced without any direct training, simply via exposure to prolonged sensory stimulation even when it is task-irrelevant (Beste & Dinse, 2013). We suggest that in this "learning without training" paradigm, focal vibrotactile adaptation plays an important role in improving spatial acuity. Future research could test this hypothesis and explore the effects of focal adaptation on perceptual learning.

The work in this thesis supports the similarity of spatial processing in touch, vision, and audition. Previous research has revealed resemblances between tactile and visual perceptions of spatial properties such as orientation, shape, and form (Phillips et al, 1983; Bensmaia et al., 2008; Hsiao, 1998; Yau et al., 2009, 2016). Moreover, tactile, visual, and

auditory perceptions are all prone to spatial illusions when the stimuli are delivered in rapid succession (Geldard & Sherrick, 1972; Goldreich, 2007; Getzmann, 2009; Khuu et al., 2011; Goldreich and Tong, 2013; Tong et al., 2016). Another spatial illusion, adaptation-induced spatial repulsion, has been well documented in vision and to a lesser extent audition (Thurlow & Jack, 1973; Kashino & Nishida, 1998; Carlile et al., 2001; Clifford et al., 2007; Kohn, 2007; Schwartz et al., 2007). Here, we verified that it occurs also in touch. The analogous repulsive aftereffects caused by adaptation in different sensory modalities may point to fundamentally similar strategies for dynamic spatial coding.

Future studies could look further into the generalizability of the spatial repulsion illusion to the perception of other tactile features. In preliminary experiments not reported in this thesis, we conducted a study to investigate the effects of adaptation on tactile orientation perception: participants compared the perceived orientations of two bars indenting their index fingertip successively, without or with adaptation to the intervening skin between the bars. Results from 19 pilot participants indicated that 5-15 s of static pressure as the adapting stimulus prior to every trial did not elicit a tactile tilt aftereffect illusion. A possible explanation is that short periods of static pressure were insufficient to cause adaptation in the slowly-adapting type-1 (SA1) afferents, whose defining characteristic is slow adaptation to static pressure. SA1s are the main afferents for conveying spatially modulated signals, thus presumably responsible for observable spatial illusions. Follow-up experiments of this study could apply vibration instead of static pressure as the adapting stimulus, because vibration is more effective in inducing adaptation of SA1 compared to static pressure (Bensmaia et al., 2005; Bensmaia et al., 2006).

The adaptation-induced repulsive effect that we observed was significant but small. It is possible that the true effect of adaptation on expanding the perceived reference distance could have been greater, but was diminished or obscured due to the fact that only one reference distance was used and that the reference point-stimuli were repeatedly applied to the same skin sites. If this happened, it could be due to a few reasons. First, participants could have developed a high prior probability for the reference distance or for the locations of the two reference points; sharpening the prior distribution around the reference distance or point positions would have counteracted the repulsion effect resulting from likelihood changes. Second, simultaneous punctate stimulation of two closely-spaced skin sites could have led to an illusory percept of a single stimulus at the middle of the sites, instead of separate stimuli at the individual sites; this phenomenon is known as the funneling illusion (Gardner & Spencer, 1972a; Chen et al., 2003; Friedman et al., 2008). If funneling occurred in perception of the reference point positions for some participants, it could have obscured the overall repulsive effect of adaptation. Third, if participants realized that the reference distance was unchanging, they could have ignored it, and simply performed the task by learning the range of the comparison distances (6 – 54 mm) and comparing each of them to an internal reference that was the average of all possible comparison distances (30 mm). In this case, ignoring sensory information from the reference site would reduce the size of the PSE shift. To address these possible factors

that could have diminished the repulsive effect, future studies could apply two or three reference distances to each participant, and test the perception of each reference with a corresponding symmetric set of comparisons.

Another future direction is to disentangle the contributions of different mechanoreceptive units to the tactile spatial repulsion illusion. Future studies could selectively activate or adapt one or a few mechanoreceptive afferent types, and assess how the presence or absence of certain afferent responses affects the generation of the illusion. A possibility for selective afferent activation is to use the OPTACON, a reading device for the blind, which has been found to activate rapidly-adapting (RA) afferents and PC afferents, but not SA1 afferents (Gardner & Palmer, 1989). The relative contribution of RA versus PC could be further disentangled by the placement of an annulus around the stimulus; this manipulation has been shown to selectively reduce stimulus-evoked PC activation relative to RA activation (Gescheider et al., 1978; Tommerdahl et al., 2005). In addition, the annulus could help control the spread of vibration and thus vibration-induced effects. Another approach is to selectively adapt PCs versus RAs (in glabrous skin) or hair units (in hairy skin). For example, Hollins and colleagues showed that prolonged suprathreshold vibration at a high (250 Hz) versus low (10 Hz) frequency selectively adapted PCs and RAs, respectively; the adapting stimulus amplitudes they used were 40 dB SL with respect to mean threshold: 4.1 μm at 250 Hz and 239 μm at 10 Hz (Hollins et al., 2001). Similarly, Gescheider and colleagues showed that when the test stimulus was 20 or 30 Hz, a 250-Hz adapting stimulus had no effect on detection threshold until it was approximately 29 dB SL suprathreshold (Gescheider et al., 1979). Furthermore, selective afferent adaptation could be combined with neurophysiological recordings that measure downstream changes following the adaptation. This could provide important insight into how channel-specific alteration of sensory representation from an earlier processing stage is read out downstream.

The Bayesian perceptual model we presented in Chapter 4 makes several predictions that could be tested psychophysically. For example, the model predicts that adaption of skin sites outside and adjacent to the reference points will cause a contraction in perceived distance. This prediction is consistent with the results from Day & Singer (1964) and Gilbert (1967), which used static pressure as the adapting stimulus and bars as test stimuli on the forearm. Also, the model predicts that in a single-point localization task, the perceived position of a point-stimulus close to the adapted site will shift away from the adapted site. Related to this, if two point-stimuli are asymmetrically positioned with respect to a single adapted site in between the points, the model predicts asymmetrical repulsive effects in point localization, with a stronger effect for the point closer to the adapted site. Furthermore, although the model focuses on adaptation effects on PSE estimates, it can also make predictions regarding the just noticeable difference (JND). For example, the model predicts that JND will decrease for two point-stimuli that straddle the adapted site, reflecting an improved discriminability. In addition, the model could try to replicate the recent empirical work of Longo and colleagues (Calzolari et al., 2017), which showed adaptation to tactile distance and suggested the possibility of distance

tuning. The model could modify its likelihood function to represent distance instead of point position, or its prior distribution to represent the effect of distance learning, and explore whether these changes may give rise to neuronal behaviour akin to distance tuning.

Last but not least, the model could be further developed to take into account more complex neural properties and adaptation effects. It could be modified to simulate a variety of additional plausible adaptation-induced changes in the RFs or tuning curves of single neurons. Furthermore, it could be developed into a network model that takes into account excitatory and inhibitory interactions within the neural circuitry. For example, the relative strength of recurrent excitation and inhibition could be assigned by adjusting simulated synaptic weights. Different combinations of dynamics in the excitatory and inhibitory input might lead to similar changes in tuning or the population response in downstream networks. These models could help explain how adaptation may alter neural responses at successive stages of processing, and generate predictions to be tested empirically by neurophysiological and psychophysical experiments.

## 5.5 Conclusion

The empirical and theoretical work presented in this thesis demonstrates that tactile spatial perception is subject to an adaptation-induced illusion that expands the perceived distance between stimuli on the skin. This work sheds light on possible mechanisms and functional organizations underlying dynamic tactile spatial processing under the influence of recent sensory events, and supports the hypothesis that tactile perception shares common processing features and computational principles with visual and auditory perception.

## 5.6 References

Barker, D. J., Shepard, P. D., & McDermott, K. L. (1982). Fatigue in cat facial mechanoreceptors. *Neuroscience Letters*, *30*, 117–122.

Barlow, H. B. (1990). A theory about the functional role and synaptic mechanism of visual after-effects. In C. B. Blakemore (Ed.), *Vision: coding and efficiency*. Cambridge University Press.

Barraclough, N. E., Page, S. A., & Keefe, B. D. (2017). Visual adaptation enhances action sound discrimination. *Attention, Perception & Psychophysics*, *79*(1), 320–332. https://doi.org/10.3758/s13414-016-1199-z

Baylis, G. C., & Rolls, E. T. (1987). Responses of neurons in the inferior temporal cortex in short term and serial recognition memory tasks. *Experimental Brain Research*, *65*,

614–622.
Belin, P., & Zatorre, R. J. (2003). Adaptation to speaker's voice in right anterior temporal lobe. *Neuroreport*, *14*(16), 2105–2109. https://doi.org/10.1097/01.wnr.0000091689.94870.85
Bensmaïa, S. J., Craig, J. C., & Johnson, K. O. (2006). Temporal factors in tactile spatial acuity: evidence for RA interference in fine spatial processing. *Journal of Neurophysiology*, *95*(3), 1783–91. https://doi.org/10.1152/jn.00878.2005
Bensmaia, S. J., Craig, J. C., Yoshioka, T., & Johnson, K. O. (2006). SA1 and RA afferent responses to static and vibrating gratings. *Journal of Neurophysiology*, *95*(3), 1771–82. https://doi.org/10.1152/jn.00877.2005
Bensmaia, S. J., Hsiao, S. S., Denchev, P. V., Killebrew, J. H., & Craig, J. C. (2008). The tactile perception of stimulus orientation. *Somatosensory & Motor Research*, *25*(1), 49–59. https://doi.org/10.1080/08990220701830662
Bensmaia, S. J., Leung, Y. Y., Hsiao, S. S., & Johnson, K. O. (2005). Vibratory Adaptation of Cutaneous Mechanoreceptive Afferents. *Journal of Neurophysiology*, *94*(5), 3023–3036. https://doi.org/10.1152/jn.00002.2005
Beste, C., & Dinse, H. R. (2013). Learning without training. *Current Biology*, *23*(11), R489–R499. https://doi.org/10.1016/j.cub.2013.04.044
Bystrzycka, B. Y. E., Nail, B. S., & Rowe, M. (1977). Inhibition of cuneate neurons: Its afferent source and influence on dynamically sensitive "tactile" neurons. *J Physiol*, *268*, 251–270.
Calzolari, E., Azanon, E., Danvers, M., Vallar, G., & Longo, M. R. (2017). Adaptation aftereffects reveal that tactile distance is a basic somatosensory feature. *Proc Natl Acad Sci USA*, *114*(17), 4555–4560.
Carandini, M., & Ferster, D. (1997). A tonic hyperpolarization underlying contrast adaptation in cat visual cortex. *Science*, *276*(5314), 949–952.
Carlile, S., Hyams, S., & Delaney, S. (2001). Systematic distortions of auditory space perception following prolonged exposure to broadband noise. *The Journal of the Acoustical Society of America*, *110*, 416–440. https://doi.org/10.1121/1.1375843
Chance, F. S., Nelson, S. B., & Abbott, L. F. (1998). Synaptic depression and the temporal response characteristics of V1 cells. *The Journal of Neuroscience*, *18*(12), 4785–4799.
Chen, L. M., Friedman, R. M., & Roe, A. W. (2003). Optical Imaging of a Tactile Illusion in Area 3b of the Primary Somatosensory Cortex. *Science*, *302*(5646), 881–885.
Chung, S., Li, X., Nelson, S. B., & Street, S. (2002). Short-Term Depression at Thalamocortical Synapses Contributes to Rapid Adaptation of Cortical Sensory Responses In Vivo. *Neuron*, *34*, 437–446.
Clifford, C. W. G., Webster, M. A., Stanley, G. B., Stocker, A. A., Kohn, A., Sharpee, T. O., & Schwartz, O. (2007). Visual adaptation: Neural, psychological and computational aspects. *Vision Research*, *47*(25), 3125–3131. https://doi.org/10.1016/j.visres.2007.08.023
Clifford, C. W. G., Wenderoth, P., & Spehar, B. (2000). A functional angle on some after-effects in cortical vision. *Proceedings of the Royal Society B: Biological Sciences*, *267*(1454), 1705–1710. https://doi.org/10.1098/rspb.2000.1198

Cooke, S. F., & Bliss, T. V. P. (2006). Plasticity in the human central nervous system. *Brain*, *129*(7), 1659–1673. https://doi.org/10.1093/brain/awl082

Day, R. H., & Singer, G. (1964). A tactile spatial aftereffect. *Australian Journal of Psychology*, *16*(I), 33–37.

Descalzo, V. F., Nowak, L. G., Brumberg, J. C., & Mccormick, D. A. (2005). Slow adaptation in fast-spiking neurons of visual cortex. *Journal of Neurophysiology*, *93*, 1111–1118. https://doi.org/10.1152/jn.00658.2004

Dewson, J. H. (1964). Cortical responses to patterns of two-point cutaneous stimulation. *Journal of Comparative Physiological Psychology*, *58*(2), 387–389.

Dragoi, V., Rivadulla, C., & Sur, M. (2001). Foci of orientation plasticity in visual cortex. *Nature*, *411*(6833), 80–86. https://doi.org/10.1038/35075070

Dragoi, V., Sharma, J., & Sur, M. (2000). Adaptation-induced plasticity of orientation tuning in adult visual cortex. *Neuron*, *28*(1), 287–298. https://doi.org/10.1016/S0896-6273(00)00103-3

Duncan, G. H., Dreyer, D. A., McKenna, T. M., & Whitsel, B. L. (1982). Dose- and time-dependent effects of ketamine on SI neurons with cutaneous receptive fields. *Journal of Neurophysiology*, *47*(4), 677–699.

Friedman, R. M., Chen, L. M., & Roe, A. W. (2008). Responses of areas 3b and 1 in anesthetized squirrel monkeys to single- and dual-site stimulation of the digits. *J Neurophysiol*, *100*(6), 3185–3196. https://doi.org/10.1152/jn.90278.2008

Gardner, E. P., & Palmer, C. I. (1989). Simulation of motion on the skin. I. Receptive fields and temporal frequency coding by cutaneous mechanoreceptors of OPTACON pulses delivered to the hand. *Journal of Neurophysiology*, *62*(6), 1410–36.

Gardner, E. P., & Spencer, W. a. (1972a). Sensory funneling. I. Psychophysical observations of human subjects and responses of cutaneous mechanoreceptive afferents in the cat to patterned skin stimuli. *Journal of Neurophysiology*, *35*(6), 925–953.

Gardner, E. P., & Spencer, W. a. (1972b). Sensory funneling. II. Cortical neuronal representation of patterned cutaneous stimuli. *Journal of Neurophysiology*, *35*(6), 954–977.

Geldard, F. A., & Sherrick, C. E. (1972). The Cutaneous " Rabbit ": A Perceptual Illusion. *Science*, *178*(4057), 178–179.

Gescheider, G. A., Capraro, A. J., Frisina, R. D., Hamer, R. D., & Verrillo, R. . (1978). The effects of a surround on vibrotactile thresholds. *Sensory Precesses*, *2*(2), 99–115.

Gescheider, G. A., Frisina, R. D., & Verrillo, R. T. (1979). Selective adaptation of vibrotactile thresholds. *Sensory Processes*, *3*(1), 37–48.

Gescheider, G. A., & Wright, J. H. (1969). Effects of vibrotactile adaptation on perception of stimuli of varied intensity. *Journal of Experimental Psychology*, *81*(3), 449–453.

Gibson, J. J., & Radner, M. (1937). Adaptation, After-Effect and Constrast in the Perception of Tilted Lines. *Journal of Experimental Psychology*, *20*(5), 453–467. https://doi.org/10.1037/h0059826

Gilbert, A. J. (1967). Tactile spatial aftereffect or adaptation level? *Journal of Experimental Psychology*, *73*(3), 450–455.

Goble, A. K., & Hollins, M. (1993). Vibrotactile adaptation enhances amplitude discrimination. *The Journal of the Acoustical Society of America*, *93*(1), 771–780. https://doi.org/10.1121/1.410314

Goble, A. K., & Hollins, M. (1994). Vibrotactile adaptation enhances frequency discrimination. *The Journal of the Acoustical Society of America*, *96*(2), 771–780. https://doi.org/10.1121/1.410314

Godde, B., Stauffenberg, B., Spengler, F., & Dinse, H. R. (2000). Tactile coactivation-induced changes in spatial discrimination performance. *The Journal of Neuroscience*, *20*(4), 1597–604. Retrieved from http://www.ncbi.nlm.nih.gov/pubmed/10662849

Goldreich, D. (2007). A Bayesian perceptual model replicates the cutaneous rabbit and other tactile spatiotemporal illusions. *PLoS ONE*, *2*(3). https://doi.org/10.1371/journal.pone.0000333

Goldreich, D., & Tong, J. (2013). Prediction, postdiction, and perceptual length contraction: A bayesian low-speed prior captures the cutaneous rabbit and related illusions. *Frontiers in Psychology*, *4*(MAY), 1–26. https://doi.org/10.3389/fpsyg.2013.00221

Goodwin, A. W., & Wheat, H. E. (2004). Sensory Signals in Neural Populations Underlying Tactile Perception and Manipulation. *Annual Review of Neuroscience*, *27*(1), 53–77. https://doi.org/10.1146/annurev.neuro.26.041002.131032

Green, B. G. (1982). The perception of distance and location for dual tactile pressures. *Perception & Psychophysics*, *31*(4), 315–323. https://doi.org/10.3758/BF03202654

Gutnisky, D. A., & Dragoi, V. (2008). Adaptive coding of visual information in neural populations. *Nature*, *452*(7184), 220–224. https://doi.org/10.1038/nature06563

Heron, J., Aaen-Stockdale, C., Hotchkiss, J., Roach, N. W., McGraw, P. V., & Whitaker, D. (2012). Duration channels mediate human time perception. *Proceedings of the Royal Society B: Biological Sciences*, *279*(1729), 690–698. https://doi.org/10.1098/rspb.2011.1131

Hollins, M., Bensmaïa, S. J., & Washburn, S. (2001). Vibrotactile adaptation impairs discrimination of fine, but not coarse, textures. *Somatosensory & Motor Research*, *18*(4), 253–262. https://doi.org/10.1080/01421590120089640

Hosoya, T., Baccus, S. A., & Meister, M. (2005). Dynamic predictive coding by the retina. *Nature*, *436*(7047), 71–77. https://doi.org/10.1038/nature03689

Hsiao, S. S. (1998). Similarities between touch and vision. In J. W. Morley (Ed.), *Neural computation* (pp. 131–165). Amsterdam ; New York: Elsevier.

Ito, M. (1989). Long-term depression. *Ann. Rev. Neurosci.*, *12*, 85–102.

Jin, D. Z., Dragoi, V., Sur, M., & Seung, H. S. (2005). Tilt Aftereffect and Adaptation-Induced Changes in Orientation Tuning in Visual Cortex Tilt Aftereffect and Adaptation-Induced Changes in Orientation Tuning in Visual Cortex. *Journal of Neurophysiology*, *94*(6), 4038–4050. https://doi.org/10.1152/jn.00571.2004

Kashino, M., & Nishida, S. (1998). Adaptation in the processing of interaural time differences revealed by the auditory localization aftereffect. *The Journal of the Acoustical Society of America*, *103*(6), 3597–3604. https://doi.org/10.1121/1.423064

Kim, K. J., & Rieke, F. (2003). Slow Na+ Inactivation and Variance Adaptation in Salamander Retinal Ganglion Cells. *Journal of Neuroscience*, *23*(4), 1506–1516.

https://doi.org/23/4/1506 [pii]
Kitagawa, N., & Ichihara, S. (2002). Hearing visual motion in depth. *Nature*, *416*(6877), 172–174. https://doi.org/10.1038/416172a
Kohn, A. (2007). Visual adaptation: physiology, mechanisms, and functional benefits. *Journal of Neurophysiology*, *97*(5), 3155–3164. https://doi.org/10.1152/jn.00086.2007
Kohn, A., & Movshon, J. A. (2004). Adaptation changes the direction tuning of macaque MT neurons. *Nature Neuroscience*, *7*(7), 764–772. https://doi.org/10.1038/nn1267
La Camera, G., Rauch, A., Thurbon, D., Lu, H., Senn, W., Fusi, S., & Camera, L. (2006). Multiple time scales of temporal response in pyramidal and fast spiking cortical neurons. *J Neurophysiol*, *96*, 3448–3464. https://doi.org/10.1152/jn.00453.2006.
Laskin, S. E., & Spencer, W. A. (1979). Geometry of excitatory and inhibitory receptive fields of single units in somatosensory cortex of the cat. *J Neurophysiol*, *42*(4), 1061–1082.
Lee, C. J., & Whitsel, B. L. (1992). Mechanisms underlying somatosensory cortical dynamics: I. In vivo studies. *Cerebral Cortex (New York, N.Y. : 1991)*, *2*(2), 81–106.
Lee, C. J., Whitsel, B. L., & Tommerdahl, M. (1992). Mechanisms underlying somatosensory cortical dynamics: II. In vitro studies. *Cerebral Cortex*, *2*(2), 107–133.
Levinson, E., & Sekuler, R. (1976). Adaptation alters perceived direction of motion. *Vision Research*, *16*, 779–781.
Lundstrom, J. (1986). Responses of mechanoreceptive afferent units in the glabrous skin of the human hand to vibration. *Scandinavian Journal of Work, Environment & Health*, *12*(4), 413–416.
Macefield, G., & Burke, D. (1991). Long-lasting depression of central synaptic transmission following prolonged high-frequency stimulation of cutaneous afferents: a mechanism for post-vibratory hypaesthesia. *Electroencephalography and Clinical Neurophysiology*, *78*, 150–158.
Mather, G. (1980). The movement aftereffect and a distribution-shift model for coding the direction of visual movement. *Perception*, *9*(4), 379–392. https://doi.org/10.1068/p090379
O'Mara, S., Rowe, M. J., & Tarvin, R. P. (1988). Neural mechanisms in vibrotactile adaptation. *Journal of Neurophysiology*, *59*(2), 607–622.
Phillips, J. R., Johnson, K. O., & Browne, H. M. (1983). A comparison of visual and two modes of tactual letter resolution. *Perception & Psychophysics*, *34*(3), 243–249. https://doi.org/10.3758/BF03202952
Poolos, N. P., & Kocsis, J. D. (1990). Elevated extracellular potassium concentration enhances synaptic activation of N-methyl-d-aspartate receptors in hippocampus. *Brain Research*, *508*(1), 7–12. https://doi.org/10.1016/0006-8993(90)91110-3
Pubols, B. H. (1982). Factors affecting cutaneous mechanoreceptor response. I. Constant-force versus constant-displacement stimulation. *Journal of Neurophysiology*, *47*(3), 515–529.
Rauch, A., Camera, G. La, & Senn, W. (2003). Neocortical pyramidal cells respond as integrate-and-fire neurons to in vivo − like input currents. *J Neurophysiol*, *90*, 1598–

1612. https://doi.org/10.1152/jn.00293.2003
Sanchez-Vives, M. V, Nowak, L. G., & McCormick, D. A. (2000a). Cellular mechanisms of long-lasting adaptation in visual cortical neurons in vitro. *Journal of Neuroscience*, *20*(11), 4286–4299.
Sanchez-Vives, M. V, Nowak, L. G., & McCormick, D. A. (2000b). Membrane mechanisms underlying contrast adaptation in cat area 17 in vivo. *Journal of Neuroscience*, *20*(11), 4267–4285. https://doi.org/20/11/4267 [pii]
Saul, A., & Cynader, M. (1989). Adaptation in single units in visual cortex: The tuning of aftereffects in the spatial domain. *Visual Neuroscience*, *2*(6), 593–607. https://doi.org/10.1017/S0952523800003527
Schwartz, O., Hsu, A., & Dayan, P. (2007). Space and time in visual context. *Nature Reviews. Neuroscience*, *8*(7), 522–535. https://doi.org/10.1038/nrn2155
Simons, S. B., Chiu, J., Favorov, O. V, Whitsel, B. L., & Tommerdahl, M. (2007). Duration-dependent response of SI to vibrotactile stimulation in squirrel monkey. *Journal of Neurophysiology*, *97*(3), 2121–9. https://doi.org/10.1152/jn.00513.2006
Simons, S. B., Tannan, V., Chiu, J., Favorov, O. V, Whitsel, B. L., & Tommerdahl, M. (2005). Amplitude-dependency of response of SI cortex to flutter stimulation. *BMC Neuroscience*, *6*, 43. https://doi.org/10.1186/1471-2202-6-43

Spain, W. J., Schwindt, P. C., & Crill, W. E. (1991). Two Transient Potassium Currents in Layer V Pyramidal Neurones from Cat Sensorimotor Cortex. *J Physiol*, *434*, 591–607. https://doi.org/10.1113/jphysiol.1991.sp018488
Stocker, A. a, & Simoncelli, E. P. (2006b). Sensory Adaptation within a Bayesian Framework for Perception. *Advances in Neural Information Processing Systems*, *18*, 1291–1298.
Tannan, V., Simons, S., Dennis, R. G., & Tommerdahl, M. (2007). Effects of adaptation on the capacity to differentiate simultaneously delivered dual-site vibrotactile stimuli. *Brain Research*, *1186*(1), 164–170. https://doi.org/10.1016/j.brainres.2007.10.024
Thurlow, W. R., & Jack, C. E. (1973). Some determinants of localization-adaptation effects for successive auditory stimuli. *The Journal of the Acoustical Society of America*, *53*(6), 1573–1577.
Toib, A., Lyakhov, V., & Marom, S. (1998). Interaction between duration of activity and time course of recovery from slow inactivation in mammalian brain Na+ channels. *The Journal of Neuroscience*, *18*(5), 1893–903.
Tommerdahl, M., Favorov, O., & Whistel, B. L. (2002). Optical imaging of intrinsic signals in the somatosensory cortex. *Behavioural Brain Research*, *135*, 83–91.
Tommerdahl, M., Favorov, O. V, & Whitsel, B. L. (2005). Effects of high-frequency skin stimulation on SI cortex: mechanisms and functional implications. *Somatosensory & Motor Research*, *22*(3), 151–169. https://doi.org/10.1080/08990220500084461
Tommerdahl, M., Hester, K. D., Felix, E. R., Hollins, M., Favorov, O. V., Quibrera, P. M., & Whitsel, B. L. (2005). Human vibrotactile frequency discriminative capacity after adaptation to 25 Hz or 200 Hz stimulation. *Brain Research*, *1057*(1–2), 1–9. https://doi.org/10.1016/j.brainres.2005.04.031
Tong, J., Mao, O., & Goldreich, D. (2013). Two-point orientation discrimination versus

the traditional two-point test for tactile spatial acuity assessment. *Frontiers in Human Neuroscience*, *7*, 579. https://doi.org/10.3389/fnhum.2013.00579

Tong, J., Ngo, V., & Goldreich, D. (2016). Tactile length contraction as Bayesian inference. *Journal of Neurophysiology*, *116*(2), 369–379. https://doi.org/10.1152/jn.00029.2016

Webster, M. (2012). Evolving concepts of sensory adaptation. *F1000 Biology Reports*, *4*(November), 1–7. https://doi.org/10.3410/B4-21

Wedell, C. H., & Cummings, S. B. . J. (1938). Fatigue of the vibratory sense. *Journal of Experimental Psychology*, *22*(5), 429–438. https://doi.org/10.1037/h0059105

Weinstein, S. (1968). Intensive and extensive aspects of tactile sensitivity as a function of body part, sex and laterality. In D. R. Kenshalo (Ed.), *The Skin Senses* (1st ed., pp. 195–222). Springfield, IL: Charles C. Thomas.

Whitsel, B. L., Kelly, E. F., Quibrera, M., Tommerdahl, M., Li, Y., Favorov, O. V, … Metz, C. B. (2003). Time-dependence of SI RA neuron response to cutaneous flutter stimulation. *Somatosensory & Motor Research*, *20*(1), 45–69. https://doi.org/10.1080/0899022031000083834

Whitsel, B. L., Kelly, E. F., Xu, M., Tommerdahl, M., & Quibrera, M. (2001). Frequency-dependent response of SI RA-class neurons to vibrotactile stimulation of the receptive field. *Somatosensory & Motor Research*, *18*(4), 263–285. https://doi.org/10.1080/01421590120089 65

Whitsel, D. L., Favorov, O. V, Kelly, D. G., & Tommerdahl, M. (1991). Mechanisms of Dynamic Peri- and Intra-columnar Interactions in Somatosensory Cortex: Stimulus-specific Contrast Enhancement by NMDA Receptor Activation. In O. Franzén & J. Westman (Eds.), *Information Processing in the Somatosensory System: Proceedings of an International Symposium at the Wenner-Gren Center, Stockholm, 3-5 July, 1989* (pp. 353–369). London: Macmillan Education UK. https://doi.org/10.1007/978-1-349-11597-6_26

Wissig, S. C., & Kohn, A. (2012). The influence of surround suppression on adaptation effects in primary visual cortex. *Journal of Neurophysiology*, *107*(12), 3370–3384. https://doi.org/10.1152/jn.00739.2011

Yates, G. K., Robertson, D., & Johnstone, B. M. (1985). Very rapid adaptation in the guinea pig auditory nerve. *Hearing Research*, *17*(1), 1–12.

Yau, J. M., Kim, S. S., Thakur, P. H., & Bensmaia, S. J. (2016). Feeling form: the neural basis of haptic shape perception. *Journal of Neurophysiology*, *115*(2), 631–642. https://doi.org/10.1152/jn.00598.2015

Yau, J. M., Pasupathy, A., Fitzgerald, P. J., Hsiao, S. S., & Connor, C. E. (2009). Analogous intermediate shape coding in vision and touch. *Proceedings of the National Academy of Sciences of the United States of America*, *106*(38), 16457–62. https://doi.org/10.1073/pnas.0904186106

Zimmerman, A., Bai, L., & Ginty, D. D. (2014). The gentle touch receptors of mammalian skin. *Science (New York, N.Y.)*, *346*(6212), 950–4. https://doi.org/10.1126/science.1254229

Zohary, E., Shadlen, M. N., & Newsome, W. T. (1994). Correlated neuronal discharge rate and its implications for psychophysical performance. *Nature*.

https://doi.org/10.1038/370140a0
Zucker, R. S., & Regehr, W. G. (2002). Short-Term Synaptic Plasticity. *Annual Review of Physiology*, *64*(1), 355–405. https://doi.org/10.1146/annurev.physiol.64.092501.114547